Targeting intracellular *Burkholderia* by directed monoclonal antibody, antibiotic and autophagy combination therapies.

Adam William Taylor

Thesis submitted in accordance with the requirements for the degree of

Doctor of Philosophy
of the
University of London

July 2022

Department of Immunology and Infection

Faculty of Infectious Tropical Diseases

LONDON SCHOOL OF HYGIENE & TROPICAL MEDICINE

Funded by UK Ministry of Defence

Research group affiliation(s): Dstl, Porton Down, Salisbury. UK.

Targeting intracellular *Burkholderia* by directed monoclonal antibody, antibiotic and autophagy combination therapies.

I Adam William Taylor, confirm that the work presented in this thesis is my own. Where information has been derived from other sources, I confirm that this has been indicated in the thesis.

Abstract.

Aim: To generate an antibody-antibiotic conjugate directed against *Burkholderia pseudomallei* and to investigate combinational therapies. This involves antibody, antibiotics and autophagy promoting compounds as potential alternative therapies for melioidosis.

Melioidosis is a severely neglected tropical disease caused by the gram negative bacterium *B. pseudomallei*. The bacterium can subvert the host immune system and form an intracellular niche protected from current antibiotic therapies. This project aims to investigate monoclonal antibodies and novel antimicrobial compounds as potential therapeutics for melioidosis. An antibody will be incorporated into an antibody-antibiotic conjugate (AAC) which has the potential to specifically target bacteria and localise delivery of antibiotics to the site of intracellular infection.

RAW 264.7 macrophage-like cell infection assays have been used to down select monoclonal antibodies based on their ability to opsonise *Burkholderia in vitro.* Imaging flow cytometry and colony count data has shown that antibodies directed against the capsule polysaccharide (CPS) of *Burkholderia* are opsonising and significantly increase bacterial uptake into RAW cells. Confocal microscopy data shows that antibody opsonised bacteria have a significant reduction in actin tail formation within RAW cells, which is required for bacterial virulence and spread between host cells. Autophagy inducing compounds have been investigated as potential alternatives to antibiotics, with one compound displaying a level of bacterial killing and autophagy induction *in vitro*.

An AAC has been developed consisting of an anti-CPS antibody conjugated to an antibiotic via a cathepsin cleavable linker. The mechanism of action relies upon opsonisation of *Burkholderia* and uptake of the AAC into phagocytes. Within the phagocyte, the linker between the antibody and antibiotic is cleaved by cathepsin, therefore releasing the antibiotic in an active form to kill the intracellular bacteria. Two antibiotics have been successfully incorporated into a cathepsin cleavable linker and antibiotic functionality demonstrated *in vitro*.

In conclusion this data is supporting the development of a novel antibody based therapy for melioidosis and gaining insight into the cell-bacterial relationship during *Burkholderia* infection. This work represents an initial proof of principle in the development of an AAC as a targeted therapy for melioidosis. By targeting intracellular infection it is hoped that this will improve current antibiotic therapy for melioidosis and reduce relapse of infection in infected individuals.

Acknowledgments.

I would like to acknowledge the support of Dstl during my PhD and the project funding provided by the UK MoD.

A very big thank you to my supervisors Jo Prior and Greg Bancroft for their help and advice throughout my PhD.

I am grateful to Dr Jenner, Dr Laws and Dr Armstrong at Dstl for their support with lab work and data analysis.

Thank you to Dr Schouten at Global Access Diagnostics for his chemistry expertise and generating antibody-antibiotic conjugate molecules.

A special thank you to my family for their support during my PhD.

Statement of contributions.

Global Access Diagnostics generated antibody-antibiotic conjugate test batches, including antibiotic-linkers and antibiotic-stub molecules. Global Access Diagnostics were previously trading as Mologic Ltd.

All hands on animal experimental work was performed by staff at the Dstl experimental animal house.

Dr D Jenner at Dstl provided advice, training, and confocal microscopy actin tail image analysis using open source Icy analysis software.

Dr S Armstrong at Dstl provided advice for the *in vivo* study and the pharmacokinetic prediction spreadsheet.

Dr T Laws at Dstl provided advice regarding statistical analysis of experimental data.

Publications and presentations.

Publications relating to this thesis

Taylor A, Jenner D, Rowland C, Laws T, Norville I, Prior J. 2021. Monoclonal antibodies opsonise *Burkholderia* and reduce intracellular actin tail formation in a macrophage infection assay. J Bacteriol doi:10.1128/jb.00244-21:Jb0024421. **Publication of antibody opsonisation and reduction in actin tail data.**

Laws, T. R., Taylor, A.W., Russell, P. (2019). "The treatment of melioidosis: is there a role for repurposed drugs? A proposal and review." Expert Rev Anti Infect Ther: 1-11. **Section on autophagy inducing compounds and repurposed drugs.**

Taylor, A., Jenner, D., Bancroft, G.J., Rowland, C.A. and Prior, J., (2017). Targeting intracellular *Burkholderia* by antibody and antibiotic combination therapies. Sri Lankan Journal of Infectious Diseases. 7, pp.S20: 25. DOI: http://doi.org/10.4038/sljid.v7i0.8187. **Publication of a conference abstract.**

Eleanor Porges, Dominic Jenner, Adam W. Taylor, James S. P. Harrison, Antonio De Grazia, Alethia R. Hailes, Kimberley M. Wright, Adam O. Whelan, Isobel H. Norville, Joann L. Prior, Sumeet Mahajan, Caroline A. Rowland, Tracey A. Newman, and Nicholas D. Evans. (2021) Antibiotic-Loaded Polymersomes for Clearance of Intracellular *Burkholderia thailandensis*. ACS Nano 15 (12), 19284-19297. **Macrophage infection assays with polymersomes and *B. thailandensis*.**

Conference presentations

- South Asian melioidosis congress, Sri Lanka 2017. Poster.
- European melioidosis congress, Oxford UK 2018. Speaker.
- Immunotherapy for infectious diseases, Texas USA 2018. Poster.

- UK Cellular Microbiology network, London UK 2019. Poster.
- World melioidosis congress, Hanoi Vietnam 2019. Speaker.
- World ADC Europe, London 2020. Poster.
- World ADC, Digital 2020. Speaker.
- World ADC Europe, Digital 2021. Speaker.
- World ADC, digital 2021. Speaker.
- World ADC Europe, London 2022. Speaker.
- European melioidosis congress, Austria 2022. Speaker.

Table of contents.

List of figures.

List of tables.

Abbreviations.

AAC	antibody antibiotic conjugate
ABTS	2,2′-azino-di-(3-ethylbenzthiazoline sulfonic acid
ACDP	advisory committee on dangerous pathogens
ADC	antibody drug conjugate
ANOVA	analysis of variance
BimA	*Burkholderia* intracellular motility A
BMDM	bone marrow derived macrophage
BOC	tert-butyloxycarbonyl
CD	cluster of differentiation
CFU	colony forming unit
Ch	channel
Cit	Citrulline
CP	cardiac puncture
CPS	capsule polysaccharide
Da	Dalton
DAR	drug antibody ratio
DMSO	Dimethyl sulfoxide
ELISA	enzyme linked immunosorbent assay
Fab	fragment antigen binding
Fc	fragment crystallisable
FcRn	neonatal fragment crystallisable receptor

FDA	food and drug administration
FITC	fluorescein isothiocyanate
GFP	green fluorescent protein
HAMA	human anti-mouse antibodies
HRP	horseradish peroxidase
IFN	interferon
Ig	immunoglobulin
IL	Interleukin
IP	intraperitoneal
IV	intravenous
J774	J774A.1 cells
LAMP	lysosomal associated membrane protein
LC3	microtubule-associated protein 1A/1B light chain 3
LD	lethal dose
LDH	lactose dehydrogenase
LLOQ	lower limit of quantification
LPS	lipopolysaccharide
mAb	monoclonal antibody
MALDI	matrix assisted laser desorption ionization
MBC	minimum bactericidal concentration
MC	maleimidocaproyl
MCSF	macrophage colony stimulating factor
MIC	minimum inhibitory concentration

MNGC	multi-nucleated giant cell
MOI	multiplicity of infection
NK	natural killer
OD	optical density
PAB	p-aminobenzyl
PABA	p-aminobenzyl carbamate
PBST	phosphate buffered saline containing Tween®
PCR	polymerase chain reaction
PK	pharmacokinetic
RAW	RAW 264.7 macrophage-like cell line
RFP	red fluorescent protein
SC	Subcutaneous
SD	standard deviation
SMCC	succinimidyl 4-(N-maleimidomethyl)cyclohexane-1-carboxylate
TA	terminal anaesthesia
TFA	trifluoroacetic acid
Val	Valine

1. Introduction.

1.1 Melioidosis.

1.1.1. *Burkholderia pseudomallei.*

B. pseudomallei is a gram negative bacterium responsible for the disease melioidosis. First described by Whitmore in 1913, Whitmore describes finding a strange glanders like bacterium during post mortems in Rangoon, and after describing the bacterium, proposed the name *pseudomallei* (1).

The bacterium has a low LD_{50}, especially via the aerosol route of infection, as shown by animal studies in which 10 or fewer bacterial colonies are fatal in BALB/c mice (2). The strain K96243 is commonly used in melioidosis studies, first isolated from a diabetic patient in Thailand. This strain has a LD_{50} in BALB/c mice of 262 and 10 bacterial colonies, from the intraperitoneal and inhalational infection route respectively (2).

B. pseudomallei is an Advisory Committee on Dangerous Pathogens (ACDP) hazard group III pathogen, it is a schedule 5 agent in the UK. The bacterium has been named as a potential bio-threat pathogen (3), this is in part due to key features including environmental persistence, a low infectious dose, together with a lengthy and complex therapy to successfully treat melioidosis.

1.1.2. Burkholderia thailandensis.

B. thailandensis is closely related to *B. pseudomallei*, first described in 1996 by Wuthiekanun *et al* as a potential new species of *Burkholderia* which is morphologically and antigenically similar to *B. pseudomallei* (4). It is possible to isolate both *B. thailandensis* and *B. pseudomallei* in the same environment (5), although *B. pseudomallei* isolation is often dominant, possibly due to the bacterium being able to inhibit the replication and motility of *B. thailandensis* (6). There are occasional reports of human infection and disease caused by *B. thailandensis* (7-9), it is probable that some of these cases are actually due to mistaken identity with *B. pseudomallei* (10). The bacterium is considered to be essentially avirulent in humans.

In small animal models, a greater than 10^5 reduction in virulence is seen with *B. thailandensis* strains compared to *B. pseudomallei* strains (2, 11). Colony morphology is similar and difficult to distinguish from *B. pseudomallei*, although one distinguishing factor is that *B. thailandensis* has the ability to assimilate L-arabinose (4, 11, 12). A *B. thailandensis* strain isolated from Cambodia expressing a *B. pseudomallei* like capsule polysaccharide (CPS) has been described in detail by Sim *et al* (13). This strain designated E555, demonstrates a greater ability to replicate and survive within the *in vitro* RAW cell infection model, when compared to non-capsulated strains (13). The E555 strain is avirulent in murine *in vivo* infection studies, demonstrating that the CPS alone is not sufficient to increase strain E555 virulence compared to other *B. thailandensis* strains (13). The E555 strain is commonly used as an ACDP hazard group II surrogate for *B. pseudomallei* within *in vitro* infection models (14, 15).

B. thailandensis E555 was used throughout this research project as a surrogate for *B. pseudomallei*. Non-capsulated strains of *B. thailandensis* such as E264 are commonly used in cell infection studies, E264 was not used in this research project since the bacterium replicates at a slower rate than *B. pseudomallei* in cell infection studies (16, 17). Additionally, E264 lacks the capsular polysaccharide, therefore lacking a major virulence factor and a specific target for monoclonal antibodies to be assessed in this research project. An attenuated strain of *B. pseudomallei* downgraded to containment level II could be used for cell infection assays, if permission could be grated for use in Dstl containment level II laboratories. Although, the characteristics for intracellular growth would have to be well defined. Capsular mutants such as JW270 (18) would not be suitable for this research project, due to the capsule being a crucial target for mAbs in this study. A study by Bayliss *et al* investigated the capsular polysaccharide of *B. thailandensis* E555, and showed that monoclonal antibody recognition of the *B. thailandensis* E555 capsule was indistinguishable from *B. pseudomallei* 1026b (19). It has also been demonstrated that *B. thailandensis* E555 replication in macrophages better represents that of *B. pseudomallei* replication, when compared to the non-capsule strain *B. thailandensis* E264 (15). *B. thailandensis* E555 shares some phenotypic characteristics with *B. pseudomallei*, such as colony wrinkling, resistance to complement and intracellular survival within macrophages (13). *B. thailandensis* E555 has been shown to be a

suitable surrogate for *B. pseudomallei* cell infection experiments enabling work at a lower level of containment. *B. thailandensis* E555 is avirulent in murine *in vivo* studies and therefore is not a suitable surrogate for *in vivo* protection studies (13).

1.1.3. Infection.

Taking into account melioidosis occurrences along with environmental and human factors, Limmathurotsakul *et al* (20) modelled the potential worldwide distribution. It is predicted that 165,000 cases of melioidosis occur a year with up to 89,000 deaths (20). The most common routes of infection by *B. pseudomallei* are through cutaneous inoculation and inhalation, with a peak of infection seen during extreme weather such as monsoon seasons, in which 75% and 81% of melioidosis cases in Thailand and Australia occur respectively (21). In Thailand, a melioidosis endemic area, the total numbers of culture-confirmed melioidosis cases in 2012, 2013, 2014, and 2015 were 1735, 1757, 1932, and 1702, respectively (22).

Cases of melioidosis in the UK are associated with travel from endemic areas, with the majority associated with travel from Thailand (23). A total of 46 cases of melioidosis were identified in the UK from January 2010 to July 2019 (23).

Melioidosis can present as an acute, chronic, or latent infection. The majority of healthy people clear the infection without complications and survive melioidosis (24, 25). Patients that do develop symptoms from an infection will most likely develop the acute form of melioidosis (25), the chronic form of infection (symptoms lasting >2 months) is less common, accounting for 11% of patients in a 20 year study from Darwin Australia (24). The latent form of melioidosis is thought to be rare and accounting for few cases, in patients that survive the initial acute melioidosis 5 - 28% experience a recurrence of infection (24, 25). Although, the recurrence in infection could be due to re-infection with a different *B. pseudomallei* strain rather than relapse in infection. Relapse however, can occur from *B. pseudomallei* that failed to be cleared from the initial infection (25-27).

1.1.4. Identification.

Early identification is key to successfully treating melioidosis, the disease is known as the great mimicker due to a wide variety of symptoms, commonly mistaken as *Mycobacterium tuberculosis* (28). The lungs are the most commonly affected organ in adults displaying symptoms such as pneumonia and fever, which can be difficult to distinguish from other infectious diseases such as tuberculosis (29). The bacterium can spread from the lungs to distant organs, such as the liver and spleen, causing abscess formation (29). Interestingly, the appearance of symptoms such as acute suppurative parotitis and central nervous system infection varies by regions (29), likely due to differences in isolates present. A recent study in Australia described an isolate of *B. pseudomallei* expressing a *Burkholderia mallei*-like *Burkholderia* intracellular motility A (*BimA*) protein, resulting in an increased virulence and central nervous system involvement in infection (30).

B. thailandensis can be present in the environment alongside *B. pseudomallei*, although rarely isolated together in the same environmental samples (6). A study in which *B. pseudomallei* and *B. thailandensis* were co-cultured, demonstrated that *B. pseudomallei* can inhibit the replication and motility of *B. thailandensis* by targeting the flagella (6). In Thailand, capsulated strains of *B. thailandensis* are less common and the presence of CPS does not seem to enhance survival in the environment (5). Seropositivity in healthy Thai farmers was shown to be due to exposure to *B. pseudomallei* rather than *B. thailandensis* (5).

Clinical diagnosis of melioidosis based on symptoms alone is extremely difficult, clinical manifestations may occur in a number of locations of the body including soft tissues, central nervous system, cardiovascular system, respiratory system, gastrointestinal and urinary tract system (25). Lab diagnosis of *B. pseudomallei* infection can be achieved by bacterial culture typically by Ashdown's selective media, in addition to detection by enzyme-linked immunosorbent assay (ELISA) and polymerase chain reaction (PCR) based technologies, although culture of *B. pseudomallei* remains the most reliable method of identification (21).

Antigen detection in clinical samples can be achieved by PCR and antibody based detection methods, these antigen diagnostic methods provide both a rapid and accurate diagnosis of melioidosis. Although, for PCR based diagnostics a laboratory

is required. This is often not available in remote endemic areas, and the cost involved also makes this approach unviable for many (25). Antibody based detection using the indirect haemagglutination assay is a specific test for *B. pseudomallei,* but this test alone is not suitable for an accurate diagnosis (31, 32). High background seropositivity in endemic areas can cause issues with misidentification and an inaccurate diagnosis of *B. pseudomallei* infection, additionally a successful diagnosis relies upon there being an antibody response in melioidosis patients (25, 31, 32).

Various PCR assays have been developed over the past 30 years, a study by Kaestli *et al* tested a panel of PCR assays against a variety of clinical samples from acute melioidosis patients (33). The study determined that a PCR assay targeting the type III secretory system TTS1-*orf2*, was the best target for detection of *B. pseudomallei* from clinical samples (33). The PCR test is highly specific and sensitive, although PCR requires expertise and laboratory facilities which are not always available, especially in remote endemic areas.

Lateral flow assays are simple to use and don't require specialist facilities. A lateral flow assay has been developed with an antibody specifically detecting the capsule polysaccharide of *B. pseudomallei* (34). The assay can detect capsule polysaccharide in a variety of samples, further studies are being undertaken with melioidosis patient samples and clinical trials to validate the *B. pseudomallei* capsule lateral flow assay. The assay has some sensitivity issues with blood samples, although can detect capsular polysaccharide in urine and sera samples from patients with severe sepsis (35, 36). The capsule polysaccharide has a low half-life with rapid excretion, and therefore a positive urine test is likely to mean an active infection (35).

1.1.5. Risk factors.

More than 80% of adult melioidosis cases are associated with the presence of risk factors, with type II diabetes and renal disease being the most common (29). With the incidence of type II diabetes rising in low to middle income countries, there is a double burden associated with diabetes together with melioidosis in poorer tropical areas (37). In non-diabetic patients the $CD4^+$ $CD8^+$ T-cell response, NK cell, and especially the production of interferon gamma (IFN-γ), have all been shown to be critical in the body's ability to control melioidosis (38, 39). In patients with type II

diabetes, the NK cell response is also important for survival, although there are some differences, such as an enhanced antibody and $CD4^-$ $CD8^-$ T cell response in melioidosis survivors (39). Lifestyle risk factors are an important consideration, including exposure to contaminated soils and water with open wounds, working in paddy fields, ingestion of soil contaminated foods and drinking untreated water (40, 41).

1.1.6. Distribution.

Melioidosis is thought to be present across all tropical regions of the world with confirmed endemic areas including Northern Australia, Thailand, the Indian subcontinent and parts of South America (20, 42-44). The bacterium survives in the tropical environment and is most commonly found within soils at depths from 30cm (45), the bacteria can also be found in water sources, especially those in close proximity or draining from *B. pseudomallei* contaminated soils (46).

Melioidosis is a neglected tropical disease (47, 48), and therefore is often undetected and unreported in less developed tropical regions. An example is the African continent, where awareness and the ability to diagnose melioidosis is lacking, leading to an estimated mortality as high as 50% (49-51). Therefore increased effort is required to diagnose, treat and increase awareness of this disease in many tropical regions worldwide.

In Northern Australia where melioidosis is endemic, the case fatality rate for critically ill melioidosis patients has dramatically reduced, from 30% in the late 1980's, to currently 15% with the introduction of improved antibiotic treatment regimens (52). This demonstrates what can be achieved in other endemic areas with improved awareness, diagnosis and availability of treatments.

1.1.7. Therapy.

The current treatment regimen for melioidosis consists of an acute stage treatment followed by an eradication stage. The aim of the acute stage therapy is to prevent the patient dying from the infection, whereas the aim of the eradication stage is to reduce the chance of a relapse in infection. Acute stage generally consists of a

therapy of two weeks IV ceftazidime, or meropenem if the infection is particularly severe (53, 54). The acute stage therapy is then followed by an eradication stage consisting of 6 months oral co-trimoxazole (Trimethoprim sulfamethoxazole) or co-amoxiclav (Amoxicillin clavulanic acid) (53, 54).

Finafloxacin is a novel fluoroquinolone antibiotic, which due to an increased activity at low pH, is being investigated as a therapy for melioidosis (55, 56). Finafloxacin has shown potential for improved treatment of other intracellular pathogens including *Listeria monocytogenes, Staphylococcus aureus* and *Legionella pneumophila* (55, 56).

1.1.8. Immune response to *B. pseudomallei*

The innate and adaptive immune response is essential for protecting our bodies against pathogens. The immune response is composed of various components that work together to detect, clear and provide long lasting immunity to pathogens. The leukocytes are the major cell component of the immune system and comprise of cells such as the lymphocytes and phagocytes.

The lymphocytes are an adaptive immune response, the lymphocytes can be divided into T cells and B cells. The B lymphocytes develop in the bone marrow and their main function is in the production of antibodies. Upon stimulation by specific antigens, the B cells differentiate into plasma cells, secreting antibody to target the specific pathogen. T cells are responsible for cellular responses and can regulate the immune response, there are different types of T cells such as the CD4+ T helper (TH) cells and regulatory T cells (Tregs). The TH cells can be further divided into the TH1, TH2 and TH17 cells. TH1 are involved in activation of phagocytic cells by IFN-γ, while TH2 cells are responsible for secretion of IL-4 IL-5 and IL13 triggering activation of cells such as B cells, basophils and eosinophils (57). TH17 cells secrete IL-17 ultimately resulting in neutrophil recruitment, TH17 cells also play a role in B cell activation (57). Another group of T cells, the CD8+ cytotoxic T lymphocytes (Tc) are responsible for cytotoxicity of infected cells. Tregs as their name suggests, regulate the immune response, and therefore protect against damage to the body and autoimmunity. Tregs regulate the T cell response and exert effects on other immune cells, through processes such as release of inhibitory cytokines, cytolysis,

metabolic disruption, and inhibition of dendritic cell maturation (58). Antigen presenting cells play an important role in activation of the T cell response, such as dendritic cell antigen presentation and cytokine release, following recognition of a pathogen by pattern recognition receptors (PRRs) (57).

Phagocytes are a group of cells which include the monocytes and neutrophils that engulf components, such as bacteria. Once internalised, the bacteria are destroyed, therefore removing pathogens from the tissues. Monocytes migrate to tissues via the blood and become specialised tissue resident phagocytes, which are long lived phagocytic cells, compared to the shorter-lived neutrophils.

The innate immune system is the initial response to a bacterial infection. PRRs recognise components of the bacterial surface known as pathogen associated molecular patterns (PAMPs). The toll like receptors (TLRs) are a group of intracellular and extracellular receptors able to detect PAMPs, such as TLR4, TLR5 and TLR9 that can detect bacterial lipopolysaccharide (LPS), flagella and CpG DNA respectively (59, 60). TLRs 1, 2, 4, 5 and 6 are extracellular on the plasma membrane, whereas TLRs 3, 7, 8 and 9 are intracellular endosomal TLRs (61). The majority of TLRs induce a pro-inflammatory cytokine response, via activation of the myeloid differentiation protein 88 (MyD88) dependent $NF_{\kappa}B$ pathway, TLR3 and TLR4 can signal via MyD88 independent TIR domain containing adaptor protein inducing interferon β (TRIF) pathway within the cell (61, 62). The TLRs TLR2 and TLR4 have been shown to play an important role in recognition of *B. pseudomallei*, genetic variations in TLR4 in particular have shown to vary susceptibility to melioidosis (63, 64). It is known that *B. pseudomallei* actively disrupts the TLR mediated $NF_{\kappa}B$ pathway with a virulence factor termed TssM (65), therefore reducing the pro-inflammatory cytokine response to infection.

1.1.9. Pathogenesis.

B. pseudomallei is a soil saprophyte and a facultative intracellular pathogen. The bacterium is opportunistic, with most common routes of exposure being through inhalation and skin inoculation in the environment (25). The disease has a variety of outcomes from asymptomatic infection, and disease ranging from acute to chronic. The severe disease state can lead to septic shock, together with pneumonia and

bacterial spread to distant organs (29). Localised infection results in symptoms such as abscess formation and pneumonia, although the bacterium over time can spread to distant organs such as the brain, spleen and also the blood, resulting in septicaemia (66, 67). The septicaemia infection of acute melioidosis is the most serious form of the disease, and is a potential target of the antibody-antibiotic therapy developed in this research project. An antibody-conjugate therapy delivered IV, would be present in the blood circulation to target a septicaemia infection, binding to the bacteria and increasing uptake into phagocytes. Within the phagocyte, the bacteria can be killed by antibiotic release from the conjugate, together with cell mediated killing mechanisms.

Asymptomatic infection leads to seroconversion, with studies in India showing seroconversion rates of between 27–29% in healthy individuals, reducing to 10% in individuals with diabetes (68, 69). The relationship between environmental exposure and seroconversion is not fully understood, with some studies showing farmers are more than twice as likely to be seropositive (69), whereas other studies show no difference within this population (68).

Once the bacterium has gained entry into the host, the bacterium is well equipped to evade killing by the immune system. The bacterium is known to reside within cells therefore avoiding detection by the immune system. Numerous virulence factors promote survival of *B. pseudomallei* within the intracellular environment. The bacterium has a large genome of 7.2 mb split between two chromosomes, encoding virulence factors such as CPS, LPS, adhesins, flagella, and secretory systems of which the type three and type six are required for optimum survival and virulence within cells (29, 70-73).

B. pseudomallei can infect a variety of phagocytic and non-phagocytic cells. The bacterial adhesins BoaA, and BoaB, as well as presence of the type IV pili, are important factors for adhesion to non-phagocytic cells (73). Following phagocytosis the bacteria are known to be able to escape endocytic vacuoles, and travel into the cell cytoplasm using the type three secretory system apparatus (T3SS) (74, 75). The T3SS is a syringe like mechanism, of which there are three types in *B. pseudomallei* encoded on chromosome 2 (76, 77). The T3SS-3 is the most characterised and is

essential for bacterial escape from endosome compartments, studies have shown it is required for full virulence in cell infection assays and for virulence in murine infection studies (77-79). The T3SS-3 transfers translocator and effector proteins into the cell, such as the *B.* pseudomallei BipB, BipC, BipD, BopE, BopA, BopB, BopC and CHBP (70, 74, 75, 77, 80).

BipB is a translocator protein secreted by the T3SS, *B. pseudomallei* mutants lacking *bipB* display reduced cell invasion, reduction in bacterial spread between cells and a reduction in multi-nucleated giant cell (MNGC) formation *in vitro* (77, 81). *BipB* mutants are also highly attenuated in murine models of infection (82). BipC is secreted by the T3SS and is a predicted translocator and effector protein. It has diverse effects on *B. pseudomallei* adhesion to host cells, invasion, phagosomal escape and intracellular survival, including effects on bacterial actin tail formation (80, 83, 84). BipC has been shown to bind directly to actin and can polymerise actin *in vitro*, although BipC is not able to stabilise the F-actin filaments (80). The full role of BipC on actin formation and how this effects *B. pseudomallei* pathogenesis is yet to be determined (80). BipD is a translocator protein secreted by the T3SS, and is a protein of the T3SS needle tip with a role in sensing host cell membrane contact (77, 85). *B. pseudomallei* mutants in *bipD* are significantly attenuated in murine studies (79).

BopE is a guanine nucleotide exchange factor shown to be important for invasion of HeLa cells and actin re-arrangement (86). BopA is involved in avoidance of LC3 associated phagocytosis (74), and bopB is a predicted phosphatase, with bacterial mutants displaying no negative effects on either intracellular replication or actin tail formation (70). *BopC* mutants show decreased invasion of cells, decreased phagosomal escape and intracellular survival (87, 88). CHBP causes cell cycle arrest, with CHBP mutants less able to form plaques (70, 74, 75, 77).

The LPS of *B. pseudomallei* is a weak inducer of inducible nitric oxide synthase (iNOS), and therefore reduces exposure and killing by reactive nitrogen species within host cells (71). The bacterium however does induce production of reactive oxygen species (ROS), which it can counteract with its ability to neutralise ROS using superoxide dismutase (71).

Once in the cytosol, the bacteria can move via actin based motility. This process involves host actin from the cytoskeleton, in the form of G actin, being assembled into F actin by mimicking host cell nucleation promoting factors (89-94). This is not unique to *B. pseudomallei* and *B. thailandensis*, other bacterial families including *Shigella* and *Listeria* strains also utilise actin based motility for intracellular motility (95, 96). Different mechanisms exist between bacteria for actin tail formation, and even between *Burkholderia* strains there are differences. *BimA* from *B. thailandensis* relies upon the ARP (actin related protein) 2-3 complex pathway for nucleation, whereas *B. pseudomallei* and *B. mallei BimA* utilises host actin via Ena/VASP (Vasodilator stimulated phosphoprotein) mimics (92). *BimA* is an essential virulence factor required for intracellular actin based motility, *BimA* is required for full virulence of *B. pseudomallei* in murine infection studies (97). *BimA* is located at the bacterial pole, and in association with other currently unknown proteins, polymerises actin propelling the bacterium forwards (93). Apart from the role of *BimA*, there are still some unknowns about the mechanisms behind actin tail formation in *B. pseudomallei*. Host cell factors required for actin polymerisation are being investigated, a scaffold protein ras GTPase activating like protein (IQGAP1) has been shown to play a role in the actin tail structure (98). As mentioned previously, *bipC* is able to bind actin and can polymerise actin *in vitro*, although the protein is unable to stabilise F-actin filaments (80).

It has been hypothesised that actin based motility may be involved in MNGC formation, this could be due to the force exhibited on the cell membrane promoting contact with adjacent cells (99). Cell fusion and MNGC formation is a hallmark of *B. pseudomallei* infection of cells, the formation possibly allows bacterial spread while avoiding the hostile extracellular environment (91). MNGC formation and granulomas are also seen in other similar infections, such as tuberculosis, although the MNGC formation in tuberculosis is not due to bacterial induced cell fusion (100). *B. pseudomallei* MNGC formation can be seen in both phagocytic and non-phagocytic cells, with intracellular bacterial replication eventually leading to cell damage and plaque formations (101). The exact role of MNGC formation in the body is unclear, it is likely MNGC formation is involved in granuloma formation and has a protective effect for the bacterium in the body (100). Chronic melioidosis patients can present with granuloma formation and require intensive IV antibiotic therapy, it is difficult to

distinguish granuloma formation from other diseases such as tuberculosis (102). The MNGC and granuloma formation could protect the bacteria from external therapies such as antibiotics, this could be a target for an antibody-conjugate therapy to deliver antibiotic to this difficult site of infection. The exact role and formation of granulomas in melioidosis is not understood, more research is required to fully characterise and target this site of infection. Melioidosis therapy is currently prolonged with an initial IV antibiotic therapy (ceftazidime) followed by an eradication therapy of 6 moths oral antibiotics (co-trimoxazole) (53, 54). The eradication stage aims to kill the bacteria in areas such as MNGC within the body, although the exact role of granuloma formation and bacterial survival is not known. In this research project an antibody-antibiotic conjugate therapy will be developed to improve antibiotic delivery to the intracellular environment. It is hoped that this could deliver antibiotic to sites such as the MNGC and granuloma, where the bacteria reside potentially avoiding current IV or oral antibiotics. This could shorten the overall antibiotic therapy required to clear the bacterial infection and potentially reduce relapse in infections.

It has been hypothesised that *B. pseudomallei* may exploit phagocytes such as neutrophils for survival and dissemination (103). It is well known that *B. pseudomallei* evades host killing mechanisms such as autophagy, for survival and replication within phagocytic cells (73). Krakauer's hypothesis suggests a method of *B. pseudomallei* spread between neutrophils and macrophages, by controlling apoptosis of neutrophils the bacteria could reside within neutrophils and spread to other phagocytes via efferocytosis (103). The ability of *B. pseudomallei* to survive inside phagocytes and avoid host mediated killing such as autophagy, is critical for survival and spread of the pathogen. It is therefore likely that processes such as autophagy are a good target for future host-directed therapies for melioidosis (104-106). This approach will be investigated with the use of potential autophagy inducing compounds within this PhD research project, investigating autophagy inducers as a host directed therapy for melioidosis.

1.1.10. The capsule of *B. pseudomallei*.

The 200kDa CPS of *B. pseudomallei,* [-3)-2-O-acetyl-6-deoxy-β-d-manno-heptopyranose-(1-], is a major virulence factor (70, 107). *B. pseudomallei* is known to express at least 5 different CPS antigens, with CPS I known to play a major role in virulence (70, 108-110). The *B. pseudomallei* CPS I is encoded by a 34.5 kb gene cluster (Figure 1) on chromosome 1 (111). Although there are different CPS, the majority of pathogenic *B. pseudomallei* strains are thought to express the same CPS serotype (13, 112). Antibodies specific for the CPS demonstrate a level of protection in *B. pseudomallei* challenge studies *in vivo* (113-115). Additionally, immunisation with *B. thailandensis* E555, which expresses CPS, is protective against a *B. pseudomallei* challenge *in vivo* (116). Further work is required to fully characterise the CPS antigens in *B. pseudomallei* and the impact of recognition of CPS by monoclonal antibodies. In this research project, monoclonal antibodies recognising the CPS of *B. pseudomallei* will be evaluated *in vitro* for development of an antibody based therapy. The antibody-antigen interaction for these antibodies has not been fully characterised, therefore the recognition of different CPS antigens by these antibodies is not currently known. Future work will be required to characterise the antibody and CPS interaction. It is important to determine antibody recognition between the different CPS antigens, to understand the impact on recognition of different *B. pseudomallei* strains by a potential therapeutic.

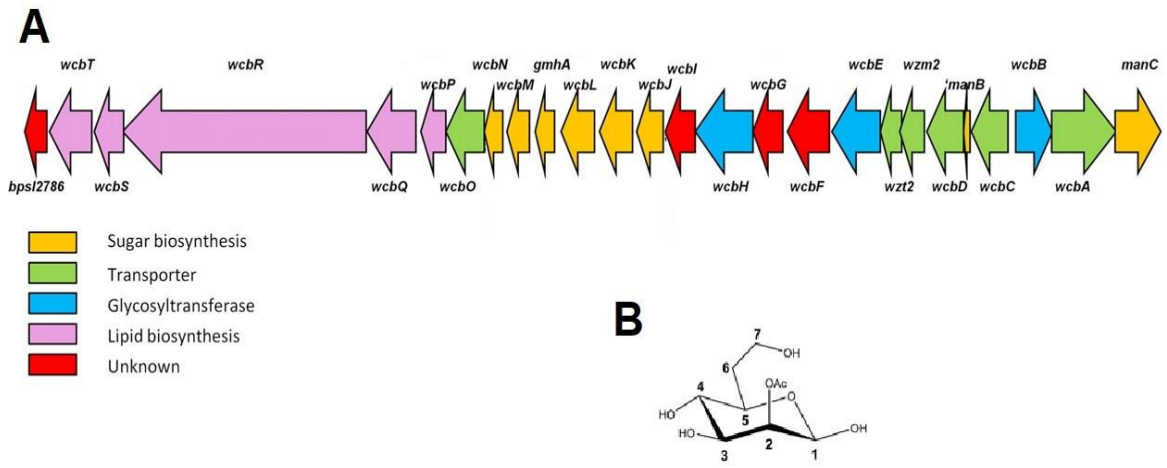

Figure 1. The capsule of *B. pseudomallei*.

The genetic organisation of the *B. pseudomallei* K96243 CPS coding region (A), image adapted from Cuccui *et al* 2012 (111). The chemical structure of the monosaccharide that makes up the *B. pseudomallei* CPS (B), image adapted from Burtnick *et al* 2012 (112).

Mutants lacking CPS are attenuated by up to 10,000 fold, as demonstrated in a hamster *in vivo* model of melioidosis (108). Importantly, *B. thailandensis* E555 expresses CPS, which has been shown to be structurally identical to that present on *B. pseudomallei* strains (19). Possessing CPS enhances intracellular survival and virulence of *B. thailandensis* E555 to a level similar to *B. pseudomallei*, with an increased survival within macrophage assays up to 9 fold compared to CPS knockout strains (13). The CPS plays a role in reducing complement deposition and opsonophagocytosis of the bacterium (108). Possessing a CPS reduces complement C3b deposition, reducing opsonisation and phagocytosis, therefore enhancing survival of the bacterium in the blood (108). It is known that *B. pseudomallei* can shed CPS, as well as LPS, during culture (117). This could be a survival mechanism, by removing or reducing the presence of surface bound anti-CPS antibodies and complement from the surface of the bacterium.

The capsule is known to be shed in the urine and blood of infected mice (118, 119), the capsular polysaccharide can be detected from patient blood and urine samples by a lateral flow assay (35, 36). This shedding has potential implications for an

antibody therapy targeting the capsular polysaccharide of *B. pseudomallei*. The shedding of CPS could have an effect on binding of therapeutic antibodies to the capsule, this is a potential limiting factor that could reduce the efficacy of anti-CPS antibody based therapies for melioidosis. The half-life of the capsule in circulation has been determined to be up to 4.4 hours (118), this could reduce the half-life of an anti-capsule antibody therapy in circulation, increasing clearance of the therapeutic along with the capsule in urine. This could result in a greater concentration of therapeutic required to target the bacterium, rather than the shed capsule in circulation.

1.1.11. Antibiotic resistance.

The increase in antibiotic resistance among microbes is a global health concern. The World Health Organisation states in a 2014 report, that bacterial resistance has reached alarming levels, it is essential that there is a focus on preserving current drugs and generation of new classes of antibacterial drugs if we are to continue curing common infections (120). The economic impacts of antimicrobial resistance as equally as great, with an estimated $21 to $34 billion dollar cost to the US health system alone per year (120). Since then, the CDC has released a 2019 report on the impact of anti-microbial resistance in the United States, it has been estimated that drug resistant bacteria and fungi are causing at least 2.8 million infections per year with 25,900 deaths per year (121). More drug resistant bacterial and fungal species have been added to the watch list, and are considered urgent threats to global health, there is a pressing need for new ways to treat drug resistant infections (121). A recent study reported that globally 1.27 million deaths in 2019 could be directly linked to bacterial drug resistance, with more than 70% of the deaths associated with resistance to fluoroquinolones and β–lactam antibiotic classes (122).

B. pseudomallei is intrinsically resistant to various classes of antibiotics, such as penicillins, aminoglycosides, cephalosporins, macrolides and polymyxins (21, 123-125). The resistance mechanisms identified in *B. pseudomallei* are all encoded in the bacterial chromosomes, including up to seven classes of β-lactamases and ten efflux systems (123). The class A β-lactamase, which is encoded by *penA* on chromosome

2, is responsible for β-lactam antibiotic resistance (124, 126). Additionally, ceftazidime resistance is associated with overproduction and mutations in *penA* (123).

Efflux is a major resistance mechanism, *B. pseudomallei* encodes at least ten different RND (resistance nodulation cell division family) efflux pumps, of which three have been characterised (124). The efflux pumps are similar between *B. pseudomallei* and *B. thailandensis* (125), making *B. thailandensis* a suitable alternative for studies at containment level II. AmrAB-OprA is responsible for intrinsic aminoglycosides and macrolides resistance, BpeAB-OprB low level resistance to tetracyclines, and BpeEF-OprC effluxes chloramphenicol, fluoroquinolones, tetracyclines and trimethoprim (124). Mutations in efflux pump regulators have been shown to alter the susceptibility of *B. pseudomallei* to a crucial front line antibiotic. An increase in meropenem resistance was observed in clinical isolates due to a mutation affecting the regulation of the *B. pseudomallei* AmrAB-OprA pump, leading to overexpression and increased meropenem resistance (127). Exclusion also plays a major role in resistance, LPS and porins both provide resistance to polymyxins by reduced drug penetration (124).

The development of resistance in *B. pseudomallei* to most front line antibiotic therapies is rare, although this does not mean it doesn't happen, instead resistance may be under reported (123). A level of resistance is seen with patients receiving trimethoprim–sulfamethoxazole during the eradication stage of therapy, with rates ranging from 2.5% in Australia to up to 16% in Thailand (123, 128-130).

B. pseudomallei is intrinsically resistant to various antibiotic classes, together with a prolonged antibiotic therapy and persistent intracellular infections, there could be more resistance seen against front line drugs in the future. This highlights a need to investigate new therapeutic options to treat melioidosis, including discovering new antibiotics, drug repurposing and using current front line antibiotics in a more effective way.

1.2. Antibody therapy.

1.2.1. Generation of monoclonal antibodies.

Hybridoma based generation of monoclonal antibodies was first discovered in the 1970s by Köhler and Milstein (131). The hybridoma fusion technique is used to generate a stable monoclonal cell line which can be cultured continuously secreting monoclonal antibody. The process first involves immunising animals, typically this will be mice, with an antigen multiple times over an immunisation schedule until hyper-immunity is reached. The spleen from the hyper-immune mouse is removed, and mashed to create a suspension of spleen cells. The spleen cells are then fused with a myeloma cell line, typically under centrifugation in the presence of polyethylene glycol. The resulting successfully fused hybridoma cells are repeatedly cultured and selected based on antibody secretion to the antigen of interest. Any non-fused cells can be removed from culture with the use of cell culture in hybridoma selective media. Techniques such as ELISA and microscopy, can be used to select hybridoma cell colonies and screen for antibody positive cell lines. The hybridoma cell lines can be kept in continuous culture, and frozen in liquid nitrogen for long term storage. Large scale continuous hybridoma culture can be achieved with the use of bioreactors, in which culture media can be continuously removed and replenished. Purification of monoclonal antibodies from the cell culture media can be performed with the use of antibody purification systems, and the use of protein G affinity columns.

1.2.2. Structure.

IgG antibodies are 150 kDa proteins, consisting of two 50 kDa heavy chains connected to two 25 kDa light chains by inter chain disulfide bonds. Each heavy (H) chain consists of one N-terminal variable domain (VH), and three constant domains (CH1-3), the light (L) chains each consist of one N-terminal variable domain (VL) and a constant domain (CL) (132-134). A hinge region connects the CH1 and CH2 domains with disulphide bonds, this hinge varies in structure between antibody isotypes (132). Two distinct light chains exist in human antibodies, an antibody can either have kappa (κ) or lambda (λ) light chains (134). The heavy chain structure determines antibody effector function, the five major heavy chain immunoglobulin

(Ig) groups are IgA (α), IgD (δ), IgE (ε), IgG (γ) and IgM (μ) (134). IgG is the most common antibody isotype present in serum, and has various subclasses in humans, IgG1, IgG2, IgG3 and IgG4. The IgG antibody will be the main focus of this research project.

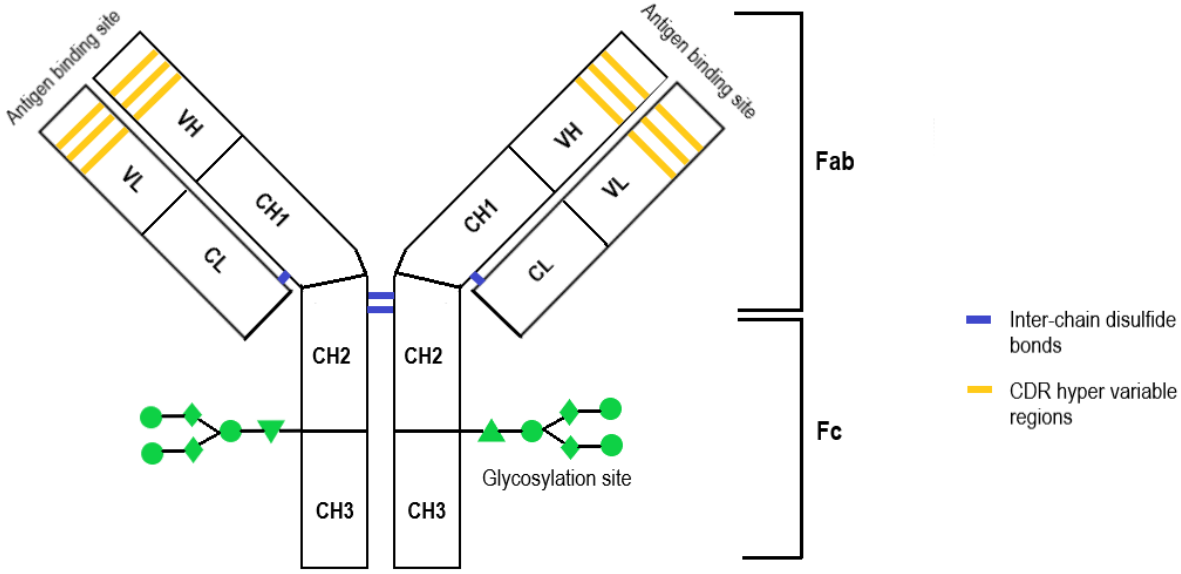

Figure 2. Structure of a typical IgG.

A representation of the structure of an IgG molecule and important features.

The Fab (fragment antigen binding) is the portion of the antibody responsible for binding to antigens. The Fab portion of the antibody contains the complementarity determining regions (CDRs), these are regions of sequence variability that form the specificity of the antigen binding site. The Fc (fragment crystallisable) is responsible for the crucial antibody effector functions, such as interaction with FcγR receptors on cells. At the interface of the CH2 and CH3 domains of the IgG Fc region is a highly conserved N- linked glycosylation site, this site has important effects on the quaternary Fc structure and interaction with receptor binding (132). The FcRn (neonatal receptor) binding site is also at the interface between the CH2 and CH3 domains, an important binding site that can determine antibody half-life and antibody transport (132).

1.2.3. Function.

Antibodies play a crucial role in the immune response to bacterial pathogens. As part of the adaptive immune response, they are generated from specific B lymphocytes to specifically target bacterial antigens. Antibodies can bind to and inactivate bacterial secreted toxins, which is a typical role for anti-bacterial antibody therapies such as the anthrax antibody therapy Raxibacumab (135).

Antibody immune complexes can activate the classical complement pathway, especially IgM, IgG1 and to a lesser extent other IgG isotypes (136). C1q interaction with antibody immune complexes activate C1r / C1s, leading to cleavage of C4 and C2, activating a complement cascade ultimately leading to the formation of a membrane attack complex and cell lysis (136). The classical complement activation pathway can also lead to opsonisation of the bacteria and activation of inflammation pathways (136).

Antibodies can opsonise bacteria directly and increase uptake into phagocytic cells via interaction between the Fc portion of the antibody and Fc receptors (FcR's) on the surface of phagocytic cells, leading to pathogen degradation via the phagolysosome. Interaction of the antibody immune complex with FcR's has diverse effects on a variety of cells. Interaction can activate phagocytosis and pro-inflammatory compound release by macrophages, phagocytosis and release of cytotoxic substances by neutrophils, release of chemoattractant and vasoactive compounds by mast cells and basophils (137). On the other hand, interaction of antibody complexes with the inhibitory FcR present on cells, modulates cell activation (137).

There are various FcγR's present on phagocytic cells, which vary depending on the cell type. Each receptor has differing activation or inhibitory functions, by possessing either ITAM (immunoreceptor tyrosine-based activation motif) or ITIM (immunoreceptor tyrosine-based inhibitory motif) in their intracytoplasmic domain (138). Murine FcγR's consist of FcγRI (activating), FcγRIIB (Inhibitory), FcγRIII (activating) and FcγRIV (activating) present to differing extents on each class of phagocytic cell (138-140). Human FcγR's consist of receptors with various allelic variants, the main groups being FcγRI (activating), FcγRIIA (activating), FcγRIIB (Inhibitory), FcγRIIC (activating), FcγRIIIA (activating) and FcγRIIIB (activating)

(140). The majority of the murine innate immune system expresses both activating and inhibitory FcγR's. Some cells only express one type, such as natural killer (NK) cells expressing activating receptors, and B cells expressing inhibitory receptors in mice (140).

In addition to binding surface receptors, antibodies can stimulate anti-microbial effects by binding to intracellular receptors. Intracellular antibody can bind to an intracellular receptor called the interferon inducible cytosolic Fc receptor tripartite motif containing-21 (TRIM21) (141). TRIM21 has the unique ability as a receptor to have a broad specificity to antibody isotypes (141, 142). In theory any therapeutic antibody can bind TRIM21, although this relies upon the antibody being able to penetrate cells in the first place (141). The binding of antibody to TRIM21 results in activation of anti-microbial processes such as antibody-dependent cellular neutralisation (ADIN), inflammation and activation of autophagy (143). An interesting question, proposed by Rhodes and Isenberg 2017, is if the intracellular delivery of antibodies can be optimised to increase antibody medicated killing via TRIM21 interaction (141). For example, if the antibody from an antibody based therapy can be engineered to have enhanced interaction with TRIM21. This could be particularly useful for an antibody-drug therapy for melioidosis, where the drug and antibody can each exert intracellular killing of the bacterium.

The Fc region of an antibody is also important for interaction with the neonatal Fc receptor (FcRn). Although there is some debate over FcRn expression in some cells, FcRn is present in various cell types including tissue specific epithelial, endothelial, monocytes and macrophage cells (144). The FcRn binds IgG in a pH dependent manner with majority of binding occurring at pH <6.5 (145). The binding of IgG to FcRn is through the Fc region histidine residues of the antibody, which due to the homodimer structure of the Fc region, allows each IgG to bind two FcRn (146). The binding of IgG to FcRn recycles IgG away from lysosomal degradation, transporting the IgG FcRn complex to a higher pH extracellular environment in which the IgG disassociates from the FcRn (144). This recycling is responsible for the long half-life of circulating IgG and is an important consideration for therapeutic antibodies. It is

possible, through antibody engineering, to improve FcRn interaction at different pH and further increase therapeutic antibody half- life (144, 145). Efforts to improve drug delivery could focus on interaction with FcRn to increase delivery across epithelial barriers, for example drug loaded nanoparticles displaying Fc (144).

Interaction with the FcRn will be crucial for any therapeutic antibody, to provide a long serum half-life typical of an IgG. Engineering to improve circulating half-life could offer huge benefits such as reducing the number of doses required for protection against a pathogen. Improving transport across epithelial barriers by engineering enhanced FcRn interactions, could increase the options for therapeutic delivery, such as inhalational or oral delivery systems involving transport across lung and intestine respectively.

Modifying glycosylation status of the antibody Fc is another important consideration. Glycosylation effects the binding of an antibody to particular FcR's. Fc glycobiology is not fully understood, the glycoengineering of a therapeutic antibody has the potential to increase antibody binding to receptors, therefore increasing desirable functions such as phagocytosis and cell activation (137). It is important to consider glycoengineering a therapeutic mAb to have a high affinity for FcR's, as the background sera IgG of approximately 15mg mL^{-1} will be competing with these FcγR's (137).

1.2.4. Therapeutic antibodies.

Blood derived polyclonal antibody therapies are approved for use as therapies for infectious diseases including anthrax, botulism, diphtheria, hepatitis, measles, rabies and staph infections (147). Monoclonal antibody based therapies (mAb) exist for a variety of diseases, mostly directed towards non-infectious diseases such as cancers. Obiltoxaximab is a chimeric IgG1 mAb FDA approved in 2016, and Raxibacumab is a human IgG1 mAb FDA approved in 2012, both are directed against protective antigen of anthrax toxin as therapies and prophylaxis for inhalational *Bacillus anthracis* infection (148-150). Palivizumab and bezlotoxumab are therapeutic monoclonal antibodies, for the treatment of respiratory syncytial virus and *Clostridium difficile* toxin B respectively (151, 152). The use of an experimental cocktail of three chimeric mAbs (ZMapp®) was approved for therapeutic use by the

world health organisation during the Ebola outbreak in Western Africa in 2014 (153-156).

Monoclonal antibodies have advantages for use as therapeutics owing to their high specificity and low toxicity. Although this is not without difficulties, such as the need of a rapid diagnosis and difficulties estimating the antibody dose required for an effective therapy (157). Antibodies have the ability to combat infectious diseases by opsonisation, complement activation, neutralisation and direct anti-microbial abilities (157). Various antibody formats exist that could be used for anti-bacterial therapies. These include humanised full IgG monoclonal antibodies, antibody fragments, bispecific, nanobodies and antibody conjugates (158). Each is not without disadvantages, but each format offers benefits depending upon target and the intended therapeutic use. Full IgG are the traditional choice for an antibody therapy, IgG is favourable over other antibody isotypes, such as IgM, due to benefits such as stability and long half-life in circulation (158). Importantly for a therapeutic, full IgG antibodies offer strong effector functions from the Fc region, such as complement activation and opsonisation, leading to uptake via FcγR into phagocytic cells.

There have been high profile failures in antibody therapy for infectious diseases such as mAbs for *Staphylococcus aureus* cytotoxin therapies (159, 160). Nagy *et al* suggests that lessons from past failures can be learnt, and when used under the right conditions, antibodies can be a successful therapy for infectious diseases (158). Antibody affinity, isotype, visibility of the target antigen and having realistic clinical aims are all important considerations for a therapeutic mAb (158).

Antibodies are not always to be considered as an alternative to antibiotic therapy, studies have shown a synergistic effect when used in combination (158). This could be beneficial for melioidosis, to enhance the effect of current antibiotics in severe cases of disease. Additionally, antibodies could be used as an initial therapy to control infection, while a full diagnosis is made and front line antibiotics administered. Alternatively, antibodies could be used as a prophylaxis for bacterial infections in specific situations and groups of people (158). This would give a similar effect to vaccination but with a shorter more immediate effect. This is a potential strategy that could work for protection from melioidosis in highly susceptible individuals, or to

protect a group of people visiting a known melioidosis endemic area for short periods of time.

Antibody drug conjugates (ADCs) are a newer approach for mAb therapies. There are over forty ADCs in development, with a focus on targeting cancers (161). Examples of licenced ADCs include Gemtuzumab ozogamicin, a humanized IgG4 ADC against CD33 for therapy of acute myeloid leukaemia (162). Brentuximab vedotin is a chimeric IgG1 ADC against CD30 for lymphomas (163). Trastuzumab emtansine (T-DM1) is a Humanized IgG1 as therapy for breast cancer (163, 164) and Inotuzumab ozogamicin is a Humanized IgG4 anti CD22 ADC (163).

Antibody-antibiotic conjugates (AAC) for bacterial infections have been developed since 2015 by Genentech inc, consisting of antibodies targeting *Staphylococcus aureus* and *Pseudomonas aeruginosa* (165-167). The AAC consists of an antibody linked to antibiotic molecules via a cathepsin cleavable linker. The AAC coats the bacterial target and delivers the antibiotic to the intracellular environment, intracellular cathepsin then cleaves the linker, releasing active antibiotic to kill the intracellular bacterial infection.

The current antibiotic therapy regimen for melioidosis is prolonged, with 2 weeks of initial IV ceftazidime antibiotic therapy followed by 6 months oral co-trimoxazole antibiotics (53). *B. pseudomallei* can potentially avoid antibiotic therapy by forming an intracellular niche, which could lead to relapse in infection post-therapy. An AAC has the potential to clear intracellular bacteria by specifically delivering antibiotic to the intracellular site of infection. The delivery of antibiotic and killing of intracellular bacteria by an AAC was demonstrated by the *S. aureus* AAC developed by Genentech Inc (165). A 20 year study of melioidosis in Australia showed that infection relapse rates were approximately 5% in treated patients, with an average onset of 8 months post-antibiotic therapy (24). An AAC for melioidosis has the potential to reduce or prevent infection relapse, by targeting the *B. pseudomallei* avoiding current antibiotic therapies residing within intracellular environments. Not only could an AAC reduce relapse of infection, the current antibiotic regimen duration could potentially also be reduced if the AAC is able to clear intracellular bacteria. The AAC for melioidosis could be used in combination with current IV and oral antibiotics to

improve efficacy of antibiotic therapy, and reduce the overall duration of therapy for patients. The disadvantage of introducing an AAC therapy is that the AAC is likely to require IV delivery, this requires medical facilities that are not always readily available in rural and developing areas of the world. Requiring IV delivery also limits the use of the AAC as a prophylactic therapy for travellers to known endemic regions. Future research for drug delivery could overcome the requirement for IV delivery of an AAC, such as development of inhalational AAC preparations or encapsulation for oral delivery. An additional consideration for an AAC therapy is ensuring delivery of a sufficient quantity of antibiotic to the intracellular environment, otherwise the AAC may aid in the intracellular uptake of *B. pseudomallei* without effective bacterial killing. Creating an AAC with a high drug-antibody ratio should help ensure that delivery of antibiotic is maximised to the intracellular infection.

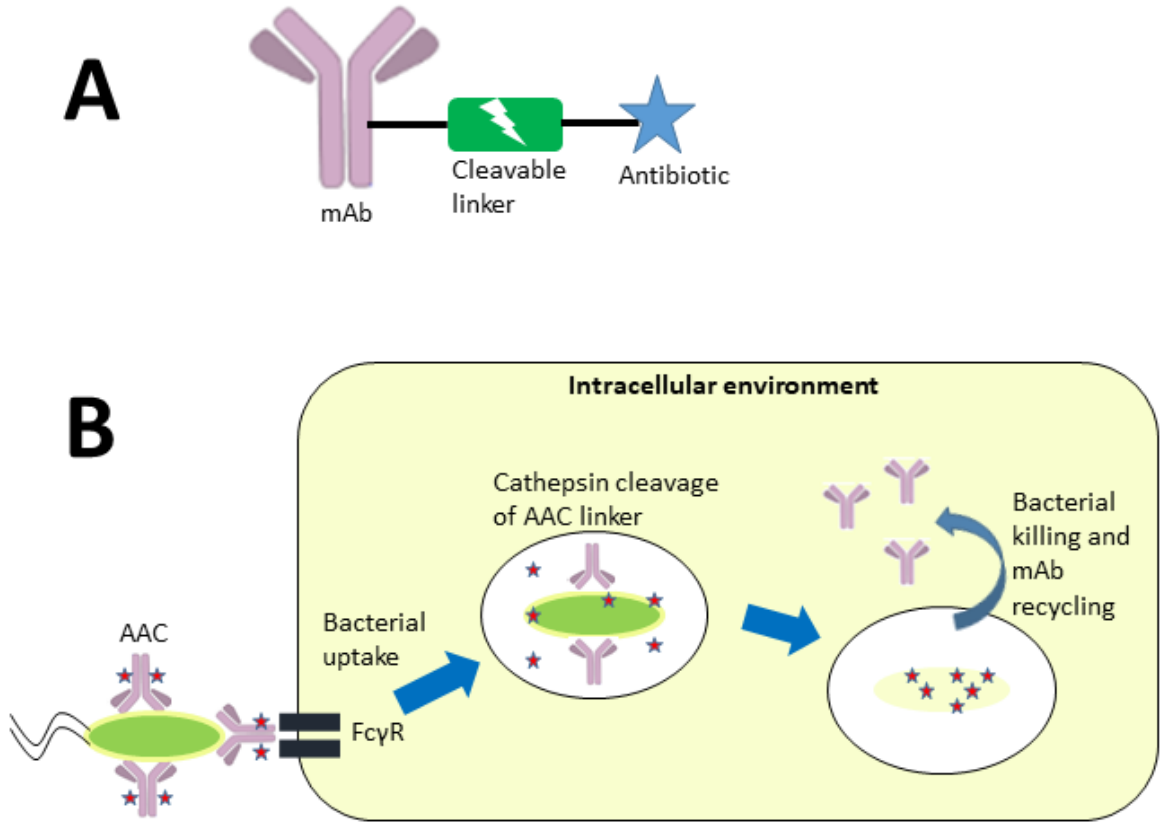

Figure 3. Antibody-antibiotic conjugate.

An AAC consists of a monoclonal antibody linked to an antibiotic via a cleavable linker (A). The AAC opsonises the bacteria and is internalised into the cell via FcγR mediated uptake (B). Intracellular cathepsin enzymes cleave the AAC linker, releasing antibiotic in an active form to kill the intracellular bacteria. The mAb can be recycled intracellularly by interaction with the neonatal receptor.

The pharmacokinetic (PK) properties are essential when designing a therapeutic mAb. The classic PK properties of an IgG mAb following administration include an initial rapid distribution phase, followed by long slow elimination phase over weeks (168). Binding of mAb to the neonatal receptor (FcRn) is beneficial in terms of mAb recycling, resulting in the characteristic long half-life of mAbs in PK studies. The FcRn can protect two thirds of the mAb taken up into acidic endosomes in the cell by binding mAb at low pH and releasing mAb extracellularly when the pH raises back to physiological levels, any mAb unbound to FcRn will be subjected to degradation by lysosomal proteases (169, 170). The distribution of mAbs is generally restricted to

the blood, with a typical 5-15% distribution to tissues (168). Clearance of mAb from the blood is generally by cell uptake and proteolytic degradation, although in some cases anti-therapeutic antibodies can target the mAb depending upon the mAb species (168). The initial PK experiments for a melioidosis mAb based therapeutic will determine how the antibody behaves in a murine body. This data would then inform future studies such as *in vivo* murine mAb *B. pseudomallei* infection studies, and PK studies involving antibody conjugates.

1.2.5. Antibody therapy for melioidosis.

Studies have shown that passive immunisation with monoclonal antibodies can protect against a lethal challenge of *B. pseudomallei*. A study carried out at the Defence Science Technology Laboratory (Dstl), demonstrated that monoclonal antibodies provide a level of protection against a lethal challenge of *B. pseudomallei* (4845) in mice (113). A delay to death was most prevalent in mice immunised with anti-CPS monoclonal antibodies and anti-LPS monoclonal antibodies. Monoclonal antibodies from this Jones *et al* study (113) will be available for use in this PhD project for further analysis as a potential therapy for melioidosis.

Antibody target is important when determining protection against a challenge of *B. pseudomallei*, often anti-CPS mAbs outperform other mAbs such as those specific to LPS or protein targets. It is logical that mAbs binding to easily accessible extracellular targets on the *B. pseudomallei* bacteria will demonstrate increased opsonisation ability *in vitro,* and therefore are more likely to be protective *in vivo* when compared to protein targets. This was the case for the Jones *et al* (113) study at Dstl, an antibody protection study by AuCoin *et al* (115) and a study by Zhang *et al* (114).

In a study by AuCoin *et al*, two mAbs directed against the LPS and CPS of *B. pseudomallei* were evaluated *in vivo* for protection against a *B. pseudomallei* intra nasal challenge. This study found that an anti-CPS and anti-LPS mAb protect 86% and 50% of mice respectively for 21 days (115). Additionally, the combination of mAbs together could offer synergistic effects and protect 88% of the mice (115), similar to observations by the Jones *et al* study in which cocktails of mAbs were protective (113).

A study by Zhang *et al* in which over a hundred mAbs were tested confirms previous statements. Zhang *et al* showed that anti-CPS outperform anti-LPS mAbs within *in vitro* opsonisation studies, and *in vivo* murine protection studies. Additionally, anti-protein target mAbs were shown to be unsuitable for opsonisation and protection from *B. pseudomallei* (114).

MAb binding to the CPS has been characterised by Marchetti *et al* (171), in this study the interaction of mAb 4C4 with the CPS antigen was assessed by techniques such as nuclear magnetic resonance (NMR) and surface plasmon resonance (SPR). The study found that an acetyl group of the CPS was essential for mAb 4C4 binding, removal of this acetyl group at position 2 of the CPS prevented mAb interaction (171). Characterising this CPS and mAb interaction will help inform future studies developing anti-CPS mAb based therapies, vaccine antigens and detection assays for melioidosis.

Antibody therapy is not just restricted to antibodies that have a target antigen on the pathogen of interest. Other targets may be the host immune response, for example the cytokine IL-1β. This cytokine has been shown to lead to a negative outcome in melioidosis, this is because of excessive neutrophil recruitment, which due to inability to undergo pyroptosis, potentially supports intracellular bacterial replication (172, 173). A commercially available anti-IL-1β monoclonal antibody was assessed by *in vivo* murine protection studies to observe the effect on disease progression and outcome (172). The IL-1β mAb in this study showed a protective effect *in vivo* from a *B. pseudomallei* challenge, the effect on bacterial counts in the study was similar to that seen with ceftazidime treatment. Mice treated with the anti-IL-1β mAb showed reduced neutrophil influx, reduced tissue damage, reduced bacterial loads in the lungs and reduced dissemination from the lungs (172).

1.3. Alternatives to an antibody therapy for melioidosis.

1.3.1 Vaccines.

There is currently no vaccine available for melioidosis, the focus has mainly been on antibiotic medical countermeasures against the disease. Despite the lack of an

approved vaccine for melioidosis, there has been significant progress in pre-clinical evaluation of vaccine candidates. Examples of potential vaccine candidates for melioidosis include live attenuated (79, 174-179), inactivated (180-182), sub unit (183-186) and glycoconjugate vaccines (187-192).

Live attenuated vaccine candidates have been investigated in murine protection studies. One such example is a study by Khakhum *et al* 2019, a *B. pseudomallei* ΔtonB Δhcp1 double mutant was investigated as an attenuated vaccine candidate (PBK001) against *B. pseudomallei* K96243 aerosol challenge in C57BL/6 mice (179). At 27 days post infection, vaccinated mice showed bacterial clearance in the lung, liver and spleen with near sterile immunity. A strong protective antibody response was seen in PBK001 vaccinated mice, which is essential for protection against the *B. pseudomallei* challenge. Vaccinated mice also showed an increased cellular response, with increased IFN-γ and IL-17 cytokine production (179). Additional live attenuated vaccine candidates include *B. pseudomallei* Δ*purN* (174), Δ*purM* (174), Δ*hisF* (176), Δ*bipD* (79), Δ*tonB* and Δ*hcp1* (179). Each with varying levels of protection in *B. pseudomallei* murine models of infection. Protection ranged from 37% protection at day 65 for Δ*purN* (174), 60% at day 75 for Δ*bipD* (79), to 100% protection for Δ*purM* (174) at day 17, Δ*hisF* at day 21 (176), Δ*tonB* and Δ*hcp1* at day 27 (179). This data highlights the potential of attenuated vaccine candidates for protection from *B. pseudomallei* infection.

B. thailandensis E555 has demonstrated potential as a live vaccine, as seen in murine protection studies at Dstl. A study by Scott *et al* (116), investigated immunising mice with *B. thailandensis* E555 and comparing survival post-challenge to mice immunised with non-capsulated *B. thailandensis* CDC2721121. Mice immunised with *B. thailandensis* E555 survived a lethal IP challenge of *B. pseudomallei* K96243, additionally these mice had an IgG response against CPS, mice immunised with non-capsulated *B. thailandensis* CDC2721121 had significantly less survival against the challenge (116). Heat inactivated *B. thailandensis* and *B. pseudomallei* have also been investigated as potential vaccine candidates, although *B. pseudomallei* offered the best level of protection (80-100% at day 21)in this murine study (182). A study by Puangpetch *et al* demonstrated that mice immunised

intramuscularly with paraformaldehyde inactivated *B. pseudomallei* displayed a level of protection *in vivo*, with a 50-60% survival at day 30 (180). An additional inactivated study immunised mice with heat killed *B. pseudomallei* and a liposome-nucleic acid adjuvant preparation, 100% survival from a *B. pseudomallei* pulmonary challenge was observed at day 40 (181).

Glycoconjugate vaccine candidates have also been researched as potential vaccine candidates for melioidosis. A synthetic hexasaccharide – TetHc (tetanus toxin Hc carrier) conjugate was used to immune mice, the result was an antibody response to CPS and protection against a *B. pseudomallei* K96243 challenge (190). Purified CPS based glycoconjugates have also been shown to offer protection in murine studies at Dstl (193). A LPS - TetHC based glycoconjugate has also shown promise as a vaccine candidate, demonstrating an antibody and protective effect from *B. pseudomallei* challenge (191). Additional glycoconjugate vaccine studies include the use of capsular polysaccharide conjugates, CPS-LolC (188), CPS-CRM_{197}-Hcp1 and CPS-CRM_{197}-TssM (189). Protection against a challenge ranged from 70% for CPS-LolC (188), to 80-100% with CPS-CRM_{197}-Hcp1 and CPS-CRM_{197}-TssM (189).

Subunit *B. pseudomallei* candidates have been investigated as vaccines for melioidosis. *B. pseudomallei* subunit studies include LolC (183), PotF (183), Omp (Omp3, Omp7, Omp85 and OmpW) (184, 194, 195) and Hcp sub unit vaccines (185). Additionally, *Burkholderia mallei* BimA and BopA have been investigated as subunit vaccine candidates (186). In murine studies LolC and PotF gave a protection level of 83% and 50% respectively at day 42 (183). Omp3 and Omp7 both provided a protection level of 50% at day 21 in murine studies (184). In comparison Omp85 and OmpW provided protection of 70% at day 15 for Omp85 (194), and 75% at day 21 for OmpW (195). Protection offered from Hcp varied, with a protection level in mice of between 33% and 80% at day 42 (185). BimA provided protection in murine studies of 100% at day 21 and 20% at day 50, in comparison BopA provided protection of 60% at day 50 (186).

A key feature between these studies is that a strong antibody response against surface targets, such as the CPS and LPS of *B. pseudomallei*, is important for protection. It is unclear exactly how important antibody response is in protection

against the intracellular infection, although survivors of melioidosis have significantly higher levels of antibody, especially to the LPS, than those patients that do not survive the infection (196, 197). Inducing an antibody response by vaccination is beneficial for targeting extracellular bacteria, conjugate vaccines have the added benefit by the synergistic effect of stimulating both humoral and cellular immunity against intracellular pathogens (198). Antibodies can have diverse anti-bacterial functions both directly, such as interfering with bacterial replication, and non-directly such as opsonisation and increased uptake into phagocytic cells by FcγR (198).

Great progress has been made identifying vaccine candidates for protection from melioidosis. It now requires potential vaccine candidates to be taken forward and developed into a melioidosis vaccine. It has been suggested that a vaccine is a cost effective measure for immunisation of high risk individuals in endemic areas (199).

1.3.2. Autophagy as a host directed therapy for melioidosis.

The Nobel Prize winner Christian de Duve first published the concept of lysosomes in 1955 whilst researching hydrolytic enzymes (200) and in 1963 during a lysosome symposium coined the term autophagy (201). The Japanese scientist and Nobel Prize winner Yoshinori Ohsumi first discovered autophagic bodies in 1992 and since then we now know that autophagy plays a role in human disease including cancers and infectious diseases (106, 202-204). Autophagy is a potential target for treatment of diseases as a host directed therapy.

There are various forms of autophagy such as macroautophagy, microautophagy, and chaperone mediated autophagy. Microautophagy consists of the direct sequestration of components into the lysosome; whereas chaperone mediated autophagy involves the translocation into the lysosome via the oligomerisation of a lysosomal membrane protein LAMP-2A (205). Macroautophagy is a cellular process in which cytoplasmic components are degraded, through a process involving the formation of an autophagosome encompassing the component to be degraded. Lysosomes containing acid hydrolases fuse with the autophagosome creating what is known as an autolysosome, in which the cargo is degraded and components

recycled (204, 205). Autophagy can be promoted by stresses such as nutrient starvation, and by a variety of chemical compounds (104, 206-209). One such compound rapamycin, which as the name suggests, targets the TOR (target of rapamycin) complex and by doing so strongly promotes autophagy of *Burkholderia* (104, 210, 211).

Host directed therapies aim to promote the host immune response to infection by a variety of mechanisms, including compounds that promote cell mediated killing such as autophagy, cytokine based therapies, mAb therapy and cell based therapies such as mesenchymal stromal cells (212).

B. pseudomallei bacteria are able to escape phagosomes via the type III secretory system and spread intracellularly, avoiding cell mediated killing processes that require compartmentalisation of the bacteria. Autophagy is a collective term for the targeted degradation and recycling of cellular components. Autophagy inducing compounds offer an alternative approach as a host directed therapy to promote killing of intracellular bacteria (xenophagy) by targeting the host autophagic pathway. Examples of autophagy promoting drugs being investigated as host directed therapies include vitamin D (213), metformin (214-217), statins (218), verapamil (207, 219-225), carbamazepine (226, 227) and valproic acid (226, 227).

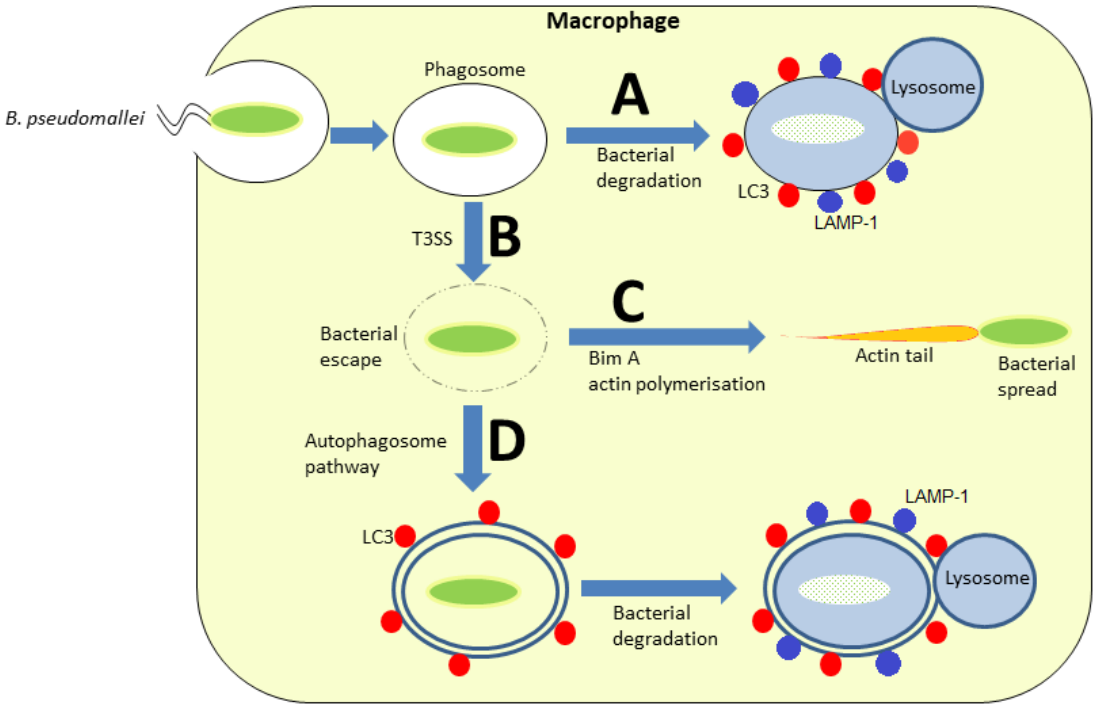

Figure 4. *B. pseudomallei* and the autophagosome pathway.

Intracellular *B. pseudomallei* can be degraded by phagosome maturation with the lysosome (pathway A), via LC3 associated phagocytosis (LAP) or without LC3 association. *B. pseudomallei* can escape from phagosomes (pathway B) using the T3SS and move intracellularly via actin tail formation (pathway C). Escaped bacteria can be targeted by auto-phagosomes (pathway D), stimulating this pathway has therapeutic potential to target intracellular bacteria.

Autophagy targets intracellular pathogens for destruction via the lysosome, although *Burkholderia* has the ability to avoid such killing by autophagy (Figure 4). The T3SS is essential for bacterial escape from autophagy (71, 74, 77). A T3SS protein bopA is known to be involved in ability of *Burkholderia* to evade autophagy (104), another T3SS protein *BimA* required for actin based motility is known to be important for avoidance of autophagy (228). The majority of *Burkholderia* bacteria will escape phagosomes into the cell cytosol, and via actin based motility move and spread between adjacent cells (73). The minority of *B. pseudomallei* that do not escape the initial phagosome are targeted by LC3 associated phagocytosis (LAP), or

phagosome maturation can occur without LC3 association, leading to fusion with the lysosome and bacterial degradation (73, 74). Autophagy promoting compounds have a potential as a host-directed therapy for melioidosis. If therapeutic compounds can be used to promote *B. pseudomallei* compartmentalisation by auto-phagosomes, then this could increase bacterial killing and prevent bacterial spread to neighbouring cells.

1.3.3. Adjuncts to antibiotics.

Adjunct therapies have potential to improve the antibiotic treatment of melioidosis by improving the efficacy of current front line antibiotics, or potentially even increasing the available antibiotics by improving drugs that were previously regarded as unsuitable therapies. One such example of a potential adjunct therapy is the drug verapamil.

Aside to being a potential autophagy inducing drug, verapamil is a potent blocker of T-type calcium channels (229). Verapamil can inhibit the action of ATP dependent multidrug pumps and other multiple drug resistance pumps, this inhibitory effect has been observed particularly in mycobacterial efflux pump studies (230). Verapamil as an adjunct with anti-tuberculosis drugs has shown promise in various *M. tuberculosis* studies (219, 224, 225, 231). Verapamil offers potential as an adjunct with antibiotics for a melioidosis therapy. Efflux pumps are crucial for anti-microbial resistance, allowing the bacterium to efflux anti-microbial compounds such as antibiotics out of the cell. Known efflux pump families in bacteria include the small multidrug resistance (SMR), major facilitator superfamily (MFS), multi-drug and toxic compound extrusion (MATE), ATP binding cassette (ABC), resistance nodulation division (RND) and proteobacterial antimicrobial compound efflux (PACE) (232-234). Efflux is a major contributor to the intrinsic antibiotic resistance of *B. pseudomallei,* and therefore blocking efflux with verapamil may increase antibiotic therapy options and increase the efficacy of antibiotics.

Antibodies in combination with anti-microbial drugs offer potential as an adjunct therapy. In a study by Olivares *et al,* polyclonal antibody from human blood donors

was assessed as a potential adjunct therapy with conventional anti-tuberculosis drugs in a murine model of lung *M. tuberculosis* infection (235). Antibody alone (2mg/g given intraperitoneal) and anti-tuberculosis drugs, reduced murine lung bacterial load *in vivo*. However, more significant was the combination of antibody and anti-tuberculosis drugs that reduced lung bacterial burden to a greater extent, and additionally reduced lung tissue damage (235). This study highlights the potential beneficial adjunct effects of combining antibody therapy and anti-bacterial drugs such as front line antibiotics. It was shown that the antibody alone had no intrinsic anti-bacterial effect, and the *in vivo* effects are likely to be due to antibody opsonisation of the bacteria and subsequent FcγR activation of phagocytic cells immune response, reducing bacterial loads (235).

1.3.4. Antibiotic delivery.

There are various alternatives to an AAC therapy for delivering an antibiotic to combat infection. These can include antibiotic conjugation or antibiotic encapsulation methods for an enhanced delivery of antibiotic.

A conjugate approach published by Su *et al*, consists of ciprofloxacin conjugated, via a cathepsin cleavable linker, to mannose and is termed a drugamer (236). This drugamer showed enhanced uptake of ciprofloxacin in lung macrophages, enhanced pharmacokinetic properties and when used in an inhalational *in vivo Francisella tularensis* infection murine model, it achieved 100% survival compared to zero survival with ciprofloxacin alone (236). This drugamer approach does not target and increase uptake of the pathogen specifically unlike with the AAC, although the mannose of the drugamer binding to the mannose receptor on the macrophage surface should increase uptake into the cell. This binding to the mannose receptor will also have the benefit of activating the macrophage and release of pro-inflammatory cytokines. Once intracellular, the cathepsin cleavable linker of the drugamer is cleaved releasing the antibiotic to kill intracellular bacteria, the same process as in the AAC approach. The drugamer approach by Su *et al* could be used as an alternative intracellular antibiotic delivery system for *B. pseudomallei* infection, although the benefit of antibody opsonisation by an AAC could prove a greater

advantage for additionally clearing extracellular bacteria and specifically targeting the delivery of antibiotic.

A polymer-drug conjugate (PDC) consisting of a biodegradable Hex-Cys-DET polymer conjugated to an antibiotic, has been developed as a concept for pH dependent antibiotic release (237). The polymer offers synergistic effects in combination with the antibiotic, the polymer interferes with the bacterial membrane creating pores, increasing antibiotic uptake and reducing efflux (237). This streptomycin PDC approach showed increased efficacy in cell and murine bacterial infection studies involving *S. aureus*, *P. aeruginosa* and *E. coli* (237). A ciprofloxacin-lectin inhibitor conjugate has been proposed as a targeted antibiotic delivery mechanism to *Pseudomonas aeruginosa* within biofilms (238). This approach specifically targets ciprofloxacin delivery to lectin receptors within biofilms, therefore accumulating antibiotic to this normally protected environment for bacteria.

An alternative delivery system for antibiotics is encapsulation of the drug. Encapsulation of antibiotic within nanoparticles is an approach that has been investigated as a therapy for melioidosis. One example is bilosome encapsulation of antibiotics as an oral drug delivery mechanism. Stable encapsulation of levofloxacin and doxycycline into bilosomes was achieved by Dstl and the University of Strathclyde (239). The antibiotic encapsulated bilosomes showed efficacy in a murine model of melioidosis, the study showed that bilosome therapy increased survival and reduced weight loss side effects when compared to the non-encapsulated antibiotic control groups (239).

An additional encapsulation approach is the use of polymersome delivery of antibiotics. In a collaborative project between Dstl and University of Southampton, antibiotic loaded polymersomes were investigated in macrophage-like cell infection assays to deliver antibiotic to intracellular *B. thailandensis*. Doxycycline and rifampicin were successfully encapsulated within polymersomes and assessed in *B. thailandensis* macrophage-like cell infection assays as a proof of principle antibiotic delivery therapy (240). Imaging flow cytometry and CFU (colony forming unit) analysis showed that polymersomes accumulate within the cells, co-localise with *B. thailandensis* and have the ability to kill intracellular bacteria (240). Further

investigations are needed such as accurate quantification of encapsulated antibiotic, defining the release and quantifying the antibiotic released within cells. In addition, further research is needed to encapsulate other antibiotics, particularly front line melioidosis therapies.

In a study by Xie *et al* (241), a bacterial 'ghost' is loaded with ciprofloxacin to deliver the antibiotic to intracellular environments such as a macrophage. This is an encapsulation method that could also be investigated for melioidosis. The bacterial 'ghost' displaying extracellular bacterial features, such as flagella and LPS, may increase uptake of the bacterial 'ghost' compared to other antibiotic encapsulation methods.

An improvement upon the nanoparticle based delivery of antibiotics could be to use antibodies to specifically target bacteria. Antibody coated nanoparticles could be an option for melioidosis, this could target delivery of antibiotic loaded nanoparticles to bacteria (242). Similar to an AAC, the antibody could opsonise the bacteria, increasing uptake of nanoparticles into the intracellular environment. This could be achieved with or without a cleavable linker between the antibody and nanoparticle. The potential benefits over an AAC is that the nanoparticle approach is potentially a simpler production method, may be easier to scale up production, and ability to switch antibiotic encapsulation without formulating new conjugation chemistry. Although, it is not known if the antibody and macrophage Fc receptor interaction would function with antibody coated nanoparticles.

1.4. Research project aims.

The current antibiotic therapy regimen for melioidosis is prolonged and can result in relapse of infection. The aim of this thesis is to investigate an alternative therapeutic option for targeting intracellular *B. pseudomallei*, which may provide an alternative and improved therapeutic option for melioidosis. The project will focus on antibody based therapy and provide proof of concept *in vitro* data for an antibody and antibiotic combination therapy. Additionally, this research project will explore drugs that are alternatives or adjuncts to antibiotics, especially drugs stimulating host intracellular killing mechanisms such as autophagy.

The aims of this research project can be summarised as the following.

- A panel of Dstl owned monoclonal antibodies (mAbs) will be selected based on previous *in vivo* data showing a level of protection from a *B. pseudomallei* challenge. The mAbs will be investigated in an *in vitro* cell infection assay, from this a single mAb will be selected for incorporation into an antibody-antibiotic conjugate.

- Potential autophagy inducing compounds will be assessed *in vitro*, as an alternative to a mAb and antibiotic based therapy. These compounds will be selected based on literature suggesting *in vitro* anti-bacterial effects.

- A decision point will be made as to develop an AAC or further investigate an autophagy inducing compound therapy. The selected therapy will be further investigated in cell infection models, and an initial pharmacokinetic study in mice will be completed. This will provide evidence for a proof of principle therapy for melioidosis.

2. Materials and Methods.

Experimental procedures were performed within ACDP containment level II and III laboratories at Dstl Porton Down, unless otherwise stated.

Generation of antibody-antibiotic conjugations were performed by Global Access Diagnostics Ltd (previously trading as Mologic), Bedford Technology Park, Thurleigh, Bedfordshire, MK44 2YA. United Kingdom.

All experimental data analysis was performed using GraphPad® prism software unless otherwise stated. GraphPad® prism version 8 for Windows, La Jolla California USA, www.graphpad.com).

2.1. Cell culture.

2.1.1 RAW 264.7 cell culture.

RAW 264.7 macrophage-like cells (ECCAC) were routinely cultured in Dulbecco's Modified Eagles Medium (DMEM) (Gibco) supplemented with 10% inactivated foetal bovine serum (Gibco) and 2mM L-Glutamine (Gibco). RAW cells were cultured within 150 cm^2 vented cell culture flasks (Corning) within a 37°C, 5% carbon dioxide humidified incubator. RAW cells were regularly passaged, by cell scraping and culture into fresh DMEM when approximately 90% confluent, RAW cells were not used past a passage number of 20. Prior to use for an infection assay, RAW cells were assessed for viability and counted by trypan blue (Sigma) cell exclusion using an automated cell counter (Nexcelom). RAW cells were cultured on 24 well cell culture plates (Corning™ Costar™) in DMEM at a concentration of $5_{x10}{}^5$ cells mL^{-1} and cultured overnight within a 37°C, 5% carbon dioxide humidified incubator until cell density reached $1x10^6$ cells mL^{-1}.

2.1.2. Isolation of bone marrow derived macrophages.

Bone marrow derived macrophages (BMDMs) were isolated as a primary macrophage source from mice. BMDMs were isolated from BALB/c mice housed within a dedicated animal facility (Dstl) in specific pathogen free conditions.

Immediately prior to bone marrow harvest, the mice were culled by cervical dislocation and transferred into a class II microbiological safety cabinet. Mice were soaked with 70% ethanol prior to removal of the femur with sterile disposable scissors and forceps. Any attached muscle was removed, and both ends of the femur removed with scissors. Holding the bone in place with forceps, 5 mL of cold sterile PBS was washed through the bone cavity using a syringe and 25-G needle. The PBS wash was collected in a sterile centrifuge tube and centrifuged at 500 x *g* for 10 minutes at room temperature. The supernatant was discarded and the pellet re-suspended into 10 mL of DMEM/F12 (Gibco®) supplemented with 10 mM L-glutamine (Gibco®), 100 units mL^{-1} penicillin (Sigma Aldrich), 100 µg mL^{-1} streptomycin (Sigma Aldrich) and 25 ng mL^{-1} murine recombinant macrophage colony stimulating factor (Sigma Aldrich). Cell flasks were incubated for 7 days within a 37°C, 5% carbon dioxide humidified incubator. The culture media was removed and replenished after 4 days of culture. After 7 days in culture, the BMDMs were harvested into fresh DMEM/F12 (Gibco®) media by gently scraping with a cell scraper. At this point BMDMs were analysed for purity and used in BMDM infection assays.

2.2. Cell infection assays.

2.2.1. RAW cell infection assay.

An overnight bacterial Luria broth culture of *B. thailandensis* E555 (or *B. pseudomallei* K96243) was centrifuged at 10,000 *g* for 5 minutes, and re-suspended into Leibovitz's L-15 media (Gibco) supplemented with 10% inactivated foetal bovine serum (Gibco) and 2mM L-Glutamine (Gibco). The bacterial suspension was diluted to an OD_{600} of 0.172 (0.4 for *B. pseudomallei*) which equates to an approximate concentration of 1_{x10}^{8} bacteria mL^{-1}. A 10% dilution of this bacterial suspension was prepared, and added to RAW cells for 1 hour at 37°C to allow bacterial uptake. Following the incubation period, the bacterial culture medium was removed and replaced with fresh Leibovitz's L-15 medium containing 1 mg mL^{-1} kanamycin (Sigma) and incubated at 37 °C. This step was considered the start of time points to monitor intracellular bacteria. Following a minimum 2 hour incubation period, the intracellular bacteria were enumerated by cell lysis and CFU enumeration. Cell lysis

was achieved with RAW cell incubation with distilled water (Gibco) for 10 minutes at room temperature, followed by serial dilution and plating onto L-agar. Agar plates were incubated at 37 °C for 48 hours prior to CFU enumeration. RAW cells were alternatively harvested intact into PBS, for analysis by imaging flow cytometry. If cell fixation was required, cells were centrifuged at 300 *g* for 5 minutes and re-suspended into 4% paraformaldehyde (Alfa Aesar) prior to analysis.

2.2.2. Monoclonal antibody opsonisation assay.

Antibody opsonisation assays were performed as the RAW cell infection assay (2.2.1), with the addition of antibody opsonisation of *B. thailandensis* prior to RAW cell infection. A culture of *B. thailandensis* at $1x10^7$ mL^{-1} was incubated with monoclonal antibody for 30 minutes at 37°C. An isotype control antibody (Invitrogen) was used in each opsonisation assay. RAW cell infection and analysis was performed as previously described in method 2.2.1.

Opsonisation assays with *B. pseudomallei* K96243 were performed the same as for *B. thailandensis* E555, apart from the experiments were performed within ACDP containment level III facilities. Samples of *B. pseudomallei* infected RAW cells were subjected to paraformaldehyde fixation, to enable analysis within ACDP containment level II laboratories. RAW cells were fixed for 48 hours in 4% paraformaldehyde at 4ºC, prior to removal from ACDP containment level III facilities.

2.2.3. Repurposed drugs infection assay.

The RAW macrophage infection assay (2.2.1) was used to assess a panel of potential anti-microbial compounds. A panel of compounds consisting of carbamazepine (Sigma), verapamil hydrochloride (Sigma), norverapamil hydrochloride (Sigma) and valproic acid (Sigma) were incubated with the macrophages post infection. Vehicle controls for each compound were DMSO ($(CH_3)_2SO$) for carbamazepine, methanol (CH_3OH) for valproic acid, dH_2O for both verapamil and norverapamil. RAW cells were infected with *B. thailandensis* at a multiplicity of infection (MOI) of 5 and incubated for an hour at 37°C in L-15 media (Gibco). Following incubation the bacteria were removed and the cell culture media

was subsequently replaced with 1mg mL^{-1} kanamycin maintenance antibiotic to kill extracellular bacteria. Additionally, test compounds were added post-infection and incubated with the infected RAW cells for up to 24 hours. GFP expressing *B. thailandensis* E555 (pBHR4-groS-eGFP) were used in the RAW cell assay to visualise bacterial infection by imaging flow cytometry. For CFU analysis RAW cells were lysed with distilled water and enumerated on L-agar. Alternatively, the cells were harvested intact into 4% paraformaldehyde for fixation and analysis by imaging flow cytometry. Subsequent experiments include staining RAW cells for autophagy, as a host-directed mechanism of bacterial killing. Staining for autophagy was achieved with anti-LC3 and anti-LAMP-1 specific fluorescent antibodies, and analysis by imaging flow cytometry.

Kanamycin RAW cell infection assay.

RAW cells were infected with *B. thailandensis* E555 at a multiplicity of infection (MOI) of 5 and incubated for an hour at 37°C in L-15 media (Gibco). Following incubation the bacteria were removed and the L-15 cell culture media (Gibco) was subsequently replaced with 1mg mL^{-1} kanamycin maintenance antibiotic to kill extracellular bacteria. After 1 hour the kanamycin media was either left at 1mg mL^{-1}, reduced to 150 µg mL^{-1} or removed completely (L-15 culture media only). Additionally, RAW cells were incubated with or without 200µm of verapamil post-infection. RAW cells were incubated for 4 and 24 hours at 37°C. At the specific time points the RAW cells were lysed with distilled water and the intracellular bacteria enumerated by serial dilution and culture on L-agar.

2.2.4. Antibody-antibiotic conjugate infection assay.

Antibody-antibiotic conjugate (AAC) batches (Global Access Diagnostics) were assessed in a RAW cell infection assay (2.2.1) with *B. thailandensis* E555. AAC was either pre-incubated with the bacteria prior to RAW cell infection, or added post-infection in the kanamycin maintenance media. Controls consisted of antibody, antibiotic, and bacterial only controls. At specific time points, the RAW cells were analysed by CFU enumeration or imaging flow cytometry.

An overnight culture of *B. thailandensis* E555 (RFP strain for imaging flow cytometry) was diluted to 1_{x10}^{8} CFU mL^{-1} (OD_{600} of 0.172) in L-15 culture media (Gibco), the bacteria culture was further diluted to 1_{x10}^{7} CFU mL^{-1}. In opsonisation experiments the bacteria were opsonised with 3VIE5 or AAC for 30 minutes at 37°C, prior to RAW cell infection. The control infection consisted of non-opsonised *B. thailandensis*. RAW cells at 1_{x10}^{6} cells mL^{-1} in L-15 media (Gibco) were infected with the opsonised or non-opsonised bacteria at an MOI of 5, and incubated for 1 hour at 37°C. Following incubation the cell culture media was removed, and immediately replaced with L-15 media containing 1mg mL^{-1} kanamycin maintenance antibiotic. At this point the AAC and ciprofloxacin were added to the RAW cells in the post-infection AAC experiments. The RAW cells incubated for up to 24 hours at 37°C. RAW cells were lysed by replacing the cell culture media with distilled water, until cell lysis occurred (checked by light microscopy). Upon cell lysis the bacteria were enumerated by serial dilution and culture on L-agar. Agar plates were incubated for a minimum of 24 hours at 37°C until colonies could be accurately counted.

Alternatively, *B. thailandensis* E555 RFP infected cells to be analysed by imaging flow cytometry were harvested intact into 4% paraformaldehyde (Alfa Aesar). RAW cells were harvested into 4% paraformaldehyde by pipetting up and down. Imaging flow cytometry was performed on the Amnis® ImageStream® X Mark II. The gating template previously described for RFP and mAb opsonisation experiments was applied to the imaging flow cytometry analysis of AAC experiments. All lasers used were set to full power (200 mW for 561nm laser), and x60 objective was used throughout. RFP excitation (peak of 555nm) was achieved with the 561nm laser and fluorescence emission (peak of 584nm) detected with channel 4. Additional bright field imagery of the RAW cell was applied throughout with channel 1. RAW cells were gated according to being in focus, single cells and containing bacterial GFP fluorescence.

Ciprofloxacin and 3VIE5 combination assay.

An overnight culture of *B. thailandensis* E555 was diluted to 1_{x10}^{8} CFU mL^{-1} (OD_{600} of 0.172) in L-15 culture media (Gibco), the bacteria culture was further diluted to 1_{x10}^{7} CFU mL^{-1}. The bacteria were opsonised with 1 µg mL^{-1} of 3VIE5 for 30 minutes

at 37°C prior to RAW cell infection. The no mAb control consisted of non-opsonised *B. thailandensis*. RAW cells at 1_{x10}^6 cells mL^{-1} in L-15 media (Gibco) were infected with the opsonised or non-opsonised bacteria at an MOI of 5, and incubated for 1 hour at 37°C. Following incubation the cell culture media was removed, and immediately replaced with L-15 media containing 1mg mL^{-1} kanamycin maintenance antibiotic. Additionally, ciprofloxacin was added to the cell culture media at concentrations ranging from 0.1 µg mL^{-1} to 5 µg mL^{-1}, and the RAW cells incubated for 4 and 24 hours at 37°C. RAW cells were lysed by replacing DMEM culture media with distilled water, until cell lysis occurred (checked by light microscopy). Upon cell lysis the bacteria were enumerated by serial dilution and culture on L-agar. Agar plates were incubated for a minimum of 24 hours at 37°C until colonies could be accurately counted.

2.2.5. Blocking of CD16 and CD32.

RAW 264.7 cells were pre-incubated with 1 µg of TruStain FcX™ (anti-mouse CD16/CD32) (Biolegend) for 15 minutes at 37°C, prior to infection. Antibody opsonisation was assessed as described previously (2.2.2), with the addition of 1 µg of TruStain FcX™ (Biolegend) present during RAW cell infection. The RAW cells were analysed as previously described for antibody opsonisation (2.2.2).

2.3. Bacterial culture and inactivation.

2.3.1 Preparation of bacterial culture media.

Luria broth, Mueller Hinton broth, and agar were all prepared by Dstl technical services.

Luria broth was prepared with 10g tryptone peptone (Gibco), 5g yeast extract (Gibco), and 5g sodium chloride (VWR) in 1L water (Milli-Q®). Luria agar was prepared with the addition of 20g of dehydrated agar (BD). The media had a pH of 7.2 and was sterilised at 121°C for 15 minutes.

Mueller Hinton broth was prepared with 21g of dehydrated Mueller Hinton broth (Oxoid) in 1L of water (Milli-Q®). Mueller Hinton agar was prepared with 38g

dehydrated Mueller Hinton agar (Oxoid) in 1L of water (Milli-Q®). The media had a pH of 7.4 and was sterilised at 121°C for 15 minutes. The Mueller Hinton media was adjusted to the desired pH with hydrochloric acid (35%, VWR) and sodium hydroxide (40%, VWR).

2.3.2. Culture of *B. thailandensis* E555.

B. thailandensis E555 was routinely cultured in Luria broth and on Luria agar at 37°C, broth cultures were incubated with shaking at 180 rpm. Florescent protein expressing strains (pBHR4-groS-eGFP/RFP) were cultured on Luria agar and Luria broth supplemented with 50 µg mL^{-1} chloramphenicol, to ensure only plasmid containing fluorescent protein expressing bacteria are cultured. Mueller Hinton broth and agar was used for bacterial culture in finafloxacin MIC studies. Culture of *B. thailandensis* E555 was performed in ACDP containment level II facilities at Dstl.

2.3.3. Culture of *B. pseudomallei* K96243.

B. pseudomallei K96243 was routinely cultured in Luria broth and on Luria agar at 37°C, broth cultures were incubated with shaking at 180 rpm. A florescent protein expressing strain (pBHR4-groS-RFP) was cultured on Luria agar and in Luria broth supplemented with 50 µg mL^{-1} chloramphenicol. Culture of *B. pseudomallei* was performed within ACDP containment level III facilities at Dstl.

2.3.4. Inactivation methods.

Inactivation of *B. thailandensis* E555 was required for ELISA analysis outside of a microbiological safety cabinet. Inactivation was performed by heat killing an overnight culture of *B. thailandensis* at 80°C for 4 hours, within a sterile glass Duran bottle. Confirmation of inactivation was achieved by culturing 10% of the bacterial suspension in Luria broth for 1 week at 37°C with shaking at 180 rpm. After the week long broth incubation, 10% of the broth was plated onto Luria agar and incubated for a further 1 week at 37°C. Inactivation was deemed successful with no visible replication in either the broth or on the agar plates. Enumeration of the stock culture,

prior to inactivation, was achieved by serial dilution and CFU enumeration on Luria agar.

Inactivation of *B. pseudomallei* K96243 was performed to enable removal and analysis of RAW cells outside of containment level III facilities. Inactivation was achieved by fixation of infected RAW cells in 4% paraformaldehyde for 48 hours at 4°C, prior to removal from containment level III facilities.

2.4 Antibiotics.

2.4.1 Ciprofloxacin.

Ciprofloxacin hydrochloride (European pharmacopoeia reference standard, Sigma), was dissolved in 1mL of 1M NaOH and 9mL of distilled water, to create a working stock solution.

2.4.2 Finafloxacin.

Finafloxacin was supplied by MerLion Pharmaceuticals Ltd. A quantity of 118mg (100mg of active finafloxacin) was dissolved in 1mL of 1M NaOH and 9mL of dH_20 to create a 10mg mL^{-1} stock, as published by Barnes *et al* (56).

2.5 Cell staining.

2.5.1. Actin tail staining.

An overnight culture of *B. thailandensis* E555 or *B. pseudomallei* K96243 was diluted to $5_{x10}6$ CFU mL^{-1}. The bacteria were opsonised with mAb 3VIE5 or a murine antibody isotype control at 1 µg mL^{-1}, for 30 minutes at 37°C prior to RAW cell infection. The RAW cells were infected with the opsonised bacteria at an MOI of 5 for 1 hour at 37°C, the cell culture media was subsequently removed and replaced with media containing 1mg mL^{-1} kanamycin maintenance antibiotic. The kanamycin prevents extracellular bacterial growth and after 16 hours the RAW cells were harvested for imaging flow cytometry analysis. RAW cells were harvested into 4%

paraformaldehyde by pipetting up and down, or left adhered to a cell culture dish for confocal microscopy. RAW cells were fixed and permeabilised with a BD Cytofix/Cytoperm™ kit, following manufacturer's instructions. Alexa Fluor® 647 phalloidin (Molecular Probes) was added to the RAW cells at 5% (vol/vol) in perm/wash buffer, and the cells incubated at room temperature for 30 minutes. Following incubation, the RAW cells were washed twice with PBS and finally re-suspended in PBS for analysis by imaging flow cytometry or remained adhered to a cell culture dish for confocal microscopy.

2.5.2. LC3 and LAMP-1 staining.

RAW cells were harvested, transferred to 200 µL fixative-permeabilisation buffer (BD Biosciences) and incubated for 30 minutes at room temperature on a roller. Following incubation, the sample volume was increased to 1mL with 800 µL of 1X permeabilisation-wash buffer (BD Biosciences) and centrifuged for 5 minutes at 300 *g*. Following centrifugation, cells were re-suspended into 200µL permeabilisation-wash buffer (BD Biosciences) containing 5 µg mL^{-1} anti-LC3 mAb (Biolegend), and incubated for 1 hour at room temperature on a roller. Following incubation, a further 800 µL of permeabilisation-wash buffer (BD Biosciences) was added to the sample. The RAW cell sample was centrifuged for 5 minutes at 300 *g,* the cell pellet was re-suspended into 200 µL permeabilisation-wash buffer (BD Biosciences) containing 10 µg mL^{-1} goat anti-mouse Alexa Fluor 647 (Invitrogen) and 3.5 µg mL^{-1} PE/Dazzle™ 594 anti-mouse CD107a (LAMP-1) Antibody (Biolegend, UK). The sample was incubated for 1 hour at room temperature on a roller. Following incubation, 800 µL of PBS (Gibco) was added and the sample centrifuged for 5 minutes at 300 *g*. Finally, cell pellets were re-suspended into 50 µL PBS (Gibco) prior to analysis by imaging flow cytometry.

2.5.3. Primary macrophage staining.

BMDM cells were stained and analysed for CD11b and CD14 markers.

BMDM cells were removed from culture by gentle scraping into DMEM/F12 (Gibco®) media. The BMDM cell suspension was centrifuged at 400 *g* for 5 minutes at room

temperature, and the supernatant discarded. The BMDM cell pellet was re-suspended into PBS containing 2% FBS (Gibco®) and separated into four separate vials. Vials consisted of a non-stained control, CD11b stained, CD14 stained and a combination of both stains. To reduce non-specific staining, BMDM cell samples were pre-incubated for 10 minutes with 1µg TruStain fcX™ anti-mouse CD16/32 antibody (BioLegend®) per 10^6 cells in a 100µL volume. Brilliant Violet 421™ anti-mouse/human CD11b antibody (Biolegend®) and Alexa Fluor® 647 anti-mouse CD14 antibody (Biolegend®) were added to the BMDM cells at 0.25 µg per 10^6 cells. All stains were incubated with BMDM cells for 45 minutes at room temperature and with gentle shaking in the dark. Cells were subsequently washed with PBS and centrifuged at 400 *g* for 5 minutes, this was repeated twice to remove unbound stain. BMDM samples were analysed by flow cytometry and confocal microscopy.

2.6. Cell analysis.

2.6.1. Cell counting.

Cells were assessed for viability and enumerated by trypan blue (Sigma) cell exclusion using an automated cell counter (Nexcelom). Trypan blue was used at 1:1 (vol/vol) with the cell suspension.

2.6.2. Confocal microscopy.

High definition imaging of RAW cells was achieved using a confocal laser scanning microscope (Zeiss). Cells were analysed on 35 mm cell culture dishes (Corning) using x20, x40, or x63 oil immersion lenses. Hoechst (Sigma) nuclei dye (excitation peak at 352 nm and emission peak at 461 nm) was added to cells at 2µg mL^{-1}, to discriminate between individual cells and multi-nucleated giant cells. A GFP expressing *B. thailandensis* E555 (excitation peak at 489 nm and emission peak at 511 nm) was used throughout confocal microscopy studies. Cells were additionally stained for bacterial actin tails with Alexa Fluor® 647 (excitation peak at 650 and emission peak at 668nm) phalloidin (red). Laser power was set between 2 – 5 mw for each laser used, 488nm (GFP), 405nm (Hoechst) and 633nm (Alexa Fluor ® 647).

Bacterial actin tail fluorescence was imaged at 12 hours post infection by confocal microscopy. Images were taken on the confocal microscope at x20 magnification, and using a 5x5 tiled image around multiple focal points of infection on a 35 mm cell culture dish (Corning). A 2 line average scan was used throughout, with a gain of 290 for green and a gain of 686 for red fluorescence. Confocal microscopy images were analysed using the Icy bio image analysis software (http://icy.bioimageanalysis.org/) (243). A ratio was generated between the green bacteria (*B. thailandensis* E555 GFP) and the red actin tail (Alexa Fluor® 647 phalloidin (Molecular Probes)).

Imaging FITC labelled AAC.

An overnight culture of *B. thailandensis* E555 RFP in L-broth was diluted to an OD of 0.172, which equates to a concentration of 1_{x10}^{8} CFU mL^{-1}. The FITC labelled AAC was added to the bacteria at a concentration of 10 µg mL^{-1}, this high concentration was selected to ensure that the fluorescence will be visible on the confocal microscope. Confocal microscopy was used to visualise fluorescence from the FITC (excitation peak of 490 and emission peak of 525) using a 488nm excitation laser, and RFP using a 543nm excitation laser (excitation peak of 555 and emission peak of 584). Laser power was set between 2 – 5 mw for each laser used, images were taken using x63 magnification.

2.6.3. Imaging flow cytometry.

Imaging flow cytometry was performed on an Amnis® ImageStream® X Mark II Imaging flow cytometer. Cell samples were analysed either live or fixed in 4% paraformaldehyde (Alfa Aesar), within an Eppendorf® tube. Ten thousand events were collected, consisting of cells gated according to being in focus and single cells. Channels 1 (bright field), 2 (GFP), 4 (RFP), 6 (side scatter) and 9 (bright field) were all used at full laser power as standard. Magnification was set at x60 for all RAW cell experiments. A compensation matrix was generated and applied to data where more than one fluorophore is present in the sample, this was to compensate for any potential cross-over between fluorescence.

Ideas® software was used to analyse data. Analysis of infected cells was performed by gating cells according to the associated bacterial fluorescence. Additionally, an erode mask was applied to exclude extracellular bacterial fluorescence from the cell analysis, as previously described by Jenner *et al* (244).

LAMP-1 analysis

RAW cells were analysed on the Amnis® ImageStream® X Mark II. The 488nm (GFP) and 561nm (PE/Dazzle™ 594) lasers were used at 100mw and 200mw power respectively. Fluorescence was detected using channel 2 (*B. thailandensis* E555 GFP, excitation peak at 489 nm and emission peak at 511 nm) and channel 4 (PE/Dazzle™ 594), magnification was set at x60 throughout. Cells were gating according to being single cells, in focus, association with GFP and co-localisation with LAMP-1 (Figure 30).

LC3 and LAMP-1 autophagy analysis

RAW cells were analysed on the Amnis® ImageStream® X Mark II. The 488nm (GFP), 561nm (PE/Dazzle™ 594) and 642nm (Alexa Fluor 647) lasers were used at 100mw, 200mw and 150mw power respectively. Fluorescence was detected using channel 2 (*B. thailandensis* E555 GFP, excitation peak at 489nm and emission peak at 511nm), channel 4 (PE/Dazzle™ 594) and channel 11 (Alexa Fluor 647 excitation peak at 650nm and emission peak at 665nm). Bright field (channel 1) was used throughout at maximum power and magnification was set at x60 throughout. Cells were gating according to being single cells, in focus, association with GFP, and co-localisation between LC3 and LAMP-1 as a marker of autophagy (Figure 40). A compensation matrix was generated in the Amnis Ideas® software and applied to the data set to compensate for fluorescence cross over between the GFP, PE/Dazzle™ 594 and Alexa Fluor 647 emissions.

2.6.4. Flow cytometry.

BMDM cells were harvested and stained with CD11b and CD14 (method 2.5.3).

BMDM cell samples were analysed on a FACS Canto II (BD Biosciences) and intact cells gated according to SSC-A and FSC-A (side scatter and forward scatter). CD11b and CD14 positive BMDM cells were gated according to pacific blue-A (violet) and APC-A (red), for detection of Brilliant Violet 421™ anti-mouse CD11b antibody (BioLegend) and Alexa Fluor® 647 anti-mouse CD14 antibody fluorescence respectively. Each laser was used at full power, violet laser at 405nm and red laser at 633nm. Brilliant violet 421 has an excitation wavelength of 405 nm and emits at 421 nm, whereas Alexa Fluor® 647 is excited at 633 nm and has a maximum emission of 668 nm. A total of 18,727 CD11b and CD14 positive BMDM cells, and 19,396 unstained BMDM cells were gated during the analysis.

2.6.5. CFU analysis.

RAW cells were lysed by replacing the culture media with dH_2O and incubated for a minimum of 10 minutes at room temperature. Lysis was confirmed with visualisation by light microscopy. Enumeration of bacteria was achieved by serial dilution and plating onto Luria agar. Agar plates were incubated for 48 hours at 37°C, prior to counting of colony forming units.

2.6.6. Analysis of LDH release from RAW cells.

Analysis of lactose dehydrogenase (LDH) release from RAW cells was achieved with the use of Promega CytoTox 96® Non-Radioactive Cytotoxicity Assay kit (Promega Corporation USA), following manufacturer's instructions. Briefly, RAW 264.7 cells (ECCAC) were cultured on 24 well cell culture plates (Corning™ Costar™) and incubated with test compounds at various concentrations. At the specified time points, the cell culture media in each well was gently mixed and 50µL of media removed for analysis. Cell culture samples were transferred to a 96 well cell culture plate (Corning™ Costar™), 50µL of CytoTox 96® reagent was added to each well. The plate was incubated in the dark at room temperature for 30 minutes prior to addition of 50µl CytoTox 96® stop solution. Absorption of each well was read on a plate reader set at 492nm wavelength. Percentage of cell lysis was calculated by comparison to a lysis control, in which all cells were lysed by CytoTox 96® lysis solution.

2.6.7. Minimum inhibitory concentration (MIC).

An overnight Luria broth culture of *B. thailandensis* E555 or *B. pseudomallei* K96243 was diluted to an approximate concentration of $1x_{10}^{8}$ bacteria mL^{-1}, using a bacterial OD reading of 0.172 OD_{600nm} and 0.4 OD_{590nm} respectively. The bacterial suspension was further diluted to 1_{x10}^{6} cfu mL^{-1} with dilutions into either L-15 cell culture media (Gibco), Luria broth or Mueller Hinton broth. A 96 well culture plate (Corning™ Costar™) was prepared with dilutions of test compounds within a 100µL volume of either L-15 cell culture media (Gibco), Luria broth or Mueller Hinton broth per well. To each well, 100µL of the 1_{x10}^{6} cfu mL bacterial suspension was added, therefore the total volume was 200 µL per well. Control wells consisted of positive bacterial culture with no test compounds, and negative controls consisted of 200 µL of culture media only. Plates were sealed with an optically clear sterile plate sealer and placed within an incubating plate reader (Multiskan FC, Thermo), with the incubator set to 37°C with gentle shaking. Automated OD readings were taken at OD_{595} every 15 minutes for 24 hours. Alternatively, plates were placed within a static incubator for 24 hours at 37°C. The MIC was calculated by a visual examination of the 96 well plate to determine wells with no bacterial replication, as stated in the Clinical and Laboratory Standards Institute (CLSI) guidelines (245). Alternatively the OD readings from the incubating plate reader (Multiskan FC, Thermo) were plotted to display bacterial replication over 24 hours.

2.6.8. Minimum bactericidal concentration (MBC).

To determine the MBC, 100µl aliquots were taken from wells of the MIC assay with no visible bacterial replication. The aliquots were plated onto Luria agar and incubated at 37°C for 24 hours to determine bacterial replication. A concentration of the compound that killed 99.9% of the bacterial inoculum was considered the MBC for that compound.

2.7. Cathepsin assays.

2.7.1 *In vitro* cathepsin cleavage assay.

Dry powder AAC preparations were dissolved in 50µL of DMF (Sigma) followed by addition of 950µL of cathepsin assay buffer (100mM sodium acetate buffer (Sigma), 2mM DTT (Sigma), 1mM EDTA (Sigma), pH 5). Solubilised AAC samples were provided by Global Access Diagnostics in PBS buffer. Cathepsin B from bovine spleen (Sigma C6286) was reconstituted into cathepsin assay buffer and added to AAC samples at between 1 and 10 unit concentrations. Cathepsin B was incubated with the AAC samples for 1 hour at 37°C to enable linker cleavage. Antibiotic function post cleavage was assessed by MIC (2.6.7) and MBC (2.6.8) analysis.

2.7.2 Cathepsin B activity.

The activity of cathepsin B (Cathepsin B from bovine spleen, Sigma C6286) was assessed in pH 5 cathepsin buffer (100mM sodium acetate buffer (Sigma), 2mM DTT (Sigma), 1mM EDTA (Sigma), pH 5) with a colorimetric Z-RR-pNA (z-arg-arg-p-nitroanalide) substrate (Sigma). The colorimetric product (p-nitroaniline) formed from cathepsin cleavage of Z-RR-pNA, was detected by OD at 405nm in a 96 well incubating micro plate reader (Multiskan FC (Thermo)), with OD readings every minute for 1 hour at 25°C.

2.8. Generation of AAC products by Global Access Diagnostics.

Octet analysis of mAbs, generation of antibiotic stub molecules, chemical conjugation of 3VIE5 to antibiotics and HPLC/MALDI analysis were performed by Global Access Diagnostics. All methods detailed in this section (2.8) were provided by Global Access Diagnostics.

2.8.1. Octet analysis of antibodies.

A heat-killed cell preparation of *B. thailandensis* E555 was prepared at Dstl (2.3.4) and sent to Global Access Diagnostics. Four mAbs (3VIE5, 4VIH12, 4VA5 and CC6) were provided for characterisation by real time label free kinetics analysis.

Data was generated using the Octet® RED Biolayer interferometry platform (ForteBio Sartorius). To test the bacterial ligand, a dilution series was set up on the reaction plate to assess whether immobilisation was taking place on the APS (aminopropylsilane) surface, and at what level the signal threshold was reached. Antibody 3VIE5 was chosen to test for analyte binding at a concentration of 333 nM. For further evaluations of antibody binding, the loading concentration was set at 1/400 dilution. A series of kinetics measurements were set up for the four candidate antibodies. In each case duration of association phase was set to between 200 and 250 seconds and the dissociation phase to between 500 and 1000 seconds.

2.8.2. Generation of antibiotic stub molecules.

Tert-Butyl-4-(hydroxymethyl)phenylcarbamate (199.6 mg, 894 µ moles, Fluorochem Ltd. Cat no. 061120, Lot no. FCB062749, MW = 223.272), was solubilised in dimethylformamide (DMF) dried over a molecular sieve (3.1 mL). A solution of thionyl chloride (Sigma-Aldrich 230464, 120 mg, 74 µL, 1009 µ moles, MW = 118.97, d = 1.638) in dichloromethane (DCM) dried over a molecular sieve (0.52 mL) was added in portions dropwise. The solution was a deep red in colour. Stirring was continued with the reaction vial septum top pierced by a syringe needle connected to a balloon of nitrogen gas. A further 65 mg (40 µL, 546 µM) $SOCl_2$ in 156 µL dry DCM was added dropwise after three hours. The solution, which was still deep red in colour, was stirred with a balloon of nitrogen in place overnight. The next day a solution of $SOCl_2$ (15 µL, i.e. 24.5 mg) in dry DCM (156 µL) was added and stirring was continued for 2 h. The volume of solution in the vial was reduced by approximately a half using a stream of nitrogen gas. One half of the solution was added to a vial containing a 196 mg aliquot of finafloxacin. HCl (÷ 434.85 = 451 µM), while the other half was added to a vial containing a 149 mg aliquot of ciprofloxacin (Sigma-Aldrich 17850, 450 µM). Each mixture was diluted with an additional 1.025 mL aliquot of DMF dried over molecular sieve, and the mixtures were stirred open to the air for 0.5

h. A 217 µL aliquot of N,N-Diisopropylethylamine (DIPEA) (2.25 mM, i.e. a 5x molar excess with respect to antibiotic) was added to each mixture, the vials were capped and stirring was continued overnight. Following overnight stirring of the reaction mixtures, 22 µL aliquots of DIPEA were added to each one and stirring was continued. After 5 hours an additional 22 µL aliquot of DIPEA was added to each reaction vial and stirring was continued overnight. Following overnight stirring of the reaction mixtures, 22 µL aliquots of DIPEA were added to each one and stirring was continued for 1 h. At this point samples were taken for high performance liquid chromatography (HPLC) analysis. A solvent control sample was run (DMF + 80/20 water/MeCN) using a Phenomenex Kinetex 5 µm C18 100Å LC column, 250 x 4.6 mm (Part no. 00G-4601-E0, batch no. 5701-0039), with a gradient of 20 – 100 % B from 2 to 16 minutes, where Solvent A = 0.1 % trifluoroacetic acid (TFA) in water and Solvent B = 0.1 % TFA in acetonitrile. Fractionation confirmed the carbamate products of ciprofloxacin and finafloxacin at retention times of 9.2 min and 9.11 min respectively. Free unreacted antibiotic eluted significantly earlier at 3 min. Liquid chromatography mass spectrometry (LC-MS) analysis confirmed the expected masses.

After HPLC purification of the target peak, pooling and lyophilisation, the de-protection was carried out to remove the tert-butyloxycarbonyl (Boc) group. A 1 mL aliquot of DCM was added to the freeze-dried material, and a 1 mL aliquot of TFA was added to the resulting solution. The de-protection mixture was incubated at room temperature. After 2 hours, the de-protection solution was transferred to a round-bottom flask and the liquid phase was removed by rotary evaporation. The de-protected material was subjected to a cold diethyl ether wash and the de-protected material was solubilised in 50/50 MeCN/water. The solution was transferred to a vial to be lyophilised.

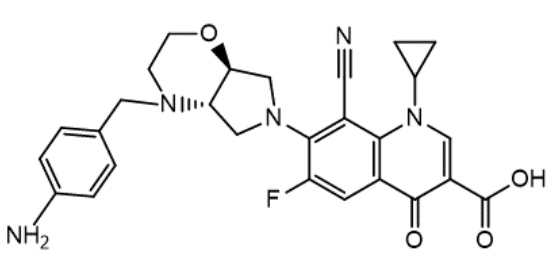

PAB-Finafloxacin

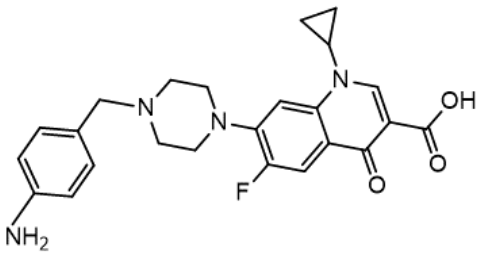

PAB-Ciprofloxacin

Figure 5. Structure of antibiotic stubs.

Finafloxacin-PAB and ciprofloxacin-PAB were generated by Global Access Diagnostics, for analysis by Dstl to determine antibiotic activity.

2.8.3. Synthesis of Boc-amine Linker intermediate.

A 2 mL aliquot of DMF dried over molecular sieve was added to a 203.67 mg aliquot of MC-Val-Cit-PABA-OH (÷ 572.66 = 356 µM) in a glass vial. A stirrer bar was added and stirring commenced to solubilise the linker. A 500 µL aliquot of 2-(Boc-amino)ethanethiol (BocAET) (= 2.96 mM, i.e. 8.3 x molar excess wrt linker) was added to the linker solution. A septum cap was fitted on the vial and a syringe needle attached to a nitrogen balloon was put through the septum. The mixture was stirred overnight at RT. Having stirred the reaction mixture overnight, a 15 µL aliquot was removed for analysis. The solution was diluted with 0.1 % TFA in 50/50 MeCN/water (300 µL) and HPLC purification was carried out using a Phenomenex Kinetex 5 µm C18 100Å LC column 250 x 4.6 mm (Part no. 00G-4601-E0, serial no. 643153-7). A gradient of 5 – 100 % B from 2 to 16 minutes was employed, where Solvent A = 0.1% TFA in water and Solvent B = 0.1 % TFA in acetonitrile. Target material was confirmed by mass spec. Expected mass = 749.38; measured MH+= 750.3.

2.8.4. Synthesis of Boc-amine linker-ciprofloxacin intermediate.

A 5.93 mg (÷ 749.92 = 7.908 µM) aliquot of Linker-BocAET was dried in the freeze-drier for 25 minutes. The material was solubilised in DMF dried over molecular sieve (90 µL), and a solution of thionyl chloride (Sigma-Aldrich 230464, 0.983 mg, 0.60 µL, 8.261 µM, MW = 118.97, d = 1.638) in DCM dried over molecular sieve (10 µL) was

added. The reaction mixture was tumbled at room temperature. After approximately 2 h, a solution of thionyl chloride (0.42 µL, 5.783 µM) in dry DCM (5 µL) was added to the reaction mixture and Tumbling at RT was continued overnight. An additional aliquot of thionyl chloride (0.42 µL, 5.783 µM) in DCM (5 µL) was added to the reaction mixture, and tumbling was continued for a further 5 h. The mixture was transferred to an Eppendorf that continued a 3.49 mg (÷ 385.82 = 9.046 µM) of ciprofloxacin hydrochloride (Abcam, Product no. ab141918, Lot no. GR193496-12). N.B. Before the solution was added to the aliquot of Cip.HCl, the volume was not reduced on this occasion using a stream of nitrogen gas. An additional aliquot of DMF (25 µL) was added to the mixture and tumbling was resumed. The Cip.HCl was not completely solubilised in the liquid phase. After 20 minutes, tumbling was interrupted to add a 6.90 µL aliquot (6.90 x 0.742 x 1000/129.247 = 39.54 µM, i.e. a 5x molar excess wrt of linker-BocAET material and ciprofloxacin.HCl) of DIPEA (Sigma-Aldrich, Product no. D125806, Lot no. STBD4638V). Tumbling of the reaction mixture was continued overnight at RT. Over 72 hours, additional aliquots of DIPEA were added until a product peak was observed on HPLC. HPLC purification was carried out with a Phenomenex Kinetex 5 µm C18 100Å LC column 250 x 4.6 mm (Part no. 00G-4601-E0, serial no. 643153-7, batch no. not stated). A gradient of 5 – 100 % B from 2 to 16 minutes was employed, where Solvent A = 0.1 % TFA in water and Solvent B = 0.1 % TFA in acetonitrile. Target material was confirmed by mass spec. Expected mass = 1062.50; Measured MH+ = 1063.3.

2.8.5. The modification of 3VIE5 antibody with sulfo-SMCC.

A 4mg/mL aqueous solution of sulphosuccinimidyl-4-(N-maleimidomethyl) cyclohexane-1-carboxylate sodium salt (sulfo-SMCC, Apollo Scientific, Cat. no. BICL207, Lot no. 29745) was prepared, and an 11.3 µL aliquot (103.6 nM) of this solution was added to an Eppendorf tube that contained a 280 µL aliquot (6.907 nM) of 3.7 mg/mL 3VIE5 diluted with PBS, pH 7.4 (220 µL). Sulfo-SMCC:Ab molar ratio = 15:1. The contents of the tube were agitated at room temperature using a rotator. After 1 hour, the tube containing the reaction mixture was removed from the rotator, and the solution was applied to a Zeba Spin column, 7K MWCO, 2 mL (Thermo Sci. Cat. no. 89890, Lot no. XA339944) that had been equilibrated with PBS, pH 7.4, + 2

mM Ethylenediaminetetraacetic acid (EDTA). A 4 µL aliquot of the eluate was removed for MALDI-TOF MS analysis.

2.8.6. Modification of linker-Ciprofloxacin with Traut's reagent.

A 0.60 mg (÷ 963 = 623 nM) aliquot of LinkerAETCiprofloxacin in an Eppendorf tube was solubilised in DMF (15 µL), and the resulting solution was diluted with a 105 µL aliquot of 20 mM borate buffer, pH 9.0, + 2mM EDTA. A 20 mg/mL soln. of Traut's reagent (2-Iminothiolane hydrochloride, Sigma-Aldrich, Cat no. I6256, Lot no. SLBZ5571, MW = 137.63) in water was prepared, and a 4.28 µL aliquot (622 nM) of this solution was added to the LinkerAETCiprofloxacin solution for a molar ratio of 1:1. The reaction mixture in the Eppendorf tube was agitated at room temperature using a rotator. After approx. 1 hour, the solution was added to the modified antibody solution (2.8.7) after a 4 µL aliquot of the Traut-modified solution had been removed for LC-MS analysis.

2.8.7. Reaction of sulfoSMCC-modified antibody with Traut-modified LinkerAETCiprofloxacin.

The sulfoSMCC-modified antibody eluate that remained, after a small sample of the solution had been taken, was transferred from a 15 mL collection tube to a 1.5 mL Eppendorf tube. The remaining Traut-modified LinkerAETCiprofloxacin solution (2.8.6) was added to the mAb eluate, and the mixture was agitated overnight at room temperature using a rotator. Theoretical calculations:

Molar ratio of Traut-modified LinkerAETCiprofloxacin:sulfoSMCC-modified Ab = 91:1

Following overnight agitation on the rotator, the conjugation solution was applied to a Zeba Spin column, 7K MWCO, 2 mL (Thermo Sci. Cat. no. 89890, Lot no. VK311740) that had been equilibrated with PBS, pH 7.4. The eluate was stored in a fridge.

2.8.8. LC-MS analysis of LinkerAETCiprofloxacin.

The aliquot of the Traut-modified solution was diluted with 0.1 % aq. formic acid in LC-MS grade water. The solution was transferred to a sample vial for LC-MS analysis, which was carried out after an LC-MS water control using a Waters BioAccord LC-MS system. A gradient of 2 – 90 % B1 from 2 to 20 minutes was used, where Solvent A1 = 0.1 % formic acid in water and Solvent B1 = 0.1 % formic acid in acetonitrile. The flow rate was 0.6 mL/min. and the injection volume = 5 µL. Column = Acquity UPLC CSH C18 130Å, 1.7 µm, 2.1 x 100 mm, Part no. 186005297, Serial no. 01703107825196.

2.8.9. MALDI-TOF MS analysis.

The analysis was carried out on a Shimadzu MALDI-8020 mass spec using the following three solutions:

3.7 mg/mL 3VIE5 Ab solution (Lot no. 3VIE51908P).

SulfoSMCC-modified 3VIE5 antibody.

The antibody-ciprofloxacin conjugate solution.

Preparation of the three sample solutions for MALDI-TOF analysis was carried out using freshly prepared sinapic acid (Sigma) (SA) solution in 50/50 MeCN/water as the matrix solution. For each sample, a 0.5 µL aliquot of matrix solution was used to pre-treat the TO-431R00 target plate. Once dry, a 0.5 µL aliquot of sample solution was applied, followed by a second 0.5 µL aliquot of matrix solution. Analysis was carried out on the MALDI-TOF MS after the plate had been allowed to air dry. The instrument parameters were:

Mass range: 10,000 – 200,000

Tuning: Linear

Spots: manual positioning (rastered)

5 shots @ 200 Hz

200 profiles

Monitor range 140,000 – 160,000

Pulsed extract: on @ 150,000

Blanking mass: 10,000

Laser power = 110

2.8.10 Conjugation of fluorescein to ciprofloxacin AAC.

A 1.4 µL aliquot of a 20 mg/mL solution of carboxyfluorescein-dPEG$_{12}$-NHS ester (Quanta Biodesign Ltd) was added to the antibody-ciprofloxacin conjugate solution at a ratio of 4:1 (fluorescein:AAC). The mixture was agitated at room temperature using a rotator. After 2 h, the reaction mixture was applied to a Zeba Spin column, 7K MWCO, 2 mL (Thermo Scientific) that had been equilibrated with PBS, pH 7.4. The yellow-coloured eluate was transferred to a 1.5 mL Eppendorf tube and stored in a fridge.

2.9. Pharmacokinetic analysis.

2.9.1 ELISA.

ELISA microtitre plates (96 well Immulon 2 HB) were coated with heat inactivated *B. thailandensis* E555 at a range of concentrations (1_{x10}^5 to 1_{x10}^8 cfu mL^{-1}) in 100 µL of 0.05M carbonate-bicarbonate buffer pH 9.6 (Sigma). The plates were coated by overnight refrigeration at 4°C and subsequently washed three times with PBST (0.01 M phosphate buffered saline containing Tween® 20 at 0.05% pH 7.4 (Sigma)). Plates were blocked with 200µL of casein blocking buffer (Sigma) for 45 minutes at 37°C, followed by a three stage wash with PBST. The mAb 3VIE5 was prepared in casein blocking buffer and added to the ELISA plates, plates were incubated at 37°C for 45 minutes. Following incubation, the plates were washed with PBST three times, and a goat anti-mouse IgG (H+L) HRP (horseradish peroxidase) conjugated secondary antibody (Sigma) was added to the plate (1 in 3000 dilution) in 100µL casein blocking buffer (Sigma). Plates were incubated at 37°C for 45 minutes followed by a three stage wash with PBST. Finally, 100µL of ABTS^{TM} (2,2′-azino-di-(3-ethylbenzthiazoline sulfonic acid) solution (Roche) was added to each well of the

plate and incubated for 45 minutes at room temperature. Absorption values were determined with a 96 well micro titre plate reader (Multiskan FC, Thermo) at a wavelength of 414nm.

2.9.2. Pharmacokinetics of mAbs *in vivo.*

A group of 15 female BALB/c mice (Charles River) were housed at the experimental animal facility at Dstl. All 15 mice received an intravenous dose of 3VIE5 mAb at 5 mg kg^{-1} into the lateral tail vein. Groups of 3 mice were subjected to blood collection by cardiac puncture under terminal anaesthesia at 24, 96, 192, 360 and 432 hours post mAb 3VIE5 dose. Blood samples were centrifuged (1500 x *g* for 10 minutes) and the sera stored at -80°C prior to testing by ELISA. Sera samples were analysed in triplicate by an immobilised antigen ELISA at 1_{x10^7} cfu mL^{-1} (2.9.1). Pharmacokinetic properties were determined by generating a standard curve from control mAb 3VIE5 ELISA data, and the subsequent interpolation of sera samples from this standard curve using GraphPad® prism (version 8 for Windows, La Jolla California USA, www.graphpad.com).

3. Antibody opsonisation of *Burkholderia in vitro*.

3.1. Introduction.

Opsonisation is the process whereby a pathogen is labelled for destruction by the immune system. First described in the early 1900's by Wright and Douglas, serum was shown to be opsonising by rendering bacteria more liable to uptake by phagocytic cells (246).

Antibodies bind to the surface of the bacterial target via the Fab (fragment antigen binding) region and interact with cell surface receptors via the antibody Fc (fragment crystallisable) region. The Fc region of antibody opsonised bacteria can interact with a variety of different FcγRs (Fc receptors) present on the surface of phagocytic cells. In this study we will be investigating opsonisation with a murine antibody and murine macrophage-like cells, murine FcγRs can have either activating or inhibitory effects on the phagocyte. The murine receptors FcγRI, FcγRIII and FcγRIV are activating, whereas FcγRIIB is inhibitory (138-140). Once the antibody is intracellular there is an additional activating cell receptor called TRIM-21 (interferon inducible cytosolic Fc receptor tripartite motif containing-21), which has a broad specificity to antibody and an ability to trigger intracellular killing mechanisms (141-143). The neonatal fragment crystallisable region receptor (FcRn) is an intracellular receptor which plays an important role in antibody recycling and saving antibody from degradation within the phagolysosome compartment, the FcRn binds the Fc portion of the antibody and binds monomeric IgG with a high binding affinity during low pH conditions (138, 247, 248). Engineering antibodies for enhancing interaction with the FcRn can promote a long half-life in circulation (248, 249), a favourable pharmacokinetic property of a potential therapeutic antibody.

The role of antibodies in opsonisation of bacteria and phagocytosis of bacteria is well documented. There has been past research in the literature investigating serum opsonins for ability to increase phagocytosis and killing of *B. pseudomallei*. Serum antibodies and complement have been shown to opsonise *B. pseudomallei*, increasing uptake into phagocytic cells (250). It has also been shown that although

antibodies and complement increase bacterial uptake, macrophages struggle to then clear *B. pseudomallei* or *B. thailandensis* without prior activation by IFN-γ (250, 251).

Antibodies play a key role and have been shown to offer a level of protection against melioidosis in *B. pseudomallei in vivo* challenge experiments (113-115). Human sera from melioidosis survivors has been tested *in vitro* and shown that antibodies play an important role of opsonising *B. pseudomallei,* and help to control intracellular bacterial replication (251). An antibody based therapy is likely to be one of the best options to provide protection against melioidosis in humans.

An aim of this chapter is to develop a suitable macrophage-like cell *in vitro* infection assay and to assess mAbs for ability to opsonise bacteria. Opsonisation ability of mAbs is not a new concept, the reason for assessing opsonisation here is that a functional antibody-antibiotic conjugate (AAC) will rely upon antibody opsonisation of *B. pseudomallei* for the AAC concept to work. In this chapter, monoclonal antibodies will be characterised based on opsonisation ability and down-selected for later incorporation into an AAC.

Antibodies previously generated at Dstl will be assessed in this study. The antibodies in this study are murine monoclonal antibodies that bind to either CPS or LPS of *B. pseudomallei*. These antibodies have been assessed in previous *in vivo* studies at Dstl, demonstrating that the anti-CPS and LPS mAbs provide a level of protection in mice against a *B. pseudomallei* challenge (113). The anti-CPS mAbs in particular, outperformed the anti-LPS and any anti-protein mAbs in protection studies carried out at Dstl. These Dstl owned mAbs are available for use in this research project, based on the previous *in vivo* protection study data the anti-LPS and anti-CPS mAbs were selected for antibody opsonisation studies in this chapter.

Initially, the cell line to be used in this research project is the RAW 264.7 macrophage-like cell line, the use of a primary cells will also be investigated for a macrophage infection assay. This RAW macrophage-like cell line has been used extensively and for many years, it is an appropriate *Burkholderia* infection cell model (75, 244, 252-254). This cell line is capable of macrophage processes such as phagocytosis, pinocytosis, nitric oxide production and antibody dependent

cytotoxicity (255, 256). The cell line has been studied for stability in continuous culture and shown to be stable, at least until passage 30 (255).

Other commonly used macrophage cells for *Burkholderia* studies are the J774 macrophage-like cell line (15, 257), and primary derived macrophage cells such as bone marrow derived macrophages (BMDM) (173, 258). There are advantages and disadvantages associated with a continuous cell line compared to primary derived macrophage cells. Primary cells are isolated from an animal and are a finite resource, a cell line can be passaged many times and much larger cell quantities are readily culturable without the requirement for animal use. A primary macrophage cell is likely to have a stronger response to infection, and better represent a response that may be seen with an *in vivo* model. In a study comparing J774 to BMDM cells in a tuberculosis infection assay, it was seen that BMDM cells responded quicker to infection and to a greater extent (259). The study compared the induction and repression of differentially expressed genes in both cell lines during infection, especially in early time points the response to infection was weaker in J774 cells (259).

The aims of this chapter can be summarised as:

- Development of a macrophage-like cell infection assay to assess antibody opsonisation.
- Assess a panel of monoclonal antibodies for opsonisation of *B. thailandensis* and *B. pseudomallei*.
- Down-select a single monoclonal antibody for further investigation as a potential therapeutic.

3.2. Development of a macrophage-like cell infection assay to assess antibody opsonisation.

The aim of this section was to modify a RAW 264.7 macrophage-like cell infection assay to assess antibody opsonisation. Initial experiments will show bacterial growth over time, followed by initial testing of antibody opsonisation and quantification of bacterial infection of RAW cells by imaging flow cytometry and by enumeration on L-

agar. This RAW cell infection assay will then be applied to assessing a panel of monoclonal antibodies for opsonisation of *B. thailandensis* and *B. pseudomallei*. A cell infection assay was chosen as the primary *in vitro* method to analyse *Burkholderia* infection of macrophage-like cells and the effect of antibody opsonisation. The initial cell line of choice is the RAW 264.7 macrophage-like cell, this cell line is a murine macrophage-like cell line purchased from the European Collection of Authenticated Cell Cultures (ECACC, 91062702) (UK Health Security Agency). The RAW 264.7 cell line was selected for its ability to be continuously cultured, and being phenotypically and functionally stable (255). Primary cell lines isolated directed from mice are more favourable as a macrophage model, but are generally harvested in lower cell densities and unsuitable for long term cell culture. Therefore the bulk of cell infection studies were performed with RAW 264.7 cells, and where possible additional studies with a primary macrophage cell line.

Initially, *B. thailandensis* E555 was used in the development and testing of cell infection assays before progressing onto infection assays with ACDP hazard group III *B. pseudomallei* K96243. *B. thailandensis* E555 expresses CPS identical in structure to *B. pseudomallei* (19); this was an important feature in the choice of this bacterium for assessing CPS specific antibodies in cell infection assays. *B. thailandensis* E555 has been shown to be a suitable surrogate for *B. pseudomallei* K96243, when compared to other *B. thailandensis* strains such as E264 (15). Data from J774 macrophage-like infection assays shows a similar intracellular replication profile and similar genetic makeup between *B. thailandensis* E555 and *B. pseudomallei* K96243 (15), thus confirming the utility of E555 as an initial ACDP hazard group II surrogate for *B. pseudomallei*.

A cell infection assay was used to demonstrate that *B. thailandensis* E555, including the GFP (green fluorescent protein) and RFP (red fluorescent protein) mutants, are able to be phagocytosed by RAW 264.7 cells (2.2.1. RAW cell infection assay.). The fluorescent expressing bacterial strains *B. thailandensis* E555 GFP / RFP and *B. pseudomallei* K96243 RFP were originally generated by Exeter University UK and provided to Dstl. The fluorescence is constitutively expressed on a plasmid pBHR4-groS-eGFP/RFP with chloramphenicol resistance. The GFP has an excitation and

emission peak of 489nm and 511nm, whereas RFP has an excitation and emission peak of 555nm and 584nm.

The RAW cell infection assay is an established and widely published method, with a *B. thailandensis* RAW 264.7 cell assay previously published by Jenner *et al* (244) at Dstl. This RAW cell infection assay was used as a tool to assess cell infection, and the effect of mAbs on intracellular bacteria. A kanamycin maintenance media was used throughout the RAW cell infection assay to prevent extracellular bacterial growth (2.2.1. RAW cell infection assay.). A 1mg mL^{-1} concentration was chosen to ensure extracellular bacterial growth was prevented during the short 2 hour incubation time points of antibody opsonisation studies. Later studies will determine the effect of kanamycin on intracellular bacteria during longer incubation time periods.

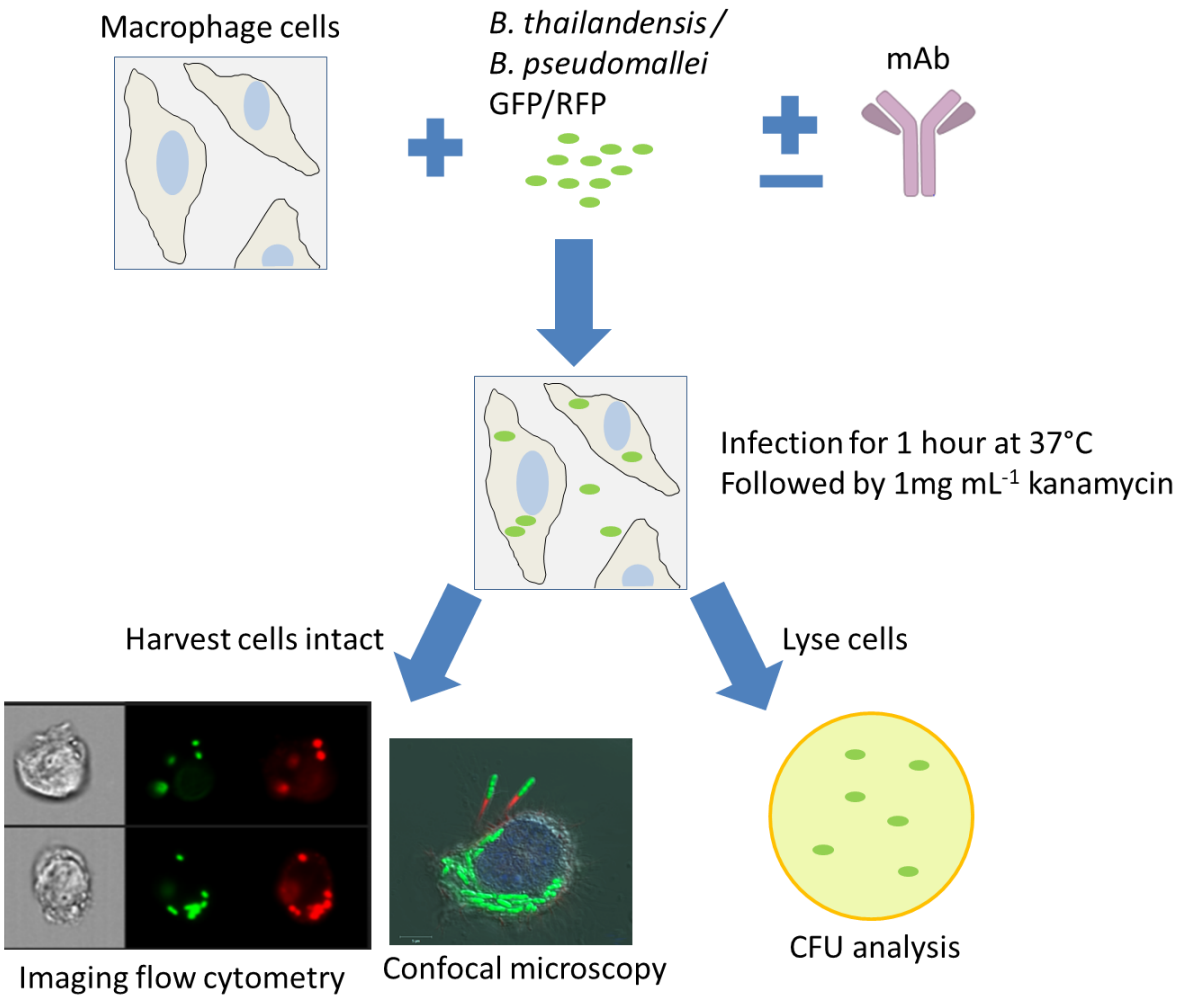

Figure 6. *In vitro* mAb opsonisation assay design.

The RAW 264.7 macrophage-like cell infection assay was selected as the primary method to analyse intracellular infection by *B. thailandensis* or *B. pseudomallei* (2.2.1. RAW cell infection assay.. *B. thailandensis* E555 and *B. pseudomallei* K96243 were cultured overnight in L-broth at 37°C with gentle shaking (2.3.2. Culture of *B. thailandensis* E555. 2.3.3. Culture of *B. pseudomallei* K96243.). The next day *B. thailandensis* and *B. pseudomallei* were diluted to 1_{x10}^{7} bacteria mL^{-1} in L-15 media using optical density (OD_{600} 0.172 and OD_{600} 0.4 respectively, equating to 1_{x10}^{8} bacteria mL^{-1}). RAW cells were infected with *B. thailandensis* or *B. pseudomallei* at a multiplicity of infection (MOI) of 5, antibody opsonised bacteria were previously incubated with monoclonal antibody for 30 minutes prior to infection of RAW cells. RAW cells were incubated with *B. thailandensis* or *B. pseudomallei* for an hour, the cell media was subsequently replaced with 1mg mL^{-1} kanamycin maintenance antibiotic to kill extracellular bacteria. Green or red fluorescent protein (GFP/RFP)

expressing *B. thailandensis* E555 and *B. pseudomallei* K96243 (pBHR4-groS-eGFP / RFP) were used in the RAW cell assay to visualise bacterial infection by imaging flow cytometry and confocal microscopy. Colony forming unit (CFU) analysis is the lysing of macrophage cells and the enumeration of bacteria on agar plates. RAW cells were lysed with distilled water and enumerated on L-agar, or alternatively harvested intact into 4% paraformaldehyde for fixation and analysis by imaging flow cytometry or confocal microscopy.

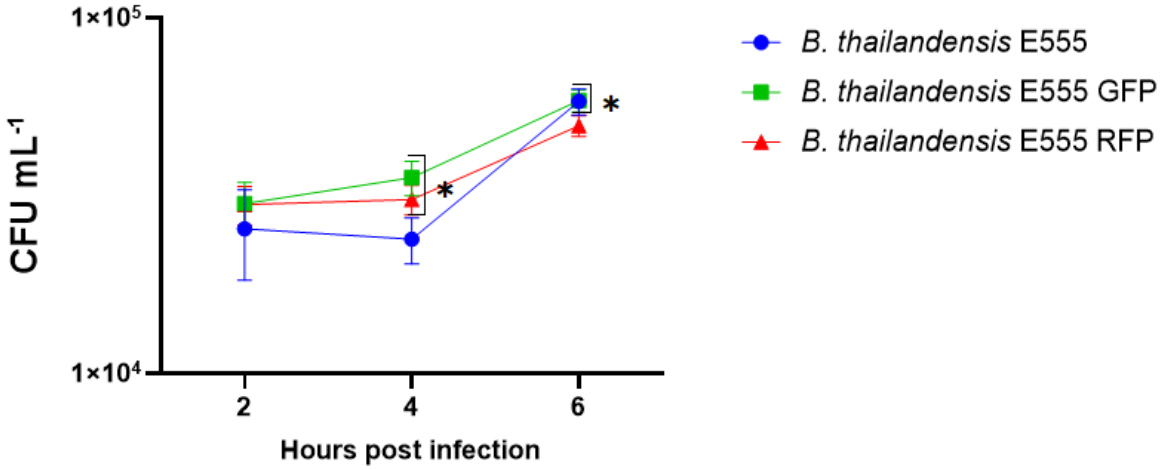

Figure 7. Infection of RAW cells with *B. thailandensis* E555, GFP and RFP.

RAW 264.7 cells were infected with *B. thailandensis* E555, GFP and RFP at a MOI of 5 for 1 hour at 37°C. Following infection, the cell culture media was replaced with culture media containing 1 mg mL^{-1} kanamycin antibiotic to kill extracellular bacteria. At 2, 4 and 6 hours post-infection the intracellular bacteria numbers were analysed by CFU enumeration on L-agar with triplicate technical replicates. Data are represented as the mean derived from two independent biological experiments, statistical data was generated from the data including all technical replicates (n=6) with error bars representing SD. No significant difference was observed at 2 hours post-infection. At 4 hours, both GFP and RFP were significantly different (P 0.0008 and P 0.0105 respectively). At 6 hours, GFP and the non-fluorescent E555 were significantly different to the RFP strain (P 0.0066 and P 0.0164 respectively) by Two-way ANOVA Tukey's multiple comparisons test.

Colony forming unit (CFU) data from the cell infection assay shows that *B. thailandensis* E555 does infect RAW264.7 cells, with intracellular replication over 6 hours post infection. Results show a similar profile of uptake and intracellular survival between GFP, RFP and wild type *B. thailandensis* E555. Some significant differences were observed at 4 and 6 hours post-infection (Figure 7). Although the differences are significant, the different fluorescent strains are not vastly different in CFU values. The data shows that the fluorescent strains each can infect cells to a similar or greater extent than the non-fluorescent stain. This demonstrates that the

GFP and RFP strains of *B. thailandensis* E555 are suitable alternatives for *in vitro* analysis of infection, when a fluorescent strain is required for analysis. Fluorescent protein expressing *B. thailandensis* strains are required for monitoring infection of cells by techniques such as confocal microscopy and imaging flow cytometry.

The RAW264.7 macrophage-like cell infection assay is the primary method that will be used to monitor infection *in vitro* and analysing monoclonal antibody opsonisation of *Burkholderia* strains.

Initial assay workup involved determining if a mAb can bind to *B. thailandensis*, this was achieved by imaging flow cytometry and an anti-CPS mAb 4VIH12. *B. thailandensis* E555 was opsonised with 4µg mL^{-1} of mAb 4VIH12 for 30 minutes prior to RAW cell infection. RAW cells were infected with the *B. thailandensis* at a MOI of 5 for 1 hour at 37°C to allow bacterial uptake. Following infection the cell culture media was removed and the RAW cells fixed and permeabilised (BD Cytofix/Cytoperm™ kit) following the manufacturer instructions. The permeabilised RAW cells were stained with 1µg mL^{-1} of Alexa Fluor® 555 Goat anti-mouse IgG (Biolegend) fluorescent secondary antibody for 30 minutes in permeabilisation wash buffer (BD Cytofix/Cytoperm™ kit), this was subsequently removed and replaced with PBS prior to imaging. . Alexa Fluor® 555 fluorescence was detected by imaging flow cytometry at x60 magnification with a 488 nm excitation laser, and the emission (565nm) detected in channel 3. Representative images were taken that showed 4VIH12 binds to *B. thailandensis,* and is bound to bacteria intracellularly within RAW cells (Figure 8 A).

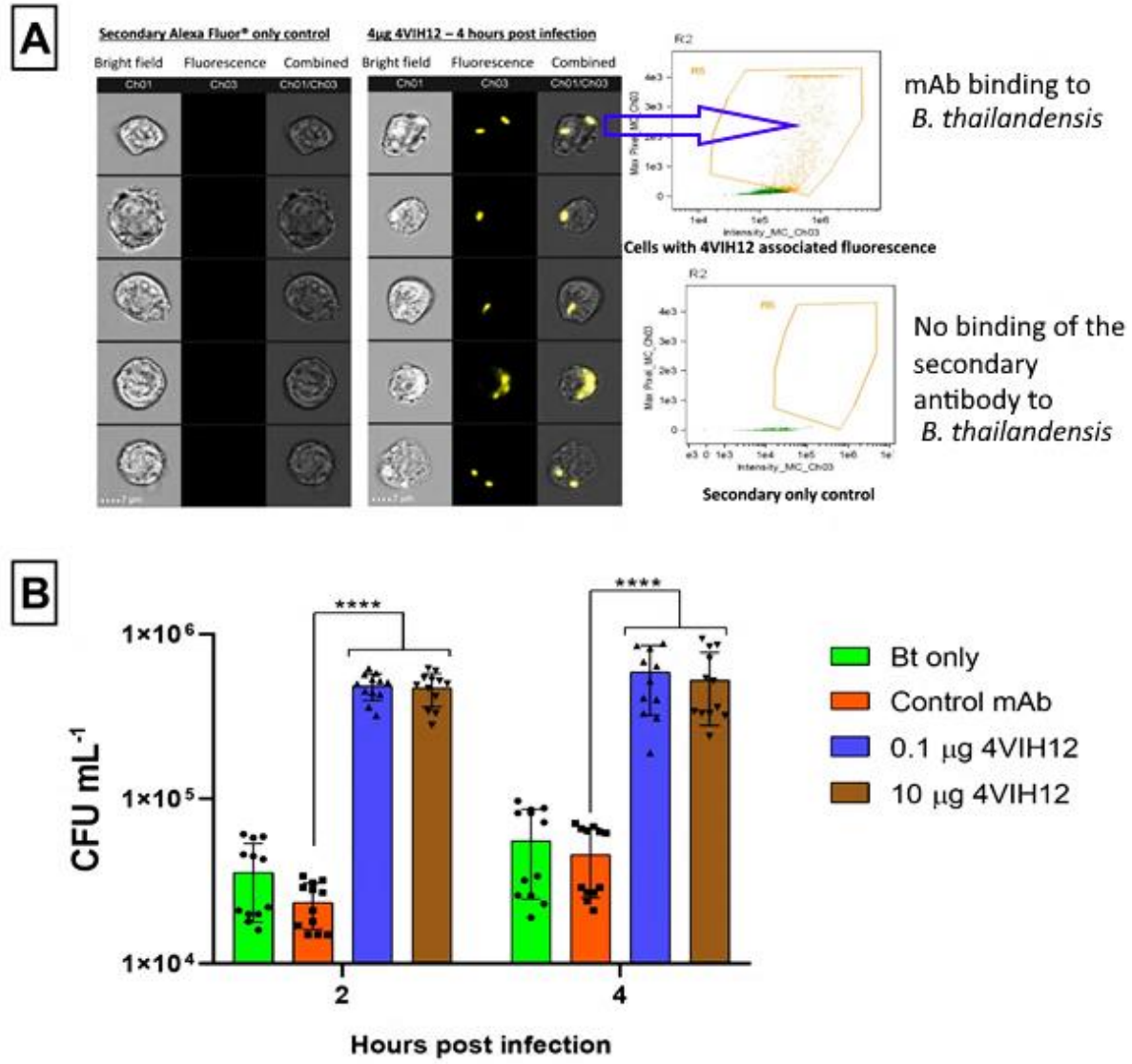

Figure 8. Imaging flow cytometry and CFU analysis of mAb 4VIH12.

A – Imaging flow cytometry representative images demonstrating mAb 4VIH12 binding to *B. thailandensis* E555 within RAW cells. The aim of this experiment was to determine if mAb 4VIH12 can bind to *B. thailandensis* E555 within RAW cells, this was achieved with the use of a fluorescent anti-IgG secondary antibody. *B. thailandensis* E555 at $5_{x10}{}^{6}$ CFU mL^{-1} was opsonised with 4 µg mL^{-1} of mAb 4VIH12 prior to RAW cell infection. RAW cells were infected with the *B. thailandensis* E555 at a MOI of 5, following infection the cells were fixed and permeabilised and subsequently stained with 1µg mL^{-1} of Alexa Fluor® 555 Goat anti-mouse IgG (Biolegend) fluorescent secondary antibody. Fluorescence was observed by imaging flow cytometry and representative images collected. **B** –The mAb 4VIH12 was added

to *B. thailandensis* E555 at 0.1 and 10 µg mL^{-1} prior to cell infection. RAW cells were then infected as described previously at an MOI of 5. RAW cells were lysed at 2 and 4 hours post-infection for CFU enumeration. Data are represented as the mean derived from two independent biological experiments, statistical data was generated from the data including all technical replicates (n=12) with error bars representing SD. **** P <0.0001 Two-way ANOVA Sidak's multiple comparisons test to control mAb.

The mAb 4VIH12 was also used to set up antibody opsonisation experiments, the mAb was used at two concentrations and two time points (Figure 8 B). *B. thailandensis* E555 was opsonised with 4VIH12 at 0.1 and 10 µg mL^{-1} for 30 minutes prior to cell infection. RAW cells were infected with opsonised *B. thailandensis* at a MOI of 5 for 1 hour at 37°C. Post-infection the media was changed and contained 1mg mL^{-1} kanamycin antibiotic to prevent extracellular bacterial growth. At 2 and 4 hours post-infection the media was removed and replaced with distilled water to lyse the RAW cells. The intracellular *B. thailandensis* were enumerated by serial dilution and culture on L-agar. A significant increase in bacterial uptake by RAWs was seen by CFU analysis at both 0.1 and 10 µg mL^{-1} of mAb 4VIH12 at either time point. This increase in CFU can be seen at 2 and 4 hours post-infection, from this data the 2 hour time point was selected for future opsonisation experiments. Later time points were not considered necessary for monitoring opsonisation. The 2 hour time point allows time for kanamycin killing of extracellular bacteria, and the data clearly shows this time point is suitable to see the mAb opsonisation effect. Later time points pose a risk of cell damage occurring due to the increase in intracellular bacteria associated with mAb opsonisation, the effect of later time points and mAb opsonisation will be determined in subsequent experiments.

Kanamycin is an aminoglycoside, considered to have low cell permeability (260) and often used as a maintenance antibiotic in cell infection assays to prevent extracellular bacterial replication. A high concentration of kanamycin (500µg - 1mg mL^{-1}) is typically used in *Burkholderia* macrophage-like cell infection assays, especially for early time points, to prevent extracellular replication of bacteria (15, 244, 250, 257). The concentration of kanamycin is reduced in some studies after an initial kill step,

this is due to concerns regarding potential intracellular accumulation. In this research project if any significant intracellular killing is observed in control infections over time, then a reduction in kanamycin will be investigated. The risk of reducing the kanamycin maintenance concentration is allowing extracellular bacterial replication. The effect of reducing kanamycin will be assessed in later experiments, especially where there will be additional anti-microbial compounds present alongside kanamycin.

3.3. Antibody opsonisation.

A panel consisting of three anti-CPS mAbs (4VIH12, 3VIE5 and 4VA5) and one anti-LPS mAb (CC6) were selected (Table 1) and investigated for opsonisation ability. The aim of this study is to down-select a mAb for incorporation into an antibody based therapy, generating a proof of principle antibody-antibiotic conjugate (AAC). Antibodies were tested *in vitro* and down-selected based on ability to opsonise *Burkholderia* strains in a cell infection assay. Opsonisation is a desired quality of the down-selected antibody, the function of an AAC relies upon antibody opsonisation to uptake antibiotic into infected cells.

Each mAb was tested in the RAW 264.7 macrophage-like cell infection assay (2.2.2. Monoclonal antibody opsonisation assay.). An overnight culture of *B. thailandensis* E555 or *B. pseudomallei* K96243 was diluted to 5_{x10}^{6} CFU mL^{-1}. The bacteria were opsonised with a range of mAb concentrations and a murine antibody isotype control at the highest concentration, for 30 minutes at 37°C prior to RAW cell infection. The RAW cells were infected with the opsonised bacteria at an MOI of 5 for 1 hour at 37°C, the cell culture media was subsequently removed and replaced with media containing 1mg mL^{-1} kanamycin maintenance antibiotic. The kanamycin prevents extracellular bacterial growth and after 2 hours the RAW cells are either harvested for imaging flow cytometry analysis or lysed for enumeration.

RAW cells were harvested into 4% paraformaldehyde by pipetting up and down, and *B. pseudomallei* samples left for a minimum of 48 hours for inactivation prior to analysis. A gating template was created and applied to all opsonisation experiments

using imaging flow cytometry. Fluorescent strains of *B. thailandensis* E555 GFP and *B. pseudomallei* K96243 RFP were excited with the 488nm and 561nm lasers respectively. GFP has an excitation and emission peak of 489nm and 511nm, whereas RFP has an excitation and emission peak of 555nm and 584nm. Fluorescence emission was detected with channel 2 and channel 4 on the imaging flow cytometer for GFP and RFP respectively. RAW cells were gated according to being in focus, single cells and containing bacterial fluorescence.

RAW cells analysed for CFU were lysed by replacing the culture media with distilled water until cell lysis occurred (checked by light microscopy). Upon cell lysis the bacteria were serial diluted and multiple dilutions plated onto L-agar spread plates, agar plates were incubated for a minimum of 24 hours until colonies can be accurately counted.

Table 1. Monoclonal antibodies evaluated in this study

Antibody	Target	Isotype	Species
4VIH12	CPS	IgG2b	Murine
3VIE5	CPS	IgG2b	Murine
4VA5	CPS	IgG1	Murine
CC6	LPS	IgG2a	Murine

CPS – capsule polysaccharide, LPS - lipopolysaccharide

3.3.1 Monoclonal antibodies opsonise *B. thailandensis* E555 in a RAW 264.7 cell infection model.

The first method to analyse antibody opsonisation was colony forming units (CFU) enumeration of *B. thailandensis* E555. Each monoclonal antibody was added to *B. thailandensis* at a concentration range from 0.1 ng mL^{-1} to 1 µg mL^{-1} (anti-CPS mAbs) and 10 ng ml^{-1} to 100 µg ml^{-1} (anti-LPS mAb). The aim of this experiment set was to determine the opsonisation ability of each mAb against *B. thailandensis* E555 in the RAW cell infection assay (2.2.2. Monoclonal antibody opsonisation assay.).

Opsonisation of each mAb was determined by an increase in intracellular bacteria analysed by both CFU (2.6.5. CFU analysis.) and imaging flow cytometry (2.6.3. Imaging flow cytometry.). Each experiment was performed in duplicate for both CFU and imaging flow cytometry. This initial opsonisation data set was then repeated with the high containment pathogen *B. pseudomallei*, generating a data set to select an antibody for further analysis based on opsonisation ability.

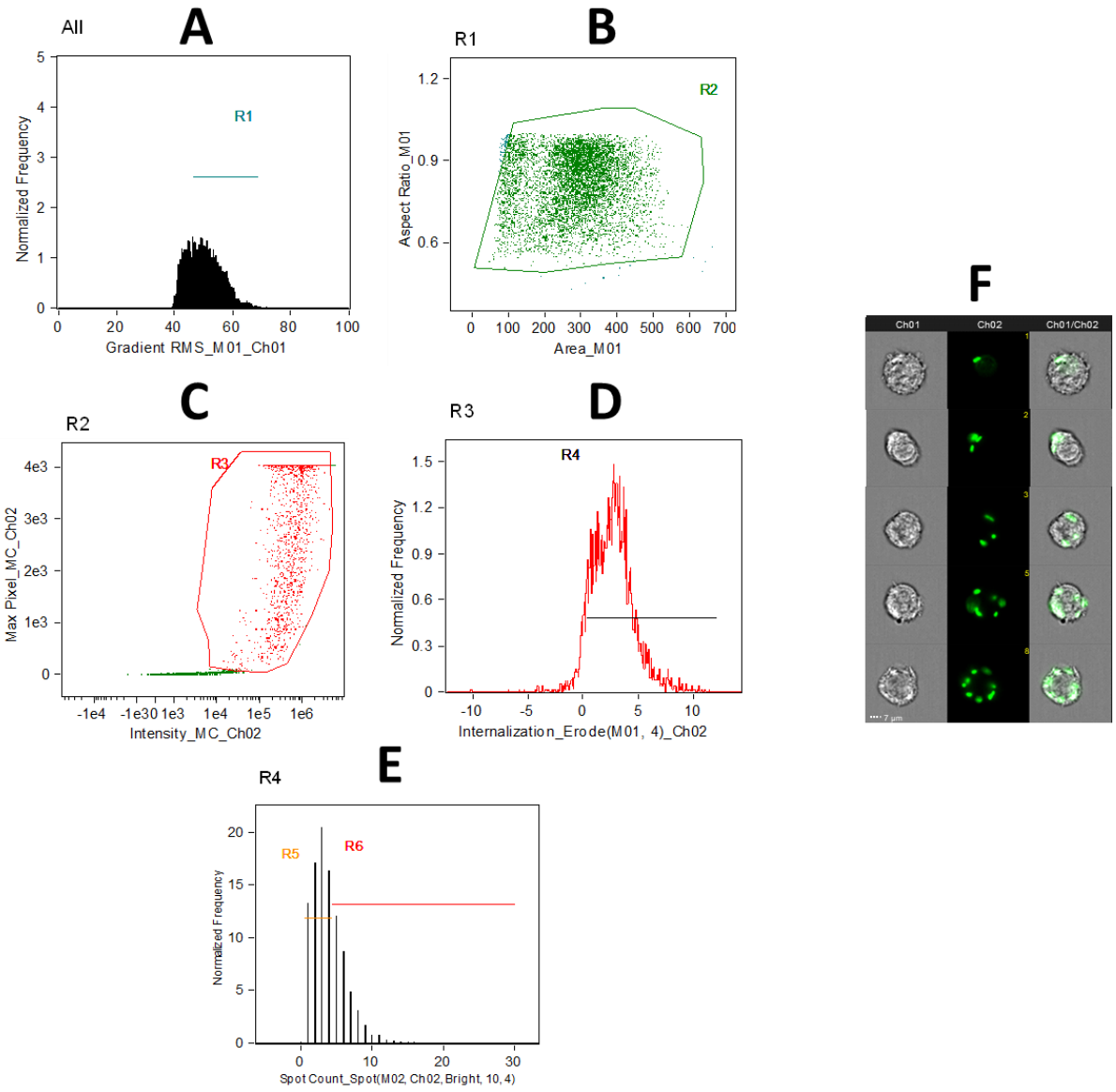

Figure 9. Imaging flow cytometry gating strategy for analysis of *B. thailandensis* GFP within RAW cells.

An analysis template was set up to be used on RAW cell infection assays involving *B. thailandensis* E555 GFP, the GFP has an excitation and emission peak of 489nm and 511nm respectively. Imaging flow cytometry was performed on the Amnis® ImageStream® X Mark II. All lasers used were set to full power (100 mW for 488nm laser), and x60 objective was used throughout. GFP excitation (peak of 489nm) was achieved with the 488nm laser and fluorescence emission (peak of 511nm) detected with channel 2. Additional bright field imagery of the RAW cell was applied throughout with channel 1. Cells were gated based on being in focus **(A)** and single cells **(B)** (10,000 cells gated). Cells associated with *B. thailandensis* E555 GFP were gated

(C) and an internalisation erode of 4 pixels applied to gate cells containing only intracellular *B. thailandensis* E555 GFP **(D)**. Spot count analysis **(E)** was applied to calculate high and low bacterial burden within cells. Spot count high and low cut off values were chosen by observing typical bacterial numbers present in opsonised and non-opsonised RAW cells, the aim of the cut off values was to give an indication of low and high bacterial burdens within the RAW cells. **(F)** Example images of spot counting *B. thailandensis* E555 GFP within RAW cells.

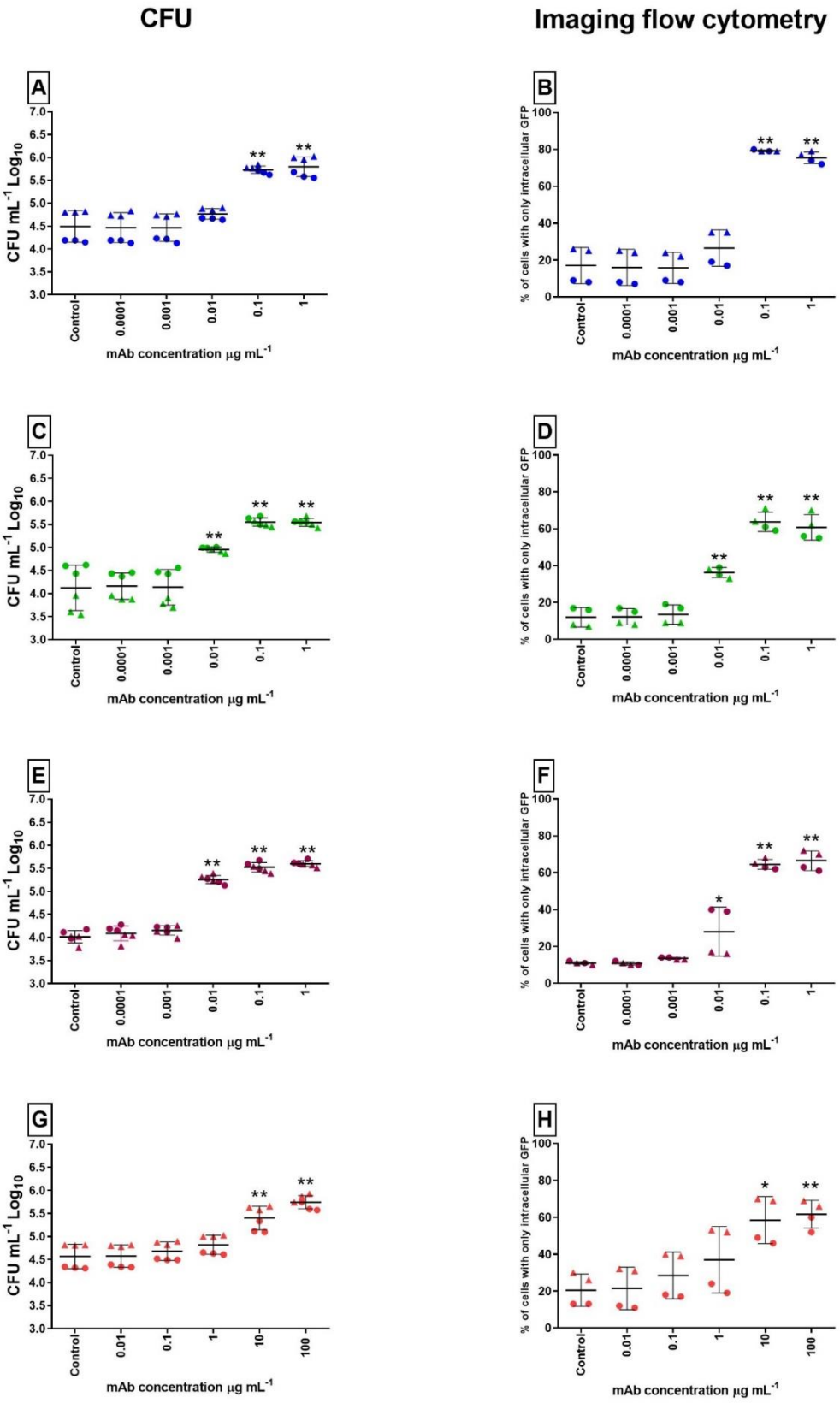

Figure 10. Monoclonal antibody opsonisation of *B. thailandensis* E555 by CFU and imaging flow cytometry.

A-B 4VIH12, **C-D** 3VIE5, **E-F** 4VA5, **G-H** CC6. *B. thailandensis* E555 (GFP expressing strain for imaging flow cytometry) was opsonised at a range of concentrations of mAb for 30 minutes at 37°C prior to RAW cell infection. RAW cells were infected for 1 hour at 37°C, the bacteria were subsequently removed and replaced with 1mg mL^{-1} kanamycin maintenance media for 2 hours. At this time point the RAWs were lysed with distilled water and the intracellular bacteria analysed by serial dilution and CFU enumeration on L-agar. Alternatively, the RAW cells were harvested intact into 4% paraformaldehyde and analysed by imaging flow cytometry. Data are represented as the mean derived from two independent biological experiments (represented by different symbols), statistical data was generated from the data including all technical replicates (n=6 for CFU and n=4 for imaging flow cytometry) with error bars representing SD. Controls consist of a non-specific isotype control mAb at the highest concentration. ** P <0.001, * P <0.01 One-way ANOVA Dunnett's multiple comparisons test to control mAb.

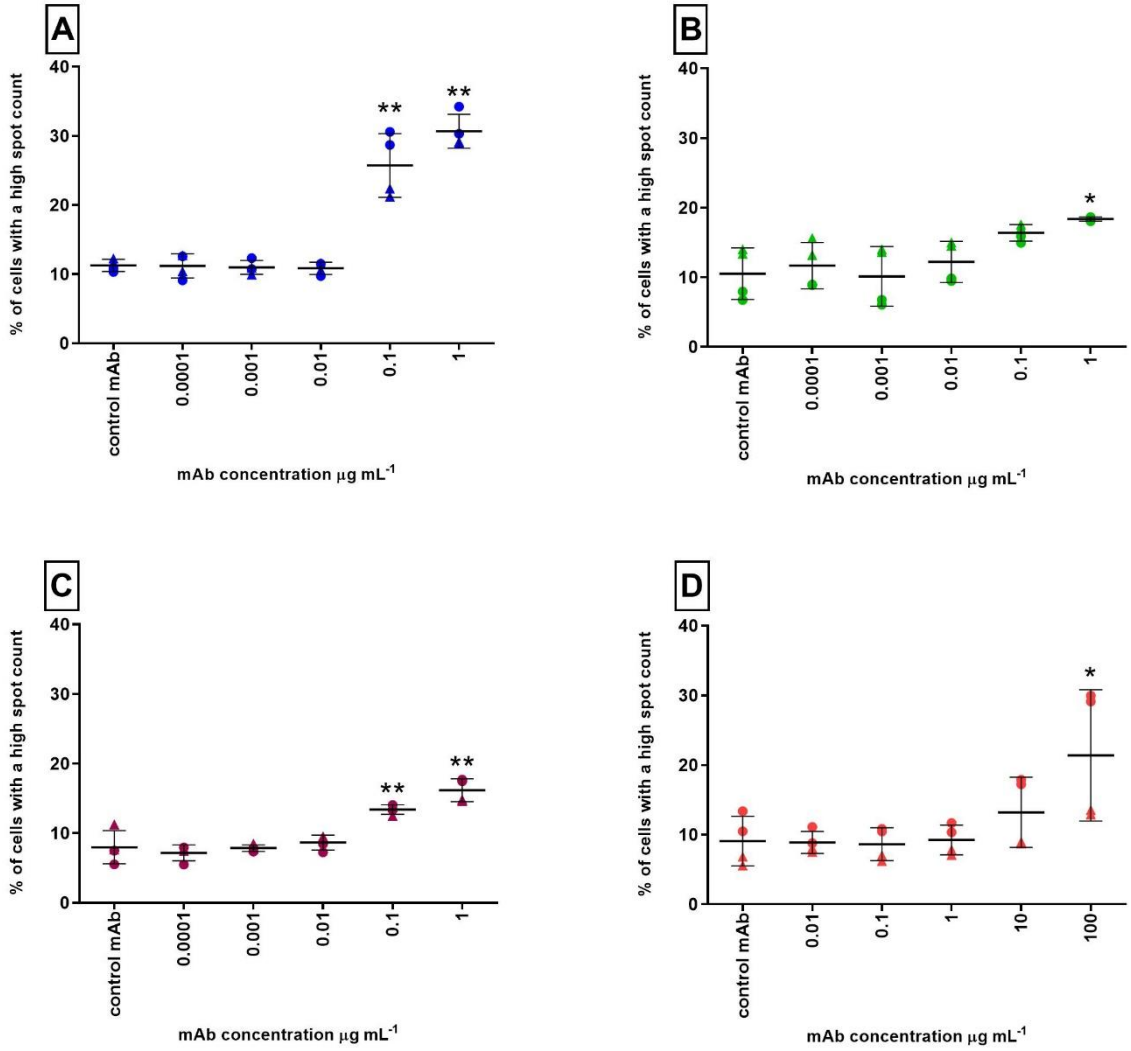

Figure 11. Bacterial fluorescent spot count profiling of intracellular *B. thailandensis* E555 by Imaging flow cytometry.

A- 4VIH12, **B**- 3VIE5, **C**- 4VA5, **D**- CC6. Imaging flow cytometry opsonisation data was further analysed to determine intracellular spot counting. A spot counting gate was applied to the channel 2 *B. thailandensis* E555 GFP fluorescence, this gated RAW cells into a high or low intracellular fluorescence spot count. Spot count high and low cut off values were chosen by observing typical bacterial numbers present in opsonised and non-opsonised RAW cells, the aim of the cut off values was to give an indication of low and high bacterial burdens within the RAW cells. Intracellular bacterial fluorescent spots were analysed comparing mAb opsonised *B. thailandensis* E555 GFP and isotype control mAbs. Data are represented as means of all technical replicates (n=4) derived from two independent biological experiments, each experiment is represented by a different symbol shape. Error bars represent

SD of all technical replicates. ** P <0.001, * P <0.01 One-way ANOVA Dunnett's multiple comparisons test to control mAb.

CFU data (2.6.5. CFU analysis.) demonstrates that each mAb is opsonising *B. thailandensis* E555 in a RAW264.7 macrophage-like infection assay (Figure 10). Each mAb increased the CFU count in a dose dependant manner compared to an isotype control mAb at the highest concentration. Two of the anti-CPS mAbs showed a significant increase in *B. thailandensis* CFU from 0.01 µg ml^{-1} with the third anti-CPS mAb from 0.1 µg mL^{-1}. There is a clear difference in CFU between the anti-CPS mAbs and the anti-LPS mAb. The concentration of anti-LPS mAb required to achieve a significant increase in *B. thailandensis* CFU is 10µg mL^{-1}, thus demonstrating a lower opsonisation ability in this RAW cell infection assay when compared to anti-CPS mAbs.

Analysis of intracellular bacteria in a macrophage-like infection assay by CFU is a well-established method and widely published in the literature. In order to gain a greater insight into bacterial infection on an individual cell level, techniques such as imaging flow cytometry can be applied. A *B. thailandensis* E555 strain expressing GFP was used to enable visualisation of intracellular bacteria. Imaging flow cytometry was performed on RAW 264.7 cells harvested intact from a *B. thailandensis* E555 GFP infection assay. The analysis of imaging flow cytometry was based upon a gating strategy (Figure 9) which ultimately results in selection of cells that have only intracellular *B. thailandensis*, the output of which is a percentage of cells with only intracellular *B. thailandensis* E555 GFP.

All mAbs analysed for opsonisation by imaging flow cytometry (2.6.3. Imaging flow cytometry.) showed a dose dependant ability to significantly increase the percentage of cells infected with *B. thailandensis* (Figure 10). Two of the anti-CPS mAbs showed a significant increase in intracellular *B. thailandensis* from 0.01 µg mL^{-1} of mAb, with the third anti-CPS mAb from 0.1 µg mL^{-1} of mAb. Again there is a clear difference between the anti-CPS mAbs and the anti-LPS mAb, mirroring the result seen by CFU analysis. Imaging flow cytometry reveals that when the bacteria are opsonised with mAb there is a significant increase in the percentage of cells infected with *B. thailandensis* (Figure 10). Additionally, spot count profiles show there is a significant

increase in the average number of intracellular bacteria per cell when opsonised with 1 μg mL^{-1} of anti-CPS mAb or 100 μg mL^{-1} of anti-LPS mAb (Figure 11). Spot count analysis on the imaging flow cytometry data allows individual bacteria to be counted in each RAW cell, therefore adding to our understanding of the effect of mAb on intracellular levels of *B. thailandensis*.

Comparing the CFU data and Imaging flow cytometry analysis, the percentage of intracellular bacteria shows a near identical profile of mAb opsonisation compared to the CFU data. This gives increased confidence in the data, since the two techniques (CFU and imaging flow cytometry) are fundamentally different in the way results are generated. CFU analysis involves the lysis of a population of cells, and does not discriminate between extracellular or intracellular bacteria. In comparison, imaging flow cytometry analyses individual intact cells, and with the use of a gating strategy (Figure 9), only analyses intracellular bacteria. Imaging flow cytometry also allows additional information to be generated, such as spot counting of individual bacteria within a large pool of infected cells. Additional data could be analysed from the imaging flow cytometry, such as fluorescence intensity values. This is a potential alternative to percentage data, which can be difficult to analyse statistically. Future studies should investigate additional data that can be collected from imaging flow cytometry macrophage infection assays, and compare this to the percentage of cell infection data generated in this study.

3.3.2 Monoclonal antibody opsonisation of *B. pseudomallei* K96243 in a RAW 264.7 macrophage-like cell infection model.

The monoclonal antibody panel was assessed to determine if the opsonisation ability demonstrated for *B. thailandensis* E555 can also be observed with the highly pathogenic ACDP hazard group III *B. pseudomallei* K96243. The clinical isolate *B. pseudomallei* K96243 was chosen as a representative strain for testing antibody opsonisation of *B. pseudomallei* (2.3.3. Culture of *B. pseudomallei* K96243.). The opsonisation of *B. pseudomallei* K96243 was determined by counting colony forming units (2.6.5. CFU analysis.) and by imaging flow cytometry (2.6.3. Imaging flow cytometry.) (Figure 13). A RFP expressing strain of *B. pseudomallei* K96243 was

used to enable visualisation of the bacterium within RAW cells (Figure 12). The RAW cell infection assay was performed in high containment laboratories using the same concentrations of RAW cells, bacteria and antibody as for *B. thailandensis* assays.

CFU data shows that opsonisation of *B. pseudomallei* K96243 by each mAb is comparable to the data for *B. thailandensis* E555 (2.6.5. CFU analysis.). Each of the three anti-CPS mAbs significantly increased *B. pseudomallei* uptake into RAW cells from 1 µg mL^{-1} of mAb, with the anti-CPS mAb significantly increasing uptake from 10 µg mL^{-1} when compared to an isotype control mAb (Figure 13).

Imaging flow cytometry data is more variable for *B. pseudomallei* opsonisation compared to *B. thailandensis* opsonisation. Although, each mAb still demonstrates opsonisation of *B. pseudomallei* from 1 µg mL^{-1}. Variability between replicates is more pronounced for *B. pseudomallei* data, as seen by a clear separation between biological replicates in the imaging flow cytometry data. Although, technical replicates in the same experiment are consistent. There is however a difference in the concentrations of mAb that are significantly opsonising between the CFU and imaging flow cytometry data for *B. pseudomallei*. This difference is likely due to the working practices in high containment laboratories, which is adding more variability to the data between biological replicates. The differences in the mAb opsonisation data between *B. thailandensis* and *B. pseudomallei* is discussed further in the discussion section.

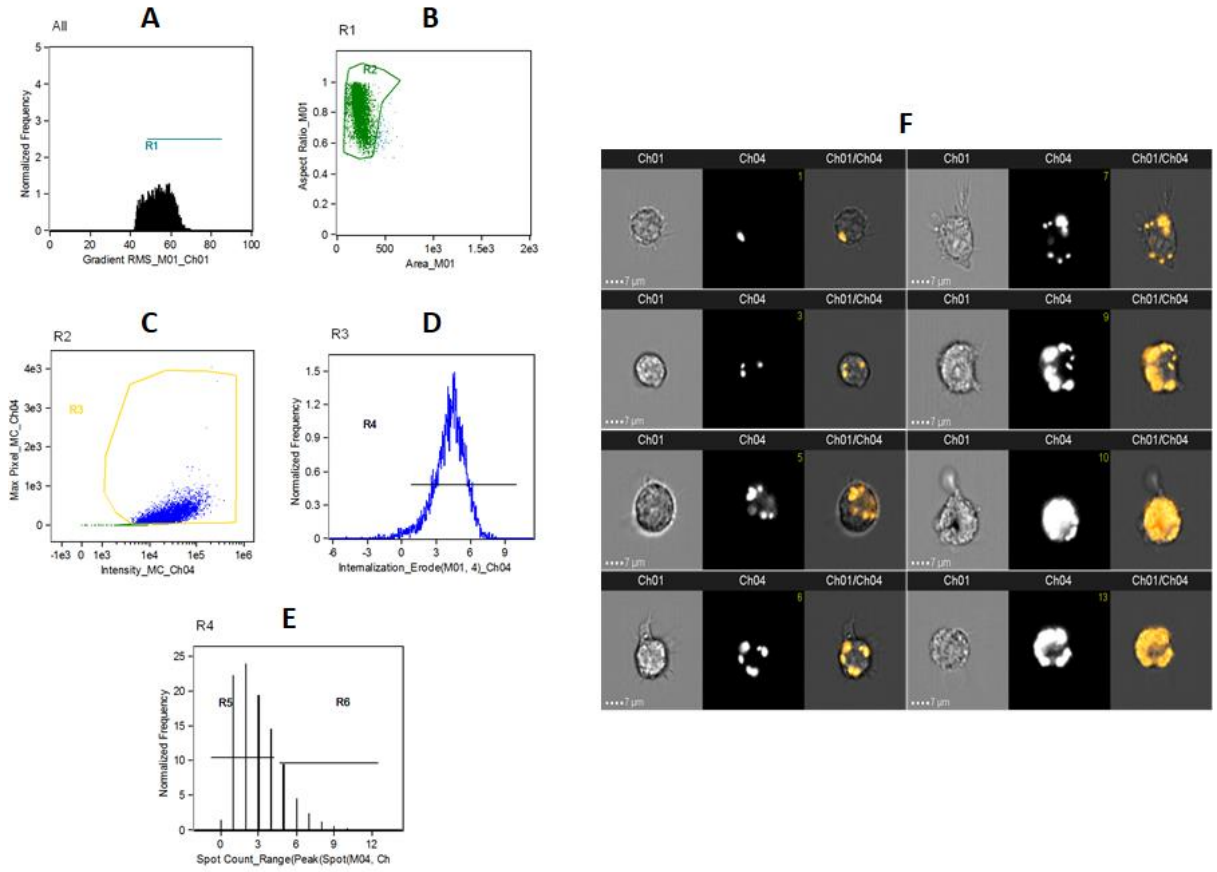

Figure 12. Imaging flow cytometry gating strategy for *B. pseudomallei* RFP within RAW cells.

An analysis template was set up to be used on RAW cell infection assays involving *B. pseudomallei* K96243 RFP. Imaging flow cytometry was performed on the Amnis® ImageStream® X Mark II. All lasers used were set to full power (200 mW for 561nm laser), and x60 objective was used throughout. RFP excitation (peak of 555nm) was achieved with the 561nm laser and fluorescence emission (peak of 584nm) detected with channel 4. Additional bright field imagery of the RAW cell was applied throughout with channel 1. Cells were gated based on being in focus **(A)** and single cells **(B)** (10,000 cells gated). Cells associated with *B. pseudomallei* K96243 RFP were gated **(C)** and an internalisation erode of 4 pixels applied to gate cells containing only intracellular *B. pseudomallei* K96243 RFP **(D)**. Spot count analysis **(E)** was applied to calculate high and low bacterial burden within cells. Spot count high and low cut off values were chosen by observing typical bacterial numbers present in opsonised and non-opsonised RAW cells, the aim of the cut off values was to give an indication of low and high bacterial burdens within the RAW cells. **(F)** Example images of spot counting *B. pseudomallei* K96243 RFP within RAW cells.

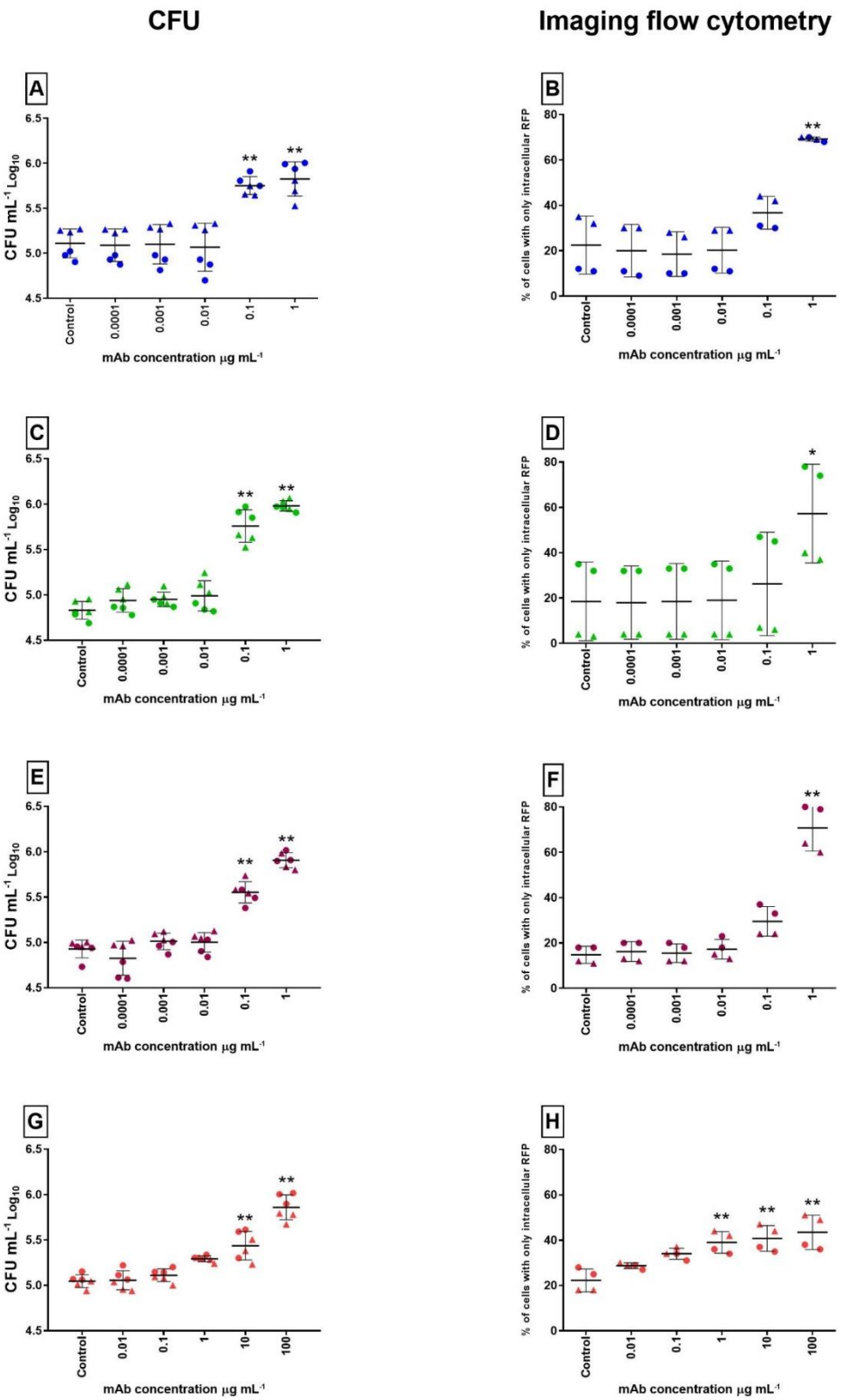

Figure 13. Monoclonal antibody opsonisation of *B. pseudomallei* K96243 by CFU and imaging flow cytometry.

A-B 4VIH12, **C-D** 3VIE5, **E-F** 4VA5, **G-H** CC6. *B. pseudomallei* K96243 (RFP expressing strain for imaging flow cytometry) was opsonised at a range of concentrations of mAb for 30 minutes at 37°C prior to RAW cell infection. RAW cells were infected for 1 hour at 37°C, the bacteria were subsequently removed and replaced with 1mg mL^{-1} kanamycin maintenance media for 2 hours. At this time point the RAWs were lysed with distilled water and the intracellular bacteria analysed by serial dilution and CFU enumeration on L-agar. Alternatively, the RAW cells were harvested intact into 4% paraformaldehyde and analysed by imaging flow cytometry 48 hours later. Data are represented as the mean derived from two independent biological experiments (represented by different symbols), statistical data was generated from the data including all technical replicates (n=6 for CFU and n=4 for imaging flow cytometry) with error bars representing SD. Controls consist of a non-specific isotype control mAb at the highest concentration. ** P <0.001, * P <0.05 One-way ANOVA Dunnett's multiple comparisons test to control mAb.

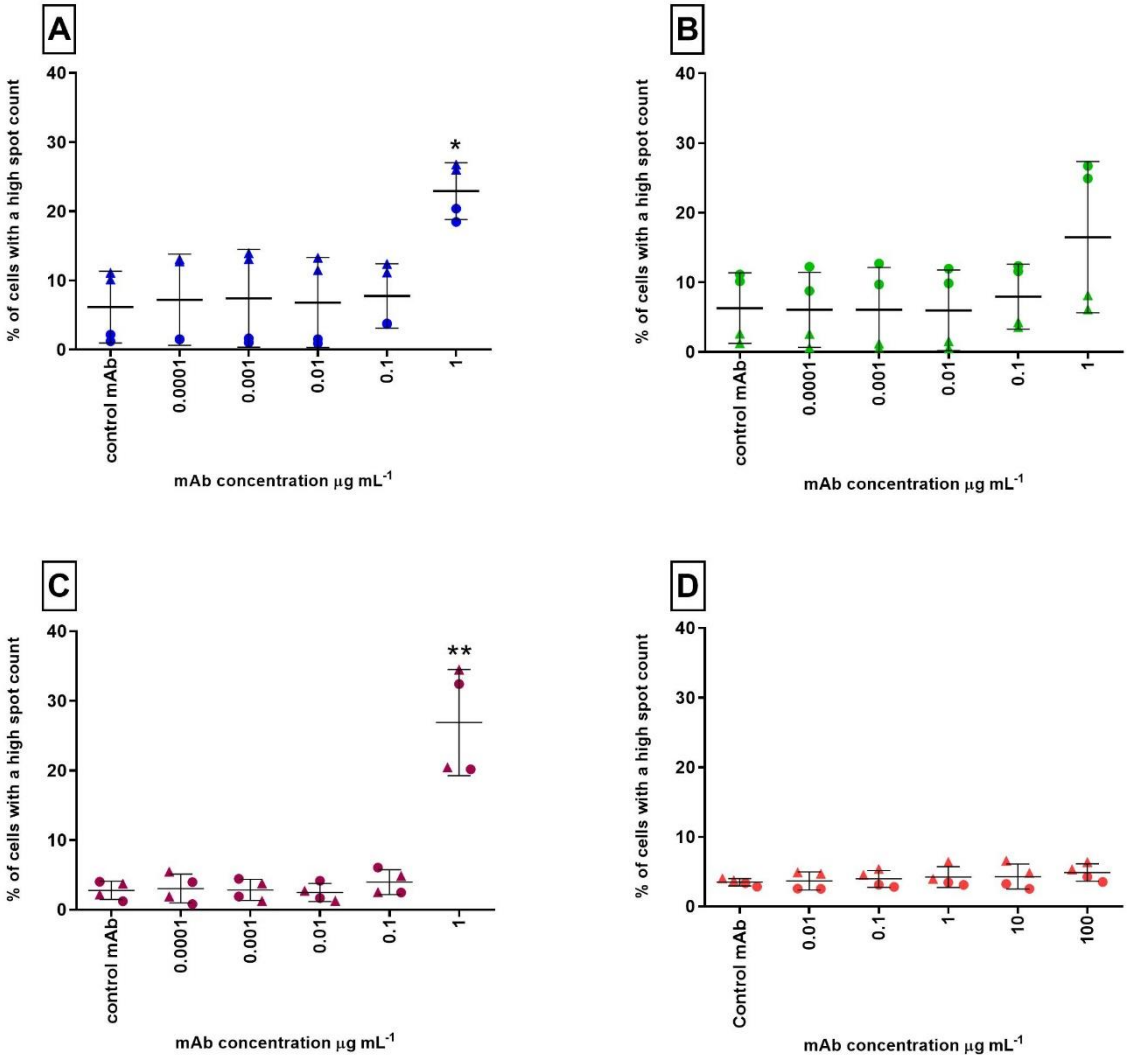

Figure 14. Bacterial fluorescent spot count profiling of intracellular *B. pseudomallei* K96243 by Imaging flow cytometry.

A – 4VIH12, **B –** 3VIE5, **C –** 4VA5 and **D –** CC6. Imaging flow cytometry opsonisation data was further analysed to determine intracellular spot counting. A spot counting gate was applied to the channel 4 *B. pseudomallei* K96243 RFP fluorescence, this gated RAW cells into a high or low intracellular fluorescence spot count. Spot count high and low cut off values were chosen by observing typical bacterial numbers present in opsonised and non-opsonised RAW cells, the aim of the cut off values was to give an indication of low and high bacterial burdens within the RAW cells. Intracellular bacterial fluorescent spots were analysed comparing mAb opsonised *B. pseudomallei* K96243 RFP and isotype control mAbs. Data are represented as means of technical replicates (n=4) derived from two independent biological experiments, each experiment is represented by a different symbol shape. Error bars

represent SD of all technical replicates. ** P <0.001, * P <0.01 One-way ANOVA Dunnett's multiple comparisons test to control mAb.

In summary, opsonisation data for both *B. thailandensis* and *B. pseudomallei* demonstrates that all 4 mAbs are opsonising. Significantly, the anti-CPS mAbs (4VIH12, 3VIE5 and 4VA5) are capable of opsonising at a lower concentration compared to the LPS mAb (CC6). This data has been used to down select mAb 3VIE5 for further investigation as a potential therapeutic antibody for melioidosis.

Although each anti-CPS mAb displayed very similar opsonisation data, antibody binding kinetic data from an Octet® RED Biolayer interferometry platform (ForteBio Sartorius) indicated that 3VIE5 has more favourable binding kinetics when compared to the other anti-CPS mAbs (generated by Global Access Diagnostics). The initial experiment on the Octet red was to determine if the heat killed *B. thailandensis* E555 can be immobilised onto the APC (aminopropylsilane) coated glass biosensor tip, the tip of the biosensor is where the antibody-antigen interaction takes place. The antibody-antigen interaction is detected by bio-interferometry on the Octet red machine, by measuring the interference pattern of white light passing through the glass sensor. This creates an off (K_{off}) and on (K_{on}) rate from antibody binding to the antigen on the sensor, along with an affinity constant (K_D) for each antibody interaction with the immobilised antigen (appendix A.3.1). A range of dilutions of heat killed *B. thailandensis* were assessed for binding onto the biosensor tip, a signal increase is observed during the loading phase indicating antigen coating the biosensor tip. A 1 in 400 dilution of heat killed *B. thailandensis* E555 was chosen as an optimum dilution based on this biosensor loading data (data not shown). This 1 in 400 dilution of antigen was then used to assess each monoclonal antibody for antigen interaction on the Octet biosensor. No interaction was observed for mAb CC6, whereas mAbs 4VIH12 and 4VA5 bound to the antigen in a nanomolar concentration range (K_D) (appendix A.3.1). The mAb 3VIE5 displayed the best affinity to the antigen, with a 690 pM affinity (K_D) to the antigen on the Octet biosensor. Therefore mAb 3VIE5 was selected as the mAb with the most favourable binding kinetics to take forward for development of an AAC.

The opsonisation experiments in this chapter were performed without addition of complement. Complement and the interaction with antibody, can increase bacterial

opsonisation and uptake into phagocytic cells, via the classical complement pathway. The classical complement pathway and the resulting complement cascade can result in effects such as increases in inflammation, opsonisation and cell lysis (via formation of a membrane attack complex) (136). The addition of complement could increase bacterial uptake, via the classical pathway and interaction with complement receptors on the present on the phagocytic cell. The addition of complement to the macrophage infection assay would better reflect antibody opsonisation of *B. pseudomallei in vivo*. It was decided to not add complement at this stage and selection of an antibody was based on antibody opsonisation alone. Future studies should investigate the effects of complement with mAb 3VIE5 on opsonisation and bacterial killing, especially in primary macrophage cells which are likely to be a more realistic model of the effects of complement *in vivo*.

3.4. 3VIE5 opsonisation ability is dependent on FcγRs CD16 and CD32.

To further characterise the down selected mAb 3VIE5, the effect of blocking CD16 and CD32 on opsonisation was investigated in a RAW cell infection assay (2.2.5. Blocking of CD16 and CD32.). The aim in this experiment was to determine the role of CD16 and CD32 in mAb 3VIE5 opsonisation, and if blocking these receptors will effect opsonisation of *B. thailandensis* E555 by RAW cells. RAW cells were pre-incubated with 1 µg of TruStain FcX™ (anti-mouse CD16/CD32) (Biolegend) for 15 minutes at 37°C (a control consisted of untreated cells), prior to cell infection. Cells were infected with 3VIE5 opsonised (1 and 0.1 µg ml^{-1}) *B. thailandensis* E555 at a MOI of 5 for 1 hour at 37°C, with 1 µg of TruStain FcX™ also present in the cell culture media. Post-infection the bacterial culture media was replaced with 1 mg mL^{-1} kanamycin antibiotic maintenance media, and the RAW cells incubated for 2 hours at 37°C. After the 2 hour incubation, RAW cells were harvested into 4% paraformaldehyde and analysed by imaging flow cytometry, using the same method and gating strategy as previously described for analysing antibody opsonisation of *B. thailandensis* GFP. Imaging flow cytometry was performed on the Amnis® ImageStream® X Mark II. All lasers used were set to full power (100 mW for 488nm laser), and x60 objective was used throughout. GFP excitation (peak of 489nm) was achieved with the 488nm laser and fluorescence emission (peak of 511nm) detected with channel 2. Additional bright field imagery of the RAW cell was applied throughout

with channel 1. RAW cells were gating according to being in focus, single cells and cells associated with GFP fluorescence. The result is a percentage of RAW cells with associated GFP fluorescence in cells treated with TruStain FcX™ (Biolegend) compared to cells without treatment. The mAb control is an isotype control antibody. The mAb 3VIE5 was used at 1 and 0.1 µg ml^{-1} which from previous data is a concentration that opsonises *B. thailandensis*, the control mAb was used at 1 µg ml^{-1}. CD16 and CD32 are the FcγR III and FcγR II which will both bind the IgG2b mAb 3VIE5, although the mAb will still be able to opsonise via the FcγR I (CD64) (139).

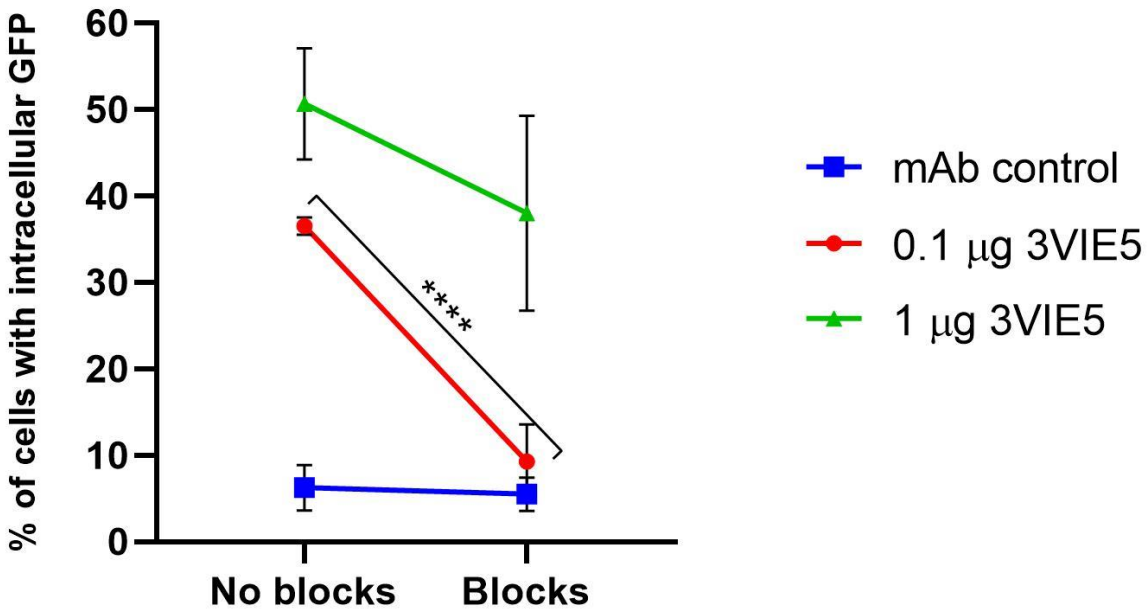

Figure 15. The effect of anti-Fc mAbs on 3VIE5 opsonisation of *B. thailandensis*.

The RAW cell Fc receptors CD16 (FcγRIII) and CD32 (FcγRII) were blocked with 1 µg of TruStain FcX™ (anti-mouse CD16/CD32) (Biolegend) in a RAW cell infection assay with *B. thailandensis* E555 GFP. RAW cells were infected at a MOI of 5 and mAb 3VIE5 was used at 0.1 and 1 µg mL^{-1} concentrations, an isotype control antibody was used at 1µg mL^{-1}. The effect of CD16 and CD32 on mAb 3VIE5 opsonisation of *B. thailandensis* E555 by RAW cells was determined by imaging flow cytometry analysis. RAW cells infected with *B. thailandensis* E555 GFP were analysed by imaging flow cytometry using the gating strategy developed from previous opsonisation studies. Data are represented as means of technical replicates (n=3) derived from two independent biological experiments. Error bars represent SD

of all technical replicates. **** P <0.0001 Two way ANOVA Tukey's multiple comparisons test.

Blocking of CD16 and CD32 reduces the ability of 3VIE5 to opsonise *B. thailandensis* E555 in a RAW 264.7 macrophage-like assay (Figure 15). At 0.1 µg mL^{-1} 3VIE5 is opsonising, shown by an increase in the percentage of cells infected compared to the isotype control antibody. When CD16 and CD32 blocks are present, the opsonisation ability of 3VIE5 at 0.1 µg mL^{-1} is reduced, and the cell infection level is comparable to the control mAb. The opsonisation ability of 3VIE5 is then reinstated at 1 µg mL^{-1} to a level comparable with no Fc blocks.

This data demonstrates that FcγRII and III are at least partly responsible for the mAb based opsonisation in the RAW cell infection assay. The ability of an increased concentration of 3VIE5 to overcome the FcγR inhibition could be due to the mAb binding to another Fc receptor such as FcγRI, or 3VIE5 outcompeting the CD16 and CD32 blocking antibody. This data builds upon the CFU and imaging flow cytometry opsonisation data, further characterising 3VIE5 opsonisation in the RAW cell assay.

3.5. The effect of mAb 3VIE5 on bacterial replication.

The aim here is to determine the effect of mAb 3VIE5 on bacterial replication, this will determine the effect of 3VIE5 mAb alone on bacteria in culture. This data will inform future studies using high concentrations of 3VIE5 mAb in bacterial culture. The effect of mAb 3VIE5 on replication of *B. thailandensis* and *B. pseudomallei* cultures was assessed by optical density readings over 24 hours within an incubating plate reader at 37°C (2.6.7. Minimum inhibitory concentration (MIC).). The mAb 3VIE5 was diluted from 100 µg mL^{-1} to 0.19 µg mL^{-1} on a 96 well culture plate. An overnight culture of *B. thailandensis* or *B. pseudomallei* was diluted to a concentration of $1x10^6$ CFU mL^{-1}, and 100 µl added to each well of the culture plate containing mAb 3VIE5. The 96 well culture plate was incubated for 24 hours at 37°C with automated OD readings every 15 minutes. A control culture plate consisted of an isotype control mAb diluted to the same concentrations as mAb 3VIE5.

Additionally, each culture plate contained positive and negative controls, consisting of bacteria only and media only controls respectively.

High concentrations of mAb 3VIE5 reduced *B. thailandensis* E555 OD compared to an isotype control mAb (Figure 16). The effect can be seen by a mAb 3VIE5 concentration of 6.25 μg mL^{-1} or greater reducing the bacterial OD at 24 hours, from a bacterial control OD of 0.6 to an OD of 0.3 for 3VIE5 treated groups. The control mAb shows little effect apart from at two concentrations where there is a trend for a reduction in OD. The reduction in OD is not seen at the highest mAb concentrations, this effect therefore seems to be an artefact of the experiment and not an antibody dose related effect. Visual inspection of the plate at all mAb 3VIE5 concentrations tested there is no inhibition of bacterial replication, therefore according to Clinical and Laboratory Standards Institute (CLSI) guidelines (245) there is no minimum inhibitory concentration (MIC) value of mAb 3VIE5 in this data.

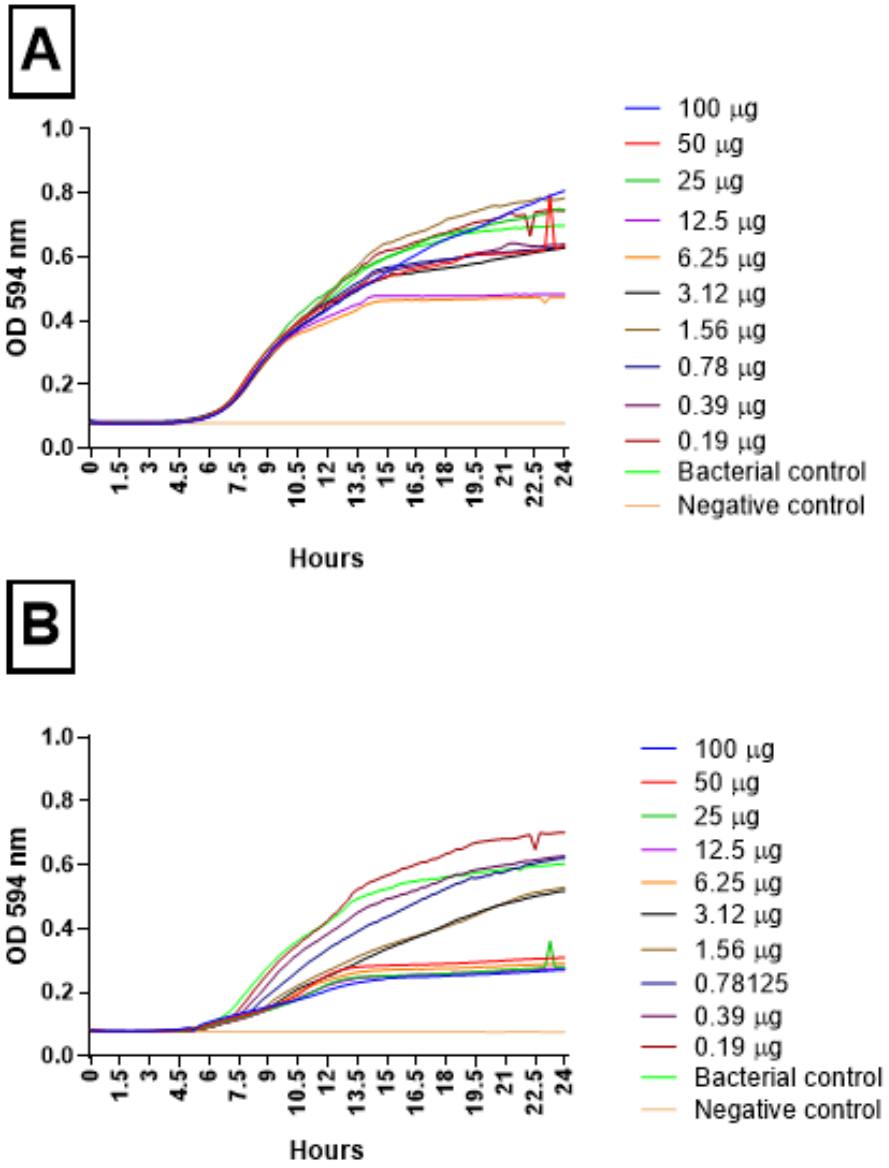

Figure 16. *B. thailandensis* replication curves with dilutions of mAb.

A – Isotype control mAb, **B** – mAb 3VIE5. The isotype control mAb and mAb 3VIE5 were diluted in a 96 well micro culture plate, to this plate a $1_{x10}6$ CFU mL^{-1} of *B. thailandensis* E555 culture was added in L-broth. An incubating plate reader was used to take optical density readings at 594nm every 15 minutes for 24 hours at 37°C. Controls consisted of a *B. thailandensis* only control and a negative L-broth only control. Data are represented as means of technical replicates (n=4) derived from two independent biological experiments.

The same method was applied to *B. pseudomallei* culture and addition of 3VIE5 has a similar effect (Figure 17), although the reduction in OD is not as great compared to the *B. thailandensis* data. With 3VIE5 concentrations of 6.25 µg mL^{-1} or greater there is a trend for reduced *B. pseudomallei* replication, from a bacterial control OD of 0.73 down to an OD of between 0.53 and 0.58 with 3VIE5 treated groups. Whereas the control mAb has no effect on the replication of *B. pseudomallei* at the concentrations tested. There was no inhibition of bacterial replication visible by observing the 96 well culture plate (2.6.7. Minimum inhibitory concentration (MIC).), therefore there was no MIC value for mAb 3VIE5 in this experiment.

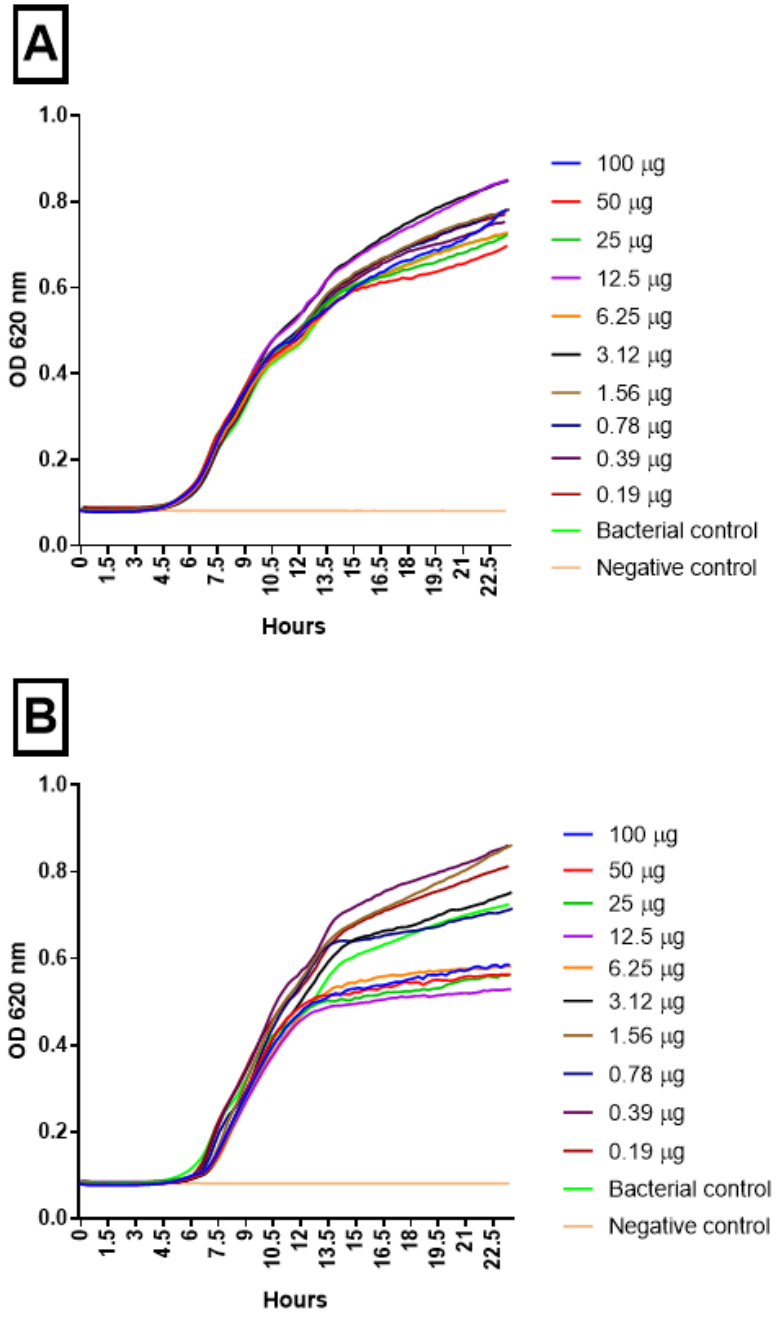

Figure 17. *B. pseudomallei* replication curves with dilutions of mAb.

A – Isotype control mAb, **B** – mAb 3VIE5. The isotype control mAb and mAb 3VIE5 were diluted in a 96 well micro culture plate, to this plate a $1_{x10}6$ CFU mL^{-1} of *B. pseudomallei* K96243 culture was added in L-broth. An incubating plate reader was used to take optical density readings at 620nm every 15 minutes for 24 hours at 37°C. Controls consisted of a *B. pseudomallei* only control and a negative L-broth only control. Data are represented as means of technical replicates (n=8) derived from two independent biological experiments.

3.6. Investigating primary cells for opsonisation infection assays.

The aim in this section is to investigate isolating murine primary cells as an alternative cell for use in infection assay studies. The RAW macrophage-like cell line has been shown to be a good model for cell infection and assessing mAb opsonisation, although primary cells isolated directly from source should better demonstrate effects that would be seen during *in vivo* studies. In this study murine primary cells were isolated, and used in cell infection assays to investigate *B. thailandensis* infection and mAb 3VIE5 opsonisation.

Initially, both bone marrow cells and peritoneal macrophages were isolated from BALB/c mice. After isolation it was apparent that extremely low numbers of cells were harvested from the mouse peritoneum, making this approach unviable for infection assays. Alternatively, it was decided to focus on harvesting bone marrow cells and differentiating these in cell culture to bone marrow derived macrophages (BMDMs) (2.1.2. Isolation of bone marrow derived macrophages.). Bones from each leg of a BALB/c mouse were harvested for bone marrow cells, the cells were cultured in media containing murine recombinant macrophage colony stimulating factor (MCSF) for a period of 7 days. The isolation of BMDMs was not without challenges, several attempts to differentiate the cells resulted in low cell numbers, cell death and contamination within cell culture. Contamination was overcome with the use of penicillin and streptomycin during initial BMDM cell culture. The issue of cell death whilst in culture, and low cell numbers, were both overcome with additional attempts of cell harvesting and culture. This resulted in a cell population that was suitable for analysis by flow cytometry, confocal microscopy (Figure 18) and a small scale *B. thailandensis* infection assay (Figure 19).

BMDM cell samples were analysed on a FACS Canto II (BD Biosciences) and intact cells gated according to SSC-A and FSC-A (side scatter and forward scatter) (2.6.4. Flow cytometry.). CD11b and CD14 positive BMDM cells were gated according to pacific blue-A (violet) and APC-A (red), for detection of Brilliant Violet 421™ anti-mouse CD11b antibody (BioLegend) and Alexa Fluor® 647 anti-mouse CD14 antibody fluorescence respectively (2.5.3. Primary macrophage staining.). Each laser was used at full power, violet laser at 405nm and red laser at 633nm. Brilliant violet 421 has an excitation wavelength of 405 nm and emits at 421 nm, whereas Alexa Fluor® 647 is excited at 633 nm and has a maximum emission of 668 nm. A

total of 18,727 CD11b and CD14 positive BMDM cells, and 19,396 unstained BMDM cells were gated during the analysis.

Additionally, BMDM cells were imaged by confocal microscopy. BMDM cells were infected with *B. thailandensis* E555 GFP as described previously for RAW cells, and imaged at 24 hours post-infection. Images were taken on a confocal laser scanning microscope (Zeiss). Cells were analysed on 35 mm cell culture dishes (Corning) using x20 magnification. Hoechst (Sigma) nuclei dye (excitation peak at 352 nm and emission peak at 461 nm) was added to cells at 2µg mL^{-1}, to discriminate between individual cells and multi-nucleated giant cells. A GFP expressing *B. thailandensis* E555 (excitation peak at 489 nm and emission peak at 511 nm) was used throughout confocal microscopy studies. The cells were additionally stained for bacterial actin tails (F-actin stain) with Alexa Fluor® 647 (excitation peak at 650 and emission peak at 668nm) phalloidin (red). Although no actin tails were visible in this cell population by confocal microscopy.

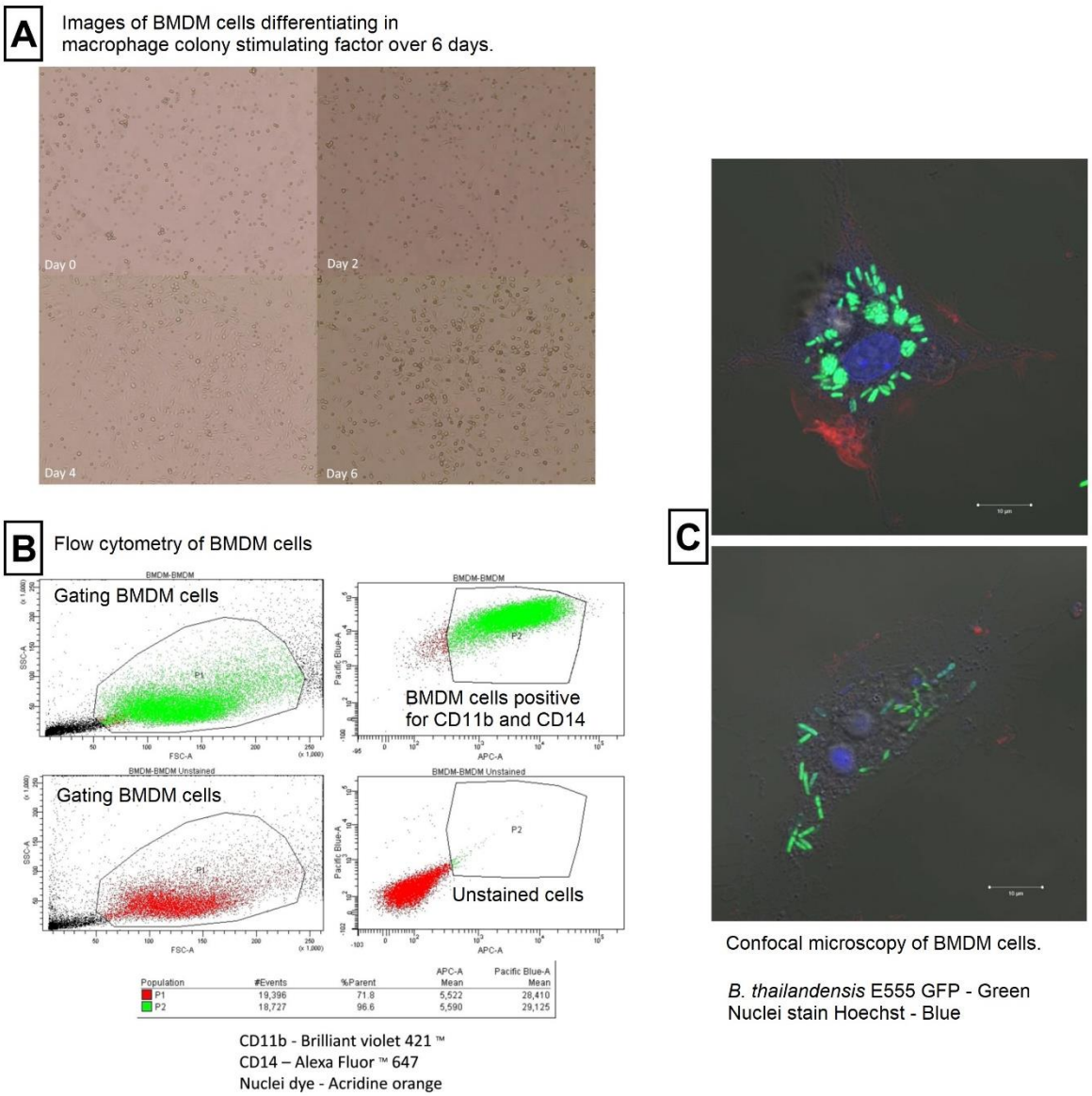

Figure 18. Characterisation of murine bone marrow derived macrophages.

A – Light microscope images of bone marrow derived macrophage (BMDM) differentiation in cell culture media containing macrophage colony stimulating factor. Cells were used for analysis from day 7 in culture. **B** – Flow cytometry analysis of BMDM cells stained with anti-CD11b and anti-CD14 fluorescent antibodies. CD11b and CD14 positive BMDM cells were gated according to pacific blue-A (violet) and APC-A (red), for detection of Brilliant Violet 421™ anti-mouse CD11b antibody (BioLegend) and Alexa Fluor® 647 anti-mouse CD14 antibody fluorescence respectively. Each laser was used at full power, violet laser at 405nm and red laser at 633nm. **C** – Example confocal microscopy images of BMDM cells infected with *B. thailandensis* E555 GFP at 24 hours post-infection. Images were taken on a confocal

laser scanning microscope (Zeiss). Cells were analysed on 35 mm cell culture dishes (Corning) using x20 magnification. The cells were additionally stained with a nuclei stain Hoechst (blue) (excitation peak at 352 nm and emission peak at 461 nm) at 2µg mL^{-1}, to discriminate between individual cells. The cells were also stained for bacterial actin tails with Alexa Fluor® 647 phalloidin (red) (excitation peak at 650 and emission peak at 668nm).

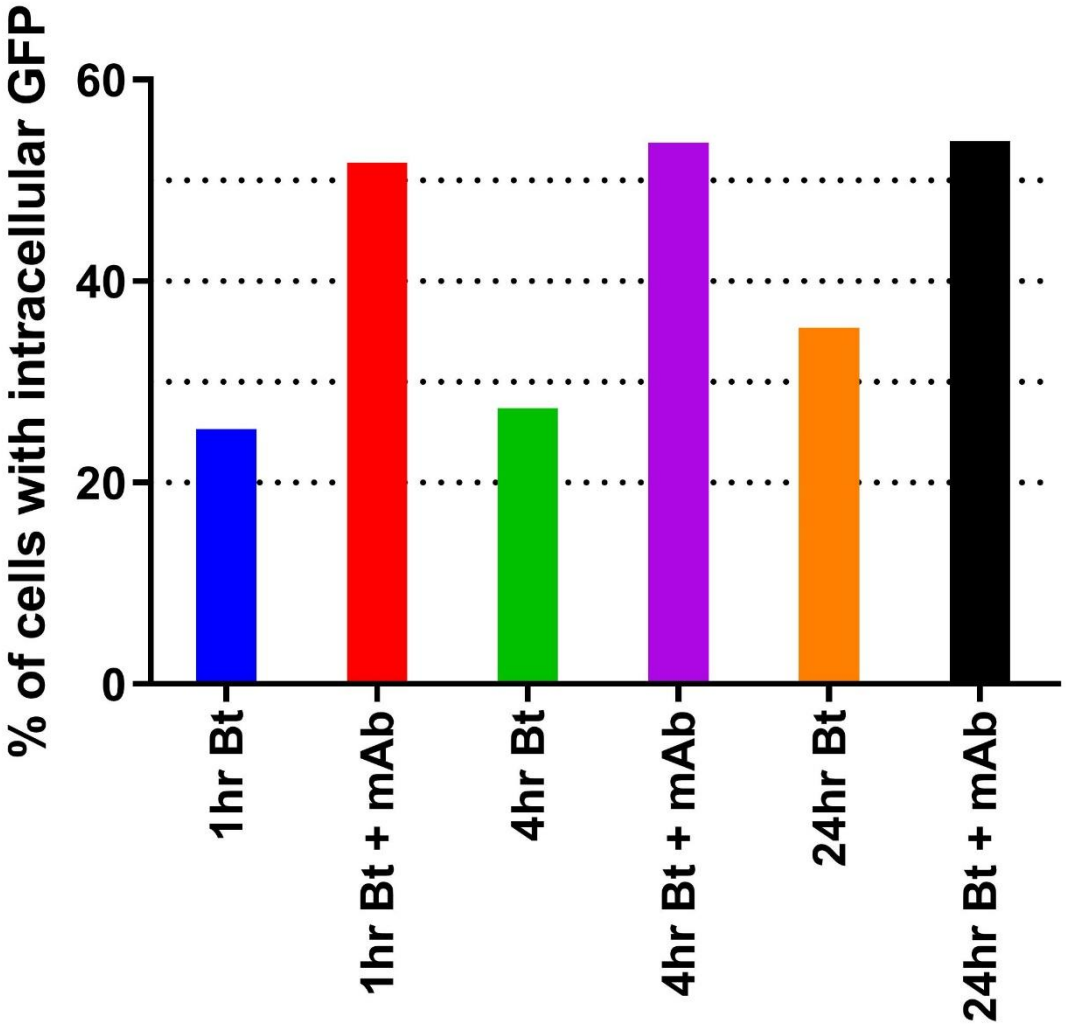

Figure 19. 3VIE5 opsonisation of *B. thailandensis* E555 in bone marrow derived macrophages.

Samples of BMDMs were infected with *B. thailandensis* E555 GFP (Bt) as described for the RAW cell infection assay (2.2.1. RAW cell infection assay.). BMDM cells were infected with *B. thailandensis* at an MOI of 5, with or without prior opsonisation with 1µg mL^{-1} mAb 3VIE5. Cells were harvested into 4% paraformaldehyde at 1, 4 and 24 hours post-infection, and subsequently analysed by imaging flow cytometry using the same *B. thailandensis* gating strategy described previously for RAW cells and GFP expressing *B. thailandensis* E555 (Figure 9). Data consists of a single cell sample for each data point with an average of 5988 cells analysed per data point. No additional data was generated with BMDM cells due to difficulties with isolation of a sufficient quantity of cells for cell infection studies.

A BMDM cell population consisting of 96.6% cells positive for CD11b and CD14 was achieved using the bone marrow isolation and MCSF culture method. The BMDM cells visualised by confocal microscopy showed that the cells can be infected with *B. thailandensis* E555 GFP, and there are examples where the bacteria can be seen compartmentalised within the cell with no actin tail formation. Due to low cell numbers, only representative images were taken of the infected BMDM cells, and the cell density was too low for actin tail image analysis. The interpretation of this primary cell data is problematic, due to the low cell population and lack of reproduced data. Therefore no firm conclusions can be made from the cell infection data and mAb opsonisation in BMDM cells. This initial data however, demonstrates that BMDM could be used as a macrophage infection assay with *B. thailandensis* E555. Although, the harvesting and differentiation of BMDM cells requires more optimisation prior to further cell infection assays.

The BMDM cells were tested as a macrophage infection assay, to determine if 3VIE5 can opsonise and increase uptake of *B. thailandensis* into BMDMs (Figure 19). The mAb 3VIE5 was opsonising with BMDMs, and an increase in the percentage of cells infected can be seen when the mAb 3VIE5 is present at 1, 4 and 24 hours post-infection. No reduction in cell infection levels can be seen over the 24 hour period, although due to the single data point no firm conclusions can be drawn from this data. In RAW cell infection assays a population of 10,000 in focus and single cells per sample are routinely analysed, in this BMDM assay an average of just under 6,000 cells was achieved per sample. This low cell population issue is the main limitation of using BMDM cells for infection assays. Imaging flow cytometry was used, rather than CFU analysis, so that identical samples with low cell numbers can be combined to enable successful analysis for infection. The cell population was too low to enable accurate analysis by CFU enumeration. No further infection assays were achieved with BMDM cells, and it was decided to not pursue additional infection assays and opsonisation data with BMDM cells.

3.7. Discussion.

The aim of this chapter was to develop an infection assay that can be used to assess a panel of mAbs for antibody opsonisation. This assay will be applied throughout this research project for assessing antibodies, antibiotics and novel anti-microbial compounds.

Initial development of a RAW macrophage-like cell infection assay to assess antibody opsonisation involved a modified assay based on published data in the literature (17, 78, 244, 250, 254, 261, 262). Macrophage infection assays are well established and a common method for analysis of bacterial infection by CFU enumeration. It has also been demonstrated by Jenner *et al* that imaging flow cytometry is a method that can also be used to assess intracellular *B. thailandensis* (244). The assessment of antibody opsonisation of *B. pseudomallei* using both CFU and imaging flow cytometry together, is a novel method for screening a panel of mAbs. The data in this chapter has shown that both methods are complimentary, and each can be used to assess a panel of antibodies for opsonisation of *B. thailandensis* and *B. pseudomallei*. Imaging flow cytometry has additional benefits, imaging flow cytometry can assess intracellular infection on a single cell level from a large population of cells in a sample. The technique is especially beneficial when using intracellular fluorescent stains, such as assessing the intracellular location of opsonised bacteria with the use of lysosomal staining. This additional level of detail is a benefit to further characterise the effect of mAb on intracellular *B. thailandensis*, and will be used in subsequent studies in this research project.

The bacterium *B. thailandensis* E555 was used in the development and testing of RAW cell infection assays, before progressing onto infection assays with *B. pseudomallei* K96243. *B. thailandensis* E555 expresses a CPS identical in structure to *B. pseudomallei* (19); this was an important feature in the choice of this bacterium for assessing CPS specific antibodies in cell infection assays. *B. thailandensis* E555 has been shown to be a more suitable surrogate for *B. pseudomallei* K96243, when compared to other *B. thailandensis* strains such as E264 (15). Data from J774 macrophage-like infection assays, shows a similar intracellular replication profile and similar genetic makeup between *B. thailandensis* E555 and *B. pseudomallei* K96243

(15), thus confirming the utility of E555 as an ACDP hazard group II surrogate for *B. pseudomallei*. The murine RAW 264.7 macrophage-like cell was selected based on its ease of use, stability and replication in continuous culture.

The opsonisation ability of the mAbs was consistent across *B. thailandensis* and *B. pseudomallei,* additionally the concentration of mAb that opsonised was consistent between analysis techniques. The consistent results between strains validated the approach of using *B. thailandensis* as a surrogate for *B. pseudomallei*. This is important since *B. thailandensis* can be handled at a lower level of containment, where a greater spectrum of analysis methods are available. It has been demonstrated that imaging flow cytometry is an alternative technique that can be successfully used to assess antibody opsonisation within a cell infection assay. Imaging flow cytometry offers advantages over CFU analysis, such as the ability to analyse individual cell infection events rather than the infection level as a whole population. This would be particularly useful with studies using a less homogeneous cell population, such as assessing infection in *ex vivo* macrophage cell populations. The process is also less labour intensive than CFU analysis in general, although with the high containment pathogen *B. pseudomallei* there is the added sterility check required to analyse cells on the imaging flow cytometer. On a cell by cell level, antibody opsonisation was shown to increase the average number of bacteria per cell, as well as increasing the overall percentage of infected cells in the population. Together, CFU and imaging flow cytometry analysis provide a robust method for analysing intracellular infection levels in cell infection assays.

Imaging flow cytometry data was more variable for *B. pseudomallei* mAb opsonisation, although each mAb still demonstrates opsonisation of *B. pseudomallei* from 1 µg mL^{-1}. Variability between replicates is more pronounced, which is possibly due to effects of the cell infection assay being performed at ACDP level III containment and the associated 48 hour fixation in paraformaldehyde prior to imaging flow cytometry.

Working practices within ACDP level III high containment laboratories may adversely affect the infection assay, potentially causing some variation between *B. pseudomallei* and *B. thailandensis* data. Potential variables include temperature

differences within high flow rate CL3 cabinets, presence of paraformaldehyde residues, sodium hypochlorite residues, and the requirement to fix cells in 4% paraformaldehyde. Infected cells containing *B. pseudomallei* were required to be fixed in 4% paraformaldehyde for a minimum of 48 hours, prior to removal from the laboratory and analysis by imaging flow cytometry at ACDP containment level II. In comparison, the CFU analysis for *B. pseudomallei* was fully performed within ACDP level III containment laboratories, and therefore not exposed to any direct paraformaldehyde treatments.

There are benefits and disadvantages of using each analysis technique. CFU analysis is a gold standard technique that provides a concentration of live intracellular bacteria from the whole cell population. In comparison, imaging flow cytometry relies upon bacterial fluorescence and therefore does not discriminate between viable and non-viable bacteria. The benefit of imaging flow cytometry is that a large number of cells (typically 10,000 per sample) can be analysed in a matter of minutes, and bacterial infection assessed on an individual cell basis. Spot counting is an additional output from the imaging flow cytometry data, this gives an indication of bacterial load per cell. Although, in this opsonisation study the spot counting data did not always correlate with the percentage of cell infection data, especially for mAb CC6. The spot counting gating on the imaging flow cytometry data is an arbitrary cut off value, to enable gating between high (>4) and low (≤4) bacterial spot counts. The spot counting analysis therefore requires more optimisation before it can be used as a standalone result. In this study the spot counting gives an indication of bacterial load in the RAW cell, with the main data set being the percentage of cell infection which was used to down select an antibody.

It has been demonstrated here that opsonisation of *B. thailandensis* by 3VIE5 involves binding to the FcγRs. Blocking CD16 and CD32 has shown that FcγR II and III are at least partly responsible for the mAb opsonisation in this RAW macrophage-like cell infection assay. The ability of a high concentration of 3VIE5 to overcome the FcγR inhibition could be due to the mAb increasingly binding to another Fc receptor such as FcγRI. Additionally, 3VIE5 mAb could be outcompeting the CD16 and CD32 blocking antibodies present in the assay.

The mAb 3VIE5 has also been shown to decrease bacterial OD in culture. This was seen by a reduction in bacterial replication OD when a high concentration of 3VIE5 is present. An explanation for this could be that 3VIE5 has aggregated the bacteria in the micro titre plate, although upon visual inspection of the plate no obvious bacterial aggregation was seen. There is an example in the literature of an IgY antibody reducing replication of *Staphylococcus aureus* in culture (263), it is not known if this effect can be seen with IgG in *B. pseudomallei* culture. It is known that *B. pseudomallei* can form micro aggregates in culture, and the reduction in OD observed is most likely due to micro-aggregations in the culture plate that are not visible by eye. There was no complete inhibition of bacterial replication in this assay, and therefore no MIC value for mAb 3VIE5. To further investigate the trend in reduction in replication with mAb 3VIE5, the bacterial culture plate could be enumerated to determine any reductions in bacterial replication.

RAW cells are simple to culture, phenotypically and functionally stable, up to passages of 30 (255). This makes them a good choice for performing multiple and consistent cell infection assays. Primary cells were assessed in this chapter as an alternative cell line for use in opsonisation *in vitro* infection assays. Primary BMDM macrophages isolated directly from a mouse could potentially be superior to RAWs at representing macrophage responses *in vivo*. However, there were challenges with BMDMs, these included low cell densities, difficulty isolating, and difficulties differentiating BMDM cells. It was therefore decided that the RAW cell assay will be taken forward for subsequent studies in this thesis.

Macrophage-like cell lines are considered to be passive to infection and require prior activation with IFN-γ to see any killing effects with *B. pseudomallei* (250), this has been shown for both RAWs and primary cells. Although we have focused on opsonisation and not investigated bacterial killing in this chapter, the effect of opsonisation on bacterial killing by activated macrophages is something that could be investigated in future studies.

The aim of this study was to develop and assess an antibody opsonisation infection assay and to down select a mAb for further development as a therapeutic, this has been achieved. It was clear from the data that an anti-CPS antibody should be down-selected based on consistent opsonisation of *B. thailandensis* and *B. pseudomallei* above the level for that of the anti-LPS mAb. Although each anti-CPS mAb generated similar results in the opsonisation studies, Octet (red) data generated by Global Access Diagnostics (appendix A.3.1) indicated that the antibody 3VIE5 has favourable binding kinetics. Therefore 3VIE5 was selected for further investigation in infection assays and in development of an AAC therapy.

Appendix.

Antibody ID	K_{on} ($M^{-1}s^{-1}$)	K_{off} (s^{-1})	K_D (nM)	Fitting Algorithm*
CC6	No Result			
3VIE5	5.5×10^{6}	3.8×10^{-3}	0.69	1:1
4VA5	3.9×10^{6}	5.2×10^{-3}	1.35	1:1
4VIH12	1.2×10^{6}	2.8×10^{-3}	2.3	1:1

* 1:1 Binding fits applied in all cases with a truncated fit applied in the dissociation phase due to incomplete release of analyte . Mass transport limited algorithms were tested but calculated unrealistic Rmax values at lower concentrations. Heterogenous ligand binding fits either gave similar values to 1:1 results or fitted more poorly to the sensorgrams.

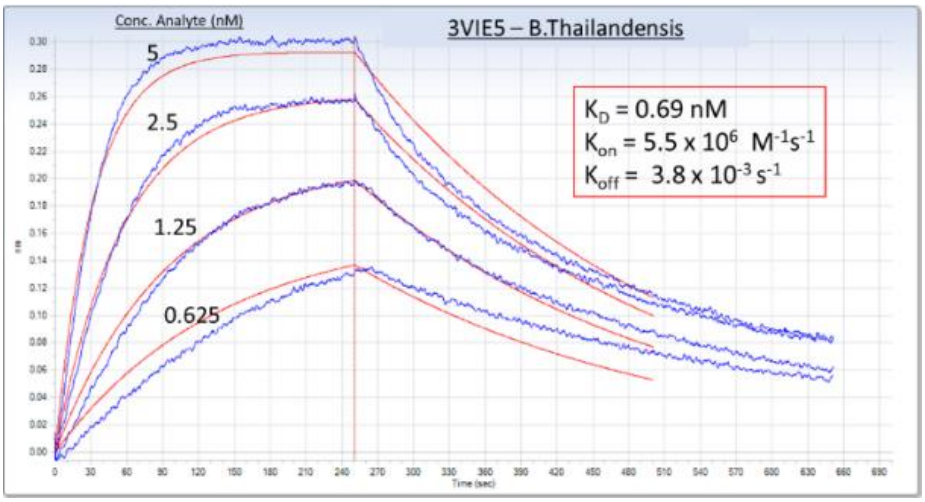

A.3.1. Antibody binding kinetic data generated by Global Access Diagnostics. Data was generated on an Octet® RED Biolayer interferometry platform (ForteBio Sartorius). A 1 in 400 dilution of antigen was used to assess each monoclonal antibody for interaction with the *B. thailandensis* E555 heat killed antigen on the Octet APC (aminopropylsilane) coated biosensor. No interaction was observed for mAb CC6, whereas mAbs 4VIH12 and 4VA5 bound to the antigen in a nanomolar affinity concentration range (K_D). The mAb 3VIE5 displayed the best affinity to the antigen, with a 690 pM affinity (K_D) to the antigen on the Octet biosensor.

4. Fate of intracellular bacteria following mAb opsonisation.

4.1. Introduction.

The mAb 3VIE5 opsonises *B. thailandensis* and *B. pseudomallei*, however it is not known what effect the mAb has on the survival of intracellular bacteria within cells, and if opsonisation disrupts the natural intracellular behaviour of this bacterium.

Following phagocytosis into macrophage cells, *B. pseudomallei* is known to be able to escape endocytic vacuoles using the type three secretory system apparatus (T3SS) (74, 75). *B. pseudomallei is* known to survive intracellularly, avoiding host cell mediated killing. Once in the cytosol, the bacteria move via actin based motility; this process involves host actin from the cytoskeleton in the form of G actin being assembled into F actin by mimicking host cell nucleation promoting factors (89-93). It is thought that actin based motility leads to multi nucleated giant cell (MNGC) formation, by the force exhibited on the cell membrane promoting contact with adjacent cells (99). The T6SS is composed of various structural proteins including the contractible sheath proteins TssB and TssC, the inner tube protein TssD, and the VgrG (TssI) spike protein (99, 264). The T6SS is a syringe like mechanism that mediates cell fusion through insertion of effector proteins across the two cell membranes, causing lipid bilayer disturbance and fusion (99). Both *B. thailandensis* and *B. pseudomallei* cause cell fusion and MNGC formation *in vitro* (72, 91, 257), the role cell fusion plays for disease progression in melioidosis patients is yet to be fully determined (264). MNGC formation is a hallmark of *B. pseudomallei* infection of cells and MNGC formation can be seen in both phagocytic and non-phagocytic cells, where intracellular bacterial replication eventually leads to cell damage and plaque formations (101).

The previous chapter has demonstrated that the mAb 3VIE5 is opsonising. This chapter will assess the fate of bacteria once they are opsonised by 3VIE5 into RAW cells. The hazard group II pathogen *B. thailandensis* E555 will be used throughout this chapter. *B. thailandensis* E555 is a proven surrogate for *B. pseudomallei* intracellular infection studies (15), allowing studies to be completed at a lower level

of containment. This is especially important when completing studies involving live confocal microscopy. For example, imaging live *B. pseudomallei* would not be possible due to the required imaging facility being a containment level II laboratory.

Initially, the effect of non-opsonised bacteria within RAW cells will be visualised by confocal microscopy, to increase our understanding whether *B. thailandensis* E555 causes cell fusion and actin tail formation in the RAW cell infection assay. The effect of mAb opsonisation on actin tail formation will then be assessed using either imaging flow cytometry or confocal microscopy analysis (Figure 20). The formation of actin tails is essential for bacterial motility in the intracellular environment, and eventual spread of the infection between cells. If this process can be disrupted by mAb 3VIE5 opsonisation, then this would be an advantage for an antibody based therapy. Additionally, the effect of opsonisation on bacterial CFU over 24 hours will be determined, together with bacterial association with lysosomal markers. The marker lysosomal associated membrane protein 1 (LAMP-1) present on the lysosomal surface, will be used to signify bacterial association with phagosome maturation, and therefore likely bacterial killing.

The aims of this chapter can be summarised as:

- Utilise the RAW macrophage-like cell infection assay to determine the intracellular fate of mAb 3VIE5 opsonised *B. thailandensis*.
- Investigate intracellular bacterial killing and if mAb 3VIE5 enhances bacterial killing.
- Image and quantify bacterial actin tail formation.
- Determine bacterial association with lysosome markers within RAW cells.

4.2. Imaging of *B. thailandensis* infected RAW cells.

The aim of this experiment was to image RAW cell infection, specifically staining for *B. thailandensis* E555 actin tail formation and observing RAW cell fusion. The bacterium *B. thailandensis* is known to form actin tails and spread between neighbouring cells causing cell fusion. This study will image this bacterial process within RAW cells, with the aim to investigate the effect of mAb 3VIE5 opsonisation on the fate of intracellular *B. thailandensis,* such as actin tail formation and bacterial

spread. High definition imaging of RAW cells was achieved using a confocal laser scanning microscope (Zeiss) (2.6.2. Confocal microscopy.).Confocal microscopy was used to visualise infection of RAW macrophage-like cells with *B. thailandensis* E555 GFP (excitation peak at 489 nm and emission peak at 511 nm), this was achieved with time lapse imaging over 24 hours. Cells were analysed on 35 mm cell culture dishes (Corning) using x20, x40, or x63 oil immersion lenses. Hoechst (Sigma) nuclei dye (excitation peak at 352 nm and emission peak at 461 nm) was added to cells at 2µg mL^{-1}, to discriminate between individual cells and multi-nucleated giant cells. Cells were additionally stained for bacterial actin tails with Alexa Fluor® 647 (excitation peak at 650 and emission peak at 668nm) phalloidin (red) (2.5.1. Actin tail staining.). Laser power was set between 2 – 5 mw for each laser used, 488nm (GFP), 405nm (Hoechst) and 633nm (Alexa Fluor ® 647).

RAW cells initially show little change in intracellular levels of *B. thailandensis* over the first 10 hours post infection (Figure 21). From 11 hours post infection, cells can be seen fusing together, forming the start of MNGCs with intracellular bacterial numbers rapidly increasing. At 20 hours post infection, many MNGCs exist with high numbers of intracellular bacteria observed. The intracellular bacteria are able to multiply within the cells, avoiding exposure to the 1 mg mL^{-1} kanamycin antibiotic present in the extracellular cell culture media.

Actin tail staining was achieved using Alexa Fluor™ 647 phalloidin (Molecular Probes) to bind to F-actin (2.5.1. Actin tail staining.). It is known that *B. thailandensis* is able to form actin tails similar to *B. pseudomallei* and *B. mallei*, and this is achieved by the conversion of G actin to F actin following bacterial escape from phagosomes into the cytosol. The formation of F-actin tails propel the bacteria forwards allowing the bacteria to move throughout the cytosol. It can be observed from confocal imaging that the intracellular *B. thailandensis* protrude outwards from the cell membrane, enabling contact with neighbouring cells (Figure 22). This actin based motility, and contact with neighbouring cells, allows the bacterial type VI secretory system of *Burkholderia* to cause MNGC formation by initiating cell fusion (99) (Figure 23 and Figure 24). Bacteria can be seen freely moving between fused cells by actin tail formation, enabling cell to cell spread while avoiding the extracellular environment, which in this infection assay contains 1 mg mL^{-1} kanamycin antibiotic.

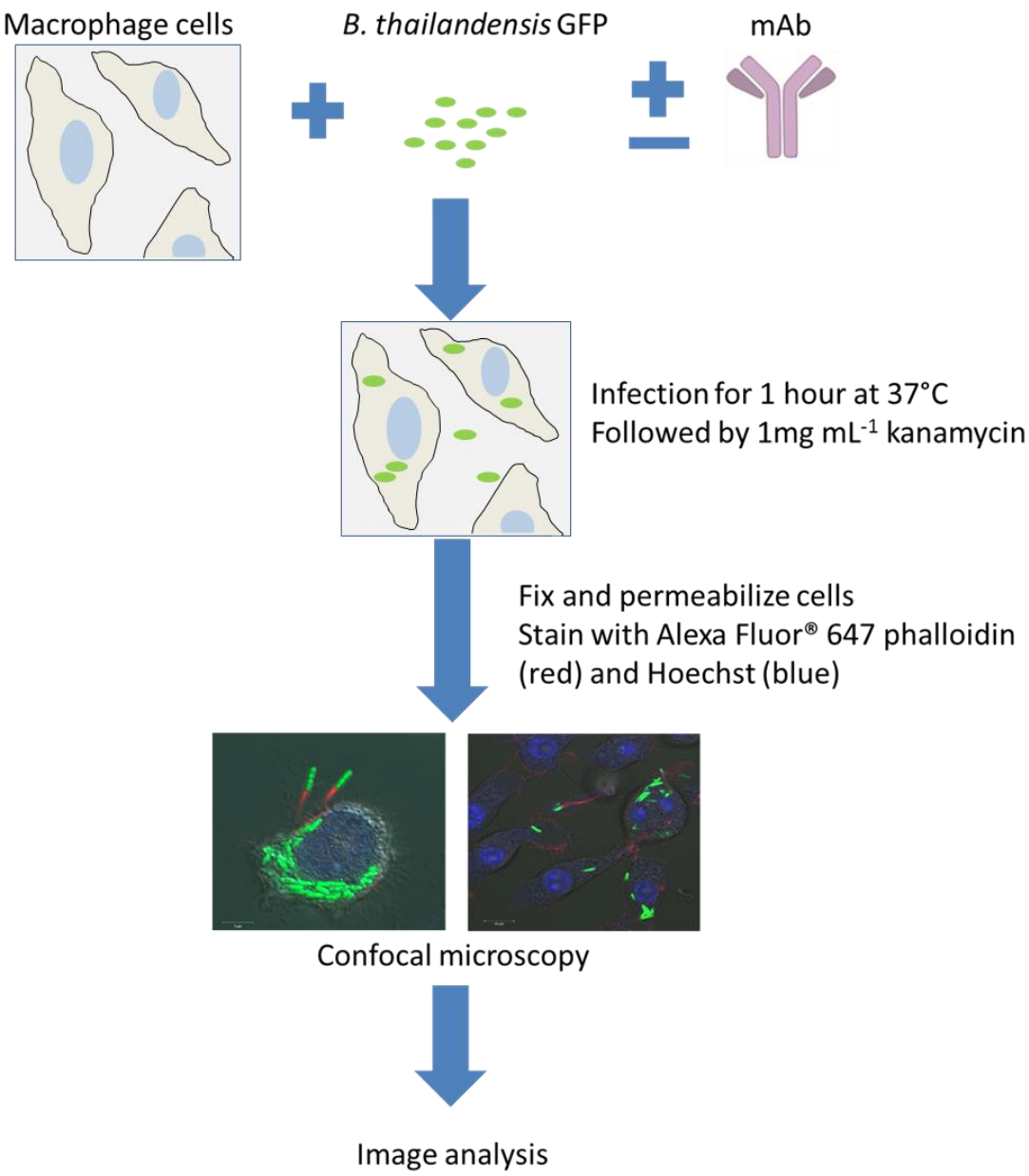

Figure 20. Flow diagram of RAW cell infection assay for actin tail analysis.

This flow diagram represents the experimental steps involved in analysing *B. thailandensis* actin tail formation in a RAW cell infection assay. The effect of mAb 3VIE5 is assessed by opsonising *B. thailandensis* prior to cell infection. The RAW 264.7 macrophage-like cell infection assay was selected as the primary method to analyse intracellular infection and actin tail formation by *B. thailandensis*. RAW cells were infected with *B. thailandensis* E555 GFP at a multiplicity of infection (MOI) of 5, antibody opsonised bacteria were previously incubated with monoclonal antibody 3VIE5 for 30 minutes prior to infection of RAW cells. RAW cells were incubated with *B. thailandensis* E555 GFP for an hour, the cell media was subsequently replaced

with 1mg mL^{-1} kanamycin maintenance antibiotic to kill extracellular bacteria. Green fluorescent protein (GFP, excitation peak at 489 nm and emission peak at 511 nm) expressing *B. thailandensis* E555 (pBHR4-groS-eGFP) were used in the RAW cell assay to visualise bacterial infection by imaging flow cytometry and confocal microscopy. RAW cells on a 35 mm cell culture dish (Corning) were fixed and permeabilised with a BD Cytofix/Cytoperm™ kit, following manufacturer's instructions. Alexa Fluor® 647 (excitation peak at 650 and emission peak at 668nm) phalloidin (Molecular Probes) was added to the RAW cells at 5% (vol/vol) in perm/wash buffer, and the cells incubated at room temperature for 30 minutes. Following incubation, the RAW cells were washed twice with PBS prior to visualisation by confocal microscopy. Alternatively, cells were re-suspended in PBS for analysis by imaging flow cytometry. Hoechst (Sigma) nuclei dye (excitation peak at 352 nm and emission peak at 461 nm) was added to cells at 2µg mL^{-1}, to discriminate between individual cells and multi-nucleated giant cells by confocal microscopy. Laser power was set between 2 – 5 mw for each laser used, 488nm (GFP), 405nm (Hoechst) and 633nm (Alexa Fluor ® 647).

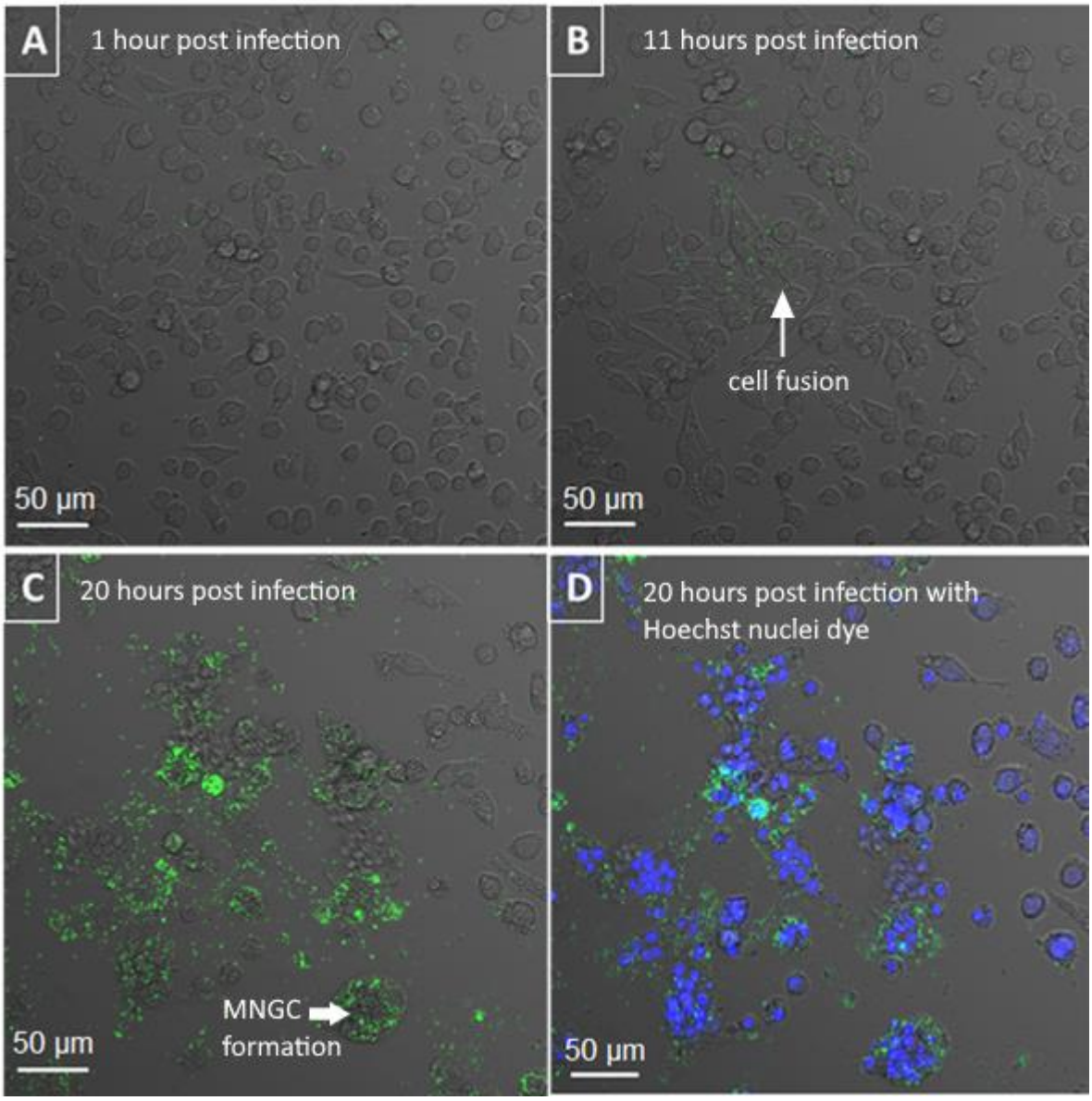

Figure 21. Confocal microscopy time course images of RAW cell infection with *B. thailandensis*.

RAW 264.7 cells were infected with *B. thailandensis* E555 GFP at a MOI of 5 on a 35 mm cell culture dish (Corning). RAW cells were incubated with *B. thailandensis* E555 GFP for an hour, the cell media was subsequently replaced with 1mg mL^{-1} kanamycin maintenance antibiotic to kill extracellular bacteria. Green fluorescent protein (GFP, excitation peak at 489 nm and emission peak at 511 nm) expressing *B. thailandensis* E555 (pBHR4-groS-eGFP) were used in the RAW cell assay to visualise bacterial infection by confocal microscopy over 20 hours. Hoechst (Sigma) nuclei dye (excitation peak at 352 nm and emission peak at 461 nm) was added to

cells at 2µg mL^{-1}, to discriminate between individual cells and multi-nucleated giant cells. Hoechst is cell permeable and stains adenine-thymine regions of the cell DNA. Laser power was set between 2 – 5 mw for each laser used, 488nm (GFP), 405nm (Hoechst) and 633nm (Alexa Fluor ® 647). **(A)** 1 hour post infection, **(B)** 11 hours post infection, **(C)** 20 hours post infection, and **(D)** 20 hours post infection with the addition of Hoechst nuclei dye. Images were taken using a confocal laser scanning microscope (Zeiss, Germany) using the x20 objective. Scale bars represent 50 µm.

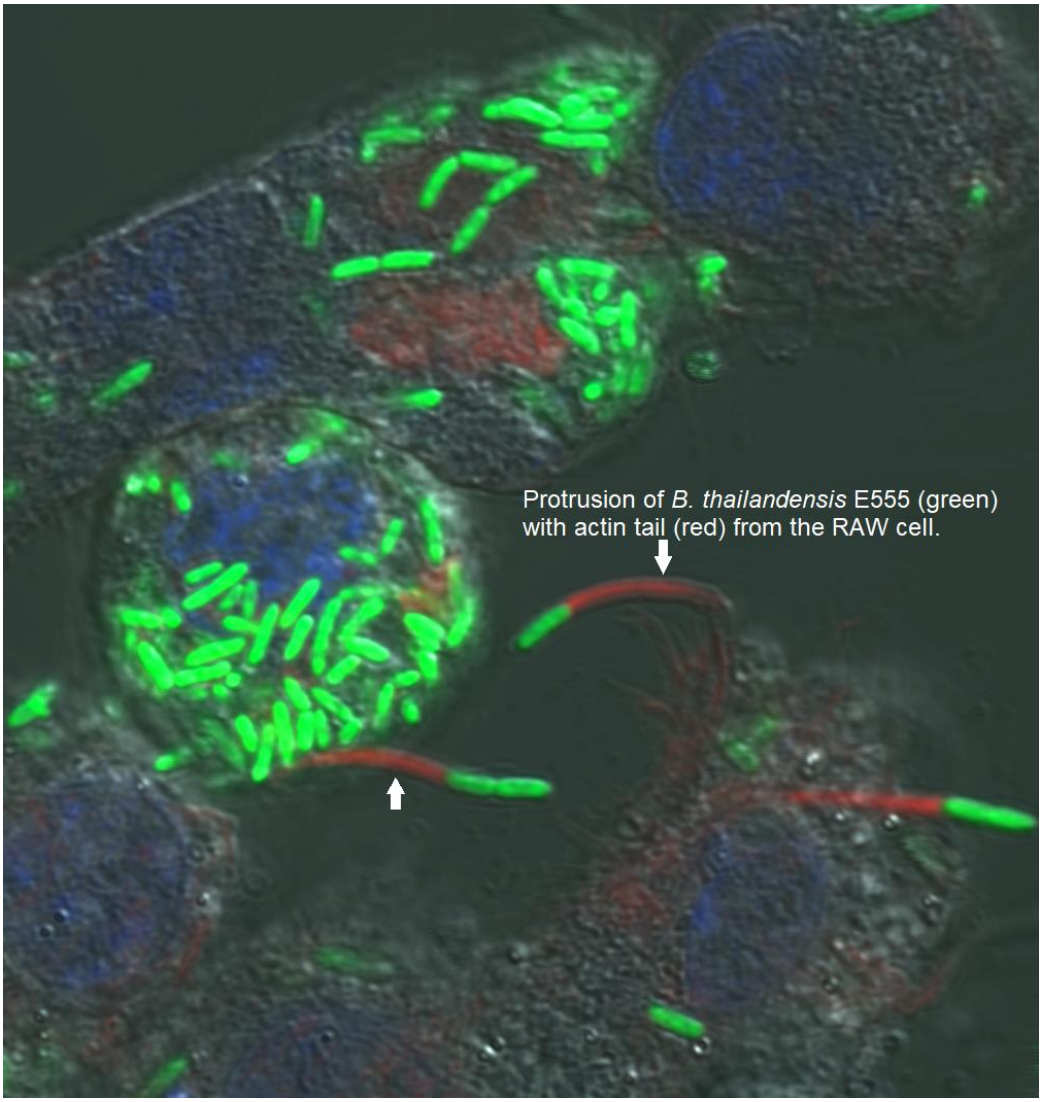

Figure 22. Confocal microscopy of *B. thailandensis* and actin tails.

Green fluorescent protein (GFP, excitation peak at 489 nm and emission peak at 511 nm) expressing *B. thailandensis* E555 (pBHR4-groS-eGFP) were used in the RAW cell assay to visualise bacterial infection by confocal microscopy. RAW cells were infected in a cell infection assay as described previously. Alexa Fluor® 647 (excitation peak at 650 and emission peak at 668nm) phalloidin (Molecular Probes) was added to the RAW cells at 5% (vol/vol). Hoechst (Sigma) nuclei dye (excitation peak at 352 nm and emission peak at 461 nm) was added to cells at 2µg mL^{-1}, to discriminate between individual cells and multi-nucleated giant cells. Cells were analysed at20 hours post infection. Arrows highlight examples of the bacterial actin tails. Image was taken using a confocal laser scanning microscope (Zeiss, Germany) at x63 objective. Laser power was set between 2 – 5 mw for each laser used, 488nm (GFP), 405nm (Hoechst) and 633nm (Alexa Fluor ® 647).

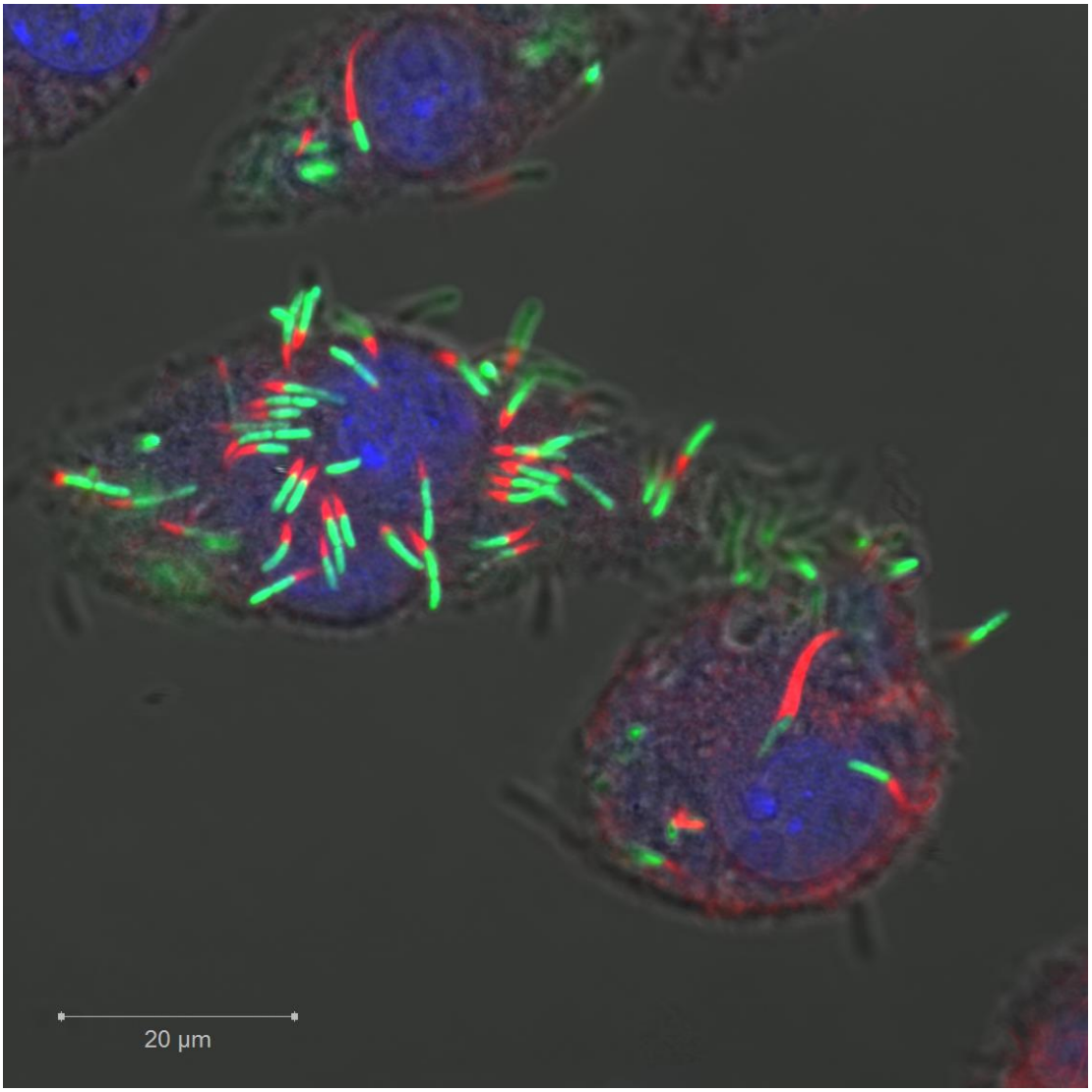

Figure 23. Confocal microscopy of cell fusion between RAW cells.

Green fluorescent protein (GFP, excitation peak at 489 nm and emission peak at 511 nm) expressing *B. thailandensis* E555 (pBHR4-groS-eGFP) were used in the RAW cell assay to visualise bacterial infection by confocal microscopy. RAW cells were infected in a cell infection assay as described previously. Alexa Fluor® 647 (excitation peak at 650 and emission peak at 668nm) phalloidin (Molecular Probes) was added to the RAW cells at 5% (vol/vol). Hoechst (Sigma) nuclei dye (excitation peak at 352 nm and emission peak at 461 nm) was added to cells at 2µg mL^{-1}, to discriminate between individual cells and multi-nucleated giant cells. Cells were analysed at 20 hours post infection. Image was taken using a confocal laser scanning microscope (Zeiss, Germany) at x63 objective. Laser power was set between 2 – 5 mw for each laser used, 488nm (GFP), 405nm (Hoechst) and 633nm (Alexa Fluor ® 647).

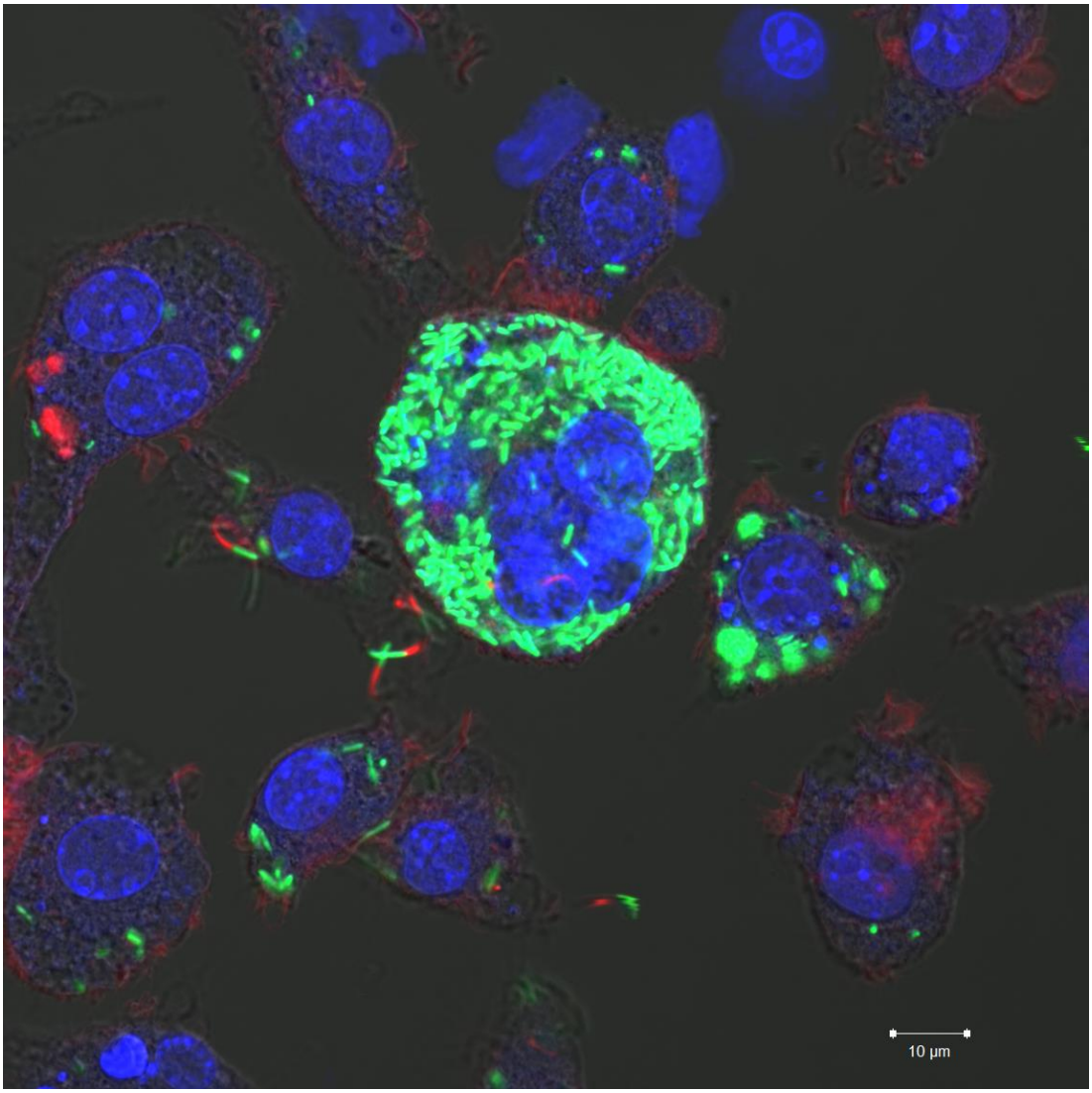

Figure 24. Confocal microscopy of a RAW cell MNGC.

Green fluorescent protein (GFP, excitation peak at 489 nm and emission peak at 511 nm) expressing *B. thailandensis* E555 (pBHR4-groS-eGFP) were used in the RAW cell assay to visualise bacterial infection by confocal microscopy. RAW cells were infected in a cell infection assay as described previously. Alexa Fluor® 647 (excitation peak at 650 and emission peak at 668nm) phalloidin (Molecular Probes) was added to the RAW cells at 5% (vol/vol). Hoechst (Sigma) nuclei dye (excitation peak at 352 nm and emission peak at 461 nm) was added to cells at 2µg mL^{-1}, to discriminate between individual cells and multi-nucleated giant cells. Cells were analysed at 20 hours post infection. Image was taken using a confocal laser scanning microscope (Zeiss, Germany) at x40 objective. Laser power was set between 2 – 5 mw for each laser used, 488nm (GFP), 405nm (Hoechst) and 633nm (Alexa Fluor ® 647).

This imaging data has demonstrated that RAW 264.7 cells infected by *B. thailandensis* E555 produce MNGCs from 11 hours post-infection, with the majority of MNGCs formed by 24 hours post-infection. This gives a time point at which to analyse bacterial actin tail formation in this cell line. This will be used to determine the effect mAb 3VIE5 has on this actin tail formation process. It has also demonstrated that *B. thailandensis* E555 bacteria form actin tails in this RAW macrophage-like cell infection assay, the concentration of phalloidin required to stain for bacterial F actin has been determined.

4.3. Quantifying bacterial actin tail formation.

Whilst imaging infected RAW cells by confocal microscopy, it was noticed that there was a clear difference in bacterial actin tail formation between mAb 3VIE5 opsonised and non-antibody opsonised *B. thailandensis*. The aim of this experiment was to investigate if opsonisation by mAb 3VIE5 reduces *B. thailandensis* E555 actin tail formation in the RAW cell infection assay (2.2.2. Monoclonal antibody opsonisation assay.). Additionally, there will be a focus on using imaging flow cytometry (2.6.3. Imaging flow cytometry.) and confocal microscopy (2.6.2. Confocal microscopy.) to determine a robust method to analyse bacterial actin tail formation in RAW cells. Imaging flow cytometry and confocal microscopy were initially both selected as techniques that can image and potentially quantify *B. thailandensis* E555 actin tail formation in the RAW cell infection assay (2.5.1. Actin tail staining..

Imaging flow cytometry was investigated for analysing actin tail formation due to the high throughput and data analysis ability. Confocal microscopy has the benefit of high definition images of the uninterrupted cell population, although confocal microscopy lacks high throughput and image analysis can be difficult. Imaging flow cytometry has the potential to quantify bacterial actin tail formation from a large population of cells. Thousands of infected RAW cells can be analysed within minutes, and fluorescent markers quantified using the imaging flow cytometry analysis software (IDEAS®).

An overnight culture of *B. thailandensis* E555 was diluted to $5_{x10}{}^{6}$ CFU mL^{-1}. The bacteria were opsonised with mAb 3VIE5 or a murine antibody isotype control at 1 µg mL^{-1} for 30 minutes at 37°C prior to RAW cell infection. Control infections

consisted of non-antibody opsonised bacteria. The RAW cells were infected with *B. thailandensis* E555 GFP at an MOI of 5 for 1 hour at 37°C, the cell culture media was subsequently removed and replaced with media containing 1mg mL^{-1} kanamycin maintenance antibiotic to prevent extracellular bacterial growth. Following 16 hours incubation the RAW cells were harvested for imaging flow cytometry analysis, or the cells remained adhered to the cell culture dish for confocal microscopy analysis from 12 hours post-infection. RAW cells were harvested into 4% paraformaldehyde for imaging flow cytometry by pipetting up and down. RAW cells were fixed and permeabilised with a BD Cytofix/Cytoperm™ kit, following manufacturer's instructions. Alexa Fluor® 647 phalloidin (Molecular Probes) was added to the RAW cells at 5% (vol/vol) in perm/wash buffer, and the cells incubated at room temperature for 30 minutes. Following incubation, the RAW cells were washed twice with PBS and finally re-suspended in PBS for analysis by imaging flow cytometry, alternatively the cells remained adhered and in PBS for confocal microscopy analysis.

For imaging flow cytometry the gating template previously described for antibody opsonisation was applied, consisting of gating cells according to being in focus, single cells and cells associated with GFP fluorescence. The fluorescent strain of *B. thailandensis* E555 GFP (excitation peak of 489 and emission peak 511nm) was excited with the 488nm laser and the Alexa Fluor® 647 (excitation peak at 650 and emission peak at 668nm) phalloidin with the 642nm laser. Fluorescence emission was detected with channel 2 and channel 11 on the imaging flow cytometer, for GFP and Alexa Fluor® 647 respectively.

Confocal microscopy was used to visualise infection of RAW cells with *B. thailandensis* E555 GFP (excitation peak at 489 nm and emission peak at 511 nm) and Alexa Fluor® 647 (excitation peak at 650 and emission peak at 668nm) phalloidin (red). This was achieved with imaging of RAW cells from 12 hours post-infection. Cells were analysed on 35 mm cell culture dishes (Corning) using an x20 objective. Laser power was set between 2 – 5 mw for each laser used, 488nm (GFP) and 633nm (Alexa Fluor ® 647).

The fluorescently stained actin tails were visible within RAW cells (Figure 25), although it was soon determined that analysing cells in a flow is not ideal for bacterial

actin tails. Bacteria and actin tails often protrude outwards from the cell membrane and fused cells are often fragile, therefore they are not suitable for the harsh conditions experienced during cell harvesting and analysis in a flow. Additionally, the fluorescent phalloidin also stained non-infected RAW cells, this was observed by a ring of fluorescence around the cell membrane (Figure 25 A). This caused issues with cell analysis, since the bacterial actin tails are also often found at the edge of cell membranes or protruding from the cell. With this in mind it was decided to focus on confocal microscopy for bacterial actin tail analysis. The RAW cells are not harvested for confocal microscopy analysis, therefore features such as giant cell formation and actin tails remain fully intact. The challenge with confocal microscopy is that data collection can be time consuming, and image analysis software is required to avoid manually counting bacterial actin tails in a large population of cells.

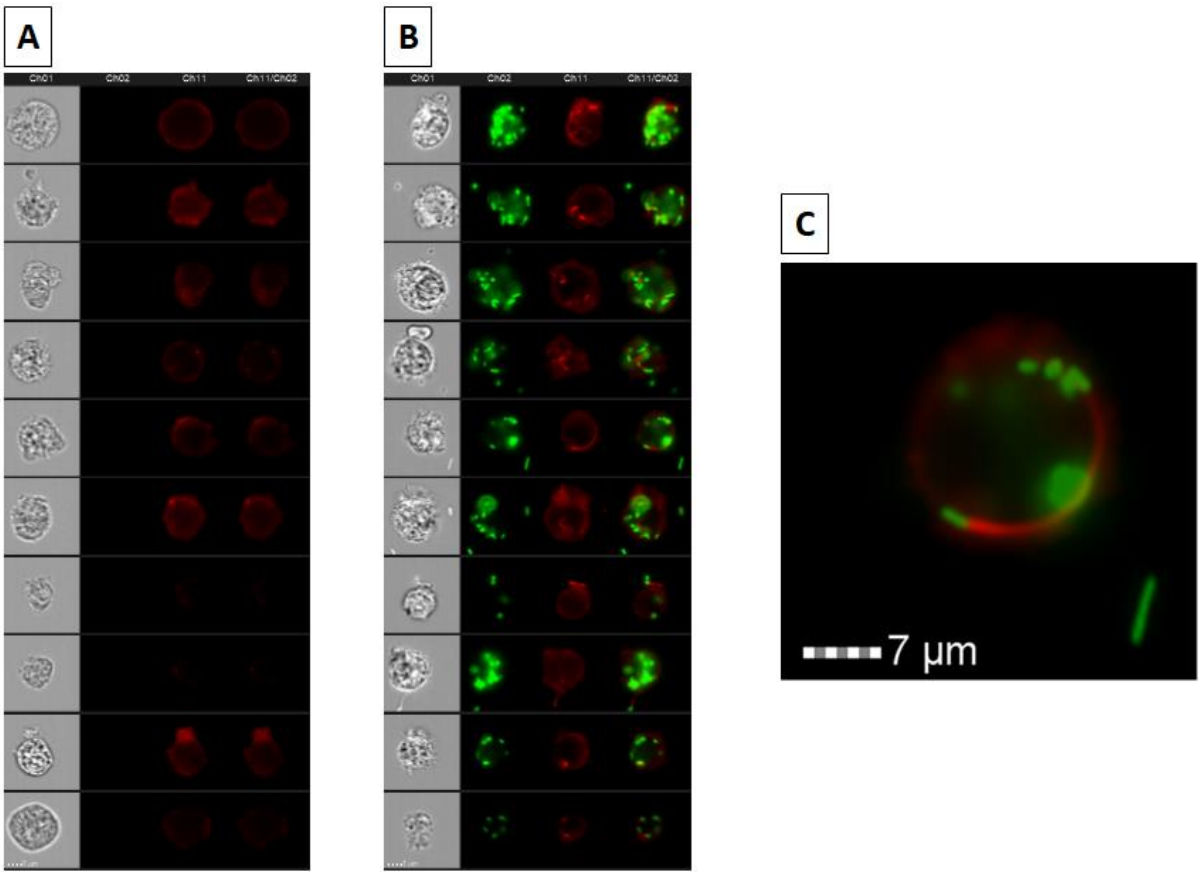

Figure 25. Examples of *B. thailandensis* actin tail images generated by Imaging flow cytometry.

A – Examples of non-infected RAW cells stained with Alexa Fluor® 647 phalloidin (red). **B** – Examples of cells infected with *B. thailandensis* E555 GFP (green) and stained with Alexa Fluor™ 647 phalloidin (red). **C** – Close up of an Imaging flow cytometry image, a bacterial actin tail is visible within the RAW cell. The fluorescent strain of *B. thailandensis* E555 GFP (excitation peak of 489 and emission peak 511nm) was excited with the 488nm laser and the Alexa Fluor® 647 (excitation peak at 650 and emission peak at 668nm) phalloidin with the 642nm laser. Fluorescence emission was detected with channel 2 and channel 11 on the imaging flow cytometer, for GFP and Alexa Fluor® 647 respectively. Representative images of *B. thailandensis* E555 GFP infected RAW cells with actin tail formation are shown. Images were taken 16 hours post-infection at x60 magnification.

Manually counting the bacteria and actin tails in a population of cells is one method that can be used to quantify bacterial actin tail formation. Manually counting is highly

time consuming and a limited number of cells can reasonably be counted. Therefore, it was decided to use an open source computer software, Icy (http://icy.bioimageanalysis.org/) (243), to analyse confocal microscopy images. This was achieved by quantifying the intensity of GFP fluorescence (*B. thailandensis*) and the intensity of the red phalloidin fluorescence (actin tails), generating a ratio between the two. The confocal microscope was set at x20 magnification to image a 5 x 5 square tiled image around a chosen field of view, giving a total image analysis area size of 675 μm^2 (Figure 26). This process was repeated at multiple other locations on the cell culture dish and replicated across three separate weeks, together this generated the final data set (Figure 27).

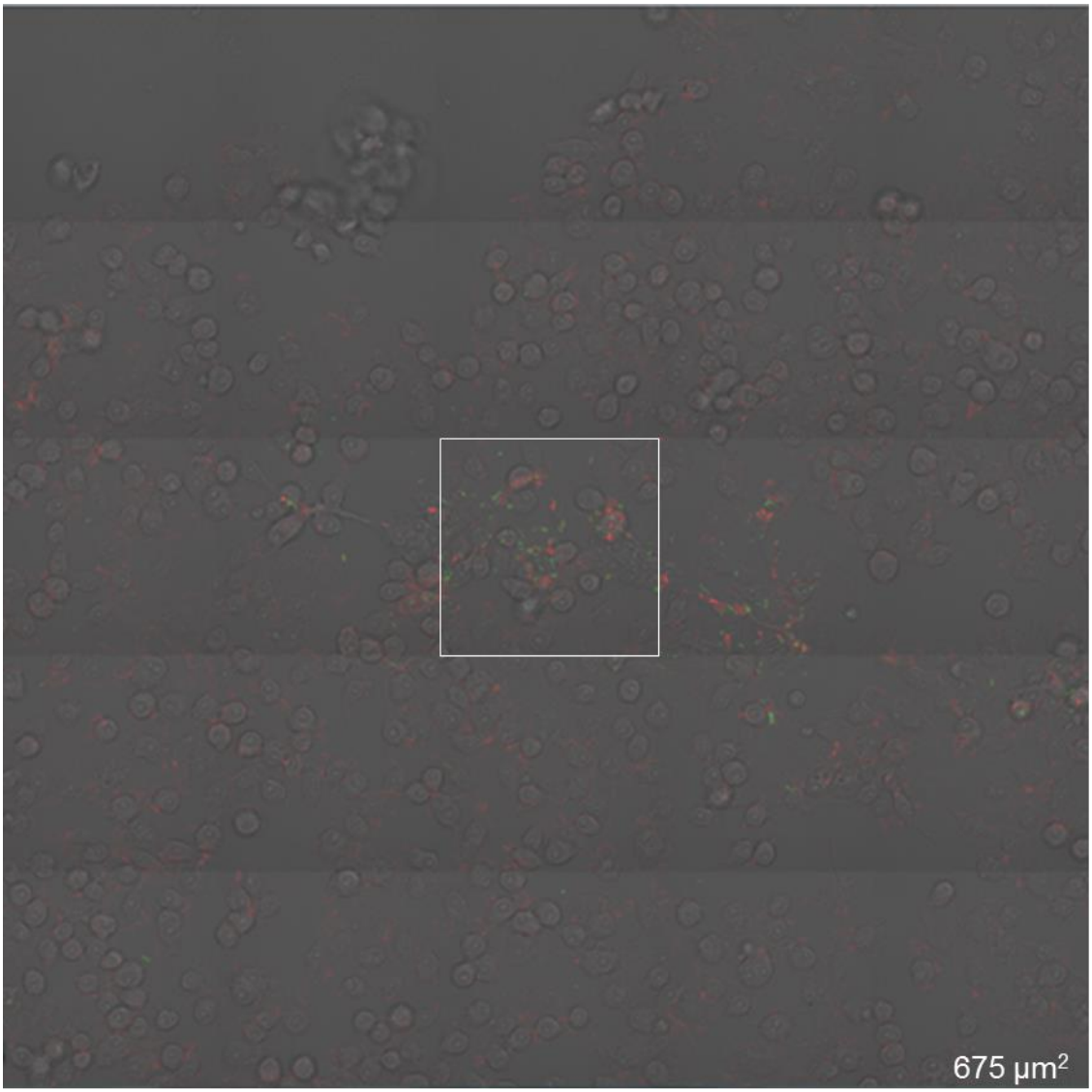

Figure 26. Actin tail analysis by confocal microscopy.

Confocal microscopy was used to visualise infection of RAW cells with *B. thailandensis* E555 GFP (excitation peak at 489 nm and emission peak at 511 nm) and Alexa Fluor® 647 (excitation peak at 650 and emission peak at 668nm) phalloidin (Molecular probes,). This was achieved with imaging of RAW cells from 12 hours post-infection, RAW cells were infected in the cell infection assay as described previously. Cells were analysed on 35 mm cell culture dishes (Corning) using an x20 objective. The white square represents one field of view with an x20 objective on a 35 mm cell culture dish (Corning), a 5x5 tiled image was generated around this central foci of infection to generate a total analysis area of 675 μm^2.

4.4. The effect of 3VIE5 opsonisation on bacterial actin tail formation.

It has been previously shown that *B. thailandensis* forms actin tails in the RAW macrophage-like infection assay, a process that is known to be crucial for intracellular bacterial motility and spread of infection between cells. The aim is now to determine the effects of mAb 3VIE5 opsonisation on the intracellular fate of the bacteria, beginning with bacterial actin tail formation.

An overnight culture of *B. thailandensis* E555 was diluted to $5_{x10}{}^{6}$ CFU mL^{-1}. The bacteria were opsonised with mAb 3VIE5 or a murine antibody isotype control at 1 µg mL^{-1} for 30 minutes at 37°C prior to RAW cell infection. Control infection consisted of non-antibody opsonised bacteria. The RAW cells on a 35 mm cell culture dishes (Corning) were infected with *B. thailandensis* E555 GFP at an MOI of 5 for 1 hour at 37°C. The cell culture media was subsequently removed, and replaced with media containing 1mg mL^{-1} kanamycin maintenance antibiotic to prevent extracellular bacterial growth. Following 12 hours incubation the RAW cells were fixed and permeabilised with a BD Cytofix/Cytoperm™ kit, following manufacturer's instructions. Alexa Fluor® 647 phalloidin (Molecular Probes) was added to the RAW cells at 5% (vol/vol) in perm/wash buffer, and the cells incubated at room temperature for 30 minutes. Following incubation, the RAW cells were washed twice with PBS, the cells remained adhered to the 35 mm cell culture dishes (Corning) and in PBS for confocal microscopy analysis.

Confocal microscopy was used to visualise infection of RAW cells with *B. thailandensis* E555 GFP (excitation peak at 489 nm and emission peak at 511 nm) and Alexa Fluor® 647 (excitation peak at 650 and emission peak at 668nm) phalloidin (red). This was achieved with imaging of RAW cells from 12 hours post-infection. Cells were analysed on 35 mm cell culture dishes (Corning) using an x20 objective. Laser power was set between 2 – 5 mw for each laser used, 488nm (GFP) and 633nm (Alexa Fluor ® 647). The open source computer software Icy (http://icy.bioimageanalysis.org/) (243) was used to analyse confocal microscopy images. This was achieved by quantifying the intensity of GFP fluorescence (*B. thailandensis*) and the intensity of the red phalloidin fluorescence (actin tails), generating a ratio between the two. The confocal microscope was set at x20 magnification to image a 5 x 5 square tiled image around a chosen field of view, giving a total image analysis area size of 675 $µm^2$ (Figure 26). This process was

repeated at multiple other locations on the cell culture dish and replicated across three separate biological experiments, together this generated the final data set (Figure 27).

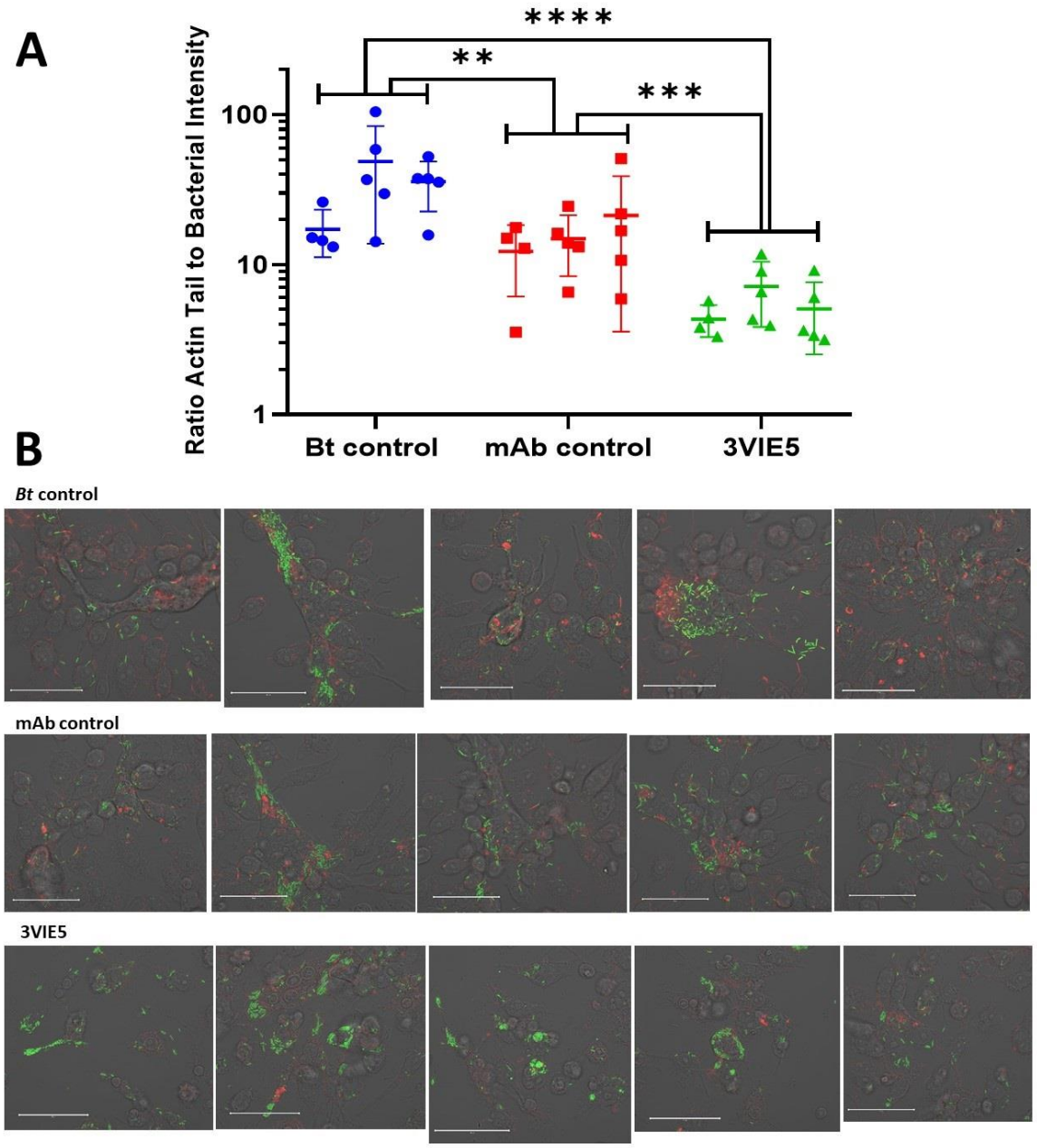

Figure 27. The effect of mAb 3VIE5 on bacterial actin tail formation.

B. thailandensis E555 GFP was opsonised with mAb 3VIE5 or a murine antibody isotype control at 1 μg mL^{-1} for 30 minutes at 37°C prior to RAW cell infection. *Bt* control consists of non-antibody opsonised *B. thailandensis*. The RAW cells on a 35 mm cell culture dishes (Corning) were infected with *B. thailandensis* E555 GFP at an MOI of 5. Bacterial actin tail formation was assessed at 12 hours post-infection of a RAW 264.7 cell infection assay. The two fluorescence markers *B. thailandensis* E555 GFP (excitation peak at 489 nm and emission peak at 511 nm) and Alexa Fluor® 647 (excitation peak at 650 and emission peak at 668nm) phalloidin (Molecular probes).

Images were taken by laser scanning confocal microscopy (Zeiss, Germany) using an x20 objective on a 35 mm cell culture dish (Corning). Laser power was set between 2 – 5 mw for each laser used, 488nm (GFP) and 633nm (Alexa Fluor ® 647). Analysis was achieved using Icy open source software (http://icy.bioimageanalysis.org/) to generate the fluorescence intensity ratio data. **A -** Data are represented as a ratio between the two fluorescent signals with each technical replicate consisting of a field of view (Figure 26), Data (n=14 technical replicates) are derived from three independent biological experiments (each represented on the graph) error bars represent SD. **B -** Example images of infected RAW cells and *B. thailandensis* E555 GFP actin tail formation. Scale bars represent 50μm. ** P 0.0038, *** P 0.0002, **** P <0.0001 One-way ANOVA Tukey's multiple comparisons test.

Plotting the ratio generated from GFP and phalloidin fluorescence, shows a significant difference in actin tail formation between mAb 3VIE5 opsonised *B. thailandensis* and non-opsonised *B. thailandensis* (2.6.2. Confocal microscopy.). The *B. thailandensis* opsonised with mAb 3VIE5 have a significantly reduced intensity of actin tail fluorescence, compared to both the isotype control antibody and the bacterial control. It is interesting that the isotype control antibody also has a significantly reduced actin tail formation ratio, when compared to the bacterial control. This is likely due to the murine IgG2b isotype control antibody cross-linking and interacting the FcγRs on the RAW 264.7 macrophage-like cells. This interaction with the FcγRs could result in an increase in phagosome compartmentalisation of the *B. thailandensis*, and therefore a reduction in bacteria associated with actin tails. The anti-CPS monoclonal antibody (3VIE5) is known to be opsonising and increase cell infection levels, although the reduction in actin tail formation of mAb opsonised *B. thailandensis* was unexpected and a novel finding. Further studies are required to characterise the effect of mAb 3VIE5 and bacterial actin tail association. Non capsular mutants and BimA mutant strains of *B. thailandensis* could be used in future studies. This could include determining if 3VIE5 has a direct effect on actin polymerisation by BimA, or if there is an indirect effect by mAb 3VIE5 and the control mAb interacting with FcγRs that is reducing cytosolic bacteria. Additionally, studies

including FcγR blocks and staining for phagolysosome formation, could add to the characterisation of mAb 3VIE5 and the reduction in bacterial actin tail association.

4.5. The effect of mAb 3VIE5 on intracellular bacterial CFU over 24 hours.

The aim of this experiment was to determine how opsonisation by mAb 3VIE5 changes the intracellular bacterial CFU count over 24 hours. After the initial increase in CFU with mAb 3VIE5 opsonisation, this experiment will determine if bacterial killing is occurring in the RAW cells when bacteria are opsonised compared to non-opsonised. The effect of mAb 3VIE5 opsonisation was determined by analysing bacterial CFU from infected RAW cells at 2, 6 and 24 hours post-infection. A mAb 3VIE5 concentration of 1µg mL^{-1} was chosen, this is a concentration that is known to be opsonising and reduce bacterial actin tail formation *in vitro*.

In this RAW cell infection assay, bacteria were opsonised with mAb 3VIE5 at 1µg mL^{-1} prior to cell infection. Alternatively, mAb 3VIE5 was added post-infection in the kanamycin maintenance media at 1µg mL^{-1}, without any prior opsonisation. Controls consisted of a *B. thailandensis* E555 control and an antibody isotype control at 1µg mL^{-1}. RAW cells were infected with *B. thailandensis* E555 as described previously, at an MOI of 5 for an hour at 37°C. Following infection, cells were incubated with 1mg mL^{-1} kanamycin maintenance media (with or without 3VIE5 present) for up to 24 hours. At each time point (2, 6 and 24 hours) RAW cells were lysed with distilled water, followed by enumeration by serial dilution and culture onto L-agar (2.6.5. CFU analysis.). The addition of mAb 3VIE5 post-infection was to determine if the antibody can opsonise any bacteria that escape from the cells over time. A reduction in CFU, compared to the control, in the later time points would indicate antibody induced bacterial killing by the RAW cell. The mAb 3VIE5 opsonised bacteria were incubated with mAb 3VIE5 for 30 minutes, prior to a 1 hour RAW cell infection step. In comparison, the post-infection group were incubated with mAb 3VIE5 in the external maintenance media for a full 2, 6 or 24 hours.

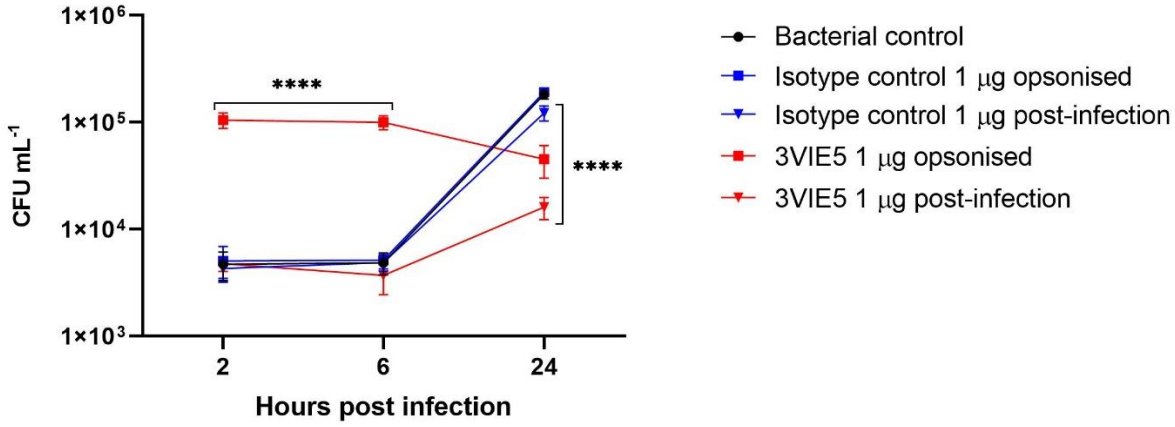

Figure 28. The effect of mAb 3VIE5 on intracellular bacterial CFU.

The effect of 1µg mL^{-1} of mAb 3VIE5 added pre and post-infection, was determined in a *B. thailandensis* RAW cell infection assay over 24 hours. RAW cells were infected with opsonised or non-opsonised *B. thailandensis* E555 at an MOI of 5. Following infection cells were incubated in kanamycin maintenance media, with the post-infection group additionally containing 1µg mL^{-1} mAb 3VIE5. The intracellular bacterial CFU count was determined by cell lysis with distilled water, with subsequent enumeration of bacteria by culture on L-agar. Controls consist of an isotype control antibody (IgG2b) and a *B. thailandensis* E555 only control. Data are represented as CFU means of all technical replicates (n=6) derived from two independent biological experiments, error bars represent SD of all technical replicates. **** P <0.0001, 2-way ANOVA Dunnett's multiple comparisons test to bacterial control.

The mAb 3VIE5, when added pre-infection, significantly increases intracellular bacterial CFU at 2 and 6 hours, compared to the controls (Figure 28). This opsonisation effect is to be expected, and is comparable to the mAb opsonisation data generated in chapter 3. At 24 hours post-infection there is a significantly lower CFU for both 3VIE5 added pre-infection and 3VIE5 added post-infection. There is also a significantly lower CFU for the isotype control antibody added post-infection. Although significant, the CFU reduction is much greater in the mAb 3VIE5 groups compared to the isotype control group.

Initially there is no significant difference between 3VIE5 added post-infection and the bacteria controls or isotype controls. At 24 hours, the CFU value for 3VIE5 added

post-infection is significantly lower by a log fold, with a CFU of 1.6 $x10^4$ CFU compared to the bacterial control of 1.8 $x10^5$ CFU. This provides evidence that mAb 3VIE5 present in the external media can interact with the RAW cell, reducing replication of intracellular bacteria over a 24 hour period. The mAb 3VIE5 added pre-infection to opsonise the bacteria, also has a significant effect in reducing CFU by 24 hours. At 24 hours there is a significantly lower CFU of $4.5x10^4$ for mAb 3VIE5 opsonised bacteria, compared to the bacterial control of 1.8 $x10^5$ CFU.

4.6. Bacterial association with LAMP-1 following mAb 3VIE5 opsonisation.

It has been demonstrated that mAb 3VIE5 can opsonise, reduce actin tail association and reduce bacterial intracellular CFU *in vitro*. The aim of this experiment was to investigate if the mAb 3VIE5 reduction in bacterial CFU is due to association with lysosomes (Figure 29). This could also add to the actin tail data, in which mAb 3VIE5 reduced bacterial association with actin. This reduction in bacterial actin tail association when opsonised by mAb 3VIE5, could be due to bacterial compartmentalisation within lysosomes. This study will determine if there is any increase in bacterial association with LAMP-1 positive lysosomes, when opsonised by mAb 3VIE5 in RAW cells. The effect of the mAb 3VIE5 on bacterial survival was investigated by analysing cell infection over 24 hours, and staining for bacterial association with lysosomes using a fluorescent anti-LAMP-1 antibody (2.5.2. LC3 and LAMP-1 staining.).

B. thailandensis E555 GFP was opsonised with 1 μg mL^{-1} mAb 3VIE5 or isotype control mAb for 30 minutes at 37°C prior to cell infection. RAW cells were infected at an MOI of 5 for an hour, bacteria were subsequently removed and RAW cells were incubated in 1mg mL^{-1} kanamycin maintenance media. At the specified time points post-infection, RAW cells were harvested by pipetting, transferred to 200 µL fixative-permeabilisation buffer (BD Biosciences) and incubated for 30 minutes at room temperature on a roller. Following incubation, the sample volume was increased to 1mL with 800 µL of 1X permeabilisation-wash buffer (BD Biosciences) and centrifuged for 5 minutes at 300 *g*. Following centrifugation, cells were re-suspended into 200µL permeabilisation-wash buffer (BD Biosciences) containing 3.5 μg mL^{-1} PE/Dazzle™ 594 (excitation peak of 566 nm and emission peak of 610 nm) anti-

mouse CD107a (LAMP-1) antibody (Biolegend, UK). The sample was incubated for 1 hour at room temperature on a roller. Following incubation, 800 µL of PBS (Gibco) was added and the sample centrifuged for 5 minutes at 300 *g*. Finally, cell pellets were re-suspended into 50 µL PBS (Gibco) prior to analysis by imaging flow cytometry (2.6.3. Imaging flow cytometry.). RAW cells were analysed on the Amnis® ImageStream® X Mark II. The 488nm (GFP) and 561nm (PE/Dazzle™ 594) lasers were used at 100mw and 200mw power respectively. Fluorescence was detected using channel 2 (*B. thailandensis* E555 GFP, excitation peak at 489 nm and emission peak at 511 nm) and channel 4 (PE/Dazzle™ 594), magnification was set at x60 throughout. Cells were gating according to being single cells, in focus, association with GFP and co-localisation with LAMP-1 (Figure 30).

A RAW cell infection assay, together with imaging flow cytometry analysis, was used to analyse cell infection levels. 3VIE5 was used at 1µg mL^{-1} to keep consistency between experiments, the time points were chosen as 2, 4, 6 and 24 hours post-infection. At each time point, cells were harvested and analysed by imaging flow cytometry, generating a percentage of cells with intracellular GFP. Additionally, bacterial association with lysosomes was assessed in the population of infected RAW cells, this was achieved by staining and gating for the lysosome marker LAMP-1.

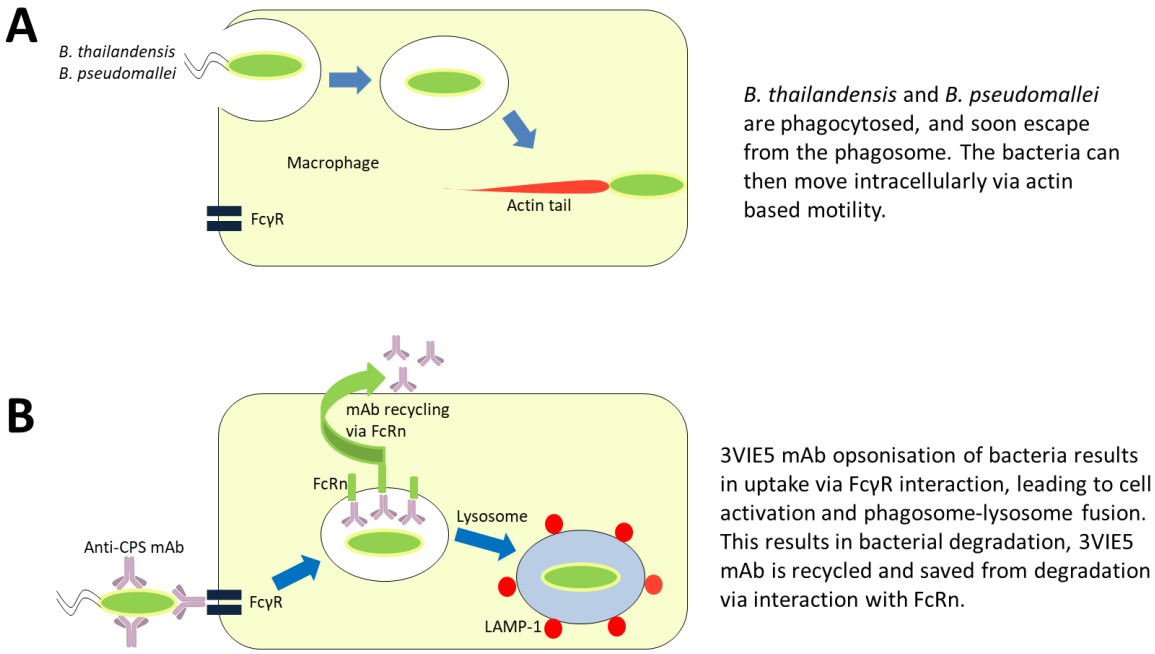

Figure 29. MAb 3VIE5 opsonisation and bacterial association with LAMP-1.

A - *B. thailandensis* and *B. pseudomallei* rapidly escape phagosomes via the type 3 secretory system. In the cell cytosol, the bacteria form actin tails by polymerising host actin. **B –** MAb 3VIE5 opsonisation and interaction with the FcγR will potentially send the bacteria down a different pathway, resulting in bacterial degradation via the phagolysosome. This theory will be investigated by mAb 3VIE5 opsonisation, LAMP-1 staining and analysis of RAW cell infection.

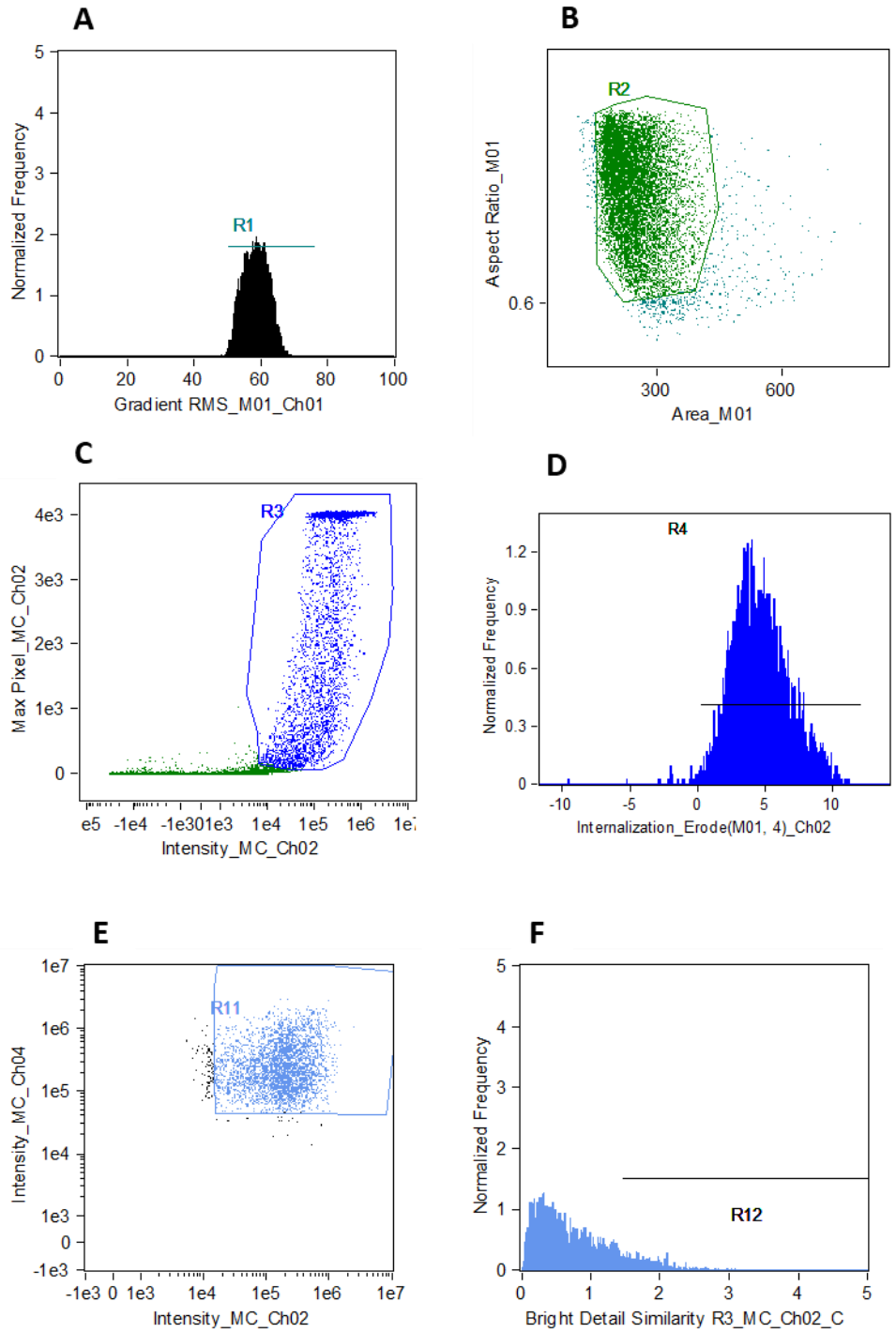

Figure 30. Imaging flow cytometry gating analysis of GFP and LAMP-1 co-localisation.

Imaging flow cytometry was used to analyse RAW macrophage-like cells for co-localisation between intracellular GFP expressing *B. thailandensis,* and a fluorescent (PE/Dazzle™ 594) antibody specific for LAMP-1. The 488nm (GFP) and 561nm (PE/Dazzle™ 594) lasers were used at 100mw and 200mw power respectively. Fluorescence was detected using channel 2 (*B. thailandensis* E555 GFP, excitation

peak at 489 nm and emission peak at 511 nm) and channel 4 (PE/Dazzle™ 594), magnification was set at x60 throughout. Cells were gated based on being in focus **(A)** and single cells **(B)**. Cells associated with *B. thailandensis* E555 GFP were gated **(C),** and an internalisation erode applied to gate cells containing only intracellular GFP **(D)**. GFP and LAMP-1 (PE/Dazzle™ 594) positive cells were gated **(E),** and the co-localisation of the two markers gated **(F)**. Each sample consisted of collecting 10,000 events of R1 and R2 per sample (average 9800).

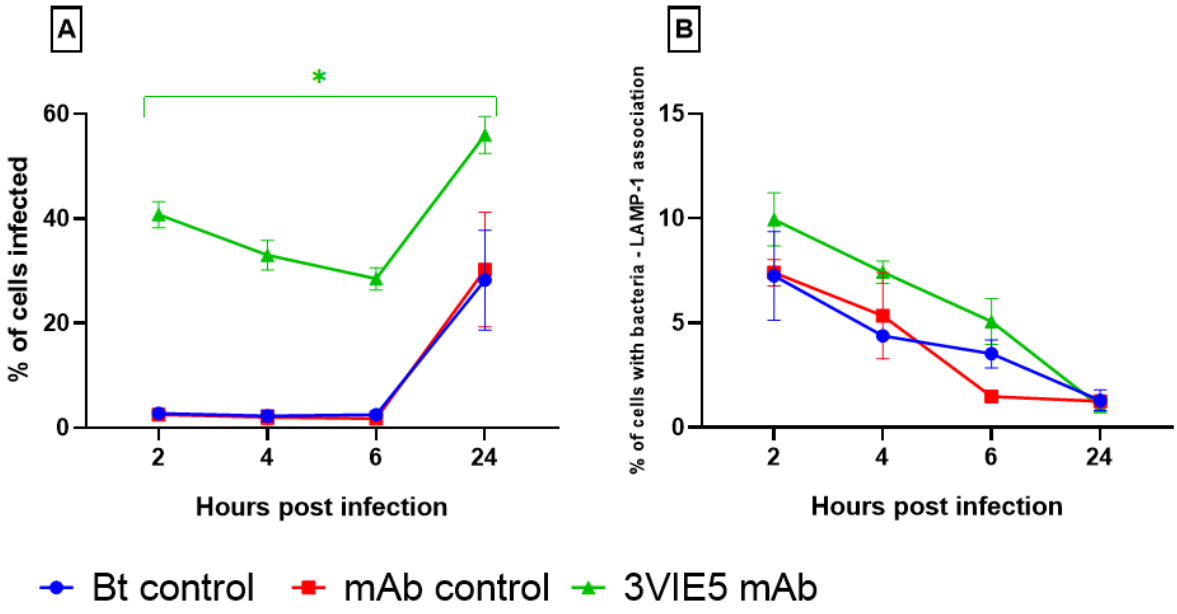

Figure 31. The effect of mAb 3VIE5 on RAW cell association to *B. thailandensis* and bacterial association with LAMP-1.

Imaging flow cytometry was used to analyse RAW cells infected with *B. thailandensis* E555 GFP (**A**), and the percentage of infected macrophages that have bacterial association with LAMP-1 (**B**). RAW cells were either incubated with *B. thailandensis* alone (Bt control), or opsonised with 1µg mL^{-1} of either control antibody or mAb 3VIE5. RAW cells were analysed on the Amnis® ImageStream® X Mark II. The 488nm (GFP) and 561nm (PE/Dazzle™ 594) lasers were used at 100mw and 200mw power respectively. Fluorescence was detected using channel 2 (*B. thailandensis* E555 GFP, excitation peak at 489 nm and emission peak at 511 nm) and channel 4 (PE/Dazzle™ 594, excitation peak of 566 nm and emission peak of 610 nm), magnification was set at x60 throughout. Cells were gating according to being single cells, in focus, association with GFP and co-localisation with LAMP-1 (Figure 30). Data are represented as the mean of all technical replicates (n=4) derived from two independent biological experiments, error bars represent SD. * $P<0.05$ repeated measures ANOVA Bonferroni's post-tests, indicating a difference in uptake between the mAb 3VIE5 group and the control groups. There is a probable time effect in both plots ($P<0.001$ ANOVA). The ANOVA indicated possible differences in LAMP-1 between groups ($P<0.05$); however, these differences were not discernible in this data set.

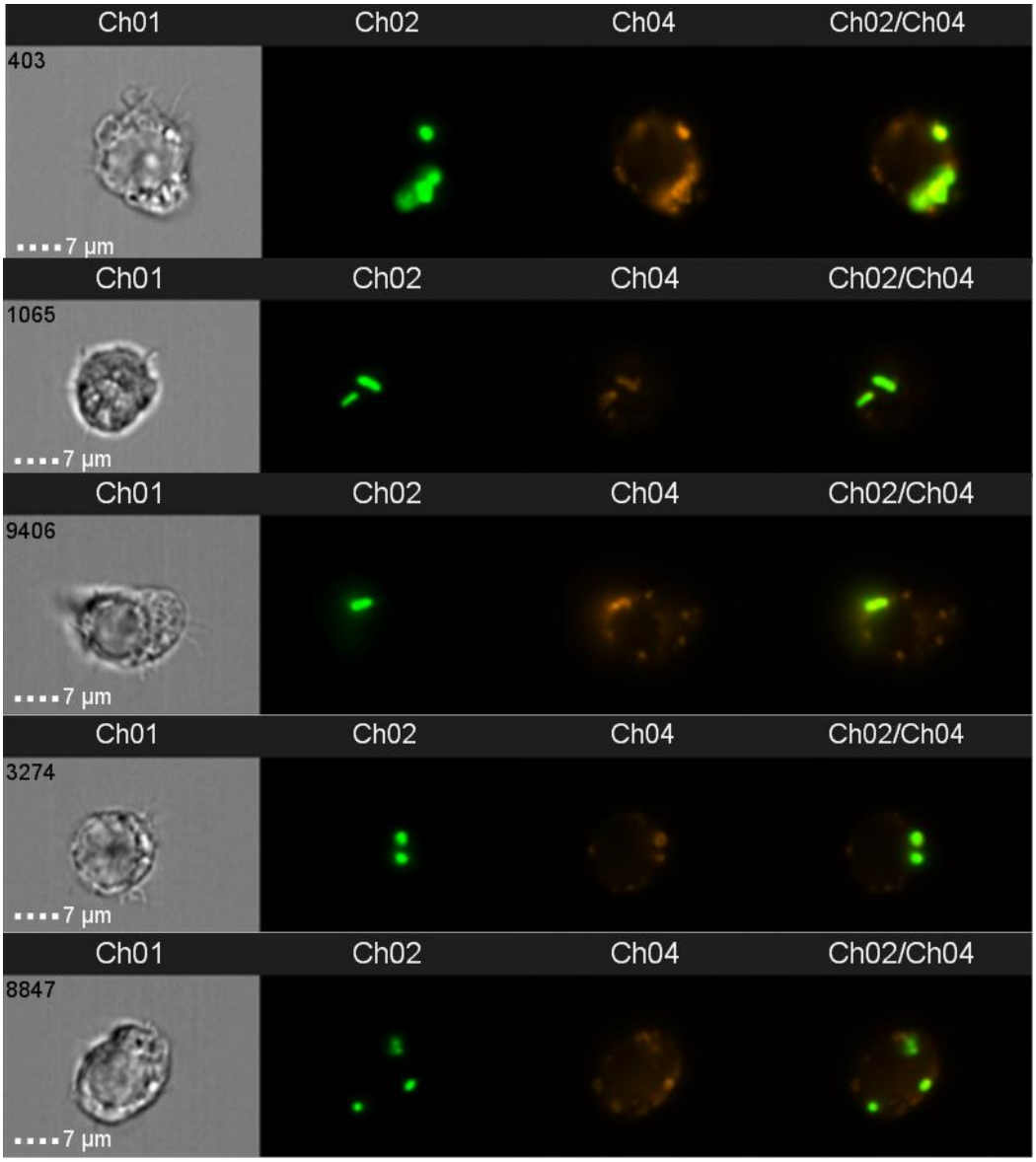

Figure 32. Examples of bacterial GFP and LAMP-1 co-localisation.

Example images of RAW cells (bright field, Ch01) with *B. thailandensis* GFP (green, Ch02) and co-localisation with LAMP-1 (red, ch04). RAW cells were analysed on the Amnis® ImageStream® X Mark II. The 488nm (GFP) and 561nm (PE/Dazzle™ 594) lasers were used at 100mw and 200mw power respectively. Fluorescence was detected using channel 2 (*B. thailandensis* E555 GFP, excitation peak at 489 nm and emission peak at 511 nm) and channel 4 (PE/Dazzle™ 594), magnification was set at x60 throughout. Cells were gating according to being single cells, in focus, association with GFP and co-localisation with LAMP-1 (Figure 30).Images are representative from the imaging flow cytometry data, the data set consisted of an average 9800 cells per sample.

As expected, 3VIE5 increases the percentage of cells infected with *B. thailandensis* GFP (Figure 31 A). The percentage of cells infected increases at 24 hours post-infection for the mAb 3VIE5 group, this is in contrast to CFU data in which there was a decrease in CFU at 24 hours for opsonised bacteria (Figure 28).

Bacterial GFP fluorescence and an anti-LAMP-1 antibody fluorescent marker can be successfully detected by imaging flow cytometry (Figure 32 and Figure 30). This was used to calculate the association between the two fluorescent markers in RAW cells. Association between bacterial GFP fluorescence and LAMP-1 fluorescence (Figure 31 B), shows a decrease in the percentage of cells with GFP and LAMP-1 association over 24 hours. Although the mAb 3VIE5 opsonised group is greater than the controls over the first 6 hours, this difference was not considered significant when analysed by ANOVA.

In this data set, there is not a significant association between mAb 3VIE5 opsonisation and bacterial co-localisation with LAMP-1. The killing effect of mAb 3VIE5 seen in RAW cell infection assays (Figure 28), could not be explained by imaging flow cytometry and LAMP-1 analysis. Under the conditions in this imaging flow cytometry experiment, mAb 3VIE5 opsonisation does not significantly reduce the percentage of cells with GFP fluorescence, or increase the bacterial GFP association with LAMP-1 in RAW cells.

4.7. Discussion.

In this chapter, the effect of 3VIE5 mAb on the fate of intracellular *B. thailandensis* was investigated. Confocal microscopy, imaging flow cytometry and CFU enumeration were all used for analysis of RAW cell infection assays. A RAW cell infection assay was used to image the intracellular infection by *B. thailandensis,* showing the presence of bacterial actin tails, cell fusion and MNGC formation. Using confocal microscopy and image analysis software, a technique was generated to determine a ratio between bacterial actin tail formation and bacterial fluorescence. This data was used to determine the effect of mAb 3VIE5 on bacterial actin tails within RAW cells. The cell infection assay was also assessed by CFU and imaging flow cytometry, to assess the effect of mAb 3VIE5 on intracellular bacterial survival.

Initially, RAW cell infection by *B. thailandensis* E555 GFP was imaged over 24 hours by confocal microscopy. Confocal imaging revealed that cell fusion and MNGC formation frequently occurs in the RAW cell infection assay, from approximately 11 hours post-infection onwards. The formation of MNGCs varies depending upon cell type, and more work is being done to characterise MNGC formation in different cell lines and primary cells (72). The extent and role of MNGC formation *in vivo* is not fully known, more work is needed to determine the relevance to granuloma formation and disease progression in patients (100). In cells that are susceptible, the *Burkholderia* T6SS plays an important role in MNGC formation (72). Cell density could play a role with MNGC formation, requiring close contact between neighbouring cells, this could explain why MNGC is commonly seen *in vitro* with infected RAW macrophage-like cells cultured as a monolayer. It has been demonstrated here that RAW cells, infected with *B. thailandensis* E555, do undergo cell fusion and MNGC formation.

Bacterial actin tail formation was imaged by staining *B. thailandensis* infected RAW cells with fluorescent phalloidin. A method to analyse confocal microscopy images for *B. thailandensis* bacterial actin tail formation has been established. An open source software was used for analysis of confocal microscopy images (http://icy.bioimageanalysis.org/) (243). Confocal microscopy images of bacterial actin tails were analysed in this software, generating a ratio between bacterial GFP fluorescence and actin tail phalloidin fluorescence. The confocal microscopy images were generated by finding a focal point containing cell infection, then expanding this area by taking a 5 x 5 tiled image around this point. This was done to expand the analysis area to include as many cell images as possible, reducing any bias selection of cells by the microscope operator. This method successfully generated a large selection of cell images, from which to generate a ratio between bacteria and actin tail fluorescence. This technique was then applied to infection assays where the GFP *B. thailandensis* was opsonised with mAb 3VIE5 or isotype control antibody. The ratios generated were then compared to a non-opsonised control infection to analyse the effect of antibody opsonisation on bacterial actin tail formation. Imaging flow cytometry was also investigated as a method to analyse bacterial actin tail formation. Although some bacterial actin tails were visible, the process of harvesting cells and

the fluidics involved in sample processing, are both likely to damage the cells from later time points. The majority of bacterial actin tails were observed in fused cells and MNGCs, these RAW cells are particularly fragile and therefore imaging by microscopy was considered to be the best option.

It has been demonstrated that the anti-CPS mAb 3VIE5 reduced bacterial actin tail formation *in vitro*. Although the mechanism for this actin tail reduction is currently unknown, reducing this bacterial virulence factor is a desirable feature of a therapeutic antibody for melioidosis. It is known that *B. thailandensis* is able to form actin tails similar to *B. pseudomallei* and *B. mallei*, and this is achieved by the conversion of G actin to F actin following bacterial escape from phagosomes into the cytosol (90, 93, 265). Is it believed that bacterial actin based motility can lead to neighbouring cells coming into contact, allowing the type VI secretory system of *Burkholderia* to cause cell fusion, leading to MNGC formation (99).

The mechanism whereby the anti-CPS mAb 3VIE5 is reducing actin tail formation is unknown. The T3SS is crucial for bacterial virulence, antibodies have been investigated as immunotherapies to target the T3SS in other pathogenic gram negative bacteria (266). It is possible in this study, that mAb 3VIE5 binding to the CPS of *B. thailandensis* is preventing bacterial escape from phagosomes, possibly by interfering with the T3SS. Alternatively, the bacteria could be escaping the phagosomes and then the mAb is preventing the function of BimA, and therefore polymerisation of host actin. In studies with *L. monocytogenes,* it has been demonstrated that an antibody against ActA can reduce bacterial actin tail formation and cell to cell spread (267). The surface protein ActA is required by *L. monocytogenes* to form actin tails (268), the anti-ActA antibody additionally demonstrated a level of protection within *in vivo* protection studies (267). Although mAb 3VIE5 is not directed against BimA, the binding of the mAb 3VIE5 to the CPS of the bacterium could potentially be blocking the action of BimA. Further studies are required to determine the effect of mAb 3VIE5 on BimA *in vitro*. Additionally, the effect of the mAb could be due to a cloud effect where the bacterium is surrounded by so much mAb that there is a general steric hindrance, preventing bacterial actin tail formation within RAW cells *in vitro*.

An alternative hypothesis is that 3VIE5 mAb opsonisation is causing cell activation by interaction with activating FcγRs, therefore sending the bacteria down a phagolysosome degradation route, rather than allowing the bacteria to escape the phagosome. It is known that binding of mAb to activating FcγRs increases bacteria associated with lysosomes (269, 270). Staining cells for lysosomal markers could gain insight into the fate of opsonised intracellular *B. thailandensis,* compared to un-opsonised bacterial controls. The isotype control mAb shows a reduction in actin tail formation, this effect could be due to the isotype control mAb binding to and activating FcγRs. The control antibody should not be binding to the bacterial surface or Fc receptors, although high concentrations of control mAb could be forming aggregates which could be triggering Fc receptors, via non-specific interactions with cellular components. Alternatively, control antibody aggregates could be interacting non-specifically with the bacterium itself, therefore to some extent interfering with *BimA* based actin tail formation.

Reducing bacterial actin tail formation *in vitro* is a desirable characteristic of a therapeutic mAb for melioidosis. The ability of the mAb to reduce actin tail formation should reduce spread of infection between neighbouring cells. Cell fusion enables the bacteria to spread intracellularly between cells, avoiding the extracellular environment. This allows the bacterium to potentially avoid antibiotic therapy, or host immune responses such as specific bacterial antibodies. The anti-CPS mAb 3VIE5 could be particularly useful as a combination therapy with antibiotics, and other host directed compounds such as autophagy inducers (271). This could involve using the mAb 3VIE5 to prevent bacterial movement within the cell, while the secondary component such as the autophagy inducer or antibiotic promotes bacterial clearance.

Opsonisation by mAb 3VIE5 reduced cell infection by CFU analysis, but not by imaging flow cytometry. Over a period of 24 hours, it was seen that the CFU significantly decreased in the RAW cell infection assay, this was not comparable to imaging flow cytometry in which the percentage of cells infected increased. An explanation for this difference could be that non-viable bacteria, and viable-but-non-culturable (VBNC) bacteria, are potentially being detected by imaging flow cytometry

and not by CFU. Various environmental stresses such as high temperature, osmotic stress and low pH can cause *B. pseudomallei* to enter a VBNC state, with differences seen in bacterial numbers between culture and flow cytometry (272, 273).

Green fluorescent protein is known to be highly stable (274), and studies have shown that there is little difference in fluorescence intensity between live and VBNC cells (275). It has been shown that dead cells do lose their GFP signal over time, although a proportion of dead cells will retain GFP fluorescence, this is likely to be dependent on membrane integrity of the dead cell (275). Imaging flow cytometry is detecting GFP fluorescence, and therefore is unable to discriminate between live, VBNC and recently dead fluorescent bacteria. In comparison, analysis by CFU gives a specific bacterial count from the whole cell population and only live bacteria are enumerated. In bacterial survival studies, CFU enumeration is therefore the analysis option if the aim is to only include live bacteria. However, CFU analysis will exclude any VBNC bacteria, the benefit of imaging flow cytometry is that VBNC bacteria can be analysed rather than excluded. Here it has been shown that 3VIE5 does significantly decrease live bacterial CFU over time, although the exact mechanism for this killing was not determined. Imaging flow cytometry indicates no significant difference in bacterial infection as shown by no significant reduction in GFP signal. Therefore, potentially the *B. thailandensis* is entering a VBNC state due to intracellular stresses, such as exposure to low pH conditions.

The MNGC's formed during the RAW cell infection assays are fragile, and are easily damaged by cell harvesting methods. These MNGC's are typically not observed by imaging flow cytometry, this is likely due to the cell harvesting process and the flow cytometry fluidics damaging the fragile giant cells. Therefore, to analyse giant cell formation and bacterial infection of MNGC's, confocal microscopy is the appropriate method. Bacterial enumeration by CFU analysis will include the fragile infected MNGC's, and therefore CFU analysis is suitable for analysing bacterial infection levels at later time points in the infection assay.

Bacterial association with LAMP-1 was assessed, this was to determine if bacterial killing by mAb 3VIE5, observed in CFU assays, is due to an increased bacterial association with lysosomes. LAMP-1 was selected as a marker for lysosomes, and

was stained with the use of a fluorescently labelled LAMP-1 specific antibody. LAMP-1, together with LAMP-2, are transmembrane proteins estimated to account for 50% of the proteins on the lysosomal membrane (276, 277). LAMP-1 is primarily located on the lysosomal surface as a transmembrane protein with a large luminal domain, however under certain circumstances LAMP-1 can be also be located on the cell surface (278, 279).

No significant increase in bacterial association with LAMP-1 was detected over the 24 hour RAW cell infection assay. There was an increase in the 3VIE5 opsonised group over the first 6 hours, but this increase was determined to be not significant by ANOVA statistical analysis. It has been determined that there is a reduction in actin tail formation and bacterial CFU when opsonised with mAb 3VIE5, the reason for this reduction remains unclear. It is possible that the bacteria are being killed via the lysosomal pathway, but the LAMP-1 antibody staining method has not been efficient at detecting lysosomes in this study. Additionally, the time points used to stain for LAMP-1 may have not been optimal for bacterial association with the lysosome.

Other commonly used lysosomal stains are available such as LysoTracker or acridine orange, these could be investigated in future studies as alternative methods to assess lysosomes. These stains accumulate in the live cell over time, although they also do have disadvantages, especially for longer time point cell experiments. Acridine orange can suffer with phototoxicity and specificity issues, LysoTracker can suffer with stability of the fluorescent signal and photoconversion issues (280-282). Bacteria opsonised with mAb 3VIE5 are taken up into phagocytic cells via interaction with FcγRs on the surface of the phagocytic cell. Non-opsonised bacteria are taken up by phagocytes via recognition of bacterial surface pathogen associated molecular patterns (PAMPs) by pattern recognition receptors (PRRs) such as the dectin-1, mannose, CD14, scavenger receptors and MARCO (macrophage receptor with collagenous structure) (57, 283). Bacterial interaction with the toll like receptor family leads to inflammation, and activation of bacterial killing pathways within the phagocyte. As mentioned in the previous chapter, future studies are required with mAb 3VIE5 and complement. When complement is present *in vivo,* the mAb 3VIE5 opsonised bacteria will likely be taken up into phagocytes via the classical complement pathway, by interaction with complement receptors on the cell surface. This complement cascade pathway not only leads to bacterial opsonisation, but

additional processes such as inflammation and cell lysis, via formation of the membrane attack complex (136). A study has shown that antibody and complement together significantly increased *M. tuberculosis* opsonisation and uptake into macrophages, additionally affecting bacterial survival *in vitro* (284). Therefore future studies should investigate complement and mAb 3VIE5 opsonisation and fate of *B. pseudomallei* in primary cells *in vitro*. These studies will more accurately demonstrate the likely effect of opsonisation of the mAb 3VIE5 when studies progress to *in vivo* models of infection.

This chapter has concluded that 3VIE5 mAb demonstrates a level of intracellular *B. thailandensis* killing, as shown by CFU analysis of a RAW macrophage-like cell infection assay. MAb 3VIE5 also has additional beneficial anti-microbial properties, such as opsonisation and reducing bacterial actin tail formation. The mAb 3VIE5 alone is not enough to effectively clear intracellular bacteria, the mAb therefore has potential for use as a combination therapy with additional anti-microbial compounds. This could be as an AAC, with the antibody effectively delivering drug to the intracellular bacteria via opsonisation, and an enhanced killing effect in combination with antibiotics. In the following chapters, mAb 3VIE5 will be investigated for incorporation into an AAC to deliver antibiotic into infected cells. Additionally, novel anti-microbial compounds as alternatives to antibiotics will be investigated to clear intracellular bacteria *in vitro*.

Data from this thesis, the opsonisation data and reduction in bacterial actin tail formation by 3VIE5, has been published as a scientific report in the Journal of Bacteriology (285).

Appendix.

A.4.1. Antibody opsonisation and the reduction in bacterial actin tail formation by 3VIE5. Publication in the Journal of Bacteriology.

AMERICAN SOCIETY FOR MICROBIOLOGY | Journal of Bacteriology®

RESEARCH ARTICLE

Monoclonal Antibodies Opsonize *Burkholderia* spp. and Reduce Intracellular Actin Tail Formation in a Macrophage Infection Assay

A. Taylor,[a,b] D. Jenner,[a] C. Rowland,[a] T. Laws,[a] I. Norville,[a] J. Prior[a,c,d]

[a]Defence Science and Technology Laboratory, Chemical, Biological and Radiological Division, Salisbury, United Kingdom
[b]London School of Hygiene and Tropical Medicine (LSHTM), London, United Kingdom
[c]University of Exeter, Exeter, United Kingdom
[d]University of Southampton, Southampton, United Kingdom

ABSTRACT Melioidosis is a neglected tropical disease caused by the bacterium *Burkholderia pseudomallei*. The bacterium is intrinsically resistant to various antibiotics, and melioidosis is therefore difficult to treat successfully without a relapse in infection. *B. pseudomallei* is an intracellular pathogen and therefore, to eradicate the infection, antimicrobials must be able to access bacteria in an intracellular niche. This study assessed the ability of a panel of monoclonal antibodies (MAbs) to opsonize *Burkholderia* species and determine the effect that each antibody has on bacterial virulence *in vitro*. Murine macrophage infection assays demonstrated that monoclonal antibodies against the capsule of *B. pseudomallei* are opsonizing. Furthermore, one of these monoclonal antibodies reduced bacterial actin tail formation in our *in vitro* assays, indicating that antibodies could reduce the intracellular spread of *Burkholderia thailandensis*. The data presented in this paper demonstrate that monoclonal antibodies are opsonizing and can decrease bacterial actin tail formation, thus decreasing their intracellular spread. These data have informed selection of an antibody for development of an antibody-antibiotic conjugate (AAC) for melioidosis.

IMPORTANCE Melioidosis is difficult to treat successfully due to the causal bacterium being resistant to many classes of antibiotics, therefore limiting available therapeutic options. New and improved therapies are urgently required to treat this disease. Here, we have investigated the potential of monoclonal antibodies to target this intracellular pathogen. We have demonstrated that monoclonal antibodies can target the bacterium, increase uptake into macrophages, and reduce actin tail formation required by the bacterium for spread between cells. Through targeting the bacterium with antibodies, we hope to disarm the pathogen, reducing the spread of infection. Ultimately, we aim to use an opsonizing antibody to deliver antibiotics intracellularly by developing an antibody-antibiotic conjugate therapeutic for melioidosis.

KEYWORDS actin, antibody, macrophage, melioidosis, opsonization

Melioidosis is a potentially fatal neglected tropical disease caused by the Gram-negative bacterium *Burkholderia pseudomallei*. It has been estimated that 165,000 cases of melioidosis occur worldwide each year, with up to 89,000 deaths (1). Melioidosis is often misdiagnosed due to the wide variety of symptoms associated with the disease (2, 3). Even with successful diagnosis and treatment, studies have shown relapse rates of between 13 and 23% in survivors (4–7), with the majority of cases occurring within 12 months of initial therapy. Due to the complex antibiotic therapy, rates of relapse and the prevalence of antimicrobial resistance, it is clear that new therapeutic approaches are required to aid in the treatment of melioidosis. Monoclonal antibody (MAb) therapies have been in development

Citation Taylor A, Jenner D, Rowland C, Laws T, Norville I, Prior J. 2021. Monoclonal antibodies opsonize *Burkholderia* spp. and reduce intracellular actin tail formation in a macrophage infection assay. J Bacteriol 203:e00244-21. https://doi.org/10.1128/JB.00244-21.

Editor Laurie E. Comstock, Brigham and Women's Hospital/Harvard Medical School

Address correspondence to A. Taylor, ataylor1@dstl.gov.uk.

Received 17 May 2021
Accepted 17 August 2021
Accepted manuscript posted online 30 August 2021
Published 12 October 2021

in the oncology field for many years (8), with research and development into antibody-based therapeutics for infectious diseases accelerating in recent years (9).

B. pseudomallei is well equipped to evade killing by the immune system. One aspect to this is its ability to reside within host cells, therefore avoiding detection and denying access to humoral defenses. The bacterium has a large genome of 7.2 Mb, which is split between two chromosomes. These chromosomes encode virulence factors such as capsular polysaccharide (CPS), lipopolysaccharide (LPS), adhesins, flagella, and secretory systems, of which the type three and type six secretory systems are required for optimum intracellular survival and virulence (10–14).

B. pseudomallei can infect a variety of phagocytic and nonphagocytic cells. *B. pseudomallei* adhesins, such as BoaA and BoaB, are important factors for adhesion to nonphagocytic cells (14). Following phagocytosis into macrophage cells, *B. pseudomallei* can escape endocytic vacuoles using the type three secretory system (T3SS) apparatus (15, 16). Once in the cytosol, the bacteria move via actin-based motility; this process is a bacterially mediated process that involves the bacteria recruiting host actin from the cytoskeleton in the form of G actin, when is then assembled into F actin by mimicking host cell nucleation-promoting factors (17–21). In *B. pseudomallei* and *Burkholderia thailandensis*, this process is driven by the BimA gene. Although the type VI secretion systems of *B. thailandensis* and *B. pseudomallei* are responsible for the cellular fusion, the motility of the bacterium is an important aspect of mobility to facilitate spread (18). Actin-based motility is not unique to *B. thailandensis*, *B. pseudomallei*, and *B. mallei*; for example, bacteria from the *Shigella* and *Listeria* genus can also utilize actin for intracellular motility (22, 23). It is thought that actin-based motility leads to multinucleated giant cell (MNGC) formation via the force exhibited on the cell membrane promoting contact with adjacent cells (24). For *B. pseudomallei* and *B. thailandensis*, MNGC formation is an important aspect of cellular invasion that can be seen in both phagocytic and nonphagocytic cells, where intracellular bacterial replication eventually leads to cell damage and plaque formation (25). The ability of *B. pseudomallei* to survive intracellularly, thus avoiding some traditional antibiotic therapies, highlights the importance of investigating novel antimicrobial therapies for melioidosis.

Burkholderia thailandensis shares many similarities to the hazard group 3 pathogen *B. pseudomallei*, although *B. thailandensis* is rarely pathogenic to humans and is therefore a hazard group 2 organism. *B. thailandensis* E555 can be used as a surrogate for *B. pseudomallei*, as the bacterium possesses a polysaccharide capsule identical to the polysaccharide capsule of *B. pseudomallei* (26) and is virulent in macrophage cell culture infection assays. Techniques for analyzing intracellular bacteria within RAW 264.7 macrophages by CFU and imaging flow cytometry have been previously reported for *B. thailandensis* (27). A range of anti-*Burkholderia* murine monoclonal antibodies developed and owned by the Defence Science and Technology Laboratory (Dstl) have previously been tested *in vivo* for protection against *B. pseudomallei* in mice (28), with the capsule-specific antibodies demonstrating a level of protection.

In this study, we test a range of *Burkholderia*-specific monoclonal antibodies for their abilities to interfere with *B. pseudomallei* and *B. thailandensis in vitro* infection and, as such, their suitability for use as therapies for melioidosis. The aim is to investigate opsonization and its effect on intracellular bacteria. These antibody data set the foundations for the generation of a proof-of-principle antibody-antibiotic conjugate (AAC) for melioidosis.

RESULTS

Monoclonal antibodies are opsonizing in a RAW 264.7 macrophage infection assay. A RAW 264.7 macrophage infection assay was used to determine monoclonal antibody opsonization. Opsonization was assessed by measuring bacterial uptake with a viable count assay and imaging flow cytometry, initially using *B. thailandensis* E555. Each MAb (Table 1) was added to *B. thailandensis* concentrations ranging from 0.1 ng · ml^{-1} to 1 μg · ml^{-1} (anti-CPS MAbs 4VIH12, 3VIE5, and 4VA5) and from 10 ng · ml^{-1} to 100 μg · ml^{-1} (anti-LPS MAb CC6). Antibodies were incubated for 30 min with the *B.*

TABLE 1 Monoclonal antibodies evaluated in this study

Antibody	Target[a]	Isotype	Species
4VIH12	Anti-CPS	IgG2b	Murine
3VIE5	Anti-CPS	IgG2b	Murine
4VA5	Anti-CPS	IgG1	Murine
CC6	Anti-LPS	IgG2a	Murine

[a]CPS, capsular polysaccharide; LPS, lipopolysaccharide.

thailandensis cells to allow binding prior to macrophage infection. Numbers of viable bacteria (CFU/well) were determined by lysis of intact macrophage cells and enumeration of the intracellular bacteria by serial dilution and culture on Luria agar plates. Imaging flow cytometry of intact macrophage cells was used as an additional method to determine antibody opsonization, together with confocal microscopy for high-definition imaging of intracellular bacterial infection.

Intracellular CFU enumeration experiments showed that each MAb analyzed was opsonizing toward *B. thailandensis* E555 in the RAW264.7 macrophage infection assay (Fig. 1A). A statistical modeling approach was taken to analyze the data, where the logarithmic transformation of dose was included as a covariate and the bacteria, antibody, and replicate experiments were included as fixed factors and with all interactions. Each anti-CPS MAb is opsonizing in a dose-dependent manner ($P < 0.001$) by increasing intracellular CFU level by a greater than 1-log fold increase. An average CFU of 2.1×10^4 CFU · ml^{-1} is observed at 0.0001 μg · ml^{-1} of anti-CPS MAb; this increases to 4×10^5 CFU · ml^{-1} at an anti-CPS MAb concentration of 0.1 μg · ml^{-1}. In comparison, an anti-LPS antibody concentration of 10 μg · ml^{-1} or greater is required to achieve a similar level of intracellular CFU increase. Modeling suggested differences between antibodies ($P < 0.001$) with a greater concentration of the anti-LPS MAb CC6 required to achieve an increase in *B. thailandensis* intracellular CFU compared to the anti-CPS MAbs 4VIH12, 3VIE5, and 4VA5 ($P < 0.001$, for all Bonferroni's posttests in which CC6 MAb was compared to each of the other MAbs).

All MAbs analyzed for opsonization by imaging flow cytometry showed a dose-dependent ability to increase the percentage of cells infected with *B. thailandensis* (Fig. 1C). A similar modeling approach was taken as with the CFU data. Again, there was a dose response for the antibodies ($P < 0.001$) and a clear difference between the anti-CPS MAbs ($P < 0.001$) (4VIH12, 3VIE5, and 4VA5) and the anti-LPS MAb (CC6), mirroring the result seen by intracellular CFU analysis ($P < 0.001$ for all Bonferroni's posttests in which CC6 MAb was compared to each of the other MAbs). Additionally, imaging flow cytometry can be used to estimate the proportional extent of bacterial presence within the cell by "spot counting" in the focal plane of each cell (see Fig. S1 in the supplemental material). Although the spot counting profiles (Fig. 1E) differ between MAbs and bacterial strains, the data indicate an increase in the average number of intracellular bacteria per cell when opsonized with MAb. The spot count analysis broadly demonstrated the same conclusions as the CFU-associated data, demonstrating a dose effect ($P < 0.001$; analysis of covariance [ANCOVA] for dose response).

The ability of monoclonal antibodies to opsonize *B. pseudomallei* K96243 is comparable to ability to opsonize *B. thailandensis* E555. The MAb panel was assessed to determine if the opsonization ability demonstrated for *B. thailandensis* E555 can also be applied to the highly pathogenic (Advisory Committee on Dangerous Pathogens, UK (ACDP, level III *B. pseudomallei* K96243 (Fig. 1B, D, and F). A red fluorescent protein (RFP)-expressing strain of *B. pseudomallei* K96243 was used to enable visualization of the bacterium within macrophage cells by imaging flow cytometry.

Analysis of intracellular bacteria by CFU enumeration and imaging flow cytometry showed that opsonization of *B. pseudomallei* K96243 by each MAb is comparable to the data for that of *B. thailandensis* E555 (Fig. 1). These data were analyzed within the modeling discussed in the previous section, alongside the *B. thailandensis* data. We found overall levels of uptake were different when measuring CFU ($P < 0.001$) or flow cytometry ($P = 0.009$). However, these differences did not seem to alter the role of

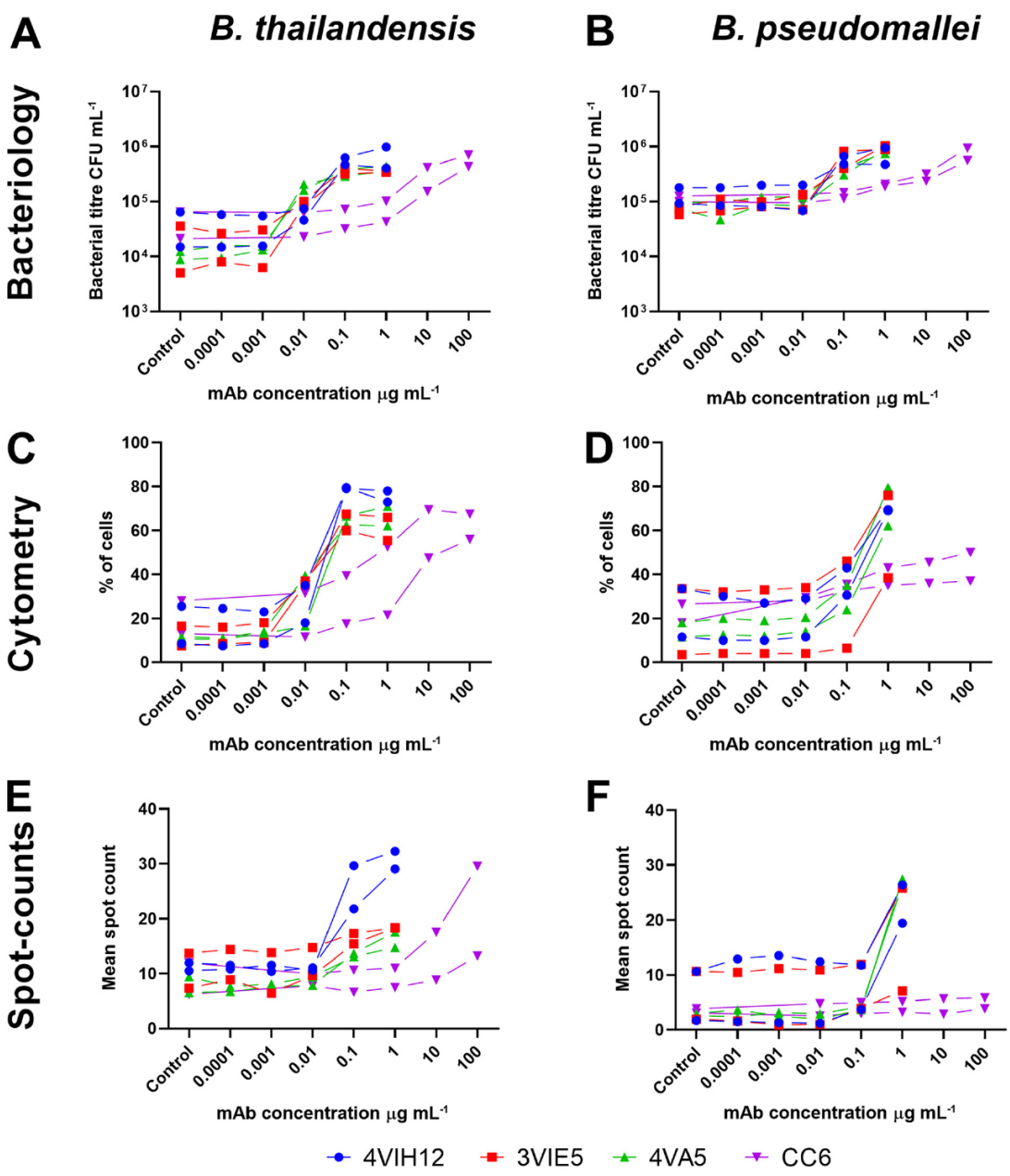

FIG 1 Monoclonal antibody opsonization. *Burkholderia thailandensis* (left) and *Burkholderia pseudomallei* (right) were opsonized at a range of concentrations of anti-capsular polysaccharide (CPS) monoclonal antibodies (MAbs) (4VIH12, 3VIE5, and 4VA5) and anti-lipopolysaccharide (LPS) MAb (CC6; note higher concentrations). Intracellular bacteria within RAW 264.7 macrophages were analyzed ay 2 h postinfection by CFU enumeration (A, B), imaging flow cytometry (C, D), and spot counts (E, F). For each concentration of MAb, replicates were performed across two separate experimental days. Controls consisted of an isotype control antibody at the highest concentration. (A to D) Statistics for bacteriology and cytometry. $P < 0.001$ (analysis of covariance [ANCOVA]) for MAb dose response); $P < 0.001$ for all Bonferroni's posttests in which CC6 MAb was compared to each of the other MAbs. (E, F) Statistics for spot counts. $P < 0.001$ (ANCOVA for MAb dose response). Imaging flow cytometry gating and spot count analysis are shown in Fig. S1 in the supplemental material.

antibody when measuring CFU ($P < 0.810$) or flow cytometry ($P = 0.891$). The conclusions are therefore the same as those with *B. thailandensis*. Each antibody was opsonizing and significantly increased bacterial uptake with dose ($P < 0.001$; ANCOVA for dose response); anti-CPS MAbs (4VIH12, 3VIE5, and 4VA5) outperformed the anti-LPS

MAb (CC6) in terms of opsonization ability ($P < 0.001$ for all Bonferroni's posttests in which CC6 MAb was compared to each of the other MAbs). Antibody opsonization data were used to select an anti-CPS antibody for further analysis in cell infection assays. The anti-CPS MAb 3VIE5 was selected because this MAb had previously been shown in other studies to have favorable binding kinetics (data not shown).

Opsonized *B. thailandensis* bacteria have a reduction in actin tail formation within RAW 264.7 macrophages. Confocal microscopy was used to visualize infection of RAW 264.7 macrophage cells with *B. thailandensis* E555 enhanced green fluorescent protein (eGFP) over 24 h. Actin tail staining using fluorescently labeled phalloidin reveals actin tail formation by intracellular *B. thailandensis* E555 (Fig. 2).

An open-source computer program, Icy (29), was used to analyze confocal microscopy images by quantifying the intensity of GFP-*B. thailandensis* and the intensity of red phalloidin-stained actin tails, generating a ratio between the two.

Plotting the ratio generated from the GFP and phalloidin fluorescence clearly demonstrates a difference in actin tail formation between 3VIE5 MAb-opsonized *B. thailandensis* and nonopsonized *B. thailandensis* in RAW 264.7 macrophages (Fig. 3). The *B. thailandensis* cells opsonized with the anti-capsule MAb 3VIE5 have a reduced intensity of actin tail fluorescence compared to that of both the isotype control antibody and the nonopsonized bacterial control ($P < 0.001$ and $P < 0.0001$, respectively, using analysis of variance [ANOVA]). It is interesting that the isotype control antibody also has a reduced actin tail formation ratio compared to that of the nonopsonized control ($P < 0.01$). Our theory to explain this observation is that the isotype control antibody is causing nonspecific activation of the RAW macrophages through the interaction with their Fc receptor, thus increasing their activation status. This, in turn, leads to compartmentalization of the bacterium, thereby suppressing bacterial actin tail formation.

Opsonization does not increase bacterial colocalization with LAMP-1-positive phagolysosomes. The MAb 3VIE5 has demonstrated the ability to opsonize and reduce actin tail formation *in vitro*. Although it is known that *B. pseudomallei* and *B. thailandensis* are both able to escape the phagolysosome (12, 14, 15), it is not known how MAb 3VIE5 will affect the intracellular fate of the opsonized bacteria. It is possible that opsonized bacteria are unable to escape from the phagolysosome, which would be a desirable characteristic for an antibody-based therapy.

A *B. thailandensis* E555 GFP macrophage infection assay with imaging flow cytometry analysis was used to investigate the uptake of opsonized and nonopsonized bacteria. The MAb 3VIE5 was used in a RAW 264.7 macrophage infection assay at 1 μg · ml^{-1}, which has already been shown to be opsonizing, compared to an isotype control antibody and no-antibody controls. At each time point, cells were harvested and analyzed by imaging flow cytometry; this generated a percentage of cells infected with *B. thailandensis* E555 GFP (Fig. 4A). Statistical analysis of these data indicated that cell association with bacteria changed over time ($P < 0.001$; repeated-measures ANOVA) and that the MAb 3VIE5 enhanced association compared to that in the two control groups ($P = 0.022$ versus no-antibody and $P = 0.020$ versus isotype control; Bonferroni's posttests). An increase in association between cell and bacteria with MAb 3VIE5 is to be expected, since we have previously demonstrated the opsonization ability of this MAb.

It is known that binding of MAb to activating FcγRs increases the number bacteria associated with lysosomes and that this process can be independent of MAb opsonization of the bacteria (30, 31). In order to assess bacterial association with lysosomes, the lysosome marker lysosomal associated membrane protein 1 (LAMP-1) was detected with the use of a fluorescently labeled antibody and image analysis software (see Fig. S2 in the supplemental material). Statistical analysis of these data indicated that LAMP-1 association with bacteria changed over time ($P = 0.003$; repeated-measures ANOVA). We also note that there was some evidence for difference between treatment groups ($P = 0.010$; repeated-measures ANOVA); however, the effects were too modest to identify the nature of which groups might be different from each other ($P > 0.05$ in all cases). These data indicate that 3VIE5 MAb opsonization enhanced bacterial uptake;

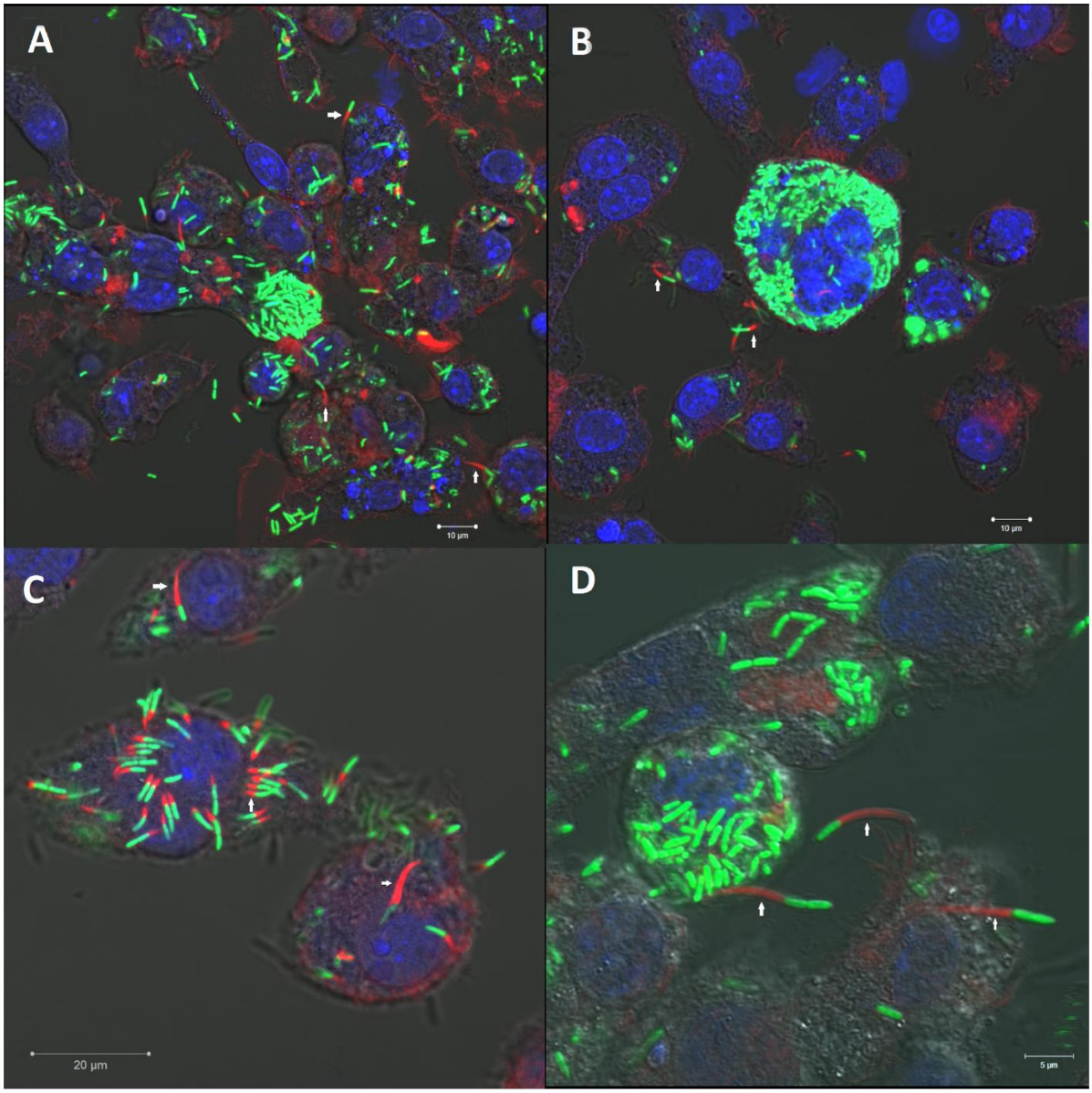

FIG 2 *B. thailandensis* E555 actin tail and multinucleated giant cell (MNGC) formation within RAW 264.7 macrophages. RAW264.7 macrophages were infected with *B. thailandensis* E555 enhanced green fluorescent protein (eGFP) and at 20 h postinfection were stained for actin using Alexa Fluor 647 phalloidin and a Hoechst nucleus stain. Images were taken using a confocal laser scanning microscope using 40× (A, B) and 63× (C, D) objectives. Arrows highlight examples of the bacterial actin tails.

however, we could not detect a significant enhancement in maturation of the phagolysosome.

DISCUSSION

Here, we investigated the ability of monoclonal antibodies to opsonize *B. pseudomallei*. A macrophage infection assay was chosen as the primary *in vitro* method to analyze intracellular infection and the effect of antibody opsonization.

Initially, *B. thailandensis* E555 was used in the development and testing of macrophage infection assays before progression to infection assays with *B. pseudomallei*

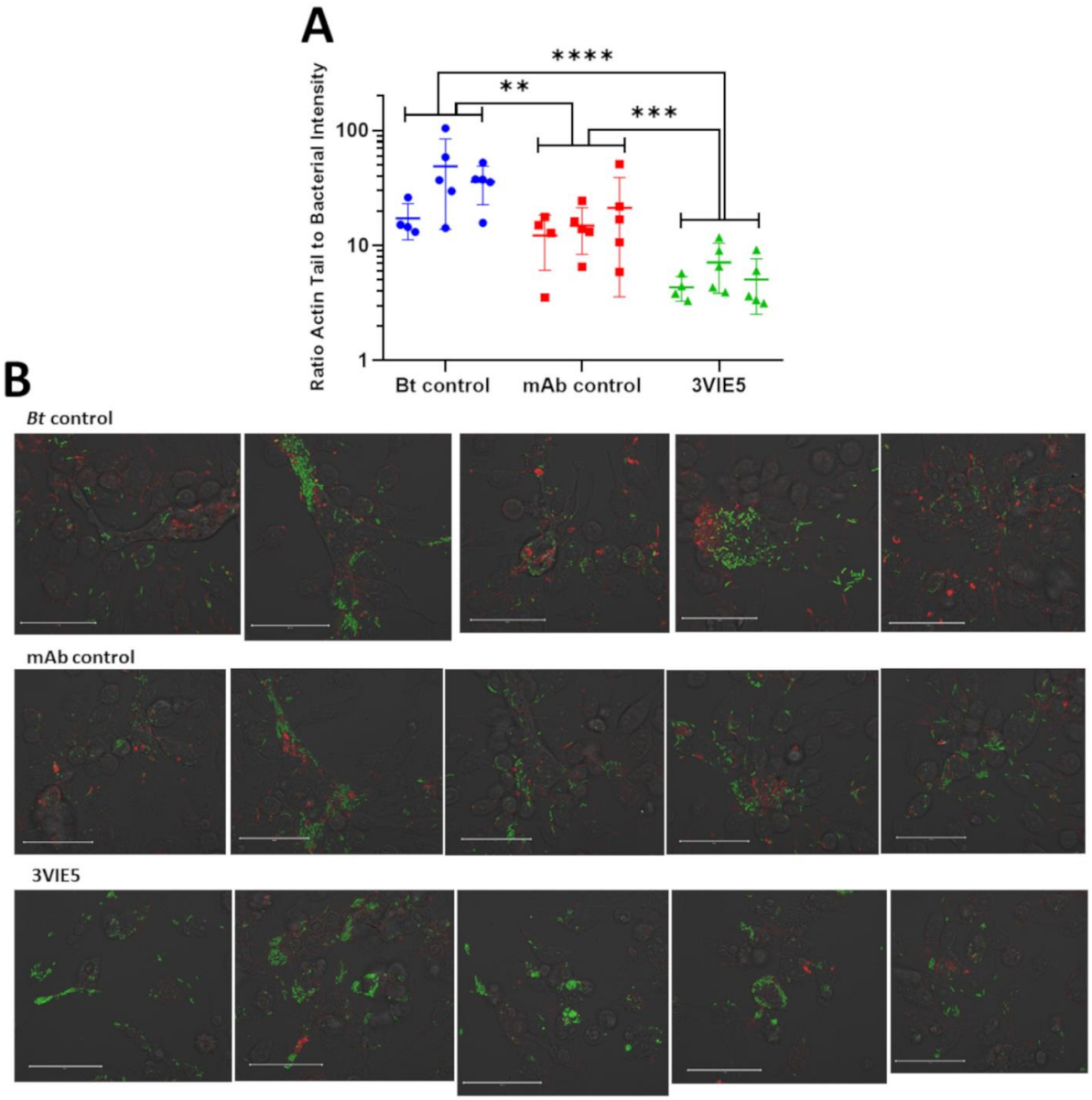

FIG 3 Ratio of actin tail fluorescence to bacterial fluorescence. (A) Bacterial actin tail fluorescence to GFP ratio was analyzed at 12 h postinfection using Icy open-source software. Data consist of 14 data points from 3 separate experimental weeks. **, $P = 0.0038$; ***, $P = 0.0002$; ****, $P < 0.0001$ (two-way analysis of variance [ANOVA] with Tukey's multiple-comparison test). (B) Example images used to calculate the actin tail to GFP fluorescence ratio. These images are a single representation of all the images taken, as the original images are 8,780 by 8,780 pixels. The images shown here are the central image from which the 5-by-5 tile scan was produced. Bar, 50 μm.

K96243. *B. thailandensis* E555 has been shown to be a suitable surrogate for *B. pseudomallei* K96243 compared to other *B. thailandensis* strains (32). Data from J774 macrophage infection assays show similar intracellular growth profiles for *B. thailandensis* E555 and *B. pseudomallei* K96243 (32), thus confirming the utility of E555 as a surrogate for *B. pseudomallei* in macrophage infection studies.

The opsonization ability of the MAbs was consistent across bacterial strain and analysis technique. The consistent results between the two *Burkholderia* species tested provided the opportunity to focus our research on *B. thailandensis*, which can be handled

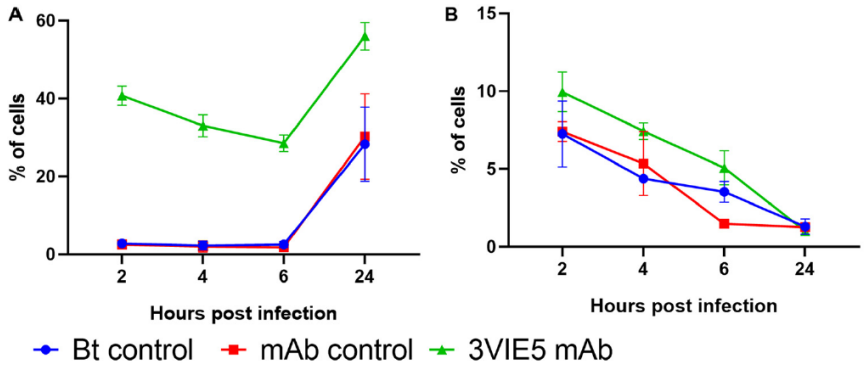

FIG 4 Effects of opsonization on RAW 264.7 macrophage association to *B. thailandensis* (A) and colocalization between intracellular *B. thailandensis* and LAMP-1 (B). Data shown are derived from two experiments (both derived from the mean of two biological replicates) and are shown as a repeated-measures plot. Repeated-measures ANOVA indicated a time effect in both plots ($P < 0.001$). Bonferroni's posttests indicate a difference in uptake between the 3VIE5 MAb and the control groups ($P < 0.05$) (A), and the ANOVA test indicated possible differences in LAMP-1 ($P < 0.05$) (B); however, these differences were not discernible by posttest.

at a lower level of containment, where a greater spectrum of analysis methods is available. Imaging flow cytometry combines the high-throughput aspects of standard flow cytometry (analyzing many cells though a flow cell) with the informative aspects of microscopy delivering thousands of images of cells. A *B. thailandensis* E555 strain expressing green fluorescent protein (GFP) was used to enable visualization of intracellular bacteria. Imaging flow cytometry was performed on RAW 264.7 macrophages harvested intact from a *B. thailandensis* E555 GFP infection assay to determine the opsonization ability of each MAb. The analysis of imaging flow cytometry was based upon a novel analysis and gating strategy (see Fig. S1 in the supplemental material). This strategy delivered information such as the proportion of cells infected and the relative bacterial load.

It has been demonstrated here that imaging flow cytometry is an alternative technique that can be successfully used to assess antibody opsonization within a macrophage infection assay. Imaging flow cytometry offers advantages over CFU analysis, such as the ability to analyze individual cell infection events, rather than the infection level of the whole population. It is to be noted that both methodologies have advantages and disadvantages. For example, CFU data are based on viable bacterial count on a population level, whereas imaging flow cytometry data are unable to distinguish between live and dead bacterial fluorescence. The comparable data from both methods increase the confidence in the data set. On a cell-by-cell level, antibody opsonization was shown to increase the average number of bacteria per cell, as well as increasing the overall percentage of infected cells in the population. Together, CFU and imaging flow cytometry analysis provide a robust method for analyzing intracellular infection levels in cell infection assays.

We observed that MAb opsonization reduced bacterial actin tail formation *in vitro*. It is known that *B. thailandensis* is able to form actin tails, similarly to *B. pseudomallei* and *B. mallei*, and that this is achieved by the conversion of G actin to F actin following bacterial escape from phagosomes into the cytosol (18, 21, 33). It is believed that bacterial actin-based motility can cause neighboring cells to contact, allowing the type VI secretory system of *Burkholderia* to cause cell fusion, leading to MNGC formation (24). The mechanism whereby the anti-capsule MAb 3VIE5 reduced actin tail formation is unknown. It is possible that MAb opsonization activates the cell, resulting in increased bacterial association with phagolysosomes and fewer cytosolic bacteria. However, in this study, no significant increase in association between bacteria and LAMP-1 was observed following antibody opsonization. Alternatively, opsonized bacteria could still be escaping from phagosomes

but the MAb prevents the bacteria from recruiting and polymerizing host actin in the cytosol. The mechanism for preventing access to host actin by the MAb is unknown; it could be as simple as the MAb essentially blocking access to the actin. However, elucidating the exact mechanism requires further research.

Reducing actin tail formation *in vitro* is a desirable characteristic of a therapeutic MAb for melioidosis. The ability of the MAb to reduce actin tail formation should, in theory, reduce the spread of infection between neighboring cells. Cell fusion enables the bacteria to spread intracellularly between cells, avoiding the extracellular environment, which may contain antibiotic therapy or host immune responses, such as specific bacterial antibodies. It is known that neutrophils (34, 35) and NK and CD8 cells (36) are likely to contribute to removal of bacteria. As an antibody therapy, the anti-CPS MAb 3VIE5 could be particularly useful as a combination therapy with antibiotics, and potentially with other host-directed compounds, such as autophagy inducers (37). This could involve utilizing the MAb to prevent bacterial motility within the intracellular environment, while the secondary component, such as the autophagy inducer or antibiotic, promotes bacterial clearance. We have shown that antibody opsonization of extracellular *B. thailandensis* can decrease actin tail formation, which in turn could reduce intracellular bacterial spread, which is a desirable property for a potential therapeutic.

It is unclear as to whether enhanced uptake by phagocytes would be of therapeutic value. The intracellular compartment may well provide a growth niche for *B. pseudomallei* (discussed in the introduction). As such, enhancing uptake may seem like folly. However, by using opsonization, we are targeting uptake into immune effector cells that could be activated to kill the bacteria. It is clear, however, that an MAb therapy alone is not the complete solution to infection. We are therefore combining MAb therapy with antibiotics by developing a proof-of-concept antibody-antibiotic conjugate (AAC) for melioidosis; at the time of writing, this work is still ongoing. Antibody conjugates have the potential to enhance killing by colocalizing antibiotic to bacterium within the intracellular phagosome environment. This has been demonstrated by recent developments of an AAC for *Staphylococcus aureus* and *Pseudomonas aeruginosa* (38–41). We are currently developing an AAC for melioidosis with the MAb 3VIE5 assessed in this opsonization study. This MAb has been linked to two different antibiotics via a cathepsin-cleavable linker and is currently undergoing *in vitro* assessment. The aim of this AAC is to use the opsonization ability of 3VIE5 to deliver antibiotic intracellularly, killing *B. pseudomallei* bacteria residing within the intracellular environment. The development of an AAC requires the use of a well-characterized antibody with a known ability to opsonize and target the bacterium of interest. In this study, the data we have outlined lays the foundation for the development of an AAC for melioidosis.

In summary, we have shown that a panel of monoclonal antibodies, directed against the capsule and LPS of *B. pseudomallei*, are opsonizing in a RAW 264.7 macrophage infection assay. Furthermore, an antibody directed against the capsule of *B. pseudomallei* has demonstrated the ability to reduce bacterial actin tail formation within macrophage cells, an important process that the bacterium requires for intracellular motility and, ultimately, for cell-to-cell spread. Imaging flow cytometry has been demonstrated to be an alternative to the CFU method for analyzing antibody opsonization of bacteria. In addition, this method offers a greater level of detail for analyzing antibody opsonization on a single-cell level. A capsule MAb analyzed in this study, 3VIE5, is being developed into an AAC as a proof-of-principle therapeutic for melioidosis.

MATERIALS AND METHODS

Macrophage cell culture. RAW 264.7 macrophages (ECCAC) were routinely cultured in Dulbecco's modified Eagle's medium (DMEM; Gibco) supplemented with 10% inactivated fetal bovine serum (Gibco) and 2 mM L-glutamine (Gibco). Macrophage cells were cultured within 150-cm^2 vented cell culture flasks (Corning) within a 37°C and 5% carbon dioxide humidified incubator. Cells were regularly passaged by cell scraping and culture into fresh DMEM when approximately 90% confluent; cells were not used past a passage number of 20.

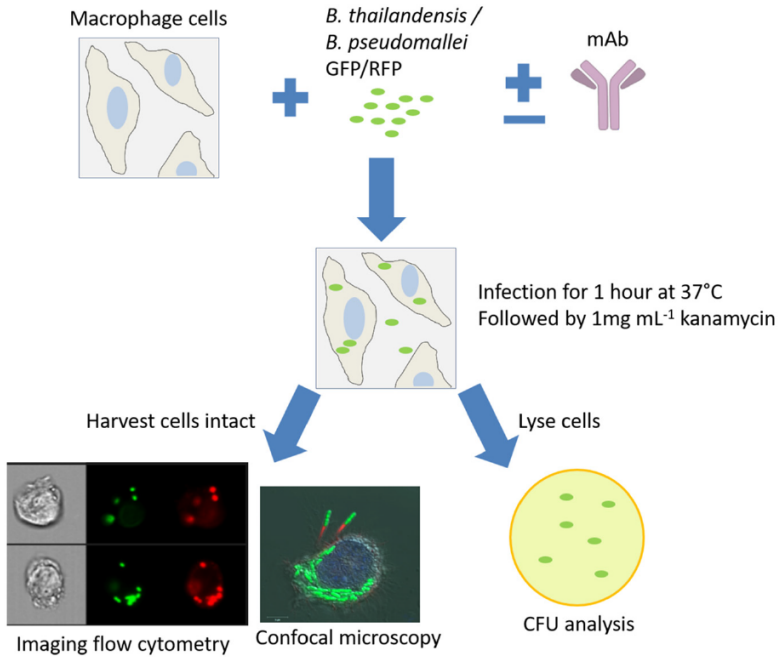

FIG 5 Macrophage infection assay. A RAW 264.7 macrophage infection assay was the primary method to analyze MAb opsonization of *B. pseudomallei* and *B. thailandensis*. Antibodies were incubated with bacteria prior to cell infection to allow for antibody-bacterium binding. Cells were infected for 1 h, followed by removal and replacement with kanamycin antibiotic medium. At specific time points, cells were harvested for analysis by imaging flow cytometry and confocal microscopy, or cells were lysed for bacterial enumeration.

Prior to use for an infection assay, macrophages were assessed for viability and counted by trypan blue (Sigma) cell exclusion using an automated cell counter (Nexcelom). Cells were typically cultured on 24-well cell culture plates (Corning) in DMEM at a concentration of 5×10^5 cells · ml^{-1} and cultured overnight within a 37°C, 5% carbon dioxide humidified incubator until cell density reached 1×10^6 cells · ml^{-1}.

Macrophage infection assay. An overnight broth culture of *B. thailandensis* E555 or *B. pseudomallei* K96243 was diluted to an approximate concentration of 1×10^8 bacteria · ml^{-1} using bacterial optical density (OD) readings of 0.172 OD at 600 nm (OD_{600}) and 0.4 OD_{590}, respectively. A 10% dilution of this bacterial suspension was prepared and added to RAW 264.7 macrophages at a multiplicity of infection (MOI) of 5 for 1 h at 37°C to allow bacterial uptake. Following the incubation period, the culture medium was removed and replaced with fresh Leibovitz's L-15 medium containing 1 mg · ml^{-1} kanamycin (Sigma) and incubated at 37°C to kill any remaining extracellular bacteria. This step was considered the start of time points to monitor intracellular bacteria. Following a specific incubation period (2 h for opsonization studies), the intracellular bacteria were enumerated by cell lysis with distilled water (Gibco) for a minimum of 10 min, serially diluted, plated onto Luria agar, and incubated at 37°C for 48 h. Macrophages were also harvested into phosphate-buffered saline (PBS) without lysis for analysis by imaging flow cytometry; in this case, macrophages were centrifuged at 300 × *g* for 5 min and resuspended into 4% paraformaldehyde (Alfa Aesar) prior to analysis. See Fig. 5 for an overview of the assay design.

Culture of *B. thailandensis* and *B. pseudomallei*. *B. thailandensis* E555 and *B. pseudomallei* K96243 were routinely cultured in Luria broth and on Luria agar plates. Green and red florescent protein-expressing strains (pBHR4-groS-eGFP and pBHR4-groS-RFP) of *B. thailandensis* E555 and *B. pseudomallei* K96243 were provided to Dstl by Exeter University, United Kingdom. Fluorescent strains were cultured in Luria broth and agar supplemented with 50 μg · ml^{-1} chloramphenicol to ensure that only plasmid-containing fluorescent protein-expressing bacteria were cultured. Culture of *B. thailandensis* was performed within containment level 2 facilities and culture of *B. pseudomallei* within containment level 3 facilities.

Actin tail staining. RAW 264.7 macrophages on a 35-mm cell culture dish (Corning) were fixed and permeabilized using a Cytofix/Cytoperm (BD Biosciences) kit following manufacturer's instructions. Alexa Fluor 647 phalloidin (Molecular Probes) was added to the RAW macrophages at 5% (vol/vol) and incubated at room temperature for 30 min. Following incubation, the RAW macrophages were washed twice with PBS, prior to visualization by confocal microscopy.

LAMP-1 staining. At the specified time point (between 2 and 24 h) postinfection, macrophages were harvested, transferred to 200 μl fixative-permeabilization buffer (BD Biosciences) and incubated for

30 min at room temperature on a roller. Following incubation, the sample volume was increased to 1 ml with 800 μl of 1× permeabilization-wash buffer (BD Biosciences) and centrifuged for 5 min at 300 × *g*. Following centrifugation, cells were resuspended into 200 μl permeabilization-wash buffer (BD Biosciences) containing 3.5 $\mu g \cdot ml^{-1}$ PE/Dazzle 594 anti-mouse CD107a (LAMP-1) antibody (BioLegend, UK) and incubated for 1 h at room temperature on a roller. Following incubation, 800 μl of PBS (Gibco) was added to the samples and centrifuged for 5 min at 300 × *g*. Finally, all cell pellets were resuspended into 50 μl PBS (Gibco) for analysis by imaging flow cytometry.

Confocal microscopy. Confocal microscopy was performed on a confocal laser scanning microscope (Zeiss). RAW 264.7 macrophages were analyzed on 35-mm cell culture dishes (Corning) using a 20×, 40×, or 63× oil immersion lens. Hoechst (Sigma) nuclei dye was added to RAW 264.7 macrophage cells at 2 $\mu g \cdot ml^{-1}$ to be able to discriminate between individual cells and multinucleated giant cells. Green fluorescent protein-expressing *B. thailandensis* E555 (pBHR4-groS-eGFP) was used throughout confocal microscopy studies.

The bacterial actin tail fluorescence to bacterial GFP ratio was calculated using Icy open-source software (http://icy.bioimageanalysis.org/) (29). To include as many cells as possible per image, the confocal microscope at ×20 magnification was set to image a 5 by 5 square tiled image around a chosen field of view, giving a total image analysis area size of 675 μm^2 (see Fig. S3 in the supplemental material). This process was repeated at multiple other locations on the cell culture dish and replicated across three separate weeks to generate the final data set.

Imaging flow cytometry. Imaging flow cytometry was performed on an Amnis ImageStream X mark II imaging flow cytometer. Cell samples were analyzed in a 50-μl volume within an Eppendorf tube. In total, 10,000 events were collected, consisting of cells gated according to being in focus and single cells. Channels 1 (bright field), 2 (GFP), 4 (RFP or LAMP-1), 6 (side scatter), and 9 (bright field) were all used at full laser power, as standard, during all analysis of *B. thailandensis* GFP- or *B. pseudomallei* RFP-infected RAW macrophages. Magnification was set at ×60 for all experiments. Compensation controls were performed on experiments consisting of more than one fluorescent marker, and the compensation matrix was then applied during data analysis. Data analysis for bacterial opsonization and LAMP-1 experiments was achieved using IDEAS (Amnis) software (see supplemental material).

Statistical analysis. GraphPad Prism v8 software was used in the preparation of all graphs. For statistical analysis, bacterial count data and actin ratio data were $\log_{10}$ transformed to better fit the test requirement for approximate Gaussian distribution equal variance. In all analyses, the test requirements were assessed using residual plots and quantile-quantile plots of the residuals against the normal distribution. Two-way ANOVA analysis of the actin ratio data was performed using GraphPad Prism v8, and the three experiments and three conditions were used as the two factors. Three-parameter ANCOVA analysis of the opsonization in the image stream and CFU data was performed using JASP v13.1 software. The three parameters were antibody, pathogen, and dose ($\log_{10}$ transformed and used as a continuous factor). Time course data were analyzed by repeated-measures ANOVA in which treatment and experimental run were factors. All posttests were performed using Bonferroni's correction.

SUPPLEMENTAL MATERIAL

Supplemental material is available online only.

SUPPLEMENTAL FILE 1, PDF file, 0.4 MB.

ACKNOWLEDGMENTS

This work was funded by the United Kingdom Ministry of Defence.

We thank Greg Bancroft at London School of Hygiene and Tropical Medicine for his support in reviewing the manuscript.

REFERENCES

1. Limmathurotsakul D, Golding N, Dance DA, Messina JP, Pigott DM, Moyes CL, Rolim DB, Bertherat E, Day NP, Peacock SJ, Hay SI. 2016. Predicted global distribution of *Burkholderia pseudomallei* and burden of melioidosis. Nat Microbiol 1:15008. https://doi.org/10.1038/nmicrobiol.2015.8.
2. Yee KC, Lee MK, Chua CT, Puthucheary SD. 1988. Melioidosis, the great mimicker: a report of 10 cases from Malaysia. J Trop Med Hyg 91:249–254.
3. Singh M, Mahmood M. 2017. Melioidosis: the great mimicker. J Community Hosp Intern Med Perspect 7:245–247. https://doi.org/10.1080/20009666.2017.1348875.
4. Currie BJ, Fisher DA, Anstey NM, Jacups SP. 2000. Melioidosis: acute and chronic disease, relapse and re-activation. Trans R Soc Trop Med Hyg 94:301–304. https://doi.org/10.1016/s0035-9203(00)90333-x.
5. Maharjan B, Chantratita N, Vesaratchavest M, Cheng A, Wuthiekanun V, Chierakul W, Chaowagul W, Day NPJ, Peacock SJ. 2005. Recurrent melioidosis in patients in northeast Thailand is frequently due to reinfection rather than relapse. J Clin Microbiol 43:6032–6034. https://doi.org/10.1128/JCM.43.12.6032-6034.2005.
6. Chaowagul W, Suputtamongkol Y, Dance DAB, Rajchanuvong A, Pattara J, White NJ. 1993. Relapse in melioidosis: incidence and risk factors. J Infect Dis 168:1181–1185.
7. Chien MFJ, Wijaya L, Tan TT. 2015. High mortality and relapse rates of melioidosis (*Burkholderia pseudomallei* infections) in Singapore. Open Forum Infect Dis 2:1628. https://doi.org/10.1093/ofid/ofv133.1181.
8. Lu R-M, Hwang Y-C, Liu IJ, Lee C-C, Tsai H-Z, Li H-J, Wu H-C. 2020. Development of therapeutic antibodies for the treatment of diseases. J Biomed Sci 27:1. https://doi.org/10.1186/s12929-019-0592-z.
9. Motley MP, Banerjee K, Fries BC. 2019. Monoclonal antibody-based therapies for bacterial infections. Curr Opin Infect Dis 32:210–216. https://doi.org/10.1097/QCO.0000000000000539.
10. Stone JK, DeShazer D, Brett PJ, Burtnick MN. 2014. Melioidosis: molecular aspects of pathogenesis. Expert Rev Anti Infect Ther 12:1487–1499. https://doi.org/10.1586/14787210.2014.970634.
11. Wiersinga WJ, van der Poll T, White NJ, Day NP, Peacock SJ. 2006. Melioidosis: insights into the pathogenicity of *Burkholderia pseudomallei*. Nat Rev Microbiol 4:272–282. https://doi.org/10.1038/nrmicro1385.

12. Willcocks SJ, Denman CC, Atkins HS, Wren BW. 2016. Intracellular replication of the well-armed pathogen *Burkholderia pseudomallei*. Curr Opin Microbiol 29:94–103. https://doi.org/10.1016/j.mib.2015.11.007.
13. Whiteley L, Meffert T, Haug M, Weidenmaier C, Hopf V, Bitschar K, Schittek B, Kohler C, Steinmetz I, West TE, Schwarz S. 2017. Entry, intracellular survival and multinucleated giant cell-forming activity of *Burkholderia pseudomallei* in human primary phagocytic and non-phagocytic cells. Infect Immun https://doi.org/10.1128/IAI.00468-17.
14. Allwood EM, Devenish RJ, Prescott M, Adler B, Boyce JD. 2011. Strategies for intracellular survival of *Burkholderia pseudomallei*. Front Microbiol 2:170. https://doi.org/10.3389/fmicb.2011.00170.
15. Gong L, Cullinane M, Treerat P, Ramm G, Prescott M, Adler B, Boyce JD, Devenish RJ. 2011. The *Burkholderia pseudomallei* type III secretion system and BopA are required for evasion of LC3-associated phagocytosis. PLoS One 6:e17852. https://doi.org/10.1371/journal.pone.0017852.
16. Burtnick MN, Brett PJ, Nair V, Warawa JM, Woods DE, Gherardini FC. 2008. *Burkholderia pseudomallei* type III secretion system mutants exhibit delayed vacuolar escape phenotypes in RAW 264.7 murine macrophages. Infect Immun 76:2991–3000. https://doi.org/10.1128/IAI.00263-08.
17. Ray K, Marteyn B, Sansonetti PJ, Tang CM. 2009. Life on the inside: the intracellular lifestyle of cytosolic bacteria. Nat Rev Microbiol 7:333–340. https://doi.org/10.1038/nrmicro2112.
18. Benanti EL, Nguyen CM, Welch MD. 2015. Virulent *Burkholderia* species mimic host actin polymerases to drive actin-based motility. Cell 161:348–360. https://doi.org/10.1016/j.cell.2015.02.044.
19. Kespichayawattana W, Rattanachetkul S, Wanun T, Utaisincharoen P, Sirisinha S. 2000. *Burkholderia pseudomallei* induces cell fusion and actin-associated membrane protrusion: a possible mechanism for cell-to-cell spreading. Infect Immun 68:5377–5384. https://doi.org/10.1128/IAI.68.9.5377-5384.2000.
20. Lamason RL, Welch MD. 2017. Actin-based motility and cell-to-cell spread of bacterial pathogens. Curr Opin Microbiol 35:48–57. https://doi.org/10.1016/j.mib.2016.11.007.
21. Stevens MP, Stevens JM, Jeng RL, Taylor LA, Wood MW, Hawes P, Monaghan P, Welch MD, Galyov EE. 2005. Identification of a bacterial factor required for actin-based motility of *Burkholderia pseudomallei*. Mol Microbiol 56:40–53. https://doi.org/10.1111/j.1365-2958.2004.04528.x.
22. Choe JE, Welch MD. 2016. Actin-based motility of bacterial pathogens: mechanistic diversity and its impact on virulence. Pathog Dis https://doi.org/10.1093/femspd/ftw099.
23. Welch MD, Way M. 2013. Arp2/3-mediated actin-based motility: a tail of pathogen abuse. Cell Host Microbe 14:242–255. https://doi.org/10.1016/j.chom.2013.08.011.
24. Toesca IJ, French CT, Miller JF. 2014. The type VI secretion system spike protein VgrG5 mediates membrane fusion during intercellular spread by *pseudomallei* group *Burkholderia* species. Infect Immun 82:1436–1444. https://doi.org/10.1128/IAI.01367-13.
25. Suparak S, Muangsombut V, Riyapa D, Stevens JM, Stevens MP, Lertmemongkolchai G, Korbsrisate S. 2011. *Burkholderia pseudomallei*-induced cell fusion in U937 macrophages can be inhibited by monoclonal antibodies against host cell surface molecules. Microbes Infect 13:1006–1011. https://doi.org/10.1016/j.micinf.2011.06.007.
26. Bayliss M, Donaldson MI, Nepogodiev SA, Pergolizzi G, Scott AE, Harmer NJ, Field RA, Prior JL. 2017. Structural characterisation of the capsular polysaccharide expressed by *Burkholderia thailandensis* strain E555:: *wbil* (pKnock-KmR) and assessment of the significance of the 2-*O*-acetyl group in immune protection. Carbohydr Res 452:17–24. https://doi.org/10.1016/j.carres.2017.09.011.
27. Jenner D, Ducker C, Clark G, Prior J, Rowland CA. 2016. Using multispectral imaging flow cytometry to assess an *in vitro* intracellular *Burkholderia thailandensis* infection model. Cytometry A 89:328–337. https://doi.org/10.1002/cyto.a.22809.
28. Jones SM, Ellis JF, Russell P, Griffin KF, Oyston PC. 2002. Passive protection against *Burkholderia pseudomallei* infection in mice by monoclonal antibodies against capsular polysaccharide, lipopolysaccharide or proteins. J Med Microbiol 51:1055–1062. https://doi.org/10.1099/0022-1317-51-12-1055.
29. de Chaumont F, Dallongeville S, Chenouard N, Hervé N, Pop S, Provoost T, Meas-Yedid V, Pankajakshan P, Lecomte T, Le Montagner Y, Lagache T, Dufour A, Olivo-Marin J-C. 2012. Icy: an open bioimage informatics platform for extended reproducible research. Nat Methods 9:690–696. https://doi.org/10.1038/nmeth.2075.
30. Joller N, Weber SS, Muller AJ, Sporri R, Selchow P, Sander P, Hilbi H, Oxenius A. 2010. Antibodies protect against intracellular bacteria by Fc receptor-mediated lysosomal targeting. Proc Natl Acad Sci U S A 107:20441–20446. https://doi.org/10.1073/pnas.1013827107.
31. Joller N, Weber SS, Oxenius A. 2011. Antibody-Fc receptor interactions in protection against intracellular pathogens. Eur J Immunol 41:889–897. https://doi.org/10.1002/eji.201041340.
32. Kovacs-Simon A, Hemsley CM, Scott AE, Prior JL, Titball RW. 2019. *Burkholderia thailandensis* strain E555 is a surrogate for the investigation of *Burkholderia pseudomallei* replication and survival in macrophages. BMC Microbiol 19:97. https://doi.org/10.1186/s12866-019-1469-8.
33. Stevens JM, Ulrich RL, Taylor LA, Wood MW, DeShazer D, Stevens MP, Galyov EE. 2005. Actin-binding proteins from *Burkholderia mallei* and *Burkholderia thailandensis* can functionally compensate for the actin-based motility defect of a *Burkholderia pseudomallei bimA* mutant. J Bacteriol 187:7857–7862. https://doi.org/10.1128/JB.187.22.7857-7862.2005.
34. Laws TR, Smither SJ, Lukaszewski RA, Atkins HS. 2011. Neutrophils are the predominant cell-type to associate with *Burkholderia pseudomallei* in a BALB/c mouse model of respiratory melioidosis. Microb Pathog 51:471–475. https://doi.org/10.1016/j.micpath.2011.07.002.
35. Easton A, Haque A, Chu K, Lukaszewski R, Bancroft GJ. 2007. A critical role for neutrophils in resistance to experimental infection with *Burkholderia pseudomallei*. J Infect Dis 195:99–107. https://doi.org/10.1086/509810.
36. Lertmemongkolchai G, Cai G, Hunter CA, Bancroft GJ. 2001. Bystander activation of $CD8^+$ T cells contributes to the rapid production of IFN-γ in response to bacterial pathogens. J Immunol 166:1097–1105. https://doi.org/10.4049/jimmunol.166.2.1097.
37. Laws TR, Taylor AW, Russell P, Williamson D. 2019. The treatment of melioidosis: is there a role for repurposed drugs? A proposal and review. Expert Rev Anti Infect Ther 17:957–967. https://doi.org/10.1080/14787210.2018.1496330.
38. Lehar SM, Pillow T, Xu M, Staben L, Kajihara KK, Vandlen R, DePalatis L, Raab H, Hazenbos WL, Hiroshi Morisaki J, Kim J, Park S, Darwish M, Lee B-C, Hernandez H, Loyet KM, Lupardus P, Fong R, Yan D, Chalouni C, Luis E, Khalfin Y, Plise E, Cheong J, Lyssikatos JP, Strandh M, Koefoed K, Andersen PS, Flygare JA, Wah Tan M, Brown EJ, Mariathasan S. 2015. Novel antibody-antibiotic conjugate eliminates intracellular *S. aureus*. Nature 527:323–328. https://doi.org/10.1038/nature16057.
39. Mariathasan S, Tan M-W. 2017. antibody-antibiotic conjugates: a novel therapeutic platform against bacterial infections. Trends Mol Med 23:135–149. https://doi.org/10.1016/j.molmed.2016.12.008.
40. Zhou C, Lehar S, Gutierrez J, Rosenberger CM, Ljumanovic N, Dinoso J, Koppada N, Hong K, Baruch A, Carrasco-Triguero M, Saad O, Mariathasan S, Kamath AV. 2016. Pharmacokinetics and pharmacodynamics of DSTA4637A: a novel THIOMAB^{TM} antibody antibiotic conjugate against *Staphylococcus aureus* in mice. mAbs 8:1612–1619. https://doi.org/10.1080/19420862.2016.1229722.
41. Kajihara KK, Pantua H, Hernandez-Barry H, Hazen M, Deshmukh K, Chiang N, Ohri R, Castellanos ER, Martin L, Matsumoto ML, Payandeh J, Storek KM, Schneider K, Smith PA, Koehler MFT, Tsai SP, Vandlen R, Loyet KM, Nakamura G, Pillow T, Seshasayee D, Kapadia SB, Hazenbos WLW, Projan SJ. 2021. Potent killing of *Pseudomonas aeruginosa* by an antibody-antibiotic conjugate. mBio 12:e00202-21. https://doi.org/10.1128/mBio.00202-21.

5. Repurposed drugs as anti-bacterial compounds.

5.1 Introduction.

With the rise in antibiotic resistance among bacterial infections there is an urgent need to research alternatives to antibiotics. Unless action is taken, by 2050 it is predicted that 10 million people a year will die from drug resistant infections, together with a cost of 100 trillion dollars to the global economy (286). To continue successful treatment of bacterial infections in the future, research into new therapeutic approaches is required now. Given the intrinsic antibiotic resistance of *B. pseudomallei*, this requirement for alternative anti-microbial therapies applies to melioidosis (271, 287, 288).

Screening of existing FDA approved drugs for anti-microbial properties can lead to drugs being repurposed as anti-microbial therapies. There are a variety of drugs that may have synergistic effects in combination with current antibiotics, for example by stimulating host cell mediated killing pathways such as autophagy. Alternatively, the repurposed drugs may have synergistic effects with current therapies as an adjunct (289, 290), thereby improving the efficacy of antibiotics. Drug repurposing offers many advantages, much of the toxicity, pharmacodynamic and pharmacokinetic data for the drug will already be known (290). This chapter focuses on FDA approved drugs that in the literature have shown potential as an anti-microbial. In the first instance, a panel of potential anti-microbial compounds will be assessed *in vitro* for ability to reduce *B. thailandensis* infection. Depending upon the outcome of the initial studies, down-selected compounds will be further assessed in cell infection assays.

As described previously, *B. pseudomallei* is an intracellular pathogen and therefore therapies that promote killing of intracellular bacteria are likely to be successful in eradiating infection. A review of the literature highlighted several compounds that have potential to reduce intracellular bacteria, which could be of interest as repurposing as antimicrobial compounds. The compounds verapamil, norverapamil, carbamazepine and valproic acid were selected to investigate further in this chapter.

Verapamil and the metabolite norverapamil, have both been investigated as potential antimicrobial compounds. Verapamil is a calcium channel antagonist, and is an FDA approved drug for heart conditions such as angina and hypertension. Verapamil demonstrates potential as a host directed therapy to reduce intracellular *M. tuberculosis* (207, 219-225). Concentrations as low as 12.5 µM verapamil have reduced intracellular *M. tuberculosis* by 40% *in vitro* (207). Norverapamil is the metabolite of verapamil, and has a similar ability to reduce intracellular bacteria within *in vitro* cell infection assays (207). Verapamil has been tested as an adjunct with antibiotics in an inhalable therapy for inhalational *M. tuberculosis*, the verapamil and antibiotic combination demonstrates an enhanced effect compared to the individual drugs alone (291). Verapamil is an efflux pump inhibitor and therefore has direct effects on the bacterium (219, 230, 231), in addition to host directed effects such as inducing autophagy (227, 292). This complicates analysis of this compound *in vitro*, since verapamil could potentially increase the effect or increase intracellular accumulation of antibiotics, such as the kanamycin present in the cell maintenance media (2.2.3. Repurposed drugs infection assay.). In this study the host directed effect of verapamil will be assessed, together with any direct bacterial effects. Additionally, the combination of verapamil and kanamycin in the *in vitro* infection assay will be investigated, this is important to determine the effect of kanamycin in combination with verapamil *in vitro*.

Carbamazepine is a FDA approved drug commonly used for treatment of epilepsy and bipolar disorder, this drug has potential to reduce intracellular *M. tuberculosis* infection in macrophages and can stimulate autophagy (226, 227). The drug has additionally demonstrated potential from *in vivo* studies involving zebrafish, and murine models of infection (226).

Valproic acid is a FDA approved anti-convulsive drug, the drug has potential to stimulate autophagy and bacterial clearance of *M. tuberculosis* in cell infection assays (226, 227). A concentration of 1mM of valproic acid increased nitric oxide production, and reduced survival of *M. tuberculosis* in J774 cells stimulated with IFN-γ (293).

Melioidosis is often misdiagnosed as tuberculosis (294), both share a strong host interferon dominated response to infection, and can be difficult to distinguish (295).

Similarities between the infections include the forming of an intracellular niche within macrophages, granuloma like formations, giant cells, and the ability to form latent infections (100). Given the similarities in intracellular infection characteristics, compounds investigated for tuberculosis infection could also offer potential as therapeutics for melioidosis.

The aims of this chapter can be summarised as:

- Investigate compounds that in the literature demonstrate potential anti-microbial properties. The compounds could offer potential as a combination therapies with antibodies or antibiotics, as an improved therapy option for melioidosis.
- Assess a panel of compounds in the RAW macrophage-like cell infection assay for bacterial killing.
- Down-select a compound for further analysis in RAW cell infection assays, including cell toxicity assays, bacterial killing and mechanism of bacterial killing.

5.2. Assessment of potential antimicrobial compounds in a RAW cell infection assay.

The aim of this set of experiments was to investigate possible alternatives to antibiotics, a panel of compounds were selected from the literature to test *in vitro* for anti-microbial activity. The compounds verapamil hydrochloride, norverapamil, carbamazepine and valproic acid were assessed for ability to reduce intracellular *B. thailandensis* infection within a RAW macrophage-like cell infection assay (Figure 33) (2.2.3. Repurposed drugs infection assay.). An initial screen of each compound at a concentration of 100μM will be used to select compounds for further investigation (Figure 34). Studies have shown that concentrations from 30μM of carbamazepine (226), 0.5mM of valproic acid (226, 296), 12.5μM of verapamil and norverapamil (207), demonstrate anti-microbial effects *in vitro*. It is not known what concentration of each compound will demonstrate killing of *B. thailandensis* in RAW cells. Therefore a concentration of 100μM was chosen, as a starting concentration for each

compound that was likely to demonstrate anti-microbial effects for the majority of the compounds tested. Down-selected compounds from the initial screen will be subsequently assessed in a RAW cell infection assay at multiple concentrations, to determine an optimum concentration for killing of *B. thailandensis in vitro* (2.2.3. Repurposed drugs infection assay.).

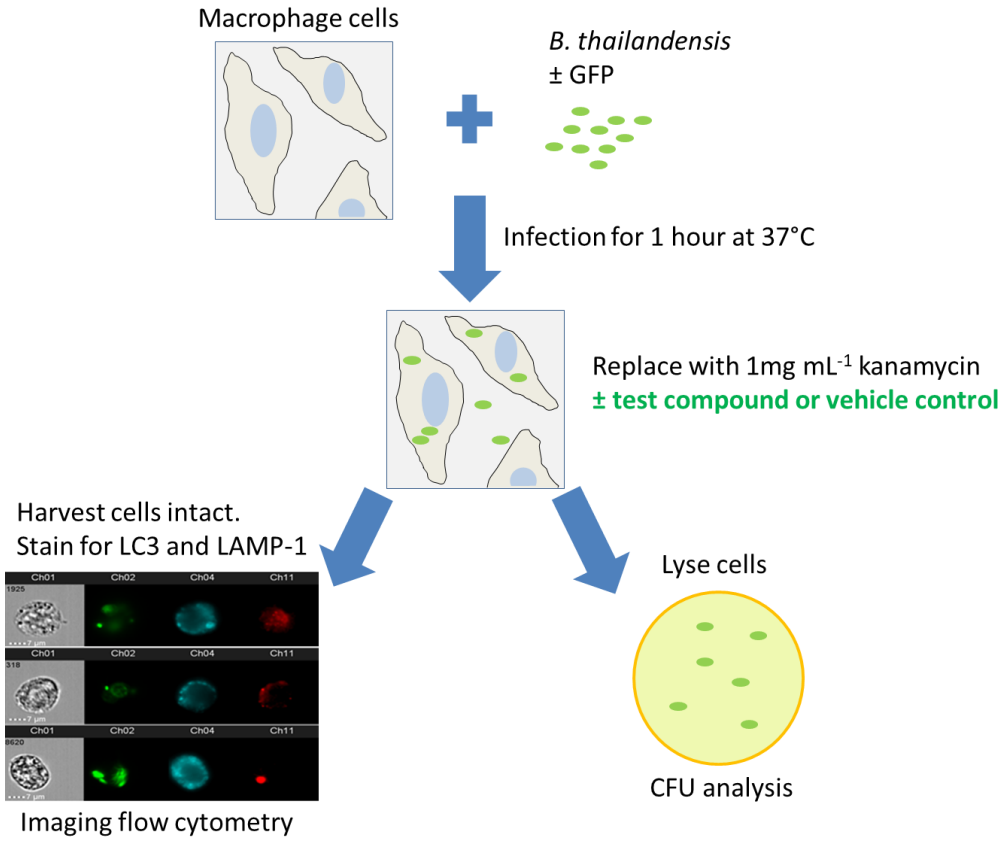

Figure 33. RAW cell infection assay to determine antimicrobial effects of each compound.

The RAW 264.7 macrophage-like cell infection assay was selected as the primary method to analyse intracellular infection by *B. thailandensis* E555 (2.2.3. Repurposed drugs infection assay.. RAW cells were infected with *B. thailandensis* at a multiplicity of infection (MOI) of 5 and incubated for an hour at 37°C. Following incubation the bacteria were removed and the cell culture media was subsequently replaced with 1mg mL^{-1} kanamycin maintenance antibiotic to kill extracellular bacteria. Additionally, test compounds were added post-infection and incubated with the infected RAW cells for up to 24 hours. GFP expressing *B. thailandensis* E555 (pBHR4-groS-eGFP) were used in the RAW cell assay to visualise bacterial infection by imaging flow cytometry. For CFU analysis RAW cells were lysed with distilled water and enumerated on L-agar. Alternatively, the cells were harvested intact into 4% paraformaldehyde for fixation and analysis by imaging flow cytometry. Subsequent experiments include staining RAW cells for autophagy, as a host-directed mechanism of bacterial killing. Staining for autophagy was achieved with

anti-LC3 and anti-LAMP-1 specific fluorescent antibodies, and analysis by imaging flow cytometry.

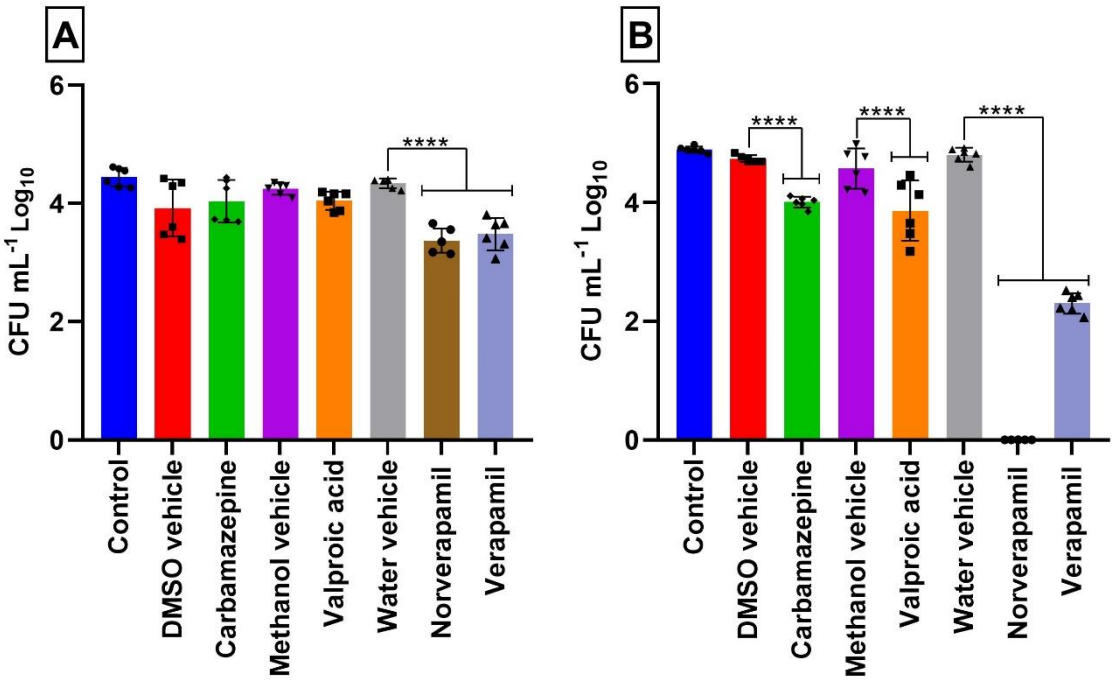

Figure 34. Effect of compounds on viability of intracellular *B. thailandensis*.

RAW cells were infected with *B. thailandensis* and incubated with 100μM of carbamazepine, valproic acid, norverapamil and verapamil. Each compound was assessed for ability to reduce intracellular *B. thailandensis,* this was achieved by CFU enumeration at 4 and 24 hours post-infection. RAW cells were infected with *B. thailandensis* E555 at a multiplicity of infection (MOI) of 5, test compounds were added post-infection at and incubated with the infected RAW cells for up to 24 hours. Intracellular *B. thailandensis* was enumerated by lysing RAW cells with distilled water, serial dilution and culture on L-agar. A separate vehicle control for each compound was incubated with RAW cells, and assessed for bacterial killing. **A –** 4 hours incubation and **B -** 24 hours incubation. Controls consist of a no compound control, DMSO vehicle (for carbamazepine), water vehicle (for verapamil and norverapamil) and methanol vehicle (for valproic acid). Data are represented as the mean of technical replicates (n=6) derived from two independent biological experiments, and error bars represent SD of all technical replicates. **** P <0.0001. One-way ANOVA Dunnett's multiple comparisons test.

There is a significant reduction in RAW cell intracellular *B. thailandensis* infection when incubated for 4 hours with verapamil hydrochloride or norverapamil. The vehicle control RAW cell intracellular CFU was 2.4 $x10^4$, this reduces significantly to 2.2 $x10^3$ and 4.3 $x10^3$ for norverapamil and verapamil respectively (Figure 34).

At 24 hours of incubation there is a significant reduction in CFU for verapamil, with a reduction from 5.5 $x10^4$ CFU for the vehicle control, to 2.5 $x10^2$ CFU for verapamil. In wells incubated with norverapamil there is complete CFU clearance at 24 hours, compared to the vehicle control of 5.5 $x10^4$ CFU. Both carbamazepine and valproic acid also significantly reduced intracellular bacterial CFU, although only at 24 hours of incubation. Carbamazepine significantly reduced intracellular CFU, from a vehicle control of 4.9 $x10^4$ CFU to $1x10^4$ CFU, at 24 hours of incubation. Valproic acid significantly reduced intracellular CFU, from a vehicle control of 5.9 $x10^4$ to 1.3 $x10^4$ CFU, at 24 hours of incubation. A significant reduction is only observed at the 24 hour post-infection time point for both compounds, and the reduction in CFU is to a lesser extent than both verapamil and norverapamil.

Based on this data set, both verapamil hydrochloride and norverapamil hydrochloride were selected for further investigation in this chapter.

5.3. The effect of verapamil and norverapamil on the viability of *B. thailandensis* bacterial culture.

The aim of this experiment was to determine if both verapamil and norverapamil can kill *B. thailandensis* E555 when there are no RAW cells present. This experiment will be a test of the effect of verapamil and norverapamil directly on a bacterial culture. An MIC (minimum inhibitory concentration) assay was used in which a visual observation of bacterial replication inhibition determines an MIC value, together with an OD reading from an automated incubating plate reader over 24 hours (2.6.7. Minimum inhibitory concentration (MIC).). A serial dilution of each compound was assessed by optical density for ability to reduce replication of *B. thailandensis*. An overnight Luria broth culture of *B. thailandensis* E555 was diluted to an approximate concentration of $1x_{10}^8$ bacteria mL^{-1}, using a bacterial OD reading of 0.172 OD_{600nm}. The bacterial suspension was further diluted to 1_{x10}^6 cfu mL^{-1} with dilutions into Luria broth. A 96 well culture plate (Corning™ Costar™) was prepared with dilutions of

verapamil and norverapamil (from 400µm) within a 100µL volume of Luria broth per well. To each well, 100µL of the 1_{x10}^{6} cfu mL bacterial suspension was added, therefore the total volume was 200 µL per well. Control wells consisted of positive bacterial culture with compounds present, and negative controls consisted of 200 µL of Luria broth only. Plates were sealed with an optically clear sterile plate sealer and placed within an incubating plate reader (Multiskan FC, Thermo), with the incubator set to 37°C with gentle shaking. Automated OD readings were taken at OD_{595} every 15 minutes for 24 hours. The MIC was calculated by a visual examination of the 96 well plate to determine wells with no bacterial replication, as stated in the Clinical and Laboratory Standards Institute (CLSI) guidelines (245). Additionally, the OD readings from the incubating plate reader (Multiskan FC, Thermo) were plotted to display bacterial replication over 24 hours.

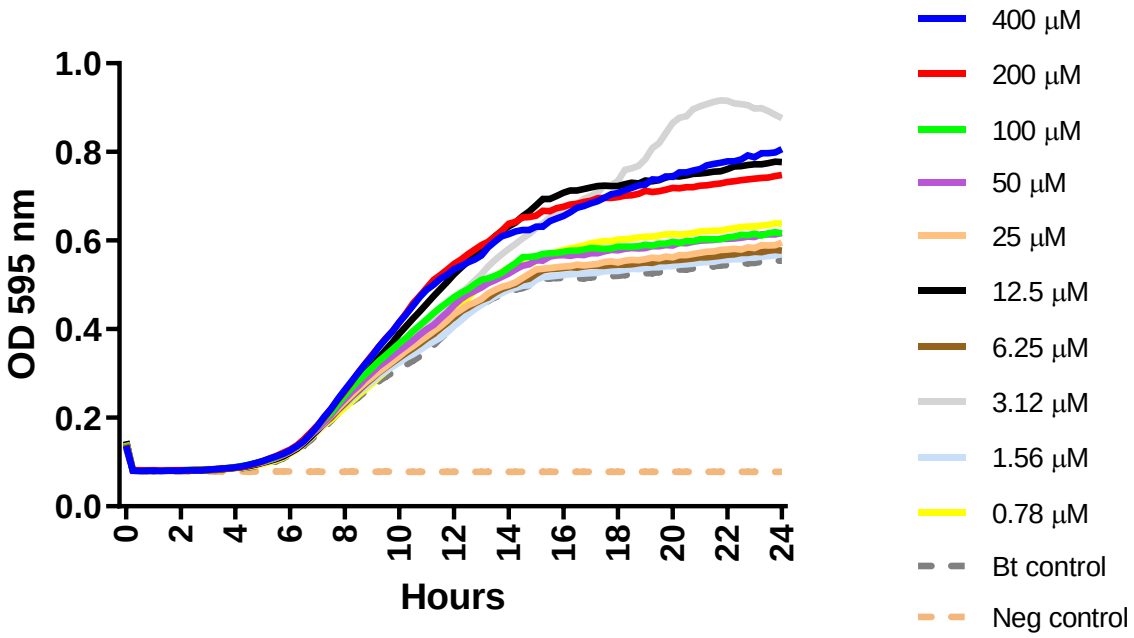

Figure 35. MIC of verapamil on a *B. thailandensis* culture.

The aim of this experiment was to determine any direct anti-microbial effects of verapamil. Verapamil hydrochloride was incubated with a culture of *B. thailandensis* over 24 hours to determine an MIC. Verapamil hydrochloride was serial diluted across a micro titre plate from 400µM to 0.7µM, and assessed for any ability to inhibit the replication of *B. thailandensis* E555. An overnight Luria broth culture of *B. thailandensis* E555 was diluted to an approximate concentration of $1x_{10}^{8}$ bacteria mL^{-1}, using a bacterial OD reading of 0.172 OD_{600nm}. The bacterial suspension was further diluted to 1_{x10}^{6} cfu mL^{-1} with dilutions into Luria broth, the culture was then added to the 96 well plate together with the verapamil dilutions. The 96 well plate was incubated at 37 °C with shaking, and optical density readings (OD 595 nm) were taken every 15 minutes for 24 hours. Controls consist of a positive *B. thailandensis* E555 bacterial only control and a negative L-broth only control. Each line represents an average OD from all technical replicates (n=4) derived from two independent biological experiments.

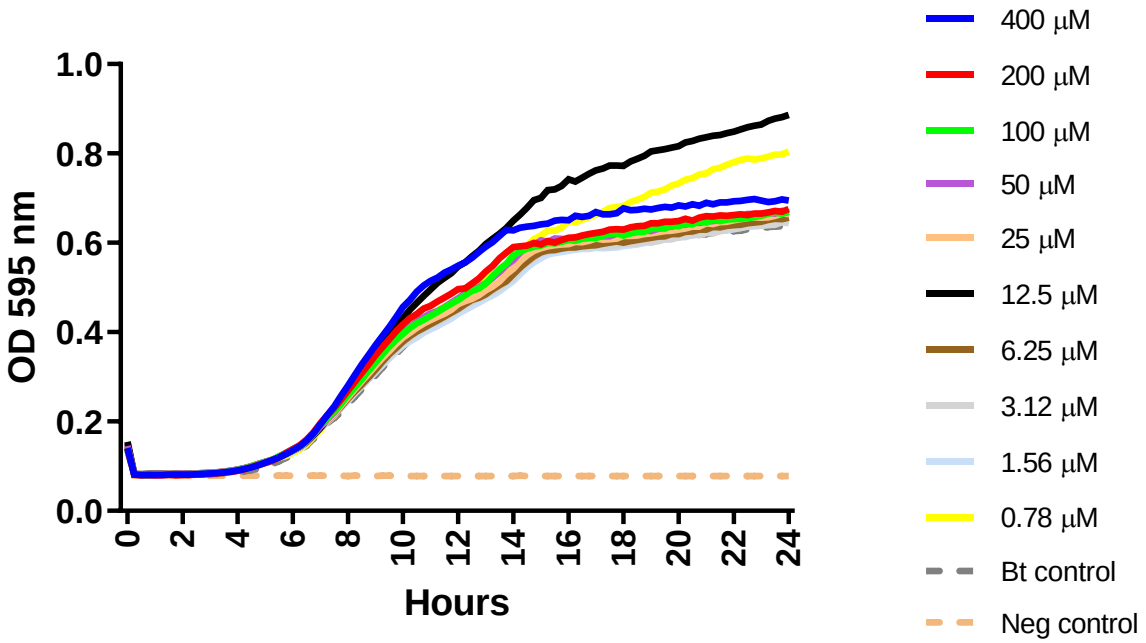

Figure 36. MIC of norverapamil on a *B. thailandensis* culture.

The aim of this experiment was to determine any direct anti-microbial effects of norverapamil. The compound was incubated with a culture of *B. thailandensis* over 24 hours to determine an MIC. Norverapamil hydrochloride was serial diluted across a micro titre plate from 400µM to 0.7µM, and assessed for any ability to inhibit the replication of *B. thailandensis* E555. An overnight Luria broth culture of *B. thailandensis* E555 was diluted to an approximate concentration of $1x_{10}^{8}$ bacteria mL^{-1}, using a bacterial OD reading of 0.172 OD_{600nm}. The bacterial suspension was further diluted to 1_{x10}^{6} cfu mL^{-1} with dilutions into Luria broth, the culture was then added to the 96 well plate together with the verapamil dilutions. The 96 well plate was incubated at 37 °C with shaking, and optical density readings (OD 595 nm) were taken every 15 minutes for 24 hours. Controls consist of a positive *B. thailandensis* E555 bacterial only control and a negative L-broth only control. Each line represents an average OD from all technical replicates (n=4) derived from two independent biological experiments.

Both verapamil and norverapamil had no direct inhibition on the replication of *B. thailandensis* at the range of concentrations tested (Figure 35 and Figure 36). No inhibition of bacterial replication was observed by visual examination of bacterial

growth after 24 hours incubation, therefore, no MIC value was determined for either compound. More quantitative analysis methods are available for determination of bacterial replication, such as Gompertz fitting and Richards models. The Richards modelling in particular has been demonstrated to be a good model for OD data (297). No inhibition of growth was observed in this experiment, therefore the visual observation of bacterial growth was deemed sufficient for the purpose of this experiment. There is an increase in OD observed at some concentrations, this is either due to a low level contamination in one of the replicates, or potentially some aggregation in the inoculum leading to that well receiving a higher inoculum. The increase is not dose dependent and therefore is not an effect of the verapamil or norverapamil. The aim of this experiment was to determine if the reduction in CFU, observed in the RAW macrophage-like cell infection assay (Figure 34), is due to the compound having direct anti-microbial activity against *B. thailandensis*. This data shows that both verapamil and norverapamil have no direct anti-microbial effect on *B. thailandensis*. Therefore to observe killing by these compounds there is a requirement for the RAW cell to be present, or another factor of the cell infection assay such as extracellular antibiotics to be present.

5.4. Cell toxicity of verapamil and norverapamil.

The aim of this experiment was to assess the toxicity of verapamil and norverapamil on the RAW 264.7 macrophage like cell line. The anti-bacterial effect of verapamil and norverapamil could be due to cell toxicity, and cell death of RAW cells leading to exposure of the intracellular *B. thailandensis* to the extracellular 1 mg mL^{-1} kanamycin maintenance media. A lactose dehydrogenase (LDH) colorimetric assay was used to determine toxicity of verapamil and norverapamil on RAW 264.7 cells over 24 hours (Figure 37) (2.6.6. Analysis of LDH release from RAW cells.). The toxicity of each compound on the cells is important, if the compound is causing cell lysis, then extracellular kanamycin could be responsible for intracellular killing observed in the *in vitro* infection assays. LDH is an enzyme present within the RAW cells, LDH is released extracellularly into the cell culture media during cell lysis. The increase in detection of LDH is therefore a quantitative measure of cell lysis caused by verapamil or norverapamil.

Analysis of lactose dehydrogenase (LDH) release from RAW cells was achieved with the use of Promega CytoTox 96® Non-Radioactive Cytotoxicity Assay kit (Promega Corporation USA), following manufacturer's instructions. Briefly, RAW 264.7 cells (ECCAC) were cultured on 24 well cell culture plates at 1_{x10}^{6} cells mL^{-1} (Corning™ Costar™) and incubated with verapamil and norverapamil at concentrations of between 10µm and 200µm. At the specified time points, the cell culture media in each well was gently mixed and 50µL of media removed for analysis. Cell culture samples were transferred to a 96 well cell culture plate (Corning™ Costar™), 50µL of CytoTox 96® reagent was added to each well. The plate was incubated in the dark at room temperature for 30 minutes prior to addition of 50µl CytoTox 96® stop solution. Absorption of each well was read on a plate reader set at 492nm wavelength. Percentage of cell lysis was calculated by comparison to a lysis control, in which all RAW cells were lysed by CytoTox 96® lysis solution.

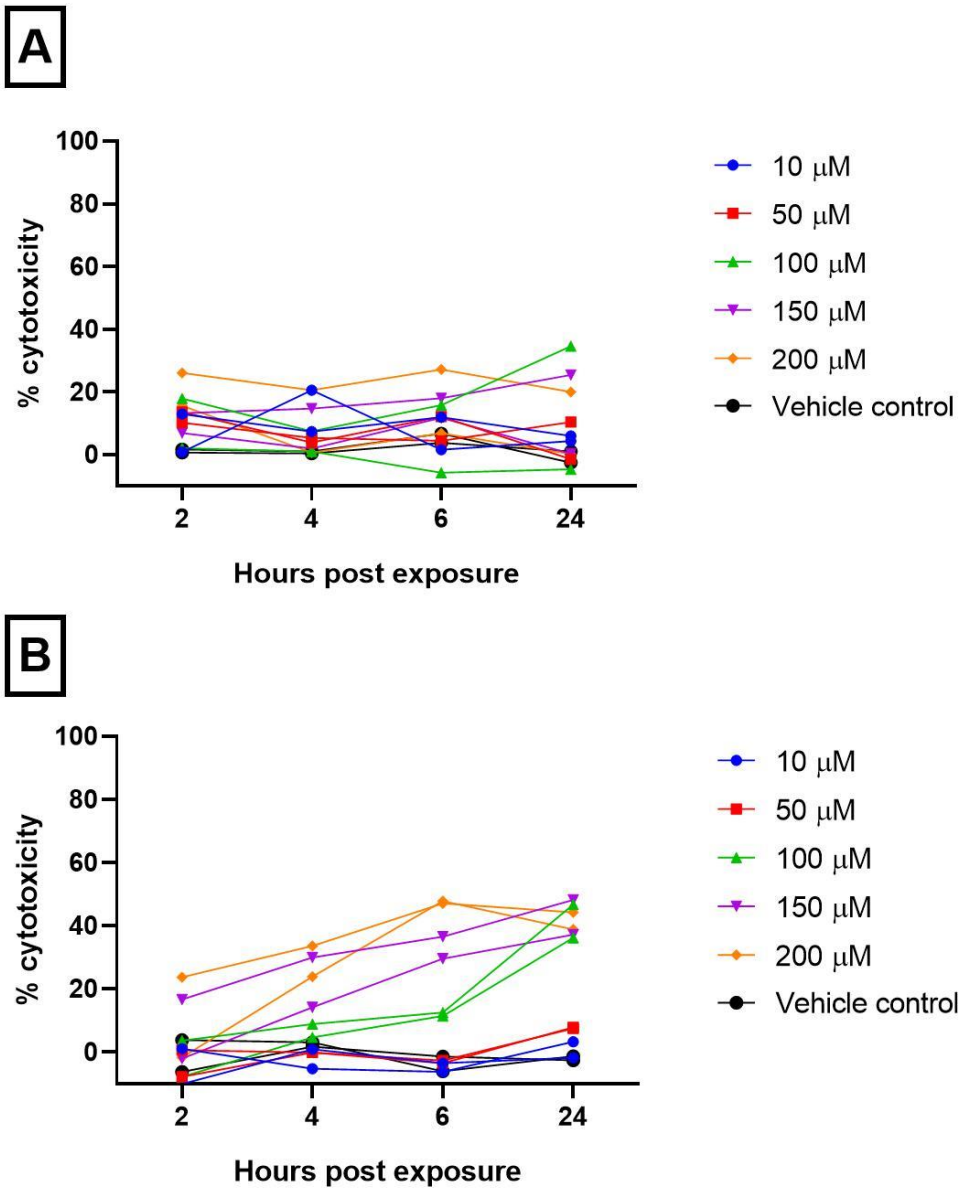

Figure 37. Determining toxicity of verapamil and norverapamil by the release of LDH from RAW cells.

RAW cells at 1_{x10}^{6} cells mL^{-1} on a 24 well cell culture plate were incubated with concentrations of verapamil and norverapamil of between 10μm and 200μm. RAW cells and the compounds were incubated at 37°C for between 2 and 24 hours. At each time point the cell culture media in each well was gently mixed and 50μL of media removed for analysis. Cell lysis releases LDH which is detected with the use of a LDH colorimetric detection kit (Promega Corporation USA). Cell toxicity was calculated based on a maximum LDH release RAW cell lysis control, the percentage cytotoxicity was calculated as the percentage above the RAW control cells. **A** –

Verapamil hydrochloride, **B** – Norverapamil hydrochloride. Each line represents the average OD of technical replicates (n=3) and two independent biological replicates are each represented by a separate line. Verapamil concentrations or the effect of hours post-exposure, were deemed not significant by two-way ANOVA. Norverapamil concentrations and hours post-exposure, both have a significant effect for norverapamil only. The source of the majority of the variation in the data set was norverapamil concentration (58.78%) ** P 0.0018, and hours post-infection (17.37%) *** P 0.0002, two-way ANOVA. Post tests could not discriminate significance between the different norverapamil concentrations.

Verapamil increased cytotoxicity when compared to the control cells. At a concentration of 200 μM, verapamil increased cytotoxicity over the 24 hours between 20% and 27% above the control. There is variability in the data between replicates, although the cytotoxicity does not rise above 34% for any verapamil concentrations throughout the 24 hour incubation. RAW cells incubated with norverapamil generally have a higher level of cytotoxicity, with a maximum of 23% at 2 hours to 48% at 24 hours. At 24 hours, norverapamil concentrations of 100μM and above have a cell cytotoxicity of between 36% and 48%, above the level of the control cells. All concentrations below 100μM have a cytotoxicity of under 7% at 24 hours incubation. The data for norverapamil is less variable, and there is a dose and time trend to the cytotoxicity data. This is reflected in the statistics, both time and concentration were significant factors in the norverapamil data, with a two-way ANOVA P-value of 0.0002 and 0.0018 respectively.

This data has highlighted that cells incubated with norverapamil concentrations of 100μM and above, have a higher cytotoxicity than the equivalent verapamil concentrations. Norverapamil reduced intracellular CFU to a greater extent than verapamil in the RAW cell infection assay (Figure 34), this could be attributed to a greater cytotoxicity on the RAW cells from incubation with norverapamil. Based on this cytotoxicity data and previous anti-microbial data, verapamil was taken forward as the primary compound of interest to investigate further.

5.5. The effect of verapamil on bacterial CFU in a RAW cell infection assay.

Verapamil hydrochloride was down selected for further investigation, based upon previous *in vitro* RAW macrophage-like cell infection assay data and cytotoxicity data. Previous *in vitro* experiments assessed verapamil at a single concentration of 100μM. The aim of this experiment is to expand upon the initial data and include a range of concentrations of verapamil, the aim is to determine if concentrations as low as 10μM can reduce intracellular bacteria in a RAW cell infection assay (2.2.3. Repurposed drugs infection assay.).

Verapamil did not inhibit bacterial replication in the previous MIC assays, and therefore the killing effect of verapamil on intracellular bacteria is likely to be host directed. There is a possibility that intracellular bacteria are directly susceptible to killing by verapamil, potentially in the low pH environment of the phagolysosome. This could be investigated in future studies by testing verapamil in MIC assays at a lower pH. This study will investigate different concentrations of verapamil for ability to kill intracellular *B. thailandensis*, this will be followed by studies to investigate the host directed killing response, such as verapamil induction of autophagy.

In this study verapamil was tested at 4 and 24 hours post infection, and at a range of concentrations from 10μM to 200μM. RAW cells were infected with *B. thailandensis* at a multiplicity of infection (MOI) of 5 and incubated for an hour at 37°C. Following incubation the bacteria were removed and the cell culture media was subsequently replaced with 1mg mL^{-1} kanamycin maintenance antibiotic to kill extracellular bacteria. Additionally, verapamil concentrations of between 10μm and 200μm were added post-infection, and incubated with the infected RAW cells for up to 24 hours. At 4 and 24 hours post-infection the RAW cells were lysed with distilled water, the intracellular *B. thailandensis* was serial diluted and enumerated by culture on L-agar (2.6.5. CFU analysis.).

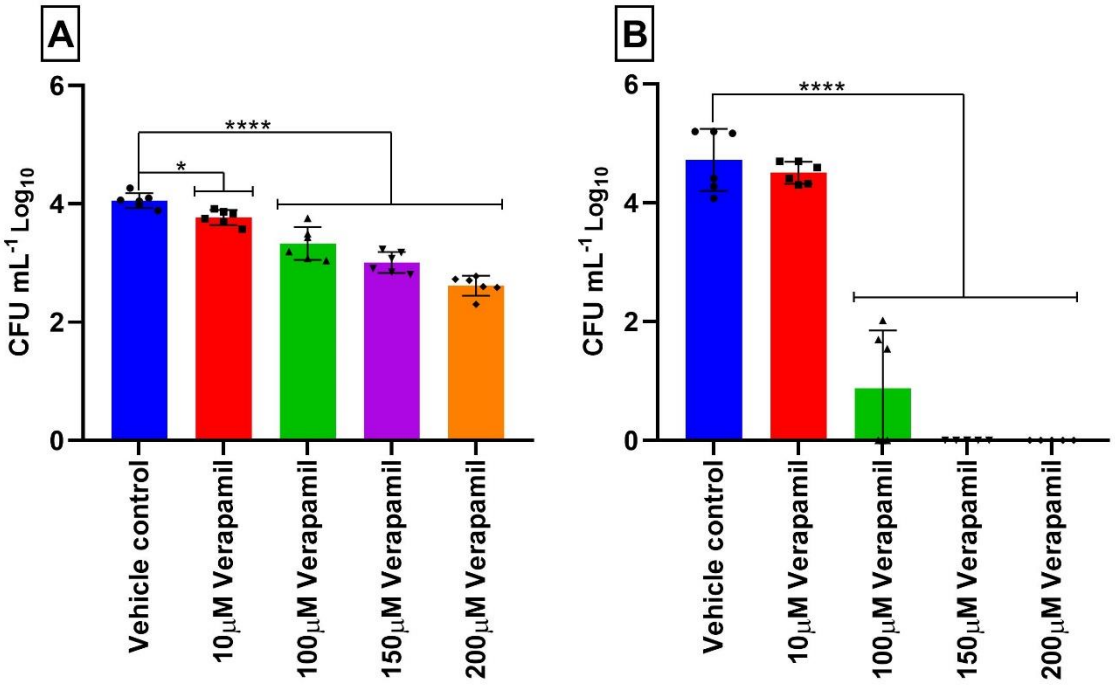

Figure 38. The effect of different verapamil concentrations on intracellular *B. thailandensis*.

RAW cells were infected with *B. thailandensis* E555 at an MOI of 5 for an hour at 37°C. Post-infection the RAW cells were incubated with a range of concentrations of verapamil of between 10μm and 200μm. Following 4 and 24 hours incubation, the RAW cells were lysed with distilled water. The intracellular *B. thailandensis* E555 CFU was enumerated by serial dilution and culture on L-agar. **A** – CFU data for 4 hours incubation, **B** – CFU data for 24 hours incubation. Data are represented as mean CFU of the technical replicates (n=6) derived from two independent biological experiments, and error bars represent SD of all technical replicates. * P 0.0423, **** P <0.0001 One-way ANOVA, Dunnett's multiple comparisons test to vehicle control.

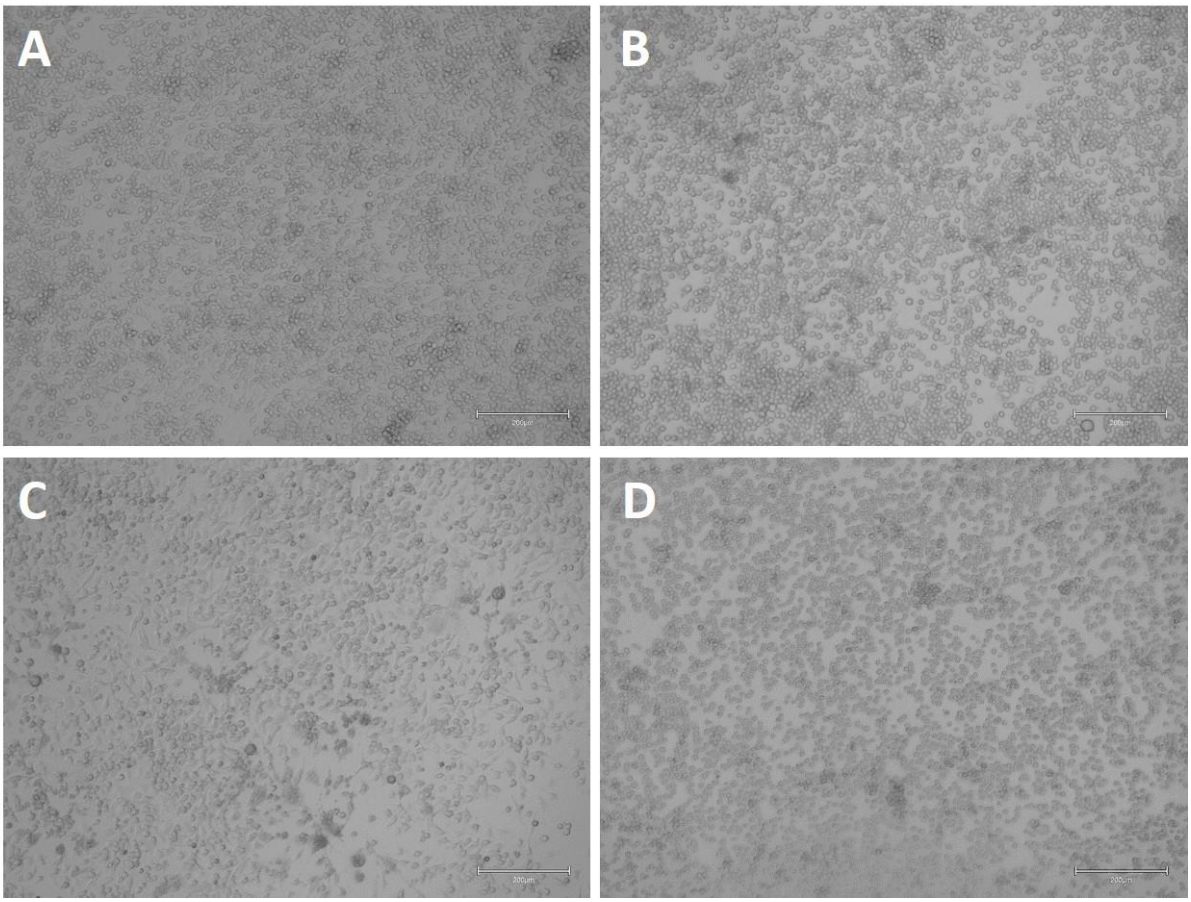

Figure 39. Images of RAW cells infected with *B. thailandensis* and incubated with verapamil.

RAW cells were infected with *B. thailandensis* at an MOI of 5 and incubated with 200μM verapamil for 4 and 24 hours. Representative light microscope images were taken of the RAW cells to compare control cells and those cells incubated with verapamil. The aim of taking representative images of cells at each time point was to demonstrate visually that cells incubated with verapamil are intact, and also at a similar cell density to the control cells at each time point. **A** – RAW cells at 4 hours post-infection. **B** – 4 hours post-infection with 200μM verapamil. **C** – RAW cells at 24 hours post-infection. **D** – 24 hours post-infection with 200μM verapamil. Images taken using an x10 objective on the Invitrogen™ EVOS™ M5000 Imaging System. Scale bar represents 200μm.

All verapamil concentrations significantly reduced intracellular bacterial CFU at 4 hours incubation, compared to the vehicle control (Figure 38). The lowest verapamil concentration of 10μM significantly (P 0.0423) reduced bacterial CFU, from a control

of $1.1x10^4$ CFU to $7.4x10^3$ CFU. The highest verapamil concentration of 200μM significantly ($P < 0.0001$) reduced bacterial CFU, from the control of $1.1x10^4$ CFU to $4x10^2$ CFU.

At 24 hours incubation, a concentration of 100μM verapamil or greater, significantly reduced intracellular bacterial CFU. A 100μM concentration of verapamil reduced CFU from a vehicle control of $8.7x10^4$ CFU, to 35 CFU with 100μM verapamil. Concentrations of verapamil greater than 100μM reduced intracellular CFU to complete clearance in this RAW cell infection assay.

Light microscope images of the RAW cells were taken as an example of the cells at each time point. The aim of these images was to show the cells exposed to 200μM verapamil are present and intact at 24 hours post-infection (Figure 39). The cells exposed to verapamil are however more rounded than the control cells, indicating that the cells are less healthy than the controls. Although not a quantitative method, these images are a visual representation of the RAW cells incubated with verapamil. The aim of the images was to visually demonstrate that the RAW cells are intact when incubated with verapamil for up to 24 hours. The images complement the cytotoxicity data, demonstrating that the reduction in intracellular *B. thailandensis* CFU by verapamil, is not solely due to RAW cell lysis.

5.6. Assessing the ability of verapamil to induce autophagy.

The aim of this experiment is to investigate the bacterial killing by verapamil within RAW cells, specifically by detecting an increase in autophagy markers in RAW cells when exposed to verapamil. This experiment will aim to show if there is an increase in autophagy within the RAW cells, which corresponds to an increase in intracellular killing of *B. thailandensis* E555. The host macrophage is able to kill intracellular bacteria through autophagy, a cell recycling process which can be enhanced upon infection, to help clear intracellular bacteria. During the formation of the autophagosome, cytosolic microtubule-associated protein 1A/1B light chain 3 (LC3) is converted to LC3 II via conjugation to phosphatidylethanolamine (298). LC3 II is membrane bound to the autophagosome, and is a common marker used for detection of autophagosome formation. The lysosomal associated membrane protein 1 (LAMP-1) is one of the main protein components of the lysosomal membrane, and

is a common marker used for detection of lysosomes. Detection of LC3 II and LAMP-1 by imaging flow cytometry (2.5.2. LC3 and LAMP-1 staining.), is a method for autophagy analysis of autolysosome formation within the cell (299) (2.6.3. Imaging flow cytometry.). In this results section, the co-localisation of LC3 and LAMP-1 will be used as a maker for autophagy, in response to RAW cell incubation with verapamil. In other cell models, verapamil can induce host cell autophagy (292), and therefore it is possible that the bacterial killing observed with verapamil here is by stimulation of autophagy in RAW cells. Verapamil was added to infected RAW cells at a range of concentrations, to investigate a concentration at which stimulation of autophagy may occur. At 16 hours post-infection, cells were harvested, stained and analysed by imaging flow cytometry. Cells were analysed for percentage of cell infection and percentage of cells with autolysosomes (Figure 40).

RAW cells were infected with *B. thailandensis* E555 GFP at a multiplicity of infection (MOI) of 5 and incubated for an hour at 37°C. Following incubation the bacteria were removed and the cell culture media was subsequently replaced with 1mg mL^{-1} kanamycin maintenance antibiotic to kill extracellular bacteria. Additionally, verapamil concentrations of between 10µm and 200µm were added post-infection, and incubated with the infected RAW cells for 16 hours. At 16 hours post-infection RAW cells were harvested, transferred to 200 µL fixative-permeabilisation buffer (BD Biosciences) and incubated for 30 minutes at room temperature on a roller. Following incubation, the sample volume was increased to 1mL with 800 µL of 1X permeabilisation-wash buffer (BD Biosciences) and centrifuged for 5 minutes at 300 *g*. Following centrifugation, cells were re-suspended into 200µL permeabilisation-wash buffer (BD Biosciences) containing 5 µg mL^{-1} anti-LC3 mAb (Biolegend), and incubated for 1 hour at room temperature on a roller (2.5.2. LC3 and LAMP-1 staining.). Following incubation, a further 800 µL of permeabilisation-wash buffer (BD Biosciences) was added to the sample. The RAW cell sample was centrifuged for 5 minutes at 300 *g,* the cell pellet was re-suspended into 200 µL permeabilisation-wash buffer (BD Biosciences) containing 10 µg mL^{-1} goat anti-mouse Alexa Fluor 647 (Invitrogen) and 3.5 µg mL^{-1} PE/Dazzle™ 594 anti-mouse CD107a (LAMP-1) Antibody (Biolegend, UK). The sample was incubated for 1 hour at room temperature on a roller. Following incubation, 800 µL of PBS (Gibco) was added and the sample centrifuged for 5 minutes at 300 *g*. Finally, cell pellets were re-suspended into 50 µL

PBS (Gibco) prior to analysis by imaging flow cytometry (2.6.3. Imaging flow cytometry.).

RAW cells were analysed on the Amnis® ImageStream® X Mark II. The 488nm (GFP), 561nm (PE/Dazzle™ 594) and 642nm (Alexa Fluor 647) lasers were used at 100mw, 200mw and 150mw power respectively. Fluorescence was detected using channel 2 (*B. thailandensis* E555 GFP, excitation peak at 489nm and emission peak at 511nm), channel 4 (PE/Dazzle™ 594) and channel 11 (Alexa Fluor 647 excitation peak at 650nm and emission peak at 665nm). Bright field (channel 1) was used throughout at maximum power and magnification was set at x60 throughout. Cells were gating according to being single cells, in focus, association with GFP, and co-localisation between LC3 and LAMP-1 as a marker of autophagy (Figure 40). A compensation matrix was generated in the Amnis Ideas® software and applied to the data set to compensate for fluorescence cross over between the GFP, PE/Dazzle™ 594 and Alexa Fluor 647 emissions.

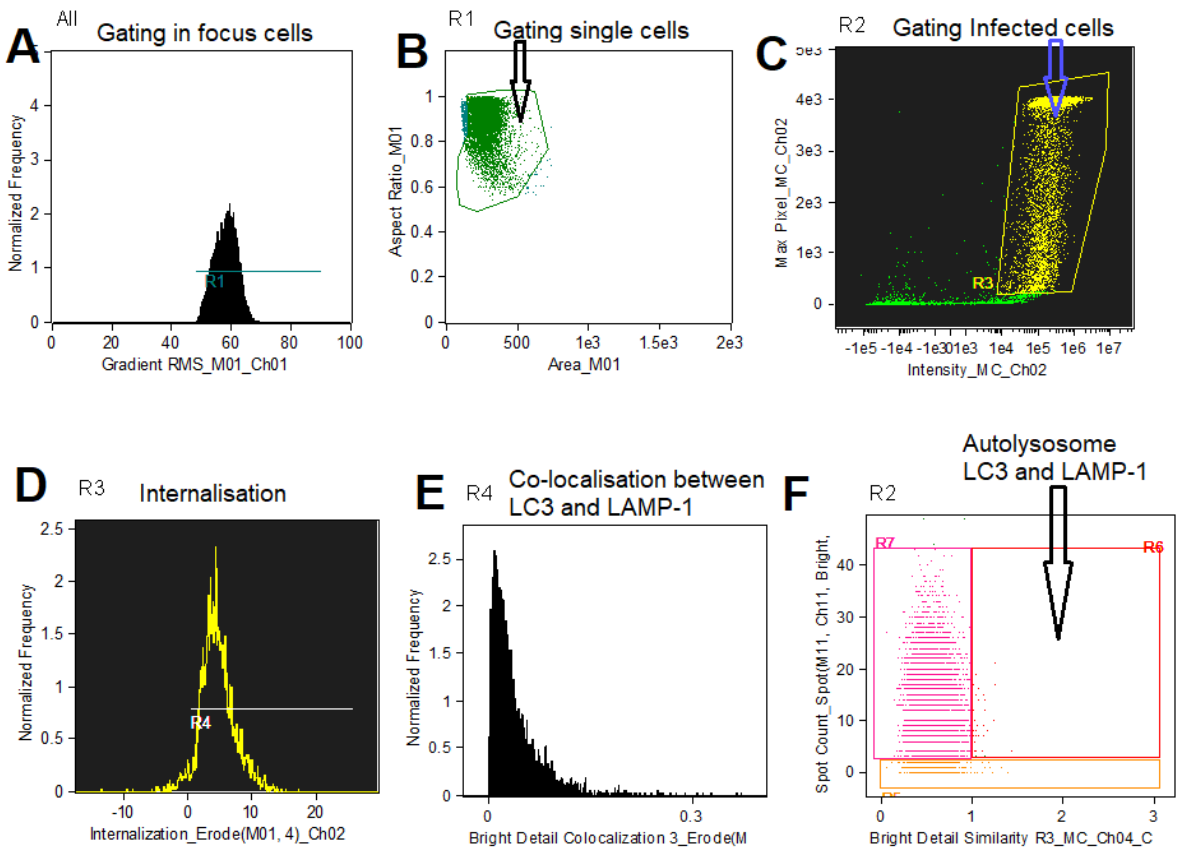

Figure 40. Imaging flow cytometry gating for identifying infected cells containing LC3 and LAMP-1 fluorescent markers.

Imaging flow cytometry was used as a method to assess the ability of verapamil to induce autophagy in RAW cells. Co-localisation between LC3 and LAMP-1 was used as a marker for autolysosome formation, and therefore autophagy occurring within infected cells. Fluorescently labelled anti-LC3 (Alexa Fluor 647 (Invitrogen)) and anti-LAMP-1 (PE/Dazzle™ 594 anti-mouse CD107a (LAMP-1) antibody (Biolegend, UK)) antibodies were used to stain RAW cells. RAW cells were previously infected with *B. thailandensis* GFP at an MOI of 5, and post-infection were incubated with verapamil as previously described (2.2.3. Repurposed drugs infection assay.). RAW cells were harvested, stained and analysed by imaging flow cytometry at 16 hours post-infection. The 488nm (GFP), 561nm (PE/Dazzle™ 594) and 642nm (Alexa Fluor 647) lasers were used at 100mw, 200mw and 150mw power respectively. Fluorescence was detected using channel 2 (*B. thailandensis* E555 GFP, excitation peak at 489nm and emission peak at 511nm), channel 4 (PE/Dazzle™ 594) and channel 11 (Alexa Fluor 647 excitation peak at 650nm and emission peak at 665nm). Bright field (channel 1) was used throughout at maximum power and magnification was set at

x60 throughout. RAW cells were gated according to being in focus (A) and single cells (B). Additionally infected cells (C) were gated according to GFP intensity and those cells with internalised GFP signal (D). Cells with co-localisation between LC3 and LAMP-1 (E, F) were gated as a population of cells with autolysosome formation. A compensation matrix was applied to the data to account for any cross over fluorescence between the different fluorescent markers.

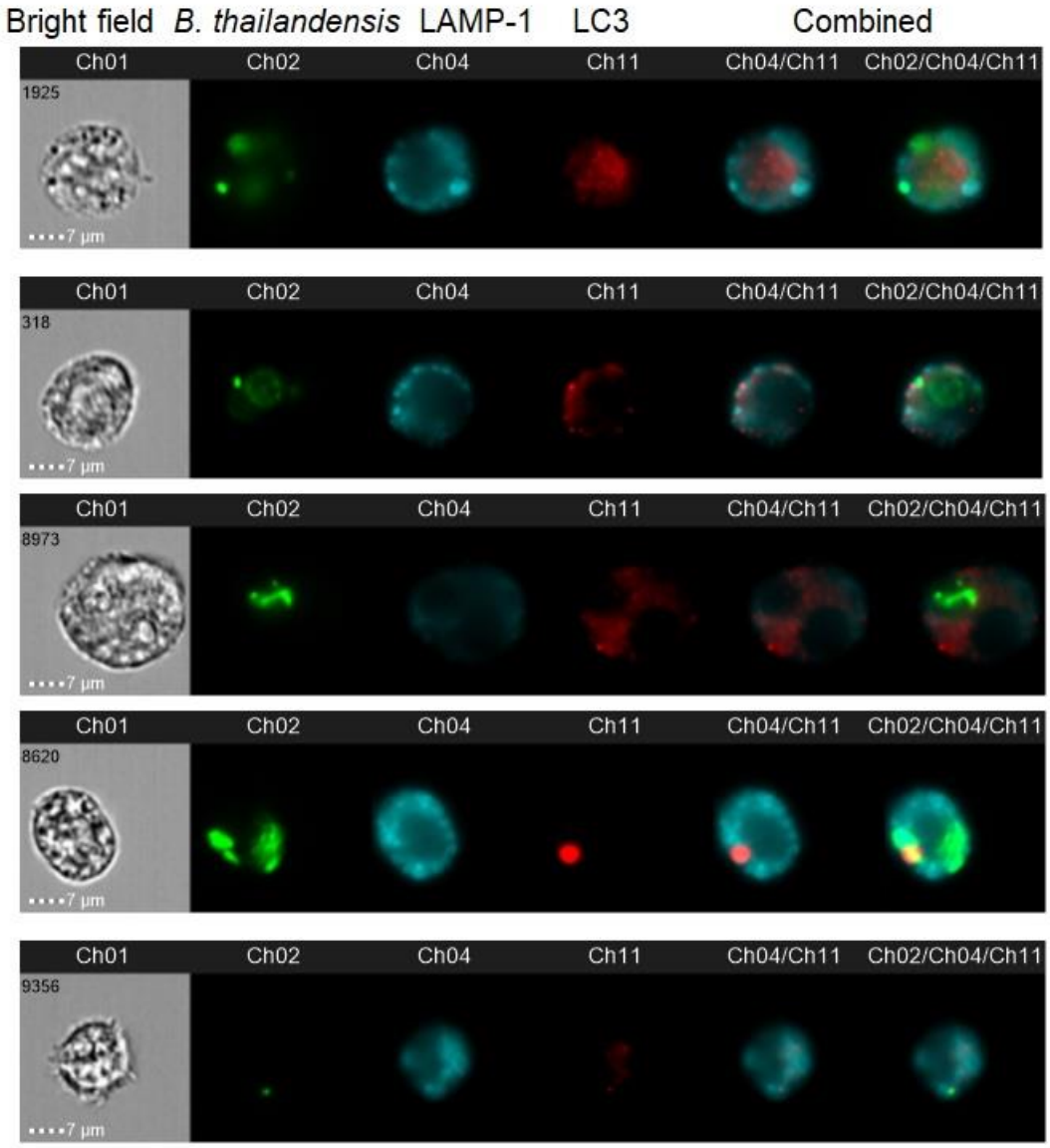

Figure 41. Examples of LC3 and LAMP-1 co-localisation by imaging flow cytometry.

Imaging flow cytometry was used to analyse *B. thailandensis* E555 GFP infected RAW cells for autolysosome formation, following incubation with verapamil. The 488nm (GFP), 561nm (PE/Dazzle™ 594) and 642nm (Alexa Fluor 647) lasers were used at 100mw, 200mw and 150mw power respectively. Fluorescence was detected using channel 2 (*B. thailandensis* E555 GFP, excitation peak at 489nm and emission peak at 511nm), channel 4 (PE/Dazzle™ 594) and channel 11 (Alexa Fluor 647 excitation peak at 650nm and emission peak at 665nm). Bright field (channel 1) was used throughout at maximum power and magnification was set at x60 throughout. Representative images of RAW cells are shown from the experimental data in Figure

42. Images shown are bright field (Ch01), infected with *B. thailandensis* E555 (Ch02, GFP), and stained with anti-LC3 (Ch11, Alexa Fluor 647), and anti-LAMP-1 (Ch04, PE/Dazzle™ 594) fluorescent antibodies. Co-localisation between LC3 and LAMP-1 (representing autolysosome formation in the RAW cells) can be observed in Ch04/Ch11. A compensation matrix was applied to the data to account for any cross over fluorescence between the emission fluorescence of the PE/Dazzle™ 594, Alexa Fluor 647 and GFP markers. This was achieved using separate samples of RAW cells with the individual markers present, and compensating for cross over fluorescence using the Ideas ® software compensation matrix generator.

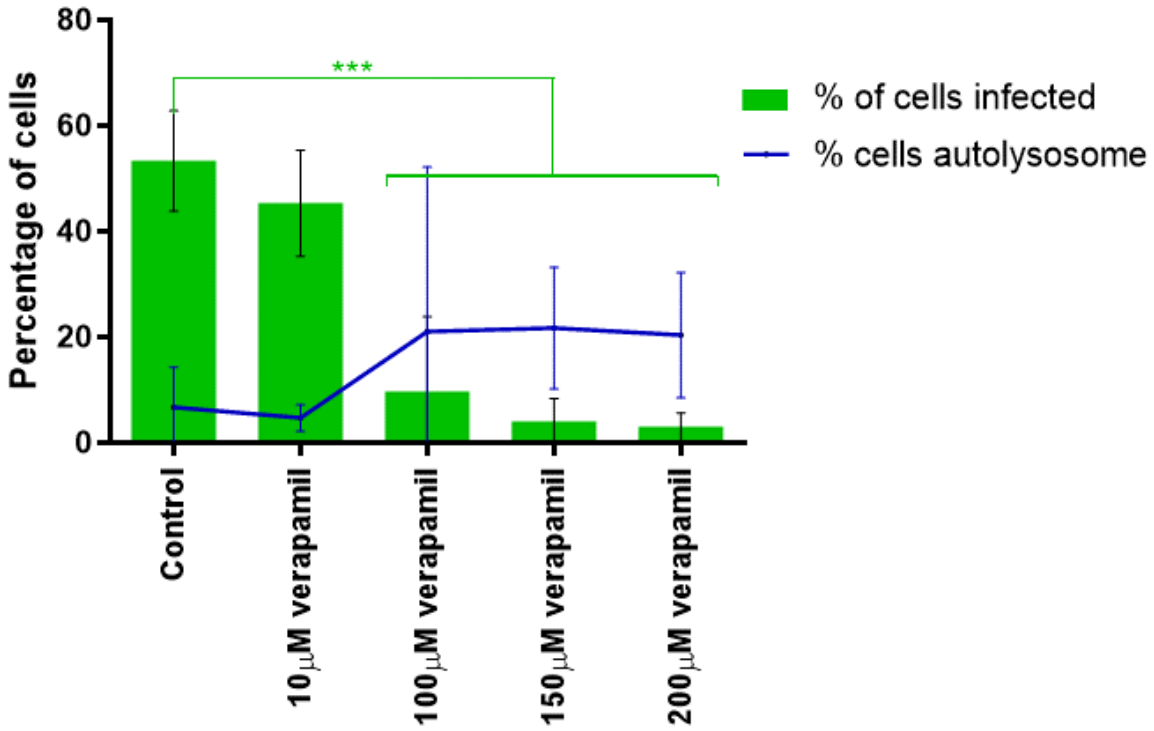

Figure 42. The effect of verapamil on autolysosome formation in infected RAW cells.

RAW macrophage-like cells infected with *B. thailandensis* E555 at an MOI of 5, post-infection the cells were incubated with concentrations of verapamil (10μm to 200μm) for 16 hours. RAW cells were harvested, stained for LC3 and LAMP-1 with specific fluorescent antibodies. RAW cells were assessed by imaging flow cytometry for cell infection with *B. thailandensis* E555 GFP and autolysosome formation. Cells were considered autolysosome positive with co-localisation between fluorescent LAMP-1 and LC3 markers. RAW cells were harvested for staining 16 hours post-infection. Control data consists of a water vehicle control comparable to that of the 200μm verapamil. Data are represented as the means (n=3) derived from three independent biological experiments, error bars represent SD of biological replicates. *** P <0.001 One-way ANOVA Dunnett's multiple comparisons test to control. No significant differences were observed in the autolysosome data by one-way ANOVA.

The aim of the analysis was to determine if the intracellular killing observed by verapamil in previous experiments, is due to verapamil stimulating an increase in

autophagy within the RAW cells. The cells were analysed by imaging flow cytometry, by gating the cell population that was in focus and single cells (Figure 40 A, B). This population was then analysed by gating for intracellular *B. thailandensis* GFP (Figure 40 C), and the fluorescent markers LC3 and LAMP-1. The LC3 and LAMP-1 markers were gating according to RAW cells with co-localisation between the two markers (Figure 40 E, F), following a published method by Pugsley *et al* (299). Co-localisation between LC3 and LAMP-1 indicates formation of an autolysosome within the cell. RAW cells were analysed to determine if incubation with verapamil increases the percentage of cells containing autolysosomes (Figure 42).

Imaging flow cytometry has demonstrated that autolysosome formation can be assessed in the *B. thailandensis* RAW macrophage-like cell infection assay (Figure 40 and Figure 41). Imaging flow cytometry has additionally detected the reduction in cell infection by verapamil, in a dose dependent manner (Figure 42). The reduction in the percentage of cells infected with *B. thailandensis* GFP is significantly reduced ($P < 0.001$ ANOVA), from a concentration of 100µM verapamil compared to the vehicle control.

Autolysosome formation within RAW cells incubated with verapamil was analysed by imaging flow cytometry (Figure 42). There is a trend towards an increase in autolysosome formation with exposure to increasing verapamil concentration, this change is not significant when analysed by ANOVA. There is a high degree of variation in the autolysosome data between the experimental replicates, as seen by the large error bars resulting in a non-significant result. This is especially apparent in the high concentrations of verapamil, for 100µM of verapamil the experimental replicates vary from 57% to as low as 3% of cells with autolysosome formation. The data for 10µM verapamil and the control is much more consistent between experimental replicates, with a consistently low percentage of RAW cells with autolysosomes. The percentage of cells with autolysosomes is between 2% and 7% for 10µM verapamil, and between 0% and 15% for the controls, between the three experimental biological replicates.

5.7. The effect of reducing kanamycin in the RAW cell infection assay.

The aim of this experiment is to determine the effect kanamycin has on the intracellular killing of *B. thailandensis* E555, when RAW cells are incubated with or without verapamil. Kanamycin is used in the RAW cell infection assay as a maintenance antibiotic to prevent extracellular *B. thailandensis* bacterial replication, the kanamycin was used at 1mg mL^{-1} throughout the RAW cell infection assays (2.2.1. RAW cell infection assay.). Verapamil significantly reduces intracellular bacterial CFU in the RAW cell infection assay. The high level of kanamycin in the extracellular media is present to reduce the replication of extracellular *B. thailandensis*, although the effect of kanamycin and verapamil in combination on the bacteria is not known. In this infection assay kanamycin was reduced or absent, this is to investigate the effect kanamycin has on bacterial CFU with and without verapamil.

RAW cells were infected with *B. thailandensis* E555 at a multiplicity of infection (MOI) of 5 and incubated for an hour at 37°C. Following incubation the bacteria were removed and the cell culture media was subsequently replaced with 1mg mL^{-1} kanamycin maintenance antibiotic to kill extracellular bacteria. After 1 hour the kanamycin media was either left at 1mg mL^{-1}, reduced to 150 µg mL^{-1} or removed completely (L-15 culture media only). Additionally, RAW cells were incubated with or without 200µm of verapamil post-infection. RAW cells were incubated for 4 and 24 hours at 37°C. At the specific time points the RAW cells were lysed with distilled water and the intracellular bacteria enumerated by serial dilution and culture on L-agar (2.6.5. CFU analysis.). The CFU data was plotted for the 4 and 24 hours post-infection to show the effect of reducing kanamycin concentrations on intracellular bacterial CFU.

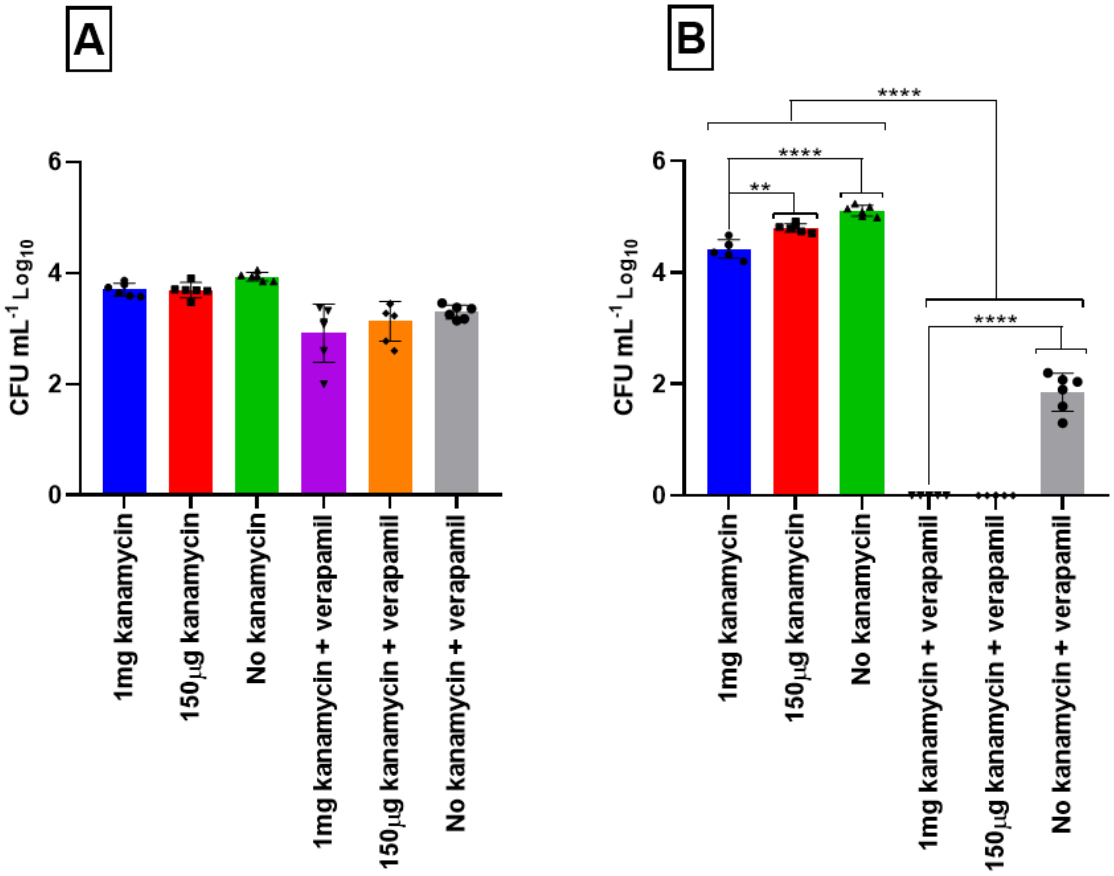

Figure 43. The effect of kanamycin on the ability of verapamil to reduce intracellular bacterial CFU.

RAW cells were infected with *B. thailandensis* at an MOI of 5 and subsequently incubated with or without 200µM verapamil. Kanamycin concentration in the cell culture media were either at a standard concentration of 1mg mL^{-1}, reduced to 150 µg mL^{-1}, or removed post-infection. Cells were lysed at 4 and 24 hours post-infection, and the intracellular CFU enumerated by serial dilution and culture on L-agar. **A –** 4 hours post-infection, **B** – 24 hours post-infection. Data are represented as technical replicate means (n=6) derived from two independent biological experiments, error bars represent SD of all technical replicates**.** ** P 0.0016, **** P <0.0001 One-way ANOVA Dunnett's multiple comparisons test.

At 4 hours post-infection, reducing the concentration of kanamycin had no significant effect on bacterial CFU when verapamil is present or absent (Figure 43). At 24 hours post-infection, reducing kanamycin does significantly increase the bacterial CFU.

When there is verapamil and kanamycin present together, there is either complete CFU clearance with high levels of kanamycin present, or a significant increase of approximately $1x10^2$ CFU when no kanamycin is present. High kanamycin concentrations in combination with verapamil, does reduce bacterial CFU to a greater extent. Although, the reduction in CFU observed with verapamil incubation is not completely due to kanamycin being present in the external media. At 24 hours, when kanamycin is removed post-infection, there is a significant reduction in bacterial CFU when verapamil is present. There is a RAW cell bacterial CFU of $1.1x10^2$ with verapamil incubation, compared to $1.2x10^5$ CFU for the control with no verapamil. This data highlights that kanamycin does have an effect on bacterial CFU to a certain extent, although kanamycin is not required for verapamil to significantly reduce intracellular bacteria.

5.8. Discussion.

In this chapter, a panel of compounds were investigated for anti-microbial activity in a *B. thailandensis* RAW macrophage-like cell infection assay. This work was a parallel set of investigations together with development of an antibody-antibiotic conjugate (AAC). Due to uncertainty in the development of an AAC, the research of anti-microbial compounds provided an alternative for investigating an anti-microbial therapy for melioidosis. A panel of compounds were selected based on literature suggesting an anti-microbial effect for similar intracellular bacterial pathogens. The panel of compounds had published activity against *M. tuberculosis* infection, which forms an intracellular niche similar to *B. pseudomallei*. Carbamazepine, verapamil, norverapamil, and valproic acid were all selected to be tested in a *B. thailandensis* RAW cell infection assay. Many other compounds in the literature show potential as anti-microbial compounds, due to the time and costs associated with screening additional compounds, there was not scope in this project to investigate further candidate compounds. The hazard group II pathogen *B. thailandensis* was used for all initial screening methods, rather than the high containment pathogen *B. pseudomallei*. Studies with *B. pseudomallei* would be required in future experiments, if verapamil was to be taken forward for further analysis as an anti-microbial compound for melioidosis.

The RAW cell infection assay highlighted that verapamil and norverapamil significantly reduced bacterial CFU, at both 4 and 24 hours post-infection (Figure 34). At 24 hours post-infection, both carbamazepine and valproic acid also significantly reduced bacterial CFU, although not to the same extent when compared to verapamil and norverapamil. This initial screen in the RAW cell infection assay was at a single concentration of 100µM, this was based on the literature that demonstrated anti-microbial effects. Ideally each compound would have been taken forward and tested at a range of concentrations, this was not possible in this project due to timescales, and therefore an initial screen and down select of compounds was required.

In the initial screen of compounds, valproic acid and carbamazepine displayed a significant reduction in bacterial CFU at 24 hours post-infection. For both valproic acid and carbamazepine, the reduction in bacterial CFU was to a lesser extent than that of verapamil and norverapamil. Valproic acid has been tested at high concentrations by Schiebler *et al* (226), although a concentration of 3 mM was required, and this was considered to not be safely achievable *in vivo*. Carbamazepine was tested at 50 µM by Schiebler *et al* (226), and shows promise *in vitro* as an autophagy inducing compound and reduction of bacterial infections. Verapamil and norverapamil were the down selected compounds, since the reduction in bacterial CFU was apparent at both 4 and 24 hours post-infection. Additionally, the reduction in CFU was to a greater extent than that of valproic acid and carbamazepine.

Verapamil and norverapamil were initially tested for any anti-microbial effects on bacteria alone (Figure 35 and Figure 36), and subsequently for RAW cell toxicity (Figure 37). This was to determine if any reduction in bacterial CFU is due to direct anti-bacterial effects, or simply due to cell death caused by the compounds toxicity. RAW cell death would lead to bacterial killing, due to the high levels of kanamycin maintenance antibiotic present externally in the cell culture media.

Both compounds were tested with a culture of *B. thailandensis* to determine any MIC over 24 hours. The data showed that neither compound inhibited the replication of *B. thailandensis* over the 24 hours, therefore both verapamil and norverapamil have a MIC of greater than 400 µM. This data shows that the anti-bacterial killing effect of each compound requires the RAW cell to be present.

The cell toxicity of both compounds was assessed with the use of a LDH cytotoxicity assay kit. The assessment of cellular integrity by LDH release is an established and widely used method (300), bacterial infection however can interfere with the assay by acidification of the media and release of proteases (301). In this study, verapamil and norverapamil were assessed by incubation with RAW cells without bacterial infection. The colorimetric LDH assay detects LDH release from the cell upon membrane damage, caused by verapamil or norverapamil toxicity. The coloured product is formed from the enzymatic activity of LDH released from the cell, therefore the colour intensity is proportional to the cell toxicity. Both compounds increased cytotoxicity above the level of control untreated cells, although the cytotoxicity of norverapamil was greater than that of verapamil. Verapamil did increase RAW cell death over a 24 hour incubation, with an increase in cytotoxicity for 200μM verapamil of between 20 and 27% above the control. The maximum increase in cytotoxicity was 34%, for 100μM verapamil at 24 hours of incubation. Norverapamil increased cell death to a greater extent, as shown by an increase in cytotoxicity of between 36% and 48% above the control, for concentrations of 100μM norverapamil and greater. Norverapamil had a maximum cytotoxicity of 48% above control, at 24 hours incubation, at a concentration of 150μM. This cytotoxicity data was used to further down select for a single compound, experiments were therefore subsequently focused on verapamil.

Verapamil did increase cell toxicity compared to control RAW cells, and imaging of the cells during the assay revealed signs of some cell damage. In the later time points the verapamil exposed cells are phenotypically less like the control cells, phenotypically they were smaller and more rounded (Figure 39). The LDH assay showed an increase in cell toxicity, although unless the cell membrane is damaged, the LHD release will be modest. The RAW cells could therefore be intact, but not a favourable environment for bacterial survival or replication. There is a possibility of kanamycin maintenance media penetrating the RAW cells, during incubation with verapamil. The data shows that removing kanamycin after the initial kill step, does allow some bacteria to survive verapamil treatment at 24 hours. Although this effect could be due to a low level of extracellular bacterial replication, especially since the media contained no kanamycin maintenance antibiotic (Figure 43). The data

provides evidence that kanamycin is not required for verapamil to significantly reduce intracellular bacterial CFU.

The effect of verapamil concentrations from 50μM to 200μM on cell viability and cell proliferation, has been investigated by Kania *et al* (292). A variety of cancer cell lines were incubated with verapamil, all cells suffered significant effects on viability and proliferation when incubated with verapamil for 48 hours. However, the effect on viability and proliferation varied between cell lines, with one cell line having a viability of 80% after 48 hours incubation with 200μM verapamil (292). Verapamil concentrations as low as 12.5 μM have been demonstrated to reduce intracellular *M. tuberculosis* by 40% *in vitro* (207).

If verapamil was to be taken further as a potential anti-bacterial therapeutic, then further analysis of cell toxicity would be required, together with expanded autophagy studies in a variety of cell lines. In primary macrophage cell lines the concentration of verapamil required for anti-microbial effects may be reduced, compared to a cell line such as RAW macrophage-like cells. The aim of this would be to identify a concentration that limits toxicity to the cell, but still significantly reduces intracellular bacteria in the majority of cell lines investigated. Norverapamil significantly reduced bacterial CFU within RAW cells, although the compound was more cytotoxic than verapamil. Norverapamil is the metabolite of verapamil, and therefore in the body both compounds will be present once partly metabolised. The cytotoxicity of norverapamil needs to be further investigated, a range of concentrations will need to be tested for cytotoxicity. It may be possible to find a concentration whereby there is a significant bacterial killing, together with a reasonable level of cytotoxicity. Finding an effective anti-microbial concentration with low toxicity may be a challenge, verapamil is known to have low bioavailability and a low half-life in circulation (302). Therefore repeated and higher therapeutic doses may be required, although slow release formulations of verapamil are available with improved pharmacokinetics (302). Verapamil plasma concentrations of between 125 to 400ng mL^{-1} is achievable with rapid release verapamil, and 16 – 77ng mL^{-1} with slow release formulations (303). Oral toxicity levels are reported to be between 3 – 14 mg kg^{-1} (303). A concentration of 100μM of verapamil hydrochloride in cell infection assays, equates to a 49μg mL^{-1} concentration. To improve therapeutic delivery of verapamil, future studies could investigate encapsulation in nanoparticles as a way to improve delivery

to the intracellular environment, and limiting drug toxicity. Antibiotics have been successfully encapsulated into polymersomes, and delivered to the intracellular site of infection for *B. thailandensis* (240), this could also be an option for verapamil.

Although verapamil significantly reduced bacterial CFU, the reason behind the killing is unclear. Autophagy is known to play a significant role in control of bacterial disease, and is likely to play an important role in control of intracellular *Burkholderia*. A study by Rinchai *et al* (304), demonstrated that *B. pseudomallei* infection increases LC3 flux in human neutrophils, with defects in autophagy significantly increasing survival of intracellular *B. pseudomallei*. Additionally, this study showed that *B. pseudomallei* stimulates autophagy in neutrophils, possibly via the type III secretory system or effector proteins (304). It is therefore reasonable to predict that individuals with defects in the autophagy pathway will have an increased susceptibility to melioidosis.

Verapamil is a known autophagy inducer, a study by Kania *et al* (292) reports that verapamil is an inducer of autophagy in a variety of cell lines. The study investigated the cytotoxic effects, autophagic induction, autophagic flux and the mechanism behind autophagy induction by verapamil. Confocal microscopy showed an increase in conversion of LC3I to LC3II with verapamil treatment, increasing LC3II puncta within a population of cells (292). A study by Juarez *et al* (227) analysed a range of drugs including verapamil, and autophagy was assessed by confocal microscopy of LC3, P62, and lysotracker co-localisation. This study showed that verapamil induced autophagy, together with a reduction in intracellular *M. tuberculosis* replication (227).

Although verapamil is a known autophagy inducer, a study by Abate *et al* (207) concluded that autophagy may not be the main mechanism behind verapamil induced *M. tuberculosis* bacterial killing. Instead the killing effect is possibly related to other factors, there is evidence of verapamil induced bacterial membrane disruption of *M. tuberculosis* (305).

In this chapter, verapamil was studied for autophagy induction in RAW cells by imaging flow cytometry, using LAMP-1 and LC3 fluorescent antibodies (Figure 40 and Figure 41). In these assays, verapamil resulted in an increase in autolysosome

formation, but this was not deemed significant by ANOVA (Figure 42). The co-localisation of LC3 and LAMP-1 markers was used as a method to monitor autophagic flux, this approach was based on published methods (299, 306). The autolysosome formation data, generated in this chapter, varied greatly between experiments. The issue with staining for autophagy is the time point selected, autophagy is a fluid process within the cell and is therefore difficult to observe at specific time points. For future work, and to further investigate the autophagic response to verapamil, more time points are required. Additionally, methods such as the use of live cell autophagy stains should be explored.

Verapamil is a known efflux pump inhibitor, and possibly concentrates antibiotics within the cell. Verapamil has shown to potentiate anti-tuberculosis drugs in both cell and murine models (219, 224, 225, 231). *B. pseudomallei* and *B. thailandensis* possess numerous RND (resistance nodulation cell division family) efflux pumps, known to contribute to the high level of antibiotic resistance of the bacterium (123-125). Three of these efflux pumps AmrAB-OprA, BpeAB-OprB and BpeEF-OprC are responsible for resistance to antibiotics from various classes including aminoglycosides, macrolides, tetracyclines and fluoroquinolones (123, 124). There is potential for verapamil as an efflux pump inhibitor therapy for melioidosis. Efflux is one of the major factors in *B. pseudomallei* resistance to antibiotics, therefore blocking the efflux with a compound such as verapamil may have the ability to enhance the efficacy of antibiotics. Combination of efflux pump inhibitors with antibiotics, may even lead to antibiotics that have previously been disregarded for melioidosis becoming viable therapeutic options.

The *B. thailandensis* RAW macrophage-like cell infection assay represents a tool that could be further utilised, especially for screening other potential anti-microbial compounds for melioidosis. One exciting compound in particular, metformin, would be an interesting comparison to verapamil. Metformin is a licenced diabetic drug that offers potential as a host directed therapy. The activity of metformin against intracellular *M. tuberculosis* has been published in the literature (214-217). Metformin has shown benefits as an adjunct therapy both *in vitro* and *in vivo* murine models of

tuberculosis infection. Singhal *et al* demonstrated that between 10^3 and 10^4 µM metformin significantly reduces survival of *M. tuberculosis,* within human monocyte derived macrophages *in vitro* (217). *In vivo* murine studies have shown that metformin enhances the efficacy of anti-tuberculosis drugs, and improves clinical outcomes of disease with improved tissue pathology, reduced inflammatory responses, together with an improved $CD8^+$ and $CD4^+$ T cell immune response (217). Diabetes is a major factor in melioidosis disease progression, and has a negative effect on the immune response to *B. pseudomallei* infection, and therefore patient survival (37, 39, 307). Metformin has been associated with a greater chance of survival from melioidosis (308). Together with the potential repurposing as an anti-microbial, metformin offers great potential for melioidosis patients. Future work should include analysis of the anti-bacterial effects of metformin and other potential anti-microbial compounds, utilising the RAW macrophage-like cell infection assay from this chapter.

Verapamil demonstrates promise as an anti-microbial compound in this study, although the mechanism of action remains unclear. The anti-microbial action seen in this project is likely to be partly due to cell toxicity, in addition to induction of cell mediated killing mechanisms such as autophagy. The focus of the research project as a whole, is to investigate antibody and antibiotic based combination therapies. This chapter has shown that there is also potential in repurposing compounds for use as alternatives to antibiotics. Although, there is more research required to fully understand the compounds tested, and their mechanisms of action on the cell and intracellular bacteria. This research was performed in parallel with development of an antibody-antibiotic conjugate (AAC), it was decided to halt verapamil studies at this point, and focus research on developing an AAC for melioidosis.

6. Generation of an antibody-antibiotic conjugate.

6.1 Introduction.

In this project, the anti-CPS mAb 3VIE5 has demonstrated the ability to opsonise and reduce bacterial actin tail formation *in vitro*. Previous work with this antibody at Dstl has demonstrated that mAb 3VIE5 offers a level of protection against *B. pseudomallei* infection in murine studies (113). In this chapter, the mAb 3VIE5 will be incorporated into an antibody-antibiotic conjugate (AAC), and tested *in vitro* as a proof of principle therapeutic for melioidosis.

Monoclonal antibody based therapies offer great potential as a therapeutic for infectious diseases. Although not a new technology, antibodies are now gaining more attention as therapeutics. As technology progresses, the costs associated with antibody production and engineering are reducing, leading to increases in therapeutic antibody development. New and improved production methods have been developed, including improved mammalian cell based production systems and plant based expression systems (309-312). Antibodies have many benefits as therapeutics especially from their stability, tolerability, ability to engineer, and their potential in combating the rise in antibiotic resistant bacterial infections (157, 159, 313-316). The therapeutic antibody market has increased dramatically in recent years and is valued at hundreds of billions of dollars (317). Engineering of mAbs is now routine, with humanisation of mAbs driving forward the potential of therapeutic mAbs (317, 318). Additionally, techniques such as phage display, transgenic mice and isolation of single B cells, have driven the development of fully human antibody therapeutics (311, 317, 318). Antibodies offer potential as a therapy for melioidosis, with several *in vivo* studies demonstrating the protective effect of anti-LPS and CPS specific mAbs (113-115, 319, 320). Antibodies also have potential to be used as combination therapies, antibody and antibiotic combinations can demonstrate synergistic effects against pathogens. Antibiotics in combination with antibodies have the ability to enhance clearance of pathogens, not only by the antibiotic action alone, but via enhancing processes such as complement mediated phagocytosis and opsonisation of pathogens (321). Several studies have highlighted synergistic effects

of antibiotic and antibody combinations (321), these include respiratory infection models of sepsis (322, 323), *P. aeruginosa* (324, 325), *S. aureus* (326, 327) and *B. anthracis* (328, 329).

ADCs are a more recent approach for mAb based therapies, aiming to specifically target delivery of a drug. ADCs are generally composed of an antibody conjugated to a payload via a linker. There are currently 14 FDA approved ADCs as cancer therapies, and hundreds more in clinical trials (330, 331). Examples include Gemtuzumab ozogamicin, a humanized IgG4 ADC targeting CD33 for therapy of acute myeloid leukaemia (162). Brentuximab vedotin is a chimeric IgG1 ADC, targeting CD30 of lymphomas (163). Adotrastuzumab emtansine (T-DM1) is a humanized IgG1 as therapy for breast cancer (163, 164) and Inotuzumab ozogamicin is a humanized IgG4 anti CD22 ADC (163). Polatuzumab vedotin (332-334) is a humanised IgG1 ADC for lymphoma therapy, and trastuzumab deruxtecan (334, 335) is a humanised IgG1 ADC for breast cancer, both of which were approved for use in 2019.

Alternative ADCs are being researched, including an ADC to specifically target *Trypanosoma brucei*, consisting of a recombinant human IgG linked to a toxin (336). This ADC takes inspiration from anti-cancer ADCs to deliver a toxin directly to the cell surface receptor on the trypanosome cell, allowing a single low dose of ADC to cure disease in a murine model of infection (336). An anti-viral ADC has been proposed, as a potential therapy for targeted drug delivery to human immunodeficiency virus (HIV) infected cells (337).

The first ADC developed for a bacterial disease is the THIOMAB^{TM} anti-*S. aureus* antibody-antibiotic conjugate (AAC), first published in 2015 and currently in development with Genentech Inc (165, 166). Since then, Genentech are also developing an AAC as a therapy for *P. aeruginosa*, similar in design to the *S. aureus* AAC consisting of an engineered monoclonal antibody conjugated to antibiotic via cathepsin cleavable linkers (167). Lehar *et al* (165) engineered an anti-*S. aureus* antibody, linked to a rifalogue antibiotic, via a cathepsin cleavable linker. The AAC mode of action relies upon opsonisation of the bacteria, and uptake via Fcγ receptors into the cell. The cleavable linker is cleaved intracellularly, releasing the antibiotic in

its active form to target intracellular bacteria. The *S. aureus* AAC was able to function *in vitro* and clear intracellular *S. aureus,* by greater than 4 logs to the limit of detection of the assay, when compared to controls of antibody alone and a non-cleavable version of the AAC (165). Lehar *et al* (165) used dithiothreitol (DTT) treatment of the antibody to engineer cysteines for conjugation, via reduction of interchain disulfides, a typical IgG antibody contains 8 interchain cysteines (338). When designing the AAC it is important to consider antibiotic incorporation ratios, as high incorporation ratios are likely to adversely affect antibody functionality. In the Lehar *et al* study (165), an incorporation ratio of 1.9 was achieved, it is thought that a ratio of 2 to 4 is optimum for an AAC (338).

The efficacy of the AAC can be influenced by various parameters including the cleavability of the linker, efficacy of the antibiotic, drug antibody ratio (DAR), antibody specificity, and pharmacokinetics (PK) of the antibody. This chapter will investigate cleavability of the AAC linker, efficacy of conjugated antibiotic, and PK properties of the mAb 3VIE5.

Ciprofloxacin and finafloxacin were selected as the antibiotics to conjugate to mAb 3VIE5. Ciprofloxacin ($C_{17}H_{18}FN_3O_3$) was first introduced in the 1980's, and like other fluoroquinolones it is a DNA gyrase inhibitor. Ciprofloxacin is known to be active intracellularly, and accumulate within phagocytic cells to a higher level multiple times that of the external ciprofloxacin concentrations (339-341). The uptake is not dependent on active transport mechanisms, and it has been shown that ciprofloxacin can rapidly leave cells once the extracellular levels decrease (339, 340).

Finafloxacin ($C_{20}H_{19}FN_4O_4$) is a novel fluoroquinolone antibiotic, which due to an enhanced activity at low pH, is being investigated as a therapy for melioidosis (55, 56). Finafloxacin has shown potential for improved treatment of intracellular pathogens including *L. monocytogenes, S. aureus, L. pneumophila* and *B. pseudomallei* (55, 56).

Fluoroquinolones are generally not considered as therapeutic options for melioidosis, in part due to efflux based resistance expressed by many *B. pseudomallei* strains (342). Ciprofloxacin is associated with high relapse rates and lower efficacy (MIC of

4 mg/L) than other front line antibiotics (53, 343-345), although ciprofloxacin does accumulate within the intracellular environment (340, 341). Ciprofloxacin is not a first choice front line therapeutic for melioidosis therapy, finafloxacin does offer potential as a future therapeutic for melioidosis. Finafloxacin demonstrates efficacy, despite bacterial efflux mediated fluoroquinolone resistance, compared to other fluoroquinolones especially at lower pH (56, 346, 347). Despite efflux pump based resistance, both ciprofloxacin and finafloxacin display efficacy against *B. thailandensis* and *B. pseudomallei* strains *in vitro*. In this study, both of these antibiotics will be investigated for incorporation into an AAC. This proof of concept AAC will be compared to the antibiotic alone in cell infection models, to demonstrate benefit of the AAC approach for antibiotic delivery. This proof of principle AAC approach using fluoroquinolones, will inform future studies whereby different antibiotic classes could also be conjugated to the AAC. Additionally, the efficacy and pharmacokinetics of the fluoroquinolones could be improved as an AAC, the AAC approach could lead to improvements and increased therapeutic options for melioidosis.

Pharmacokinetics is the study of how a drug behaves in a body; this involves the analysis of properties such as distribution, metabolism and excretion of a drug. Determining the PK of a therapeutic antibody is essential to be able to determine parameters such as antibody distribution and clearance, to inform dosing regimens. IgG is generally characterised by a slow clearance and long half-life in circulation, this is due to properties such as binding to the neonatal receptor (FcRn), which saves antibody from lysosomal degradation (168). The major factors affecting the PK properties of the antibody include the antibody charge, glycosylation pattern and antibody engineering modifications (169). Therapeutic antibody delivery is most commonly achieved by intravenous (IV) and subcutaneous (SC) dosing, the distribution of the therapeutic antibody in the body is generally limited to the vascular system, together with interstitial spaces (348).

A PK study of the Genentech AAC (DSTA4637A) showed that in non-infected mice the AAC behaved the same as a monoclonal antibody, displaying short distribution, slow clearance and long half-life (166). In infected mice, the *S. aureus* had minimal

effect on the PK of the AAC, demonstrating prolonged strong anti-bacterial activity at 25 and 50mg kg^{-1} in multiple organs and tissues, including the kidneys, heart and bone (166).

Following on from the murine PK study (166), DSTA4637A has been further assessed in studies involving rats and cynomolgus monkeys (349). The AAC and antibody behaved as expected, mirroring the previous murine studies with a short distribution phase and a long elimination phase (349). The conjugation of antibiotic onto the *S. aureus* antibody has overall not adversely affected the PK behaviour of the antibody, as shown in murine, rat, and monkey studies (166, 349). The use of cynomolgus monkeys is considered a suitable model for predicting the PK properties of AAC in humans; this is due to similarities in antibody binding receptor pathways and antibody elimination pathways between non-human primates and humans (349). The study created a human model of AAC PK, predicted from the cynomolgus monkey PK analysis, to inform and predict the behaviour of the AAC in human clinical trials (349).

In this chapter, a proof of principle AAC targeting intracellular *B. thailandensis* will be assessed *in vitro.* Additionally, the pharmacokinetic properties of mAb 3VIE5 will be determined in BALB/c mice. This work represents the initial steps in developing an AAC therapeutic for melioidosis.

The aims of this chapter can be summarised as:

- Work in collaboration with Global Access Diagnostics to develop the first proof of principle AAC for melioidosis.
- *In vitro* testing of initial antibody conjugations, and analysis of conjugate cleavage by cathepsin.
- Test AACs in RAW cell infection assays and assess intracellular bacterial killing by the AAC.
- Determine the pharmacokinetic properties of mAb 3VIE5.

6.2 Development of a cathepsin cleavable linker-antibiotic.

6.2.1 Antibiotic stub conjugations.

The aim of this experiment is to investigate the AAC cleavage product, the products of AAC cathepsin cleavage being the active antibiotics ciprofloxacin and finafloxacin. This initial experiment is crucial to ensure antibiotic function post-cleavage. Cathepsin cleavage of the AAC linker, releases the antibiotic from the antibody, during this cathepsin cleavage a stub consisting of a portion of the linker (PAB, p-aminobenzyl) is retained on the antibiotic molecule (Figure 44). This stub has the potential to interfere with antibiotic function, it is therefore essential to investigate the effect of having the stub on the antibiotic, prior to developing the full AAC molecule. Antibiotic stubs were generated for both ciprofloxacin and finafloxacin (2.8.2. Generation of antibiotic stub molecules.) (Global Access Diagnostics), mimicking the final product generated from cathepsin cleavage of a full AAC. The purity of the antibiotic stub molecules (HPLC analysis, Global Access Diagnostics) were determined to be 90% and 95%, for finafloxacin-stub and ciprofloxacin-stub respectively. The antibiotic stubs were each tested *in vitro* in comparison to free antibiotic, this was to determine any differences in activity.

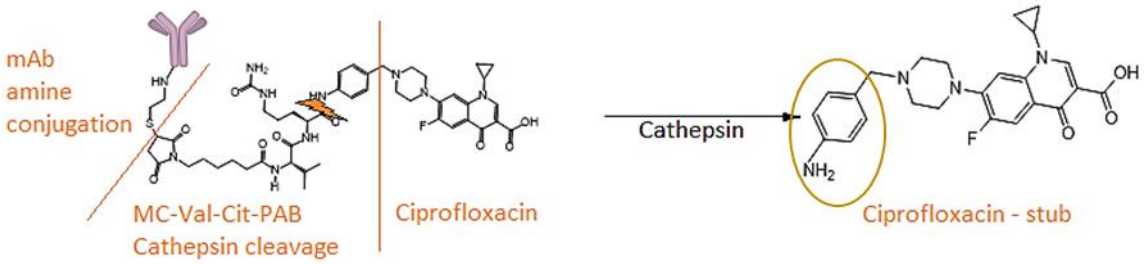

Figure 44. Amine conjugated AAC.

An AAC consists of an antibiotic conjugated to an antibody via a cleavable linker. The linker is cathepsin cleavable within the intracellular environment, releasing active antibiotic-stub. The cathepsin cleavage site is highlighted with a bolt on the AAC structure, and the stub is circled on the ciprofloxacin structure. Structures have been provided by Global Access Diagnostics.

Antibiotic stub molecules were assessed in a MIC assay (2.6.7. Minimum inhibitory concentration (MIC).). A visual observation of bacterial replication inhibition was used as a determination of an MIC value, together with an OD reading from an automated incubating plate reader over 24 hours. A time point of 24 hours was chosen as a point where antibiotic activity by inhibition of *B. thailandensis* replication is clearly visible. More quantitative analysis methods are available for determination of bacterial replication, such as Gompertz fitting and Richards models (297). The aim of this experiment was to observe bacterial growth inhibition by the antibiotic-stub molecules, therefore a visual examination of bacterial replication was sufficient for this purpose. A serial dilution of each compound was assessed by optical density for ability to reduce replication of *B. thailandensis*. An overnight Luria broth culture of *B. thailandensis* E555 was diluted to an approximate concentration of $1x_{10}^{8}$ bacteria mL^{-1}, using a bacterial OD reading of 0.172 OD_{600nm}. The bacterial suspension was further diluted to 1_{x10}^{6} cfu mL^{-1} with dilutions into Luria broth (Mueller Hinton broth for finafloxacin). A 96 well culture plate (Corning™ Costar™) was prepared with dilutions (75µg mL^{-1} to 0.14µg mL^{-1}) of ciprofloxacin, finafloxacin and the associated sub molecules, within a 100µL volume of Luria broth (Mueller Hinton broth for finafloxacin) per well. To each well, 100µL of the 1_{x10}^{6} cfu mL bacterial suspension was added, therefore the total volume was 200 µL per well. Control wells consisted of a positive *B. thailandensis* E555 only, and a negative control of 200 µL Luria broth (Mueller Hinton broth for finafloxacin). Plates were sealed with an optically clear sterile plate sealer and placed within an incubating plate reader (Multiskan FC, Thermo), with the incubator set to 37°C with gentle shaking. Automated OD readings were taken at OD_{595} every 15 minutes for 24 hours. The MIC was calculated by a visual examination of the 96 well plate to determine wells with no bacterial replication, as stated in the Clinical and Laboratory Standards Institute (CLSI) guidelines (245). Additionally, the OD readings from the incubating plate reader (Multiskan FC, Thermo) were plotted to display bacterial replication over 24 hours.

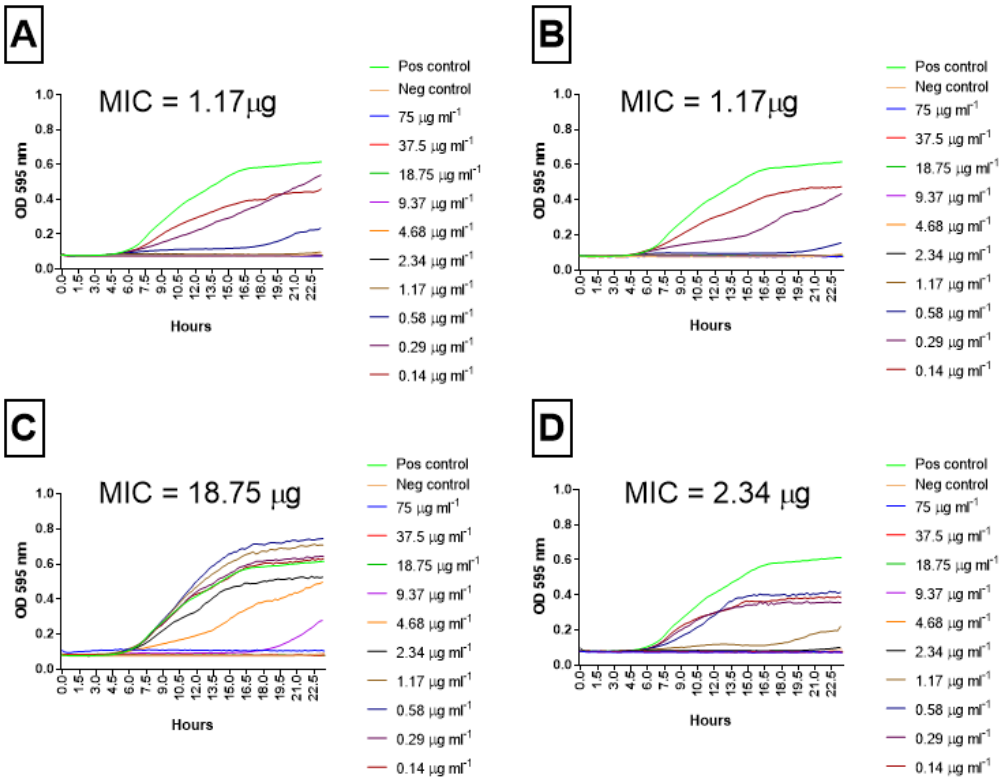

Figure 45. Minimum inhibitory concentration of antibiotic-stubs.

The MIC of the antibiotic-stubs was assessed by serial dilution on a 96 well micro titre plate from 75µg mL^{-1} to 0.14 µg mL^{-1} in Luria broth (Mueller Hinton broth for finafloxacin). An overnight Luria broth culture of *B. thailandensis* E555 was diluted to an approximate concentration of $1x_{10}^{8}$ bacteria mL^{-1}, using a bacterial OD reading of 0.172 OD_{600nm}. The bacterial suspension was further diluted to 1_{x10}^{6} cfu mL^{-1} with dilutions into Luria broth (Mueller Hinton broth for finafloxacin), the culture was then added to the 96 well plate together with the antibiotics and antibiotic-stubs. Plates were incubated for 24 hours at 37°C in an incubating plate reader (Multiskan FC, Thermo), additionally OD_{595nm} readings were taken every 15 minutes. The MIC was determined by visual inspection of the wells, the MIC was determined as the well with no bacterial replication after 24 hours incubation. Additionally, the bacterial replication curves were plotted by taking OD_{595nm} readings every 15 minutes for 24 hours. **A** – Ciprofloxacin stub, **B** – Ciprofloxacin control, **C** – Finafloxacin stub, **D** – Finafloxacin control. Positive (Pos) control and negative (Neg) controls consist of *B. thailandensis* and Luria broth (Mueller Hinton broth for finafloxacin) respectively. Each data point is the average of two technical replicates from a single biological experiment, due to the quantity of antibiotic-stub product available.

Antibiotic stubs were analysed by serial dilution and incubation with bacterial culture over 24 hours. Ciprofloxacin stub displayed efficacy, reducing bacterial replication to the same extent of the ciprofloxacin control (Figure 45 A and B), with an MIC of 1.17µg mL^{-1} at 24 hours. Finafloxacin stub also inhibited bacterial replication, although to a lesser extent than that of the finafloxacin control (Figure 45 C and D). The finafloxacin stub preparation suffered with precipitation issues, with a visible precipitate present in the antibiotic-stub preparation. Potentially, this is a solubility issue resulting in a lower active concentration of finafloxacin stub being applied to the assay.

In this assay, the stub does not inhibit ciprofloxacin function. This could also be the case for finafloxacin, once the issue with precipitation is solved. Overall this data provides evidence that successful cleavage of the AAC will release antibiotic in an active form.

6.2.2 Cathepsin cleavage of linker-antibiotic preparations.

The aim of this experiment was to determine if linker-antibiotic molecules can be successfully cleaved by the enzyme cathepsin B. Linker-antibiotic molecules were cleaved by cathepsin B *in vitro*, and the cleaved products tested by an MIC assay. A MC-Val-Cit-PAB(N-[(2S)-1-[[(2S)-5-(carbamoylamino)-1-[4-(hydroxymethyl) anilino]-1-oxopentan-2-yl]amino]-3-methyl-1-oxobutan-2-yl]-6-(2,5-dioxopyrrol-1-yl) hexanamide) cathepsin cleavable linker was conjugated to ciprofloxacin and to finafloxacin (2.8.4. Synthesis of Boc-amine linker-ciprofloxacin intermediate.), as separate linker-antibiotic batches (Global Access Diagnostics). The purity of the linker-antibiotic preps were 98% and 95%, for ciprofloxacin and finafloxacin respectively (Global Access Diagnostics LC-MS analysis). Conjugates were sent to Dstl for testing, to determine if cathepsin B can cleave the linker (2.7.1 *In vitro* cathepsin cleavage assay.), therefore releasing active antibiotic.

Cathepsin B from bovine spleen (Sigma) was used to cleave the MC-Val-Cit-PAB-ciprofloxacin / finafloxacin linker, the reaction was performed in cathepsin buffer (100mM sodium acetate buffer (Sigma), 2mM DTT (Sigma), 1mM EDTA (Sigma), pH 5) for 1 hour at 37°C (2.7.1 *In vitro* cathepsin cleavage assay.). Post cleavage, antibiotic activity was assessed by serial dilution and MIC analysis. Antibiotic-linker

molecules were assessed in a MIC assay (2.6.7. Minimum inhibitory concentration (MIC).). A visual observation of bacterial replication inhibition was used as a determination of an MIC value, together with an OD reading from an automated incubating plate reader over 24 hours. A serial dilution of cathepsin B cleaved and intact linker-antibiotics was assessed by optical density, to determine reduction in replication of *B. thailandensis*. An overnight Luria broth culture of *B. thailandensis* E555 was diluted to an approximate concentration of $1x_{10}^{8}$ bacteria mL^{-1}, using a bacterial OD reading of 0.172 OD_{600nm}. The bacterial suspension was further diluted to 1_{x10}^{6} cfu mL^{-1} with dilutions into Luria broth (Mueller Hinton broth for finafloxacin). A 96 well culture plate (Corning™ Costar™) was prepared with dilutions of ciprofloxacin, finafloxacin and the antibiotic-linker molecules (cleaved and intact), within a 100µL volume of Luria broth (Mueller Hinton broth for finafloxacin) per well. To each well, 100µL of the 1_{x10}^{6} cfu mL bacterial suspension was added, therefore the total volume was 200 µL per well. Control wells consisted of a positive *B. thailandensis* E555 only, and a negative control of 200 µL Luria broth (Mueller Hinton broth for finafloxacin). Plates were sealed with an optically clear sterile plate sealer and placed within an incubating plate reader (Multiskan FC, Thermo), with the incubator set to 37°C with gentle shaking. Automated OD readings were taken at OD_{595} every 15 minutes for 24 hours. The MIC was calculated by a visual examination of the 96 well plate to determine wells with no bacterial replication, as stated in the Clinical and Laboratory Standards Institute (CLSI) guidelines (245). Additionally, the OD readings from the incubating plate reader (Multiskan FC, Thermo) were plotted to display bacterial replication over 24 hours.

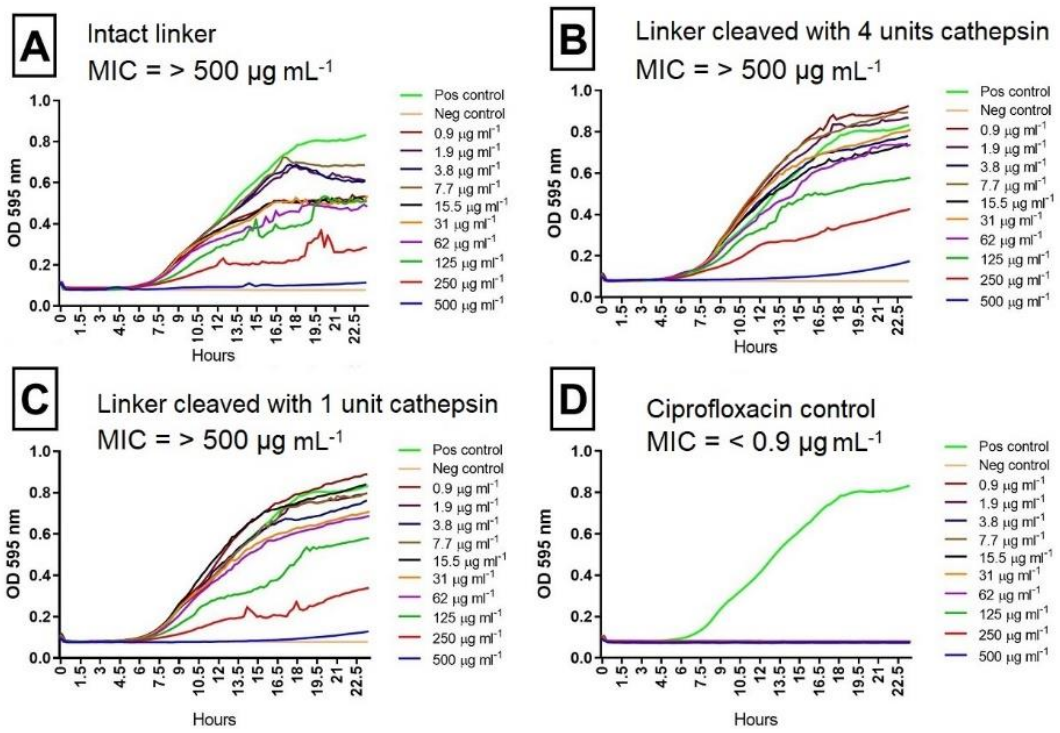

Figure 46. Cathepsin cleavage of linker-ciprofloxacin.

The MIC of the linker-ciprofloxacin was assessed by serial dilution on a micro titre plate from 500µg mL^{-1} to 0.9µg mL^{-1}. Linker-ciprofloxacin was either tested intact or with prior cleavage by cathepsin B at 4 units and 1 unit concentrations. An overnight Luria broth culture of *B. thailandensis* E555 was diluted to an approximate concentration of $1x_{10}^{8}$ bacteria mL^{-1}, using a bacterial OD reading of 0.172 OD_{600nm}. The bacterial suspension was further diluted to 1_{x10}^{6} cfu mL^{-1} with dilutions into Luria broth (Mueller Hinton broth for finafloxacin), the culture was then added to the 96 well plate together with the linker-ciprofloxacin products (cleaved and intact) and ciprofloxacin control. Plates were incubated for 24 hours at 37°C in an incubating plate reader (Multiskan FC, Thermo), additionally OD_{595nm} readings were taken every 15 minutes. The MIC was determined by visual inspection of the wells, with no visible bacterial replication after 24 hours incubation. Additionally, the bacterial replication curves were plotted by taking optical density (OD) readings every 15 minutes for 24 hours. **A** – Intact linker-ciprofloxacin, **B** – Cleaved linker-ciprofloxacin with 4 units cathepsin, **C** – Cleaved linker-ciprofloxacin with 1 unit cathepsin and **D** – Ciprofloxacin control. Positive (Pos) control and negative (Neg) controls consist of *B. thailandensis* E555 and Luria broth respectively. Each data point is the average of two technical replicates from a single biological experiment, due to quantity of linker-ciprofloxacin available.

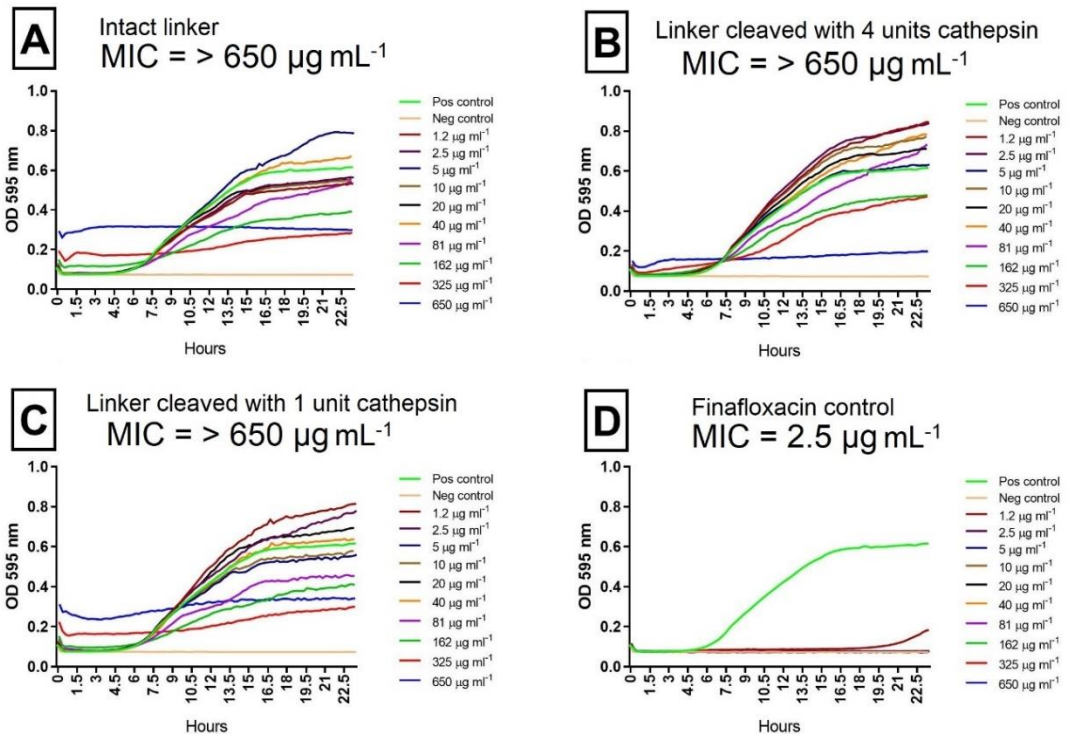

Figure 47. Cathepsin cleavage of linker-finafloxacin.

The MIC of the linker-finafloxacin was assessed by serial dilution on a micro titre plate from 650µg mL^{-1} to 1.2µg mL^{-1}. Linker-finafloxacin was either tested intact or with prior cleavage by cathepsin B at 4 units and 1 unit concentrations. An overnight Luria broth culture of *B. thailandensis* E555 was diluted to an approximate concentration of $1x_{10}^{8}$ bacteria mL^{-1}, using a bacterial OD reading of 0.172 OD_{600nm}. The bacterial suspension was further diluted to 1_{x10}^{6} cfu mL^{-1} with dilutions into Luria broth (Mueller Hinton broth for finafloxacin), the culture was then added to the 96 well plate together with the linker-ciprofloxacin products (cleaved and intact) and ciprofloxacin control. Plates were incubated for 24 hours at 37°C in an incubating plate reader (Multiskan FC, Thermo), additionally OD_{595nm} readings were taken every 15 minutes. The MIC was determined by visual inspection of the wells, with no visible bacterial replication after 24 hours incubation. Additionally, the bacterial replication curves were plotted by taking optical density (OD) readings every 15 minutes for 24 hours. **A** – Intact linker-finafloxacin, **B** – Cleaved linker-finafloxacin with 4 units cathepsin, **C** – Cleaved linker-finafloxacin with 1 unit cathepsin and **D** – Finafloxacin control. Positive (Pos) control and negative (Neg) controls consist of *B. thailandensis* E555 and Mueller Hinton broth respectively. Each data point is the average of two technical replicates from a single biological experiment, due to quantity of linker-finafloxacin available.

There was no clear difference in bacterial replication inhibition between intact or cathepsin cleaved linkers, this was the result for both ciprofloxacin and finafloxacin linkers. It was expected that the intact linker-antibiotic would have no efficacy, based on published literature on the activity of AAC conjugated antibiotic for the *S. aureus* AAC (165). Although once the linker is cleaved, the antibiotics should then be released in the active stub-antibiotic form, and show efficacy to a MIC similar to the antibiotic control MIC. The stub-antibiotic form has previously shown efficacy in the MIC assay (Figure 45), therefore if the linker had been cleaved successfully then this efficacy should have been demonstrated in this MIC assay. The MIC assay gives an indication of cleavage efficiency, since the antibiotic is only active post-cleavage and the MIC value should reflect the concentration of antibiotic on the AAC. In future studies, fluorescent linkers or colorimetric linkers could be developed to more accurately quantify AAC cleavage by cathepsin B. For example, a linker incorporating Z-RR-pNA could be developed, this would release pNA which can be quantified in a colorimetric assay to determine the efficiency of linker cleavage by cathepsin B. Alternatively, a fluorescent linker could be developed in which fluorescence is detected post-cleavage, this method could also be used to visualise AAC cleavage within infected cells *in vitro* (165).

This data shows that, either the linker itself was not cathepsin cleavable in this initial linker-antibiotic product, or the cathepsin B used to cleave the linker was inactive. Based on this data, cathepsin B was replaced with a new batch, and the enzymatic activity tested prior to any further AAC cleavage experiments.

6.2.3. Cathepsin B activity.

The aim of this experiment was to test the activity of cathepsin B, this was important to demonstrate that the cathepsin B is active in the pH5 sodium acetate buffer and the cathepsin B is able to cleave the AAC *in vitro*. Additionally, the effect of cathepsin B on bacterial replication was assessed in a MIC assay, to determine any anti-bacterial effect at high concentrations. A colorimetric Z-RR-pNA (Sigma) substrate was used to test the enzymatic activity of cathepsin B from bovine spleen (Sigma). A concern from previous linker-antibiotic data was that the cathepsin from bovine spleen may not be active in the cathepsin buffer (100mM sodium acetate buffer

(Sigma), 2mM DTT (Sigma), 1mM EDTA (Sigma), pH 5), and therefore would not cleave the linker-antibiotic samples. To investigate this, the lyophilised cathepsin B from bovine spleen (Sigma) was prepared in cathepsin buffer (100mM sodium acetate buffer (Sigma), 2mM DTT (Sigma), 1mM EDTA (Sigma), pH 5), then added at a concentration of one unit to a range of concentrations (30µm to 120µm) of colorimetric Z-RR-pNA (Sigma) on a 96 well plate (2.7.2 Cathepsin B activity.). The colorimetric product (p-nitroaniline) formed from cathepsin cleavage of Z-RR-pNA, was detected by OD at 405nm in a 96 well incubating micro plate reader (Multiskan FC (Thermo)), with OD readings every minute for 1 hour at 25°C.

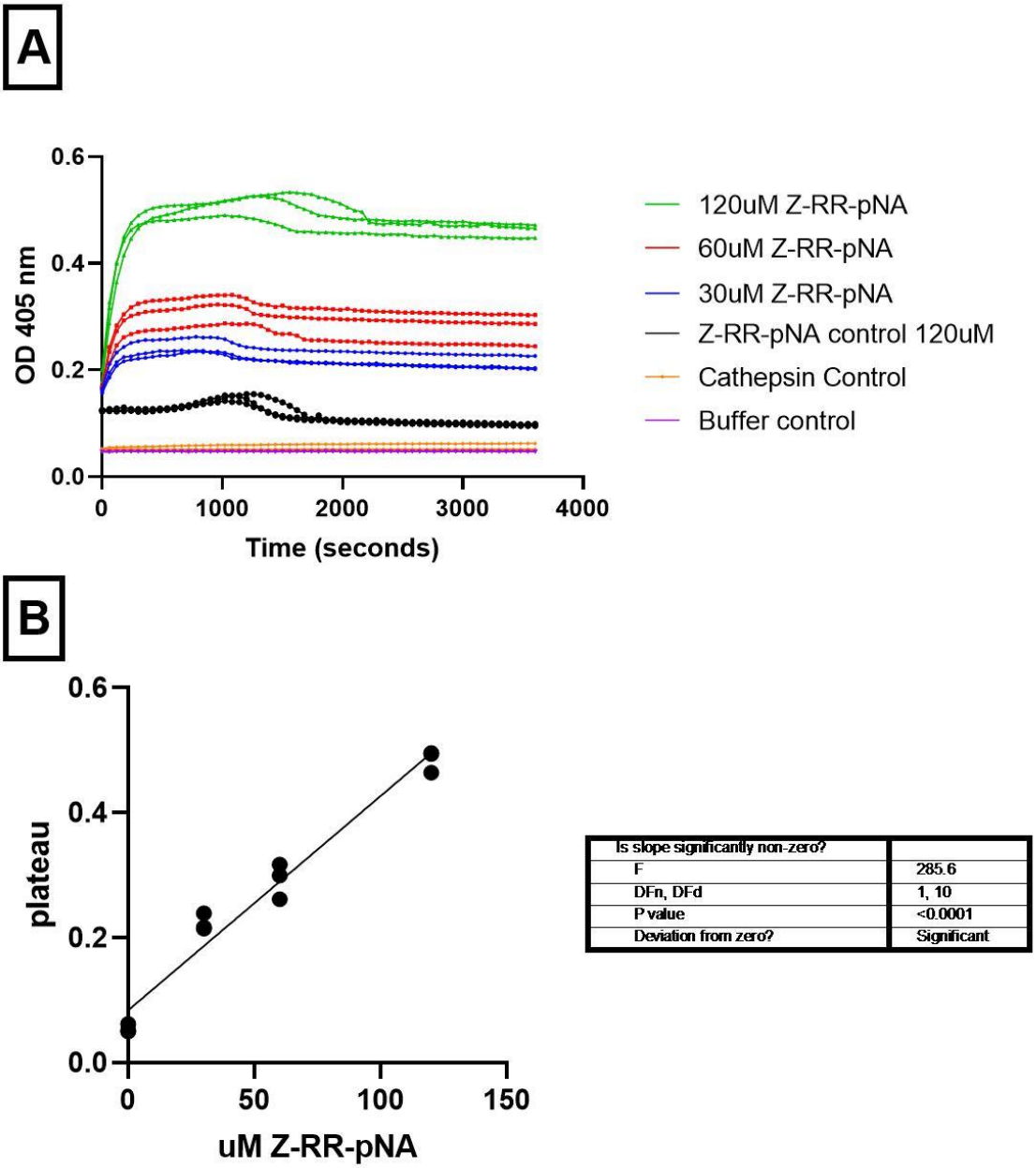

Figure 48. Cathepsin B activity with a colorimetric Z-RR-pNA substrate.

The activity of cathepsin B in cathepsin buffer (100mM sodium acetate buffer (Sigma), 2mM DTT (Sigma), 1mM EDTA (Sigma), pH 5) was assessed by cleavage of Z-RR-pNA. The colorimetric product (p-nitroaniline) formed from cathepsin cleavage of Z-RR-pNA, was detected by OD at 405nm in a 96 well incubating micro plate reader (Multiskan FC (Thermo)), with OD readings every minute for 1 hour at 25°C. **A** - Cathepsin cleavage of Z-RR-pNA colorimetric substrate at 405nm. Data are the average of replicates (n=3) from separate vials of cathepsin B, and each

biological replicate is shown as a separate line on the graph. **B** – The plateau of the slope for each data was assessed by an F test. There is a significant ($P < 0.0001$) association between Z-RR-pNA concentration and the OD data plateau.

The activity of cathepsin B from bovine spleen in the pH 5 cathepsin buffer, was confirmed using the colorimetric Z-RR-pNA (z-arg-arg-p-nitroanalide) substrate. The product p-nitroaniline, formed from cathepsin cleavage of Z-RR-pNA, was detected at 405nm. The cathepsin reaction yielded detectable p-nitroaniline, and in a concentration dependent response over 1 hour. This data shows that the cathepsin B reagent from bovine spleen is enzymatically active.

The effect of cathepsin B on bacterial replication, was assessed by MIC (2.6.7. Minimum inhibitory concentration (MIC).). This was to determine if cathepsin B has any direct anti-microbial activity. A visual observation of bacterial replication inhibition was used as a determination of an MIC value, together with an OD reading from an automated incubating plate reader over 24 hours. A serial dilution of cathepsin B was assessed by optical density, to determine reduction in replication of *B. thailandensis*. An overnight Luria broth culture of *B. thailandensis* E555 was diluted to an approximate concentration of $1x_{10}^{8}$ bacteria mL^{-1}, using a bacterial OD reading of 0.172 OD_{600nm}. The bacterial suspension was further diluted to 1_{x10}^{6} cfu mL^{-1} with dilutions into Luria broth. A 96 well culture plate (Corning™ Costar™) was prepared with dilutions of cathepsin B (10 units diluted to 0.01 units) within a 100µL volume of Luria broth per well. To each well, 100µL of the 1_{x10}^{6} cfu mL bacterial suspension was added, therefore the total volume was 200 µL per well. Control wells consisted of a positive *B. thailandensis* E555 only, and a negative control of 200 µL Luria broth. Plates were sealed with an optically clear sterile plate sealer and placed within an incubating plate reader (Multiskan FC, Thermo), with the incubator set to 37°C with gentle shaking. Automated OD readings were taken at OD_{595} every 15 minutes for 24 hours. The MIC was calculated by a visual examination of the 96 well plate to determine wells with no bacterial replication, as stated in the Clinical and Laboratory Standards Institute (CLSI) guidelines (245). Additionally, the OD readings from the incubating plate reader (Multiskan FC, Thermo) were plotted to display bacterial replication over 24 hours.

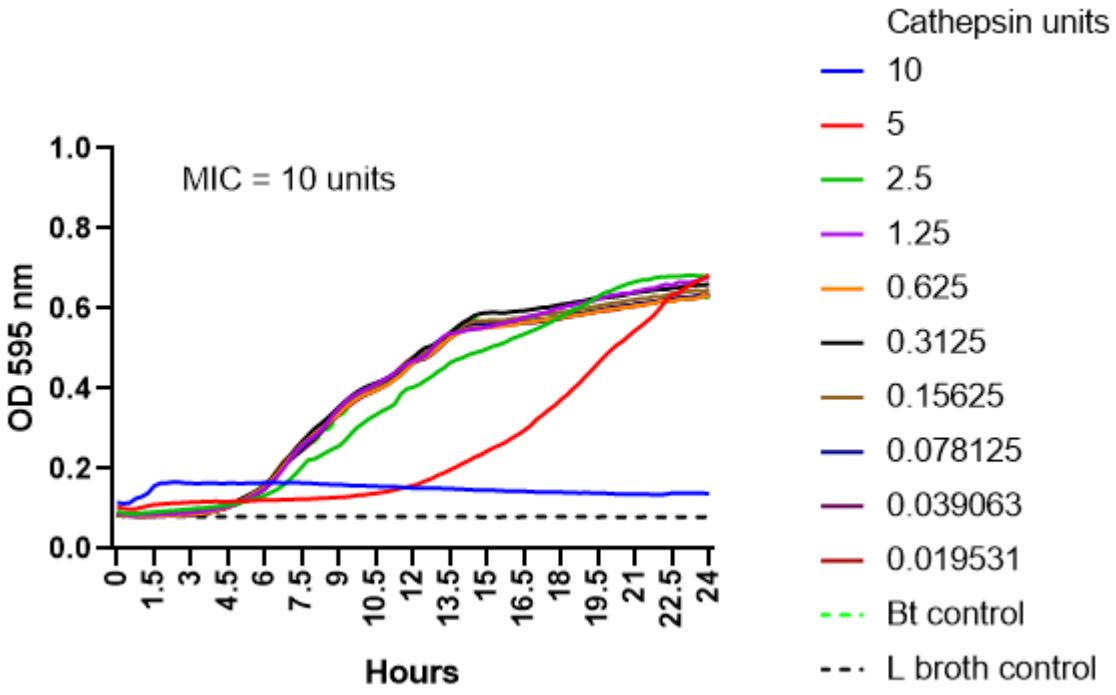

Figure 49. Effect of cathepsin B on bacterial replication.

The MIC of cathepsin B was assessed by serial dilution of cathepsin B on a micro titre plate and incubation with *B. thailandensis* E555. The 96 well plate was incubated at 37°C for 24 hours to determine the effect of cathepsin B on replication of *B. thailandensis*. The MIC was determined by visual inspection of the wells, with no visible bacterial replication after 24 hours of incubation. Additionally, the bacterial replication curves were plotted by taking OD readings every 15 minutes for 24 hours. Controls consist of a positive *B. thailandensis* E555 only control (Bt control) and a negative Luria broth only control (L broth control). Data are the average from two biological experiments.

High levels of cathepsin B (10 units) directly onto the bacteria inhibited replication, with a delay in replication at 5 units. Although 10 units inhibited replication, and 5 units delayed bacterial replication, the cathepsin that will be used for MIC assays is diluted multiple times before adding to the bacteria. In AAC cleavage assays, a maximum cathepsin B concentration that bacteria will be exposed to is 2.5 units. This data shows that cathepsin levels directly on the bacteria, need to be diluted to an

equivalent of 2.5 units or below, this is to avoid cathepsin inhibition of replication during MIC analysis of AACs.

6.3 Generation of a full ciprofloxacin AAC.

Conjugation of finafloxacin to a cathepsin cleavable linker, and as a stub-finafloxacin molecule, resulted in issues with precipitation. The precipitation was evident in the stock solution of stub-finafloxacin and at high concentrations in MIC assays. This is visible in the data as a consistent high OD reading across the MIC assays at 650µg mL^{-1} of linker-finafloxacin (Figure 47). Precipitation is an issue with MIC assays and especially when using OD readings, any precipitation will show as a high OD and could be mistaken as bacterial replication by OD and also visually. The precipitation in the stock solution will also result in inaccurate concentrations of finafloxacin being used in experimental assays, therefore future work with finafloxacin will require the precipitation issue to be resolved prior to further *in vitro* analysis. A loss of activity was evident when testing finafloxacin-stub conjugations in MIC assays (Figure 45). No such precipitation issues or loss of activity was evident with the ciprofloxacin-linker molecules, therefore it was decided to focus on developing a proof of principle ciprofloxacin AAC.

6.3.1 Unconjugated ciprofloxacin and mAb 3VIE5 in a RAW 264.7 cell infection assay.

The aim of this experiment was to determine any benefit of mAb 3VIE5 and ciprofloxacin together as a combination, without any physical conjugation as an AAC. A *B. thailandensis* RAW cell infection assay was used to assess combining both mAb 3VIE5 and ciprofloxacin, as a non-conjugated therapy (2.2.1. RAW cell infection assay.). Synergistic effects of antibody and ciprofloxacin has been reported in the literature for other bacterial diseases, with synergistic effects including reductions in antibiotic MIC, and improving efficacy in animal challenge studies (350-352). In this assay, it is expected that mAb 3VIE5 will opsonise and increase bacterial CFU, the effect mAb 3VIE5 will have on the efficacy of ciprofloxacin will be determined over 24 hours. It has previously been demonstrated that ciprofloxacin has a MIC of approximately 1 µg mL^{-1} directly on *B. thailandensis* bacterial culture (Figure 45), the

data generated here will determine the bactericidal concentration of ciprofloxacin on intracellular *B. thailandensis* at 4 and 24 hours of incubation. Any synergistic effects of ciprofloxacin with mAb 3VIE5 will be determined, although no increase in ciprofloxacin efficacy is expected with mAb 3VIE5. This assay will provide the initial data of the mAb and ciprofloxacin combination in a RAW cell infection assay, prior to assessing bacterial killing as an AAC in later studies.

An overnight culture of *B. thailandensis* E555 was diluted to 1_{x10}^{8} CFU mL^{-1} (OD_{600} of 0.172) in L-15 culture media, the bacteria culture was further diluted to 1_{x10}^{7} CFU mL^{-1}. The bacteria were opsonised with 1 µg mL^{-1} of 3VIE5 for 30 minutes at 37°C prior to RAW cell infection. The no mAb control consisted of non-opsonised *B. thailandensis*. RAW cells at 1_{x10}^{6} cells mL^{-1} in L-15 media were infected with the opsonised or non-opsonised bacteria at an MOI of 5, and incubated for 1 hour at 37°C. Following incubation the cell culture media was removed, and immediately replaced with L-15 media containing 1mg mL^{-1} kanamycin maintenance antibiotic. Additionally, ciprofloxacin was added to the cell culture media at concentrations ranging from 0.1 µg mL^{-1} to 5 µg mL^{-1}, and the RAW cells incubated for 4 and 24 hours at 37°C. RAW cells were lysed by replacing DMEM culture media with distilled water, until cell lysis occurred (checked by light microscopy). Upon cell lysis the bacteria were enumerated by serial dilution and culture on L-agar. Agar plates were incubated for a minimum of 24 hours at 37°C until colonies could be accurately counted.

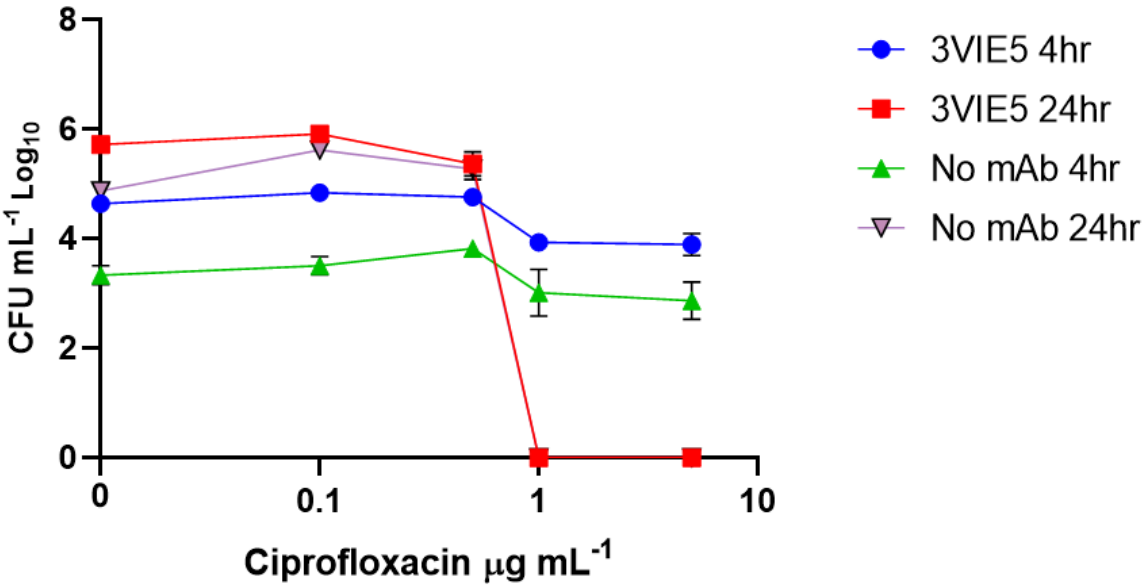

Figure 50. The effect of ciprofloxacin and mAb 3VIE5 on bacterial CFU.

A range of ciprofloxacin concentrations were assessed in a RAW cell infection assay, for ability to kill mAb 3VIE5 opsonised and non-opsonised *B. thailandensis*. The *B. thailandensis* E555 bacteria were opsonised with 1 μg mL^{-1} of 3VIE5 for 30 minutes at 37°C, prior to RAW cell infection. The no mAb control consisted of non-opsonised *B. thailandensis* E555. RAW cells were infected with the opsonised or non-opsonised bacteria at an MOI of 5, and incubated for 1 hour at 37°C. Following incubation the cell culture media was removed, and immediately replaced with L-15 media containing 1mg mL^{-1} kanamycin maintenance antibiotic and ciprofloxacin ranging from 0.1 μg mL^{-1} to 5 μg mL^{-1}. Following incubation at 37°C for 4 or 24 hours, intracellular bacterial CFU were enumerated by serial dilution and culture on L-agar. Data points are the mean of all technical replicates (n=4) derived from two separate biological experiments. Error bars represent SD of all technical replicates.

Table 2. Three way ANOVA statistical analysis of ciprofloxacin and mAb 3VIE5 combination CFU data.

3 way ANOVA	% of total variation	P value	
Cipro concentration	58.42	<0.0001	****
mAb or no mAb	2.883	0.0002	***
Time 4 vs 24	2.171	0.0022	**
Cipro concentration x mAb or no mAb	0.3488	0.0003	***
Cipro concentration x Time 4 vs 24	34.37	<0.0001	****
mAb or no mAb x Time 4 vs 24	1.173	<0.0001	****
Cipro concentration x mAb or no mAb x Time 4 vs 24	0.07091	0.1085	ns

A 3 way ANOVA was performed using GraphPad Prism comparing each variable in the CFU infection assay. Variables were ciprofloxacin concentration, presence or absence of mAb 3VIE5, and time (post-infection).

The RAW cell infection assay was used to determine the effect of mAb 3VIE5 together with ciprofloxacin, on intracellular CFU. The data shows that the major determining factors on intracellular bacterial CFU, are the ciprofloxacin concentration and the ciprofloxacin concentration over time. The effect of mAb 3VIE5 on CFU is significant, although no reduction of bacterial CFU is observed. The significance is due to an increase in CFU by mAb 3VIE5 opsonising the bacteria, at 4 hours post-infection the opsonisation effect of mAb 3VIE5 is most apparent. Therefore, mAb 3VIE5 does not affect the concentration of ciprofloxacin at which there is bacterial killing. This is most apparent at 24 hours post-infection (Figure 50), both mAb 3VIE5 and the no antibody control, demonstrate bacterial CFU clearance at 1µg mL^{-1} of ciprofloxacin.

In this *in vitro* cell infection assay, there is no apparent bacterial killing advantage of a ciprofloxacin and mAb 3VIE5 non-conjugated combination therapy. This data provides a starting point to determine the beneficial effect of conjugating mAb 3VIE5 to ciprofloxacin as an AAC. It has also been determined that in the RAW cell infection assay, 1 µg mL^{-1} of ciprofloxacin is bactericidal at 24 hours of incubation.

6.3.2 Amine to amine conjugation to create a cathepsin cleavable AAC.

The mAb 3VIE5 was conjugated to ciprofloxacin via a cathepsin cleavable linker, this was achieved by an amine to amine conjugation method developed by Global Access Diagnostics (Figure 51) (2.8. Generation of AAC products by Global Access Diagnostics.. The amine group on the AAC linker is initially protected using a Boc (tert-butyloxycarbonyl) group, this Boc group protects the linker anime during ciprofloxacin conjugation to the linker. Protection of the amine group is essential, this ensures that the amine is available for later conjugation to the mAb 3VIE5. This Boc group is subsequently removed with TFA (trifluoroacetic acid) treatment, thus de-protecting the amine group for conjugation. A lysine on the antibody displays a maleimide group via treatment with SMCC (succinimidyl 4-(N-maleimidomethyl) cyclohexane-1-carboxylate), the linker amine is treated with traut's reagent (2-Iminothiolane) to display a thiol group, allowing conjugation to the maleimide group of the antibody. The end result is a proof of principle mAb 3VIE5 - ciprofloxacin AAC, a heterogeneous product with an average DAR of 2. Samples of AAC were prepared by Global Access Diagnostics and sent to Dstl for *in vitro* analysis.

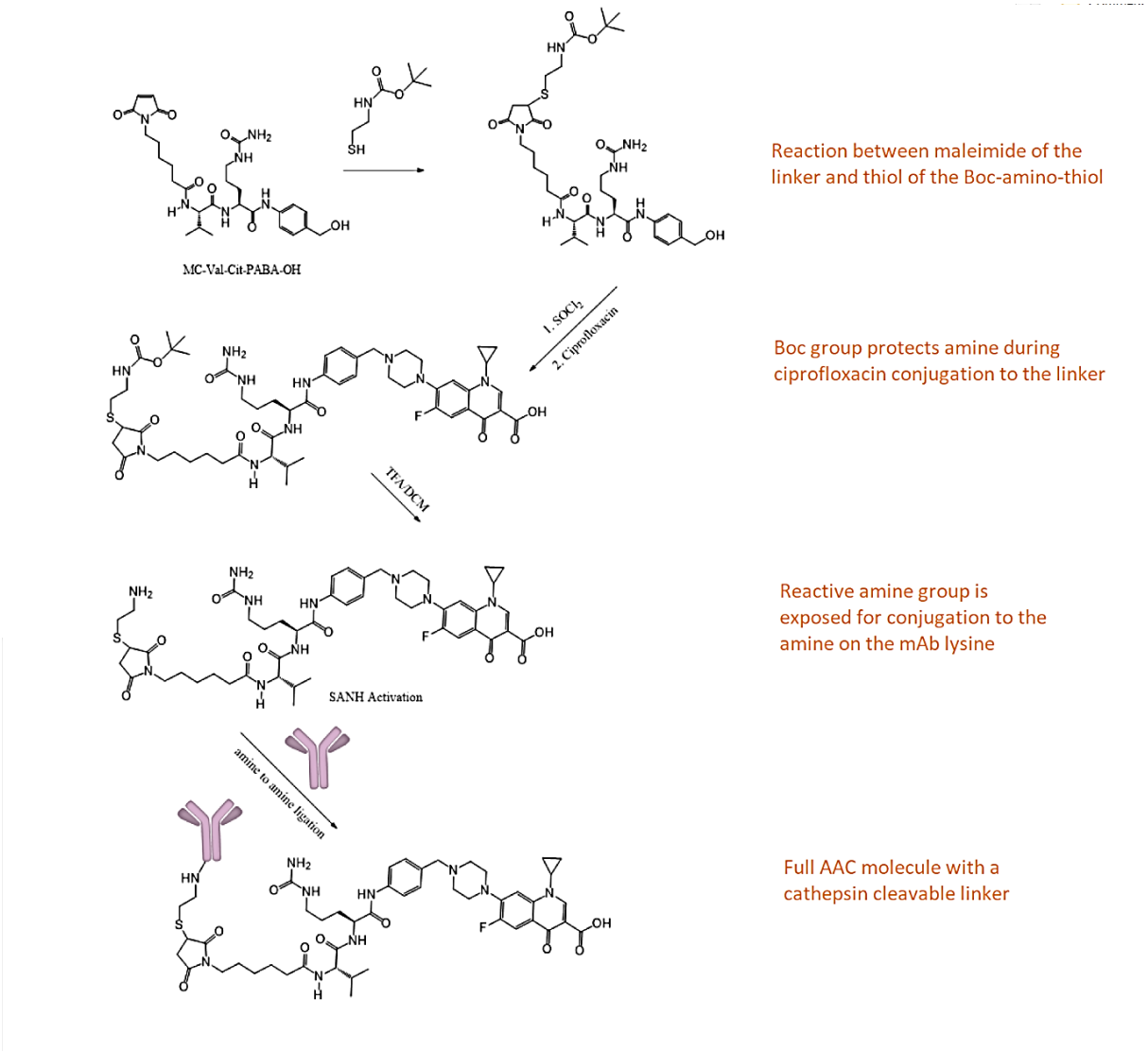

Figure 51. Generation of a cathepsin cleavable AAC by amine to amine conjugation.

An overview of the amine based conjugation method for development of an AAC, mAb 3VIE5 was conjugated to ciprofloxacin via a cathepsin cleavable linker. A MC-val-cit-PAB-OH linker undergoes a reaction with a Boc (tert-butyloxycarbonyl)-amino-thiol, this provides an amine group to conjugate to an amine on the mAb lysine. The Boc group protects the amine during ciprofloxacin conjugation to the linker, this Boc group is later removed by TFA (trifluoroacetic acid) so that the reactive amine is available for mAb conjugation. Structures provided by Global Access Diagnostics.

The ciprofloxacin AAC (generated by Global Access Diagnostics) was labelled with FITC (fluorescein isothiocyanate), the AAC was added to red fluorescent protein (RFP) expressing *B. thailandensis* to visualise binding of the AAC to the bacterial CPS. An overnight culture of *B. thailandensis* E555 RFP in L-broth was diluted to an OD of 0.172, which equates to a concentration of 1_{x10}^{8} CFU mL^{-1}. The FITC labelled AAC was added to the bacteria at a concentration of 10 µg mL^{-1}, this high concentration was selected to ensure that the fluorescence will be visible on the confocal microscope. The AAC and *B. thailandensis* were incubated for 30 minutes at 37°C prior to imaging. Confocal microscopy was used to visualise fluorescence from the FITC (excitation peak of 490 and emission peak of 525) using a 488nm excitation laser, and RFP using a 543nm excitation laser (excitation peak of 555 and emission peak of 584). Images were taken using x63 magnification.

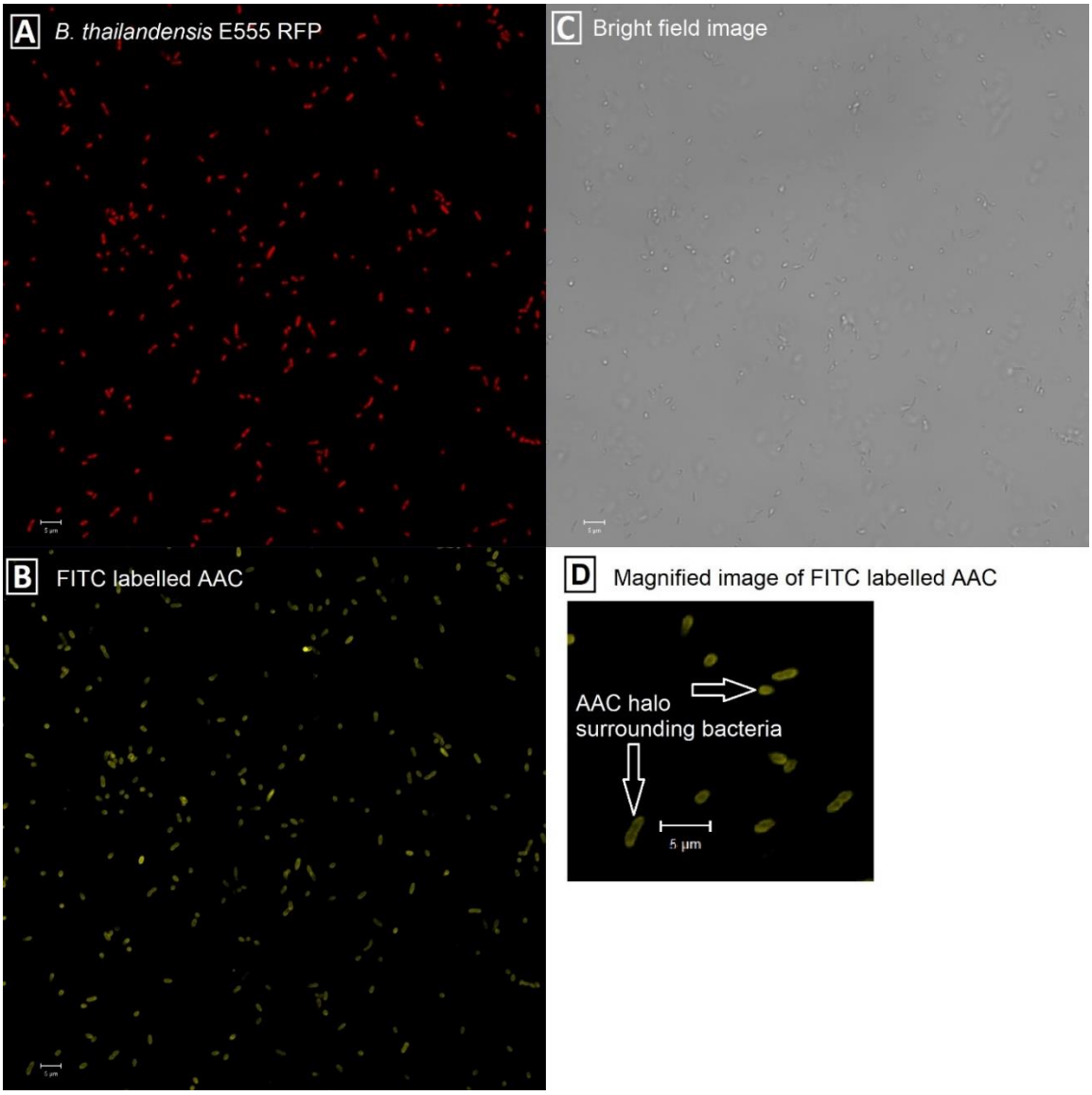

Figure 52. Confocal imaging of ciprofloxacin AAC labelled with FITC.

Confocal microscopy was used to visualise FITC labelled AAC binding to *B. thailandensis*. The FITC labelled AAC was added at 10µg mL^{-1}, to a *B. thailandensis* E555 RFP culture of $1_{x10}{}^{8}$ CFU mL^{-1}. Images were taken after 30 minutes of incubation at 37°C. Split confocal images were generated of RFP expressing *B. thailandensis* and FITC labelled AAC. FITC (excitation peak of 490 and emission peak of 525) fluorescence was imaged using a 488nm excitation laser, and RFP fluorescence using a 543nm excitation laser (excitation peak of 555 and emission peak of 584). Images were taken using x63 magnification. **A** – RFP expressing strain of *B. thailandensis* E555, **B** – FITC labelled AAC, **C** – light image of bacteria and AAC. **D** – A magnified example of AAC bound to *B. thailandensis*. Scale bar represents 5 µm.

The aim of this experiment was to visualise the binding of the FITC labelled AAC to the *B. thailandensis* bacteria. It is expected that the AAC is binding to the capsule surrounding the *B. thailandensis*. It was observed that the fluorescent AAC binds as a halo around the bacteria (Figure 52), this image provided reassurance that the AAC is binding to the CPS of the bacteria, prior to assessment of the AAC in RAW cell infection assays. The binding of the FITC labelled AAC to *B. thailandensis* has not been quantified in this experiment, generation of further fluorescent AAC molecules are required. Additional studies with fluorescent AAC molecules are required to quantify AAC binding to the capsule of *B. thailandensis*, by analysing fluorescence intensity of the bound FITC labelled AAC molecule. This experiment confirmed that the AAC can be successfully labelled with FITC, this will inform future experiments for tracking the intracellular location of the AAC by confocal microscopy.

Table 3. Details of AAC batches.

Reference	Concentration mg.mL	DAR	Date of production
WR1365	1.13	2	09/01/20
WR1382	1	2.7	19/02/20
WR1498	2.82	2	15/07/20
WR1568	2	2	10/11/20
WR1691	1.5	2.9	01/12/21

Details of amine conjugated AAC, each reference is an AAC batch generated by Global Access Diagnostics. DAR – drug antibody ratio.

6.3.2 *In vitro* MIC and MBC testing of ciprofloxacin AAC.

The MIC of the AAC for *B. thailandensis* was assessed *in vitro*. The aim of the MIC and MBC experiments was to determine the activity of intact and cleaved AAC compared to controls (ciprofloxacin and mAb 3VIE5). The activity of the AAC was determined by inhibition of replication (2.6.7. Minimum inhibitory concentration (MIC).) and killing (2.6.8. Minimum bactericidal concentration (MBC).) of *B.*

thailandensis E555. The MIC of the AAC was compared to a ciprofloxacin control and a mAb 3VIE5 control, at a range of concentrations.

An overnight Luria broth culture of *B. thailandensis* E555 was diluted to an approximate concentration of $1x_{10}^{8}$ bacteria mL^{-1}, using a bacterial OD reading of 0.172 OD_{600nm}. The bacterial suspension was further diluted to 1_{x10}^{6} cfu mL^{-1} with dilutions into Luria broth. A 96 well culture plate (Corning™ Costar™) was prepared with dilutions of AAC, ciprofloxacin and mAb 3VIE5 within a 100µL volume of Luria broth per well. AAC was previously cleaved with 10 units of cathepsin B in cathepsin assay buffer (100mM sodium acetate buffer (Sigma), 2mM DTT (Sigma), 1mM EDTA (Sigma), pH 5), once diluted the maximum concentration of cathepsin B in the MIC assay was equivalent to 1.25 units. To each well, 100µL of the 1_{x10}^{6} cfu mL bacterial suspension was added, therefore the total volume was 200 µL per well. Control wells consisted of positive bacterial culture and negative controls consisted of 200 µL of L-broth. Plates were placed within a static incubator for 24 hours at 37°C. The MIC was calculated by a visual examination of the 96 well plate to determine wells with no bacterial replication, as stated in the Clinical and Laboratory Standards Institute (CLSI) guidelines (245). To determine the MBC, 100µl aliquots were taken from wells of the MIC assay with no visible bacterial replication. The aliquots were plated onto Luria agar and incubated at 37°C for a minimum of 24 hours. A concentration of the AAC, ciprofloxacin and mAb 3VIE5 that killed 99.9% of the bacterial inoculum was considered the MBC value.

Table 4. Amine conjugated AAC MIC and MBC data.

	WR1382	WR14981		WR1568		WR1691	
	MIC (µg mL)	MIC (µg mL)	MBC (µg mL)	MIC (µg mL)	MBC (µg mL)	MIC (µg mL)	MBC (µg mL)
Intact AAC	Nd >250	350	Nd >350	Nd >250	Nd >250	Nd >187.5	Nd >187.5
Cleaved AAC	62.5	87.5	350	62.5	250	46.8	Nd >187.5
Ciprofloxacin	0.3	0.6	2.5	0.3	2.5	0.15	2.4
Antibody	250	Nd >350	Nd >350	Nd >250	Nd >250	Nd >187.5	Nd >187.5

Amine conjugated AAC batches (WR1382, WR14981, WR1568 and WR1691) were analysed for ability to inhibit replication and kill *B. thailandensis* E555. The AAC was tested intact or with prior cleavage by cathepsin B. MIC was determined by eye as the dilution with no visible bacterial replication after 24 hours incubation at 37°C. MBC (minimum bactericidal concentration) was determined by plating a bacterial culture onto L-agar, the MBC is the concentration that resulted in no visible bacterial replication on L-agar after 24 hours incubation at 37°C. Nd – not detected, MIC and MBC are greater than the maximum concentration tested.

The MIC was calculated by a visual examination of the 96 well plate to determine which wells visually had no replication, as stated in the CLSI guidelines (245). A modification to the CLSI guideline was that Luria broth was used as the bacterial culture media during all MIC assays, this was for consistency in bacterial culture methods across all experiments.

The MIC and MBC data shows that the un-cleaved AAC does not inhibit replication of *B. thailandensis*. Once cathepsin cleaved, the AAC is then able to inhibit replication of bacteria in the MIC and MBC assay. This to be expected, since the ciprofloxacin attached to the antibody has not undergone cleavage from the

cathepsin B cleavable linker. This is a desirable characteristic of the AAC, by limiting off target effects of the antibiotic, potentially allowing lower concentrations of antibiotic to be used as a targeted therapy.

To compare ciprofloxacin control and cleaved AAC, it was calculated that 1mg mL^{-1} of AAC (DAR of 2) is approximately 4.4 µg mL^{-1} of ciprofloxacin, based on molecular weight of antibody being 150,000 kDa and ciprofloxacin of 331 kDa. This equates to 0.44% ciprofloxacin, which correlates with the MIC data between the ciprofloxacin control and AAC cleaved. For example, in Table 4 the cleaved AAC MIC is 62.5 µg which contains 0.275 µg (0.44%) ciprofloxacin, this compares to the ciprofloxacin control MIC of 0.3 µg. This demonstrates that the AAC has undergone full cleavage by cathepsin B in the MIC assay, releasing active ciprofloxacin to inhibit bacterial replication.

6.3.3 *In vitro* AAC RAW macrophage-like cell infection assay.

The aim of this experiment was to assess the AAC in a RAW cell infection assay, to determine the killing ability of the AAC against *B. thailandensis* E555 *in vitro*. An additional aim was to investigate differences in bacterial killing when the AAC is added pre or post-infection of RAW cells (2.2.4. Antibody-antibiotic conjugate infection assay.).

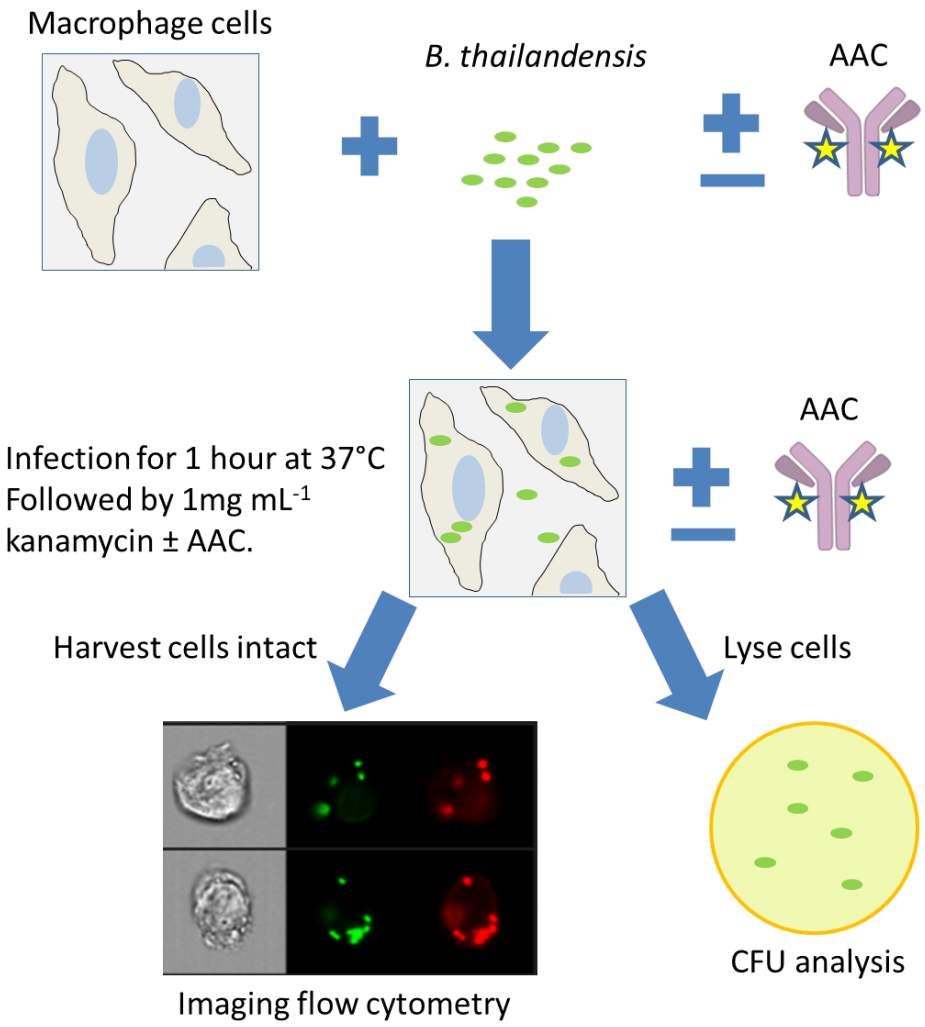

Figure 53. Testing of the AAC in a RAW cell infection assay.

A RAW 264.7 cell infection assay was used to assess the AAC for ability to kill intracellular *B. thailandensis*. An overnight culture of *B. thailandensis* E555 (RFP strain for imaging flow cytometry) was diluted to 1_{x10}^{8} CFU mL^{-1} (OD_{600} of 0.172) in L-15 culture media (Gibco), the bacteria culture was further diluted to 1_{x10}^{7} CFU mL^{-1}. In opsonisation experiments the bacteria were opsonised with 3VIE5 or AAC for 30 minutes at 37°C, prior to RAW cell infection. The control infection consisted of non-opsonised *B. thailandensis*. RAW cells at 1_{x10}^{6} cells mL^{-1} in L-15 media (Gibco) were infected with the opsonised or non-opsonised bacteria at an MOI of 5, and incubated for 1 hour at 37°C. Following incubation the cell culture media was removed, and immediately replaced with L-15 media containing 1mg mL^{-1} kanamycin maintenance antibiotic. At this point the AAC and ciprofloxacin were added to the RAW cells in the post-infection AAC experiments. The RAW cells incubated for up to

24 hours at 37°C. RAW cells were lysed by replacing the cell culture media with distilled water, until cell lysis occurred (checked by light microscopy). Upon cell lysis the bacteria were enumerated by serial dilution and culture on L-agar. Agar plates were incubated for a minimum of 24 hours at 37°C until colonies could be accurately counted.

Alternatively, *B. thailandensis* E555 RFP infected cells to be analysed by imaging flow cytometry were harvested intact into 4% paraformaldehyde (Alfa Aesar). RAW cells were harvested into 4% paraformaldehyde by pipetting up and down. Imaging flow cytometry was performed on the Amnis® ImageStream® X Mark II. The gating template previously described for RFP and mAb opsonisation experiments was applied to the imaging flow cytometry analysis of AAC experiments. All lasers used were set to full power (200 mW for 561nm laser), and x60 objective was used throughout. RFP excitation (peak of 555nm) was achieved with the 561nm laser and fluorescence emission (peak of 584nm) detected with channel 4. Additional bright field imagery of the RAW cell was applied throughout with channel 1. RAW cells were gated according to being in focus, single cells and containing bacterial GFP fluorescence.

Stars on the AAC represent ciprofloxacin antibiotic, with a DAR of 2.

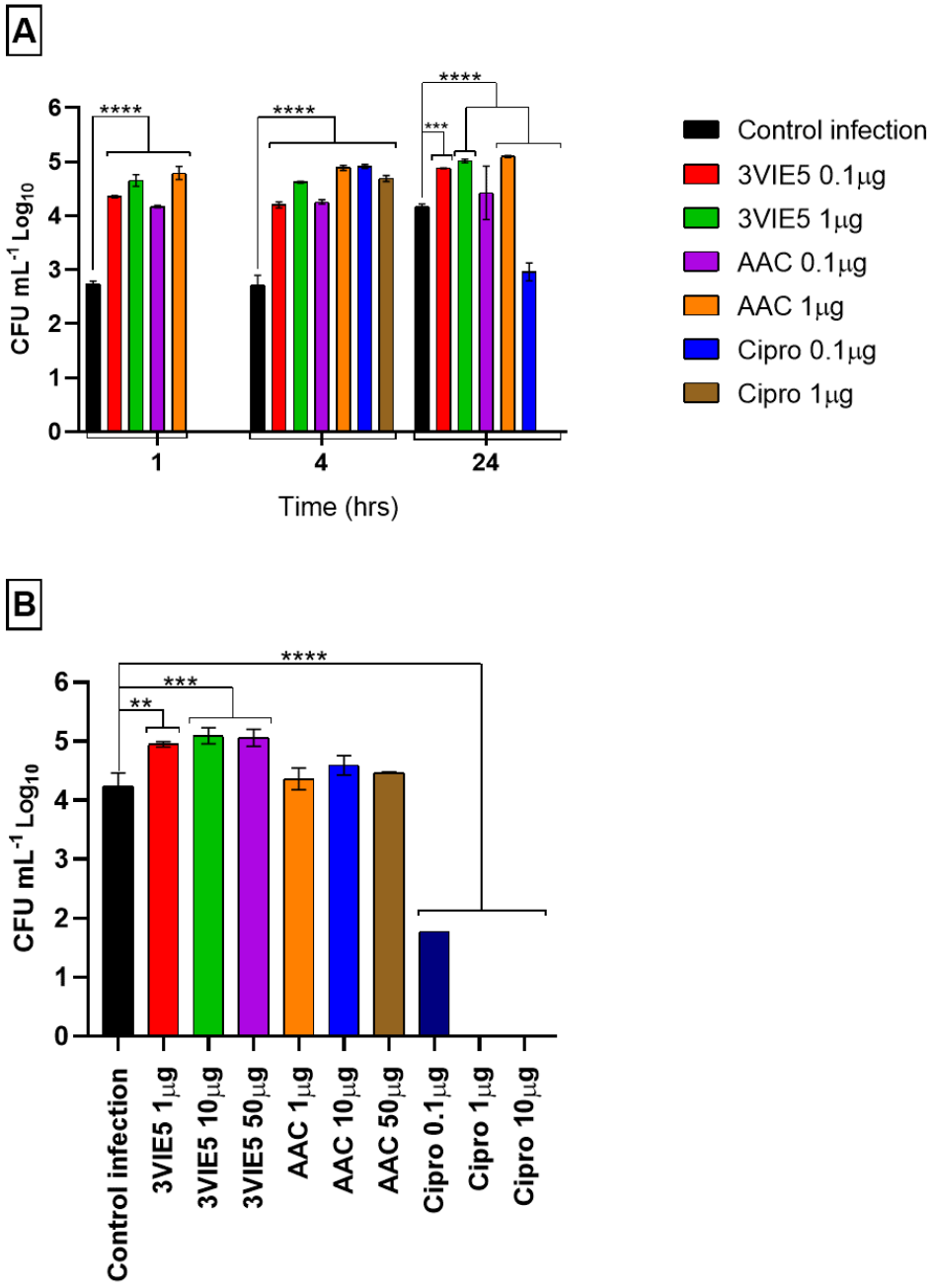

Figure 54. Assessing bacterial killing by the AAC in a RAW cell infection assay.

A RAW cell infection assay was used to assess the ability of the AAC to kill intracellular *B. thailandensis*. RAW cells were infected with AAC or mAb 3VIE5 opsonised *B. thailandensis* E555 at a MOI of 5. Ciprofloxacin was added to the RAW cells post-infection in the kanamycin maintenance media, AAC was also added to the kanamycin maintenance media in post-infection experiments. AAC and ciprofloxacin killing of *B. thailandensis* E555 was assessed by RAW cell lysis and CFU enumeration on L-agar between 1 and 24 hours post-infection. **A.** AAC (Ref -

WR1365 DAR 2) and mAb 3VIE5 were both added pre-infection at 0.1 and 1 µg mL^{-1}. Ciprofloxacin control was added post-infection at 0.1 and 1 µg mL^{-1}. Each data point is the average of two technical replicates from a single experiment (Due to limited AAC product). All concentrations stated are in 1mL of volume. Error bars represent SD. **** P <0.0001, *** P 0.0001. Two way ANOVA Dunnett's multiple comparisons test. **B**. AAC (Ref – WR1365 DAR 2) and mAb 3VIE5 were both added pre-infection and post-infection, intracellular bacteria were enumerated after a 24 hour incubation. Each data point is the average of two technical replicates from a single experiment (Due to limited AAC product). All concentrations stated are in 1mL of volume. Error bars represent SD. **** P <0.0001, *** P 0.0004, ** P 0.0013. One way ANOVA Dunnett's multiple comparisons test.

The one hour time point (Figure 54 A) demonstrates the opsonisation ability of the AAC compared to mAb 3VIE5, both mAb 3VIE5 and AAC increase CFU compared to the control infection. This clearly shows that the AAC is able to opsonise *B. thailandensis,* at a similar level as unconjugated mAb 3VIE5. This result is promising since the action of the AAC relies upon the antibody being functional and opsonising the bacteria, interacting with FcγR's to increase uptake of bacteria coated with AAC. The ciprofloxacin conjugated to the mAb 3VIE5 (at DAR of 2) is not adversely effecting this important function.

This assay was continued for 4 and 24 hours post-infection, to determine any anti-bacterial effects of the AAC (Figure 54 A). At 4 hours post-infection, there is no significant reduction in CFU for the AAC opsonised bacteria, compared to the mAb opsonised bacteria. Ciprofloxacin did not reduce CFU at 4 hours post-infection, ciprofloxacin was added after mAb 3VIE5 opsonisation, but did not kill bacteria at this time point. The ciprofloxacin was added post-infection, and therefore there is a delay while the ciprofloxacin enters the cells, and increases to a level required for intracellular killing of *B. thailandensis*. In this assay, the AAC and mAb were not added post-infection, and therefore any effects are purely from the initial opsonised *B. thailandensis*. At 24 hours post-infection, the anti-bacterial effect of ciprofloxacin can be observed with 1µg of ciprofloxacin clearing bacterial CFU. Interestingly there

is no reduction in CFU with the AAC at 0.1 and 1 µg. Although the AAC was opsonising, there is no killing effect observed in this assay.

The AAC was investigated to determine if there is a reduction in bacterial CFU when the AAC is added both pre and post-infection, and incubated for 24 hours (Figure 54 B). By adding post-infection, in the same method as with the ciprofloxacin control, this will give a greater chance for the AAC to be taken up into the RAW macrophage-like cells. The AAC and mAb concentrations were also increased, to a level that was possible with the quantity of available AAC product supplied from Global Access Diagnostics. The ciprofloxacin controls significantly reduced the CFU, at concentrations below 1µg mL^{-1}. The AAC did not reduce the bacterial CFU compared to the control infection, although the CFU was not significantly higher than the control infection.

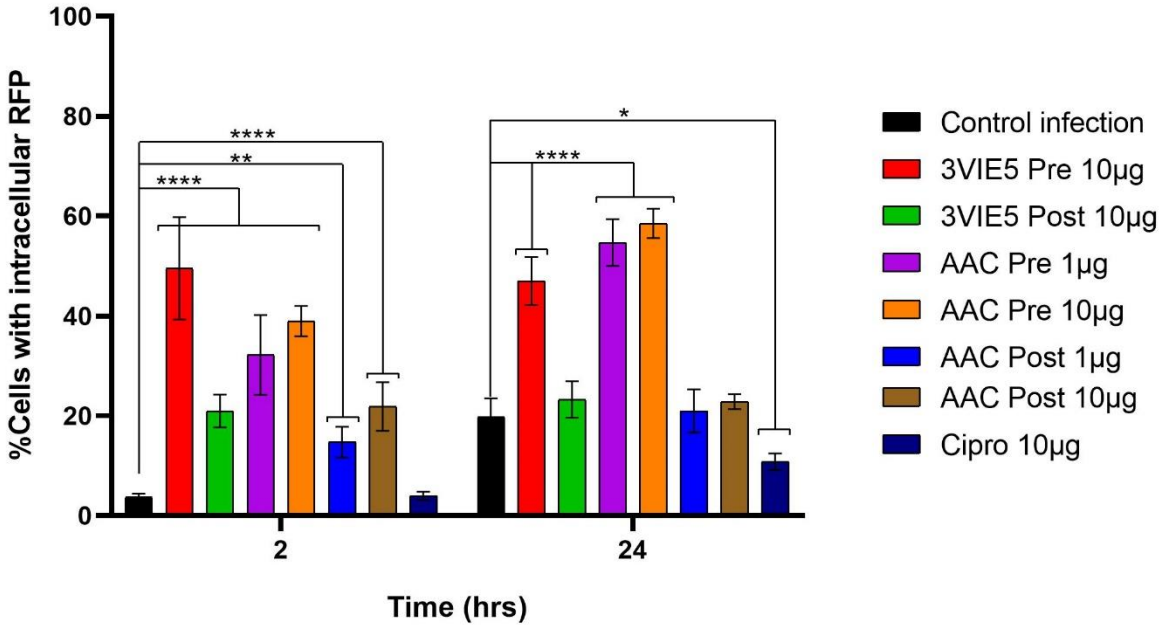

Figure 55. Assessing AAC bacterial killing by Imaging flow cytometry.

A RAW cell infection assay was used to assess the ability of the AAC to kill intracellular *B. thailandensis*. AAC killing of bacteria was assessed by imaging flow cytometry of intracellular *B. thailandensis* RFP (red fluorescent protein). Imaging flow cytometry was performed on the Amnis® ImageStream® X Mark II. The gating template previously described for RFP and mAb opsonisation experiments was applied to the imaging flow cytometry analysis of AAC experiments. All lasers used were set to full power (200 mW for 561nm laser), and x60 objective was used throughout. RFP excitation (peak of 555nm) was achieved with the 561nm laser and fluorescence emission (peak of 584nm) detected with channel 4. AAC (WR1568 DAR 2) was added to a RAW cell infection assay at 1 and 10µg mL^{-1}, both pre-infection and post-infection. A minimum of 7800 cells were assessed per sample. Data consists of the mean of technical replicates (n=4) derived from two biological experiments. **** P <0.0001, ** P 0.0089, * P 0.0465 Two Way ANOVA Sidak's multiple comparisons test to control infection. Error bars represent SD of all technical replicates.

Imaging flow cytometry confirms that the AAC is opsonising, as seen by a significant increase in the percentage of cells infected in the pre-infection groups, compared to

the control infection (Figure 55). AAC added post-infection did significantly increase the percentage of cells infected at 2 hours, displaying some opsonisation effect on the bacteria. No significant killing effect was seen with the AAC at 24 hours in this assay. The ciprofloxacin control did significantly reduce the percentage of cells infected at 24 hours.

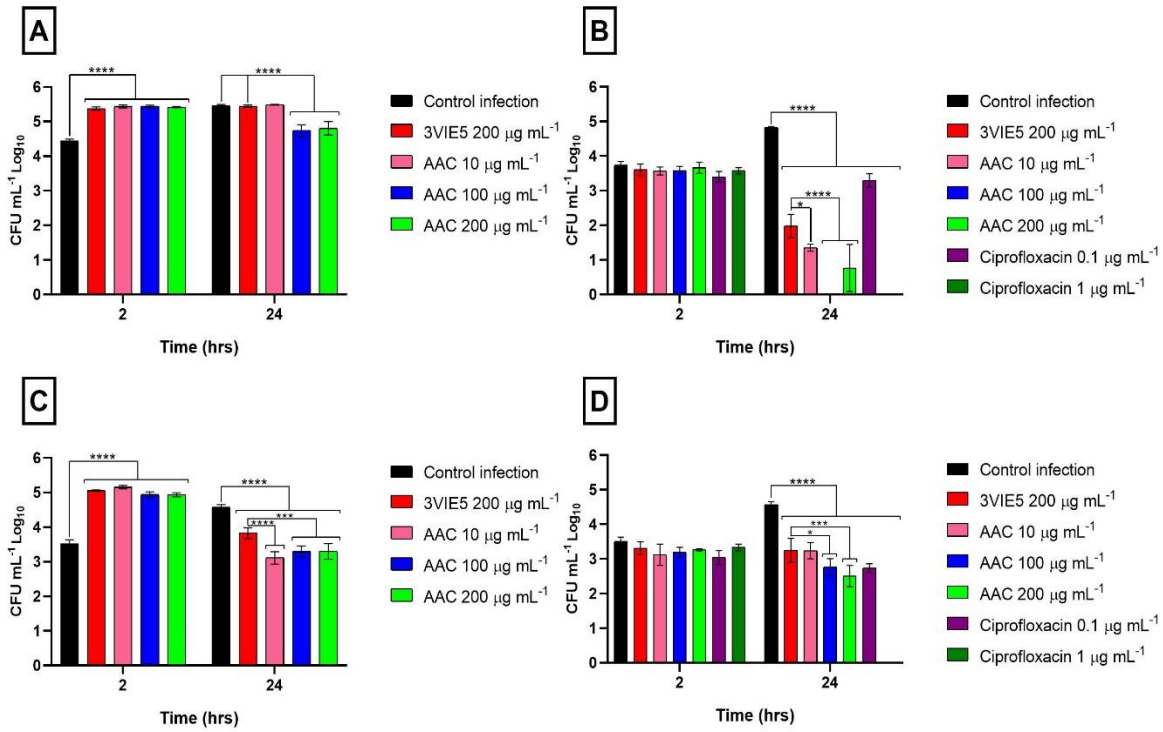

Figure 56. Testing increased concentrations of AAC pre and post-infection by CFU analysis.

A RAW cell infection assay was used to assess the ability of the AAC to kill intracellular *B. thailandensis* E555. RAW cells were infected with AAC or mAb 3VIE5 opsonised *B. thailandensis* E555 at a MOI of 5. Ciprofloxacin was added to the RAW cells post-infection in the kanamycin maintenance media, AAC was also added to the kanamycin maintenance media in post-infection experiments. AAC and ciprofloxacin killing of *B. thailandensis* E555 was assessed by RAW cell lysis and CFU enumeration on L-agar between 1 and 24 hours post-infection. Control infection consists of non-opsonised *B. thailandensis* infection of RAW cells. **A** - AAC opsonised *B. thailandensis* pre-infection (AAC ref – WR1568 DAR 2), **B** - AAC added post-infection (AAC WR1568 DAR 2). **C** - AAC opsonised *B. thailandensis* pre-infection (AAC WR1691 DAR 2.9), **D** - AAC added post-infection (AAC WR1691 DAR 2.9). Each data point is the mean of technical replicates (n=3) with each graph representing a biological experiment. Biological experiments were repeated with separate batches of AAC (Due to availability of product for each AAC batch). Error bars represent SD. **** P <0.0001, *** P 0.0005, * P 0.01 (B) * P 0.02 (D), Two Way ANOVA Dunnett's multiple comparisons test.

Concentrations of AAC were increased further, to determine killing ability pre and post-infection by CFU analysis (Figure 56). The AAC is opsonising the bacteria when added pre-infection, this is seen as a significant increase in CFU at 2 hours (Figure 56 A and C). At 24 hours, there is a significant reduction in bacterial CFU for AAC treated cells, when compared to the control infection and mAb 3VIE5 control. The reduction in bacterial CFU is enhanced when the AAC is added to the cells as a post-infection therapy (Figure 56 B and D). Especially from 100 µg mL^{-1} of AAC, where a significant bacterial killing effect at 24 hours post-infection is observed. The high concentration of mAb 3VIE5 also significantly reduced bacterial CFU, when compared to the infection control at 24 hours post-infection (Figure 56 B and D), although the AAC reduced the bacterial CFU to a greater extent. The ciprofloxacin control significantly reduced bacterial CFU at 24 hours post-infection, with complete clearance seen at a concentration of 1 µg mL^{-1}.

6.4 Pharmacokinetics of mAb 3VIE5.

The pharmacokinetic (PK) properties are important to understand when designing a therapeutic mAb. The aim of this initial PK experiment is to determine how the mAb 3VIE5 behaves in a murine system. This data will inform future studies, such as *B. pseudomallei* protection studies, and PK studies involving mAb 3VIE5 as part of an antibody-antibiotic conjugate (AAC) in mice.

6.4.1 ELISA development.

The aim of this experiment was to design an ELISA to detect mAb 3VIE5, with the ultimate aim to detect mAb 3VIE5 in sera samples from an *in vivo* PK study. An ELISA was developed by testing a range of heat killed *B. thailandensis* E555 concentrations bound to a 96 well ELISA plate (2.9.1 ELISA.). An overnight culture of *B. thailandensis* E555 was enumerated and heat inactivated (80°C for 4 hours), for use in this ELISA. MAb 3VIE5 was diluted across the plate, in order to determine the lower limit of quantification (LLOQ) of the ELISA. The LLOQ data for mAb 3VIE5 binding to $1x10^7$ cfu ml^{-1} of *B. thailandensis* E555 was used as a calculation for the concentration of mAb to deliver to mice, for a mAb 3VIE5 PK study. Murine control sera (Sigma) was used as a control, to determine the dilution required to eliminate

any background sera cross reactivity to *B. thailandensis* E555. It was established that a dilution of 1:9 or greater, was required to eliminate sera cross reactivity in this ELISA.

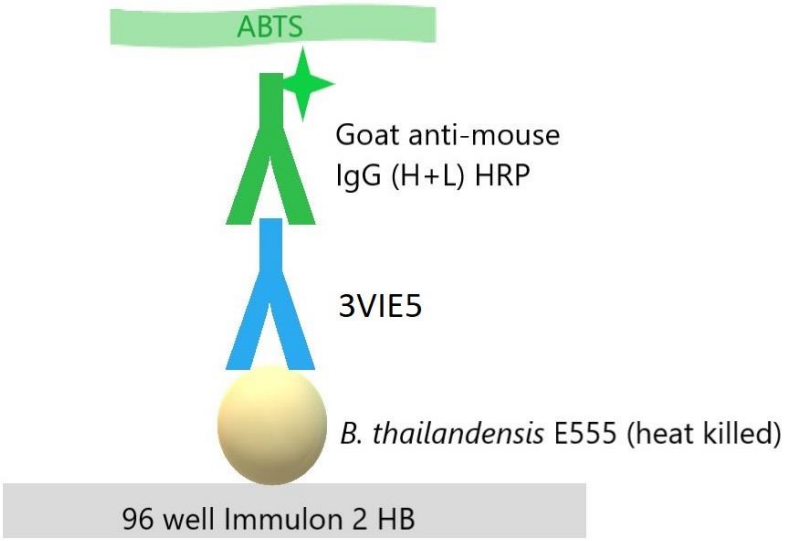

Figure 57. ELISA detection of mAb 3VIE5 in sera.

The detection of mAb 3VIE5 in sera was achieved by designing an immobilised antigen ELISA. *B. thailandensis* E555 was heat killed for use as the immobilised antigen in the ELISA. ELISA microtitre plates (96 well Immulon 2 HB) were coated with heat inactivated *B. thailandensis* E555 at a range of concentrations (1_{x10}^{5} to 1_{x10}^{8} cfu mL^{-1}) in 100 µL of 0.05M carbonate-bicarbonate buffer pH 9.6 (Sigma). Plates were blocked with 200µL of casein blocking buffer (Sigma) prior to addition of mAb 3VIE5 or sera containing mAb 3VIE5. A secondary goat anti-mouse HRP antibody was used at a 1 in 3000 dilution to detect mAb 3VIE5 bound to the immobilised antigen. A plate reader (Multiskan FC, Thermo) at 414nm was used to measure the absorption values following the addition of ABTS ((2,2′-azino-di-(3-ethylbenzthiazoline sulfonic acid)) to the ELISA.

Calibration curves in plasma used 11 points between 170 pg mL^{-1} and 10 µg mL^{-1}, the LLOQ of the ELISA (mean background + 10SD) was calculated as 15.8 ng ml^{-1}.

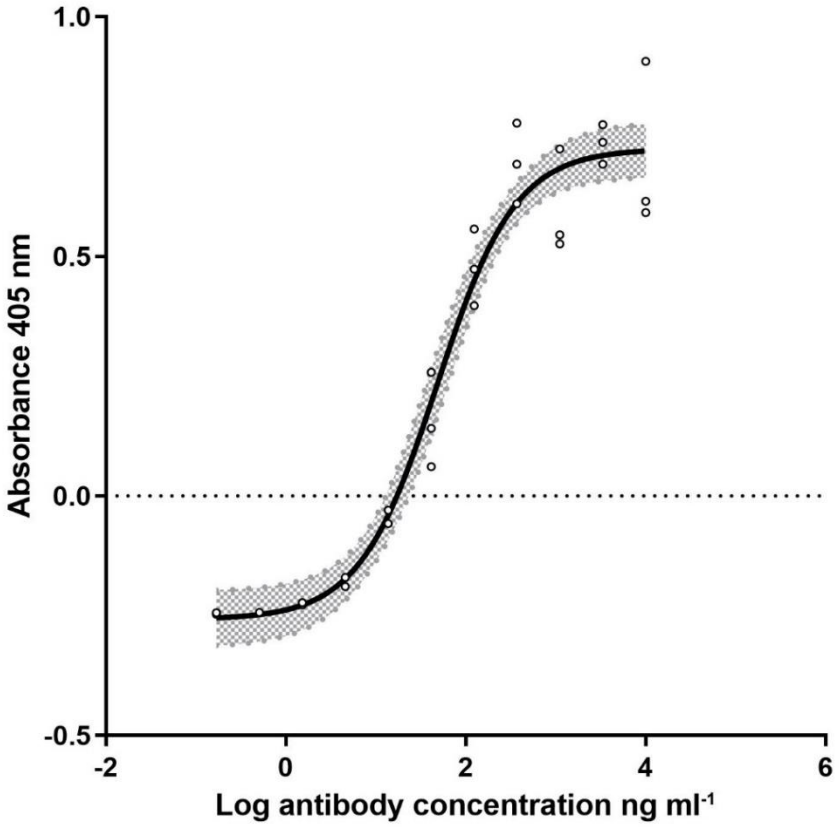

log(agonist) vs. response (three parameters)	
Best-fit values	
Bottom	-0.2579
Top	0.7245
LogEC50	1.684
EC50	48.27
Span	0.9824
Std. Error	
Bottom	0.02860
Top	0.02781
LogEC50	0.07917
Span	0.03729
95% CI (asymptotic)	
Bottom	-0.3166 to -0.1992
Top	0.6674 to 0.7816
LogEC50	1.521 to 1.846
EC50	33.20 to 70.16
Span	0.9058 to 1.059
Goodness of Fit	
Degrees of Freedom	27
R squared	0.9626
Sum of Squares	0.1886
Sy.x	0.08357
Number of points	
# of X values	33

Figure 58. MAb 3VIE5 ELISA LLOQ.

A dilution of mAb 3VIE5 in the ELISA was used to generate a curve, to enable interpolation of murine sera samples of mAb 3VIE5 for PK analysis. The ELISA LLOQ was calculated as the mean background + 10SD (15.8 ng mL^{-1}). The generated curve has been corrected for the ELISA LLOQ, and the 95% confidence interval is highlighted in grey. Replicates were performed in triplicate and are displayed as individual points on the graph.

6.4.2 Pharmacokinetic analysis of mAb 3VIE5 in BALB/c mice.

The aim of this murine *in vivo* study was to investigate the PK properties of mAb 3VIE5. A group of 15 BALB/c mice (weight of 19 ± 0.97 g (mean ± standard deviation)) were injected with mAb 3VIE5 (2.9.2. Pharmacokinetics of mAbs *in vivo.*), at 5 mg kg^{-1} in a 50µL volume by IV injection (performed by Dstl experimental animal house staff). At the specified time points, 3 mice were removed for terminal anaesthesia and cardiac puncture (performed by Dstl experimental animal house staff). Time points for cardiac bleeds were 1, 4, 12, 15 and 18 days post mAb injection. The mAb 3VIE5 dosage and study plan time points were chosen based on ELISA LLOQ data and PK estimations (appendix A.6.2), based on an antibody half-life of 120 hours (353) and volume of 72 mL kg^{-1} (354).

Table 5. PK experimental study plan.

Day	**Procedure**
0	15 BALB/c mice dosed IV with 5 mg kg^{-1} mAb 3VIE5
1	3 BALB/c TA and CP
4	3 BALB/c TA and CP
12	3 BALB/c TA and CP
15	3 BALB/c TA and CP
18	3 BALB/c TA and CP

A group of 15 BALB/c mice received an IV dose of mAb 3VIE5. At between 1 and 18 days a group of 3 mice were culled, and cardiac punctures performed to provide sera for detection of mAb 3VIE5 by ELISA. IV – Intravenous, TA – Terminal anaesthesia, CP – Cardiac puncture

Table 6. Descriptive statistics of mAb 3VIE5 plasma concentrations.

Time (hours)	**N**	**Mean** (µg mL^{-1})	**Minimum** (µg mL^{-1})	**Median** (µg mL^{-1})	**Maximum** (µg mL^{-1})	**Geometric mean** (µg mL^{-1})
24	3	46.1	31	40.4	67	43.8
96	3	35.8	26.7	35.7	44.9	34.9
192	3	7	5.3	5.9	9.9	6.7
360	3	2.8	1.9	2.9	3.4	2.7
432	3	1.7	1.5	1.7	2	1.7

Concentrations of mAb 3VIE5 measured in BALB/c mouse plasma following intravenous administration of mAb 3VIE5. Triplicate groups of mice were culled at each time point and the blood sera harvested from each mouse. Concentrations of mAb 3VIE5 in the murine sera were determined by the *B. thailandensis* E555 immobilised antigen ELISA previously described.

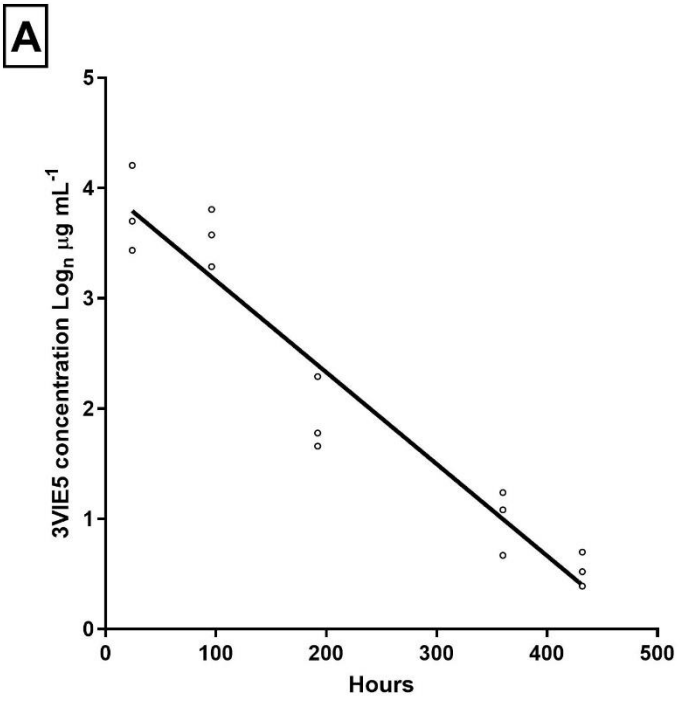

Line	
Best-fit values	
YIntercept	3.991
Slope	-0.008319
Std. Error	
YIntercept	0.1787
Slope	0.0006634
95% CI (asymptotic)	
YIntercept	3.605 to 4.378
Slope	-0.009752 to -0.006886
Goodness of Fit	
Degrees of Freedom	13
R squared	0.9236
Sum of Squares	2.044
Sy.x	0.3966
Number of points	
# of X values	15

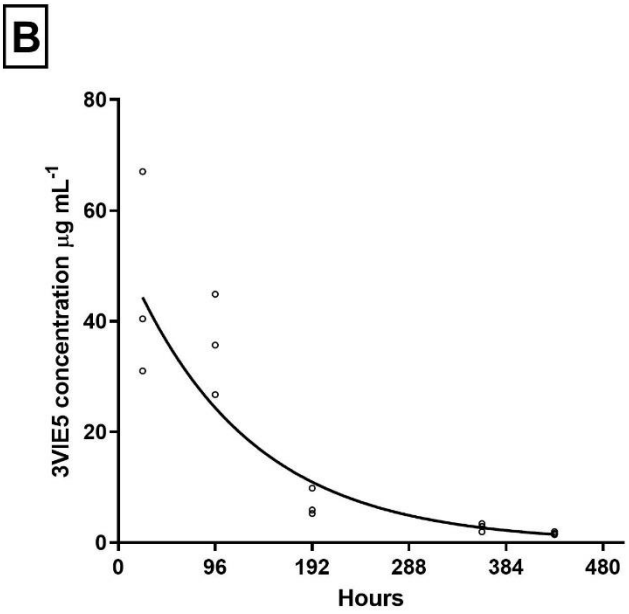

Baseline	0
Total Area	5987
Std. Error	900.9
95% Confidence Interval	4221 to 7752
Total Peak Area	5987
Std. Error	900.9
95% Confidence Interval	4221 to 7752
Number of Peaks	1

Figure 59. Pharmacokinetic analysis of mAb 3VIE5 in BALB/c mice.

The concentrations of mAb 3VIE5 in murine sera at specific time points were determined by ELISA. Data are plotted as both a line graph with log$_n$ of 3VIE5 concentrations (**A**) and a curve of 3VIE5 concentrations (**B**). The PK parameters of mAb 3VIE5 calculated from the figure parameters.

Table 7. Pharmacokinetic analysis of mAb 3VIE5 mAb in BALB/c mice.

PK parameter	
Dose	5 mg kg^{-1} mAb 3VIE5
C0	54.1 µg mL^{-1}
V	92.4 mL kg^{-1}
T½	83.5 h
AUC	5987 µg hr mL^{-1}
C	0.83 mL hr kg^{-1}

A summary of the details of the pharmacokinetic analysis of mAb 3VIE5. C0 – maximum concentration of mAb, V – Volume of distribution, T½ - Half-life of mAb, AUC – Area under curve, C – clearance of mAb

The standard curve, generated from the mAb 3VIE5 ELISA, was used to interpolate sera sample concentrations of mAb 3VIE5 at each sample time point. From this data, the pharmacokinetic properties of mAb 3VIE5 were determined.

The PK properties of mAb 3VIE5 were calculated based on the equation $c=C0.e^{-k.t}$, where c is concentration of the mAb 3VIE5. Using this equation the concentration of mAb 3VIE5 at any time point in the murine sera can be calculated. The value for C0 (Y intercept) (Figure 59) was determined to be 54.1 µg mL^{-1} (log_n 3.991), k is the slope of the line 0.0083 1/h (Figure 59), and t represents time (hours).

The volume (V) that the mAb 3VIE5 is dosed into is determined by the equation V = dose (5000 µg kg^{-1}) / C0. This calculated to a volume of 92.4 mL kg^{-1} for the BALB/c mouse in this experiment.

The half-life ($T\frac{1}{2}$) of mAb 3VIE5 was calculated using the equation $T\frac{1}{2}$ = Ln (2) / k, which calculated as 83.5 hours.

Clearance (C) of the mAb 3VIE5 was calculated based on the equation C = dose / area under curve (5987 µg hr mL^{-1}) (Figure 59), which calculates to a mAb 3VIE5 clearance of 0.83 mL hr kg^{-1}.

This study data has successfully determined the pharmacokinetics of mAb 3VIE5 in BALB/c mice. It has been calculated that mAb 3VIE5 has a half-life of 3.5 days (83.5 hours) and a clearance rate of 0.83 mL hr kg^{-1}.

6.5. Discussion.

In this chapter, a proof of principle AAC has been generated and tested against *B. thailandensis in vitro*.

Cathepsin cleavage of the AAC MC-Val-Cit-PAB linker, releases antibiotic with a stub attached. This stub is part of the linker remaining with the antibiotic post cleavage. An initial concern was that this stub would impact the efficacy of ciprofloxacin and finafloxacin in an AAC. Global Access Diagnostics created antibiotic-stub molecules to represent the antibiotics post AAC cathepsin cleavage. These antibiotic stubs were analysed by bacterial replication curve experiments, to determine any impacts on efficacy compared to native antibiotics. The result of the antibiotic MIC experiments was that the stub did not have an impact on the efficacy of ciprofloxacin. It is likely that solubility issues with the finafloxacin stub samples resulted in the higher MIC. Although still functional, the finafloxacin stub MIC was not at the same level as the control.

Once it was established that the antibiotic stub was active, the next step was to determine if the antibiotic bound to the MC-Val-Cit-PAB linker can be released by cathepsin B cleavage. Cathepsin B from bovine spleen was selected, based on a previous AAC publication using this method to cleave cathepsin cleavable linkers (165). Linker and antibiotic preparations initially showed no difference in activity between intact and cathepsin cleaved samples. It was expected that cathepsin cleavage of the linker would release the antibiotic in an active form. In the linker finafloxacin samples, there was no evidence of finafloxacin antibacterial activity in cathepsin cleaved samples. The ciprofloxacin preparations did show some activity, but no differences could be determined between intact and cleaved samples. For this reason, together with solubility issues with finafloxacin preparations, it was decided to focus on development of a ciprofloxacin AAC in this project. The activity of

cathepsin B from bovine spleen was assessed with a colorimetric Z-RR-pNA substrate. This experiment confirmed that the cathepsin B was active *in vitro,* therefore enzymatically functional and able to cleave an intact AAC molecule with a MC-Val-Cit-PAB linker.

Cathepsin B is a 30 kDa bilobal protein, an endopeptidase and protease responsible for protein degradation within lysosomes (355). There are various classes of the cathepsin proteases in the human body, and present in the majority of tissues. High levels of cathepsin enzymes are expressed in macrophages (356), the RAW 264.7 macrophage-like cell possess a variety of cathepsin enzymes for cleavage of Val-Cit linkers (357). Although the AAC generated in this project is cathepsin B cleavable, there are likely to be other cathepsin proteases present in lysosomes that can contribute to cleavage of the Val-Cit linker. In a study by Caculitan *et al*, cathepsin B knockout cells were used to demonstrate that other cathepsin enzymes (K, L and S) can compensate for the loss of cathepsin B (357). Cathepsin S in particular was shown to have a similar level of activity compared to cathepsin B in cleaving a Val-Cit linker (357). The PAB spacer is an important part of the linker, this allows access of cathepsin to the cleavage site (358), without the PAB spacer the cathepsin cleavage site is not accessible and therefore the linker cannot be cleaved. Cathepsins are not restricted to the low pH environment of the lysosome, it is now known that cathepsin has diverse roles outside of the lysosome and is implicated in a variety of diseases (359, 360). Extracellular cathepsin is mostly associated with disease states, such as cancers and inflammation (360). Release of antibiotic at extracellular sites of inflammation would reduce the AAC available for intracellular delivery. Although, if the inflammation is at a site of infection, then release of antibiotic at this site by the AAC would be beneficial.

In this chapter, mAb 3VIE5 has been successfully conjugated to ciprofloxacin, via a cathepsin cleavable linker by an amine to amine conjugation method (Global Access Diagnostics). A lysine on the antibody displays a maleimide group via treatment with SMCC (succinimidyl 4-(N-maleimidomethyl) cyclohexane-1-carboxylate), the linker amine is treated with traut's reagent (2-Iminothiolane) to display a thiol group, allowing conjugation to the maleimide group of the antibody. The DAR varies

between batches, this is due to the lysine conjugation method which results in the AAC product being heterogeneous. The DAR varied between 2 and 3 based on mass spectrometry data (Global Access Diagnostics).

Ideally an ADC should be a homogenous preparation, although this is not always essential for a therapeutic. Brentuximab vedotin and adotrastuzumab emtansine are both FDA approved heterogeneous ADC's, generated by cysteine and lysine conjugation methods respectively (163, 164, 361). Traditional heterogeneous ADC conjugation techniques are achieved by conjugation to lysines and hinge cysteines (362). Conjugation by reduction of hinge cysteines will produce a more homogenous population of ADCs compared to lysines, this is due to the number of available binding sites on the antibody producing a lower DAR (362). Conjugation to reduced cysteines can yield a potential homogeneous DAR of 8 with full reduction, or a heterogeneous DAR of between 0 and 8 with partial reduction (361, 363). In contrast, conjugation to lysine residues can be to any of up to 40 different lysine sites, with a typical heterogeneous DAR of between 0 and 8 (361, 363). The potential problem with heterogeneous ADCs, is that each ADC will have individual PK and drug release properties. To overcome this, antibodies can be engineered to contain cysteines available for conjugation, resulting in a more homogenous approach. This was achieved by the THIOMAB™ approach used by Genentech in the development of an AAC for *S. aureus* (165). The resulting homogeneous ADC is well tolerated and stable, with a long half-life in circulation (166).

Lehar *et al* (165) used dithiothreitol (DTT) treatment of the antibody to engineer cysteines for conjugation via reduction of interchain disulfides, a typical IgG antibody contains 8 interchain cysteines (338). When designing the AAC it is important to consider DAR, as high incorporation ratios could interfere with antibody functionality, and potentially adversely affect the PK of the ADC by reducing half-life in circulation (361). In the Lehar *et al* study (165) an incorporation ratio of 1.9 was achieved, it is thought that a ratio of 2 to 4 is optimum for an AAC (338). The choice of linker chemistry is crucial and can have major effects on the antibody function, it is important to protect the antibody Fab and Fc region, for antigen binding and Fc receptor interactions.

Techniques other than cysteine and lysine conjugation exist that can generate a homogeneous ADC product. These include, site directed mutagenesis to incorporate additional cysteine conjugation sites, glycol-conjugation, unnatural amino acid incorporation, and the use of peptide tags (361-363). Not all ADC's have protease cleavable linkers, FDA approved adotrastuzumab emtansine functions via a non-cleavable linker, requiring lysosomal degradation of the conjugate to release the active drug (164, 361). In this project, a proof of concept AAC has been developed. Future projects should investigate alternative linker chemistry and conjugation sites, enhancing this initial proof of concept AAC for melioidosis.

The mAb 3VIE5 was incorporated into the proof of concept AAC. Antibody selection is crucial for an ADC, the antibody should ideally be humanised to limit anti-species reactivity in the host. It is also essential for the antibody to be specific for the bacterial target, to limit off site effects in the host. There is potential to increase the half-life of conjugated drugs, by selecting an antibody with favourable PK properties. Data from a recently published *S. aureus* AAC (165), showed that binding antibiotic to the antibody increased half-life of the antibiotic from 3-4 hours to 4 days (364). Therefore the PK properties of ciprofloxacin are likely to be improved when conjugated to mAb 3VIE5.

Initially, the AAC was tested in the RAW cell infection assay at lower concentrations of 0.1 μg mL^{-1} and 1 μg mL^{-1}, resulting in no bacterial killing by CFU analysis. The concentrations were subsequently increased, and analysed by both CFU and imaging flow cytometry. It was clear that the AAC opsonised the bacteria at all concentrations tested, the AAC increased intracellular CFU and the percentage of cells infected. Once the AAC was tested by CFU analysis at higher concentrations, then bacterial killing was observed. This was especially evident when the AAC was added post-infection, although some bacterial killing could be seen in pre-infection groups at 24 hours. Greater concentrations of AAC are required to achieve killing, due to the low concentration of ciprofloxacin per AAC molecule. Increasing the DAR should therefore reduce the concentration of AAC required to observe bacterial killing *in vitro*. The data in this research project is encouraging and demonstrates that the AAC concept has potential for a melioidosis therapy. Although the *in vitro* data does

not demonstrate killing to the same extent of the ciprofloxacin control, there are advantages of the AAC approach. One such advantage is that *in vivo* the antibiotic on the AAC will be targeted to the intracellular site of infection, this has the potential to reduce the antibiotic required to treat the infection successfully. The AAC approach also has the potential to accumulate antibiotic in the intracellular environment. The higher the DAR of the AAC, the more antibiotic can be delivered to the site of infection. The *in vitro* data generated here has demonstrated that the AAC can deliver antibiotic to the intracellular environment, and kill intracellular *B. thailandensis*. Further enhancements are required to the AAC, such as increasing antibiotic loading to increase antibiotic delivery *in vitro*.

It is difficult to directly compare the actions of the ADC with the free ciprofloxacin control. The ADC functions in a targeted method and contains a lower quantity of ciprofloxacin antibiotic, approximately 0.44% (DAR of 2). The AAC in theory can target the delivery of ciprofloxacin, and therefore a much lower concentration of ciprofloxacin should show a killing response. Stimulating the RAW cells with IFN-γ could be a method to increase cathepsin activity within the cell, and then the anti-bacterial effect of ADC may be observed at lower concentrations. The cathepsin activity could be monitored with the use of fluorescent labels, with and without IFN-γ stimulation, to determine if the enzymatic activity is present to efficiently cleave the ADC. To improve the efficacy of AAC's at lower concentrations, the DAR of the AAC can be increased to deliver a much higher payload of ciprofloxacin to the intracellular environment. This is one of the major improvements that should be made to future AAC development projects, although care must be taken not to adversely affect the functionality of the antibody.

Analysis of the AAC in RAW cells represents an initial evaluation, prior to testing the AAC *in vivo*. Differences in AAC efficacy may be observed when the AAC is evaluated in future *in vivo* studies. Ideally, the AAC would be tested in primary macrophage cells to better represent *in vivo* conditions. The Genentech *S. aureus* AAC (DSTA4637A) showed good translation between efficacy *in vitro* and *in vivo*. The AAC was tested in a variety of primary and cultured cell lines, the AAC demonstrated potent killing of *S. aureus* in all cells tested (165). The *S. aureus* AAC

displayed efficacy *in vivo*, with a single dose of AAC given 24 hours post-infection more effective than an equivalent dose of antibiotic. The cleavability of the *S. aureus* AAC was essential for efficacy both *in vitro* and *in vivo*, with a non-cleavable version of the AAC exhibiting no efficacy (165).

When the AAC is tested *in vivo,* the AAC will come into contact with all the immune cells and the associated cytokines, compared to *in vitro* where the AAC is tested on a cultured layer of RAW macrophage-like cells. Neutrophils are the largest population of immune cells present in human blood, these short lived cells are produced in the bone marrow (365). Neutrophils are the predominant cells that are associated with *B. pseudomallei* in murine lung infection studies (366). *B. pseudomallei* aerosol challenge studies *in vivo* have shown that the neutrophil response is crucial to survival, especially during the early stage *B. pseudomallei* infection (367). Neutrophils play an important role in engulfing *B. pseudomallei,* and release of pro-inflammatory cytokines (367). The immune cells cytokine response is crucial for controlling infection, the role of IFN-γ has been characterised and known to be essential for control of *B. pseudomallei* infection, determining if the infection is acute and lethal, or a chronic infection (368, 369). Stimulation of the J774 macrophage-like cell line by IFN-γ has shown to increase the cells ability to kill intracellular *B. pseudomallei* (370), further demonstrating the importance of the IFN-γ response in control of infection. Neutrophil elastase, a protease secreted from neutrophils, has shown to increase expression of cathepsin B in macrophages (371). IFN-γ also increases cathepsin B expression in macrophages (372). This activation by neutrophils would be of benefit to the cleavage of the AAC within infected macrophages, likely increasing the efficacy of the AAC *in vivo*. The AAC is likely to opsonise and increase uptake into neutrophils, in addition to macrophages. Neutrophils contain proteases, including cathepsin G (365), that possibly will cleave the AAC releasing antibiotic to kill intracellular bacteria. Neutrophils also release proteases, including cathepsin G (365), which could potentially cleave the AAC at sites of inflammation, allowing extracellular antibiotic release at these sites of infection.

Once the infection spreads to tissues, resident macrophages will engulf the AAC coated *B. pseudomallei*, delivering antibiotic to the intracellular environment. This is a benefit, reducing the latent infection in the long lived macrophage cells within

tissues. There is a balance to be made between increasing uptake of bacteria into cells and the bacterial killing. A certain level of antibiotic is required to kill the bacteria, without this there is a risk an AAC could assist uptake of bacteria into the intracellular environment and promote infection. This is a reason why DAR is important for an AAC, since an AAC with a high DAR will deliver more antibiotic per antibody to the intracellular environment.

We have determined the PK properties of the mAb 3VIE5, and this data will inform future *in vivo* studies with this mAb. Although, a PK study of the full AAC is required to know exactly how the AAC behaves *in vivo*. The antibody conjugate therapy for melioidosis will likely follow a similar path as the *S. aureus* PK studies, with PK studies with the full AAC in mice prior to larger animal studies. In this project, an initial PK study has been completed with mAb 3VIE5 in BALB/c mice. Properties such as half-life and clearance of 3VIE5 have been determined, the data shows that 3VIE5 has a half-life of 3.5 days (83.5 hours) in BLAB/c mice. A typical IgG2b monoclonal antibody in mice has a half-life of approximately 5 days (120 hours) (353). IgG has the potential for an elimination half-life of up to 21 days (169), depending upon antibody isotype and target binding. As a comparison, an engineered antibody recently incorporated into a *S. aureus* AAC therapeutic (165) displayed a half-life of approximately 16 days and 5 days, for non-infected and infected mice respectively (166). A clearance rate for 3VIE5 was determined to be 0.83 mL hr kg^{-1}. In comparison the clearance rate for the *S. aureus* AAC antibody ranged from 5 to 15 ml day kg^{-1}, for non-infected and infected mice respectively (166). The data generated here will inform future studies such as *in vivo* murine mAb protection studies, to determine the therapeutic potential of the mAb given to mice infected with *B. pseudomallei*. The PK data such as mAb clearance, will also be used to determine the effects of antibiotic conjugation on the mAb.

The classic PK properties of an IgG mAb following administration include an initial rapid distribution phase, followed by long slow elimination phase over weeks (168). Binding of mAb to the neonatal receptor (FcRn) is beneficial in terms of mAb recycling, resulting in the characteristic long half-life of mAbs in PK studies. The FcRn can protect two thirds of the mAb taken up into acidic endosomes in the cell, by

binding mAb at low pH and releasing mAb extracellularly when the pH raises back to physiological levels (169, 170). The distribution of mAbs is generally restricted to the blood, with a typical 5-15% distribution to tissues (168). Clearance of mAb from the blood is generally by cell uptake and proteolytic degradation, although in some cases anti-therapeutic antibodies can target the mAb depending upon the mAb characteristics such as species (168). It has been suggested that a homogeneous low antibiotic coupling ratio should not have a negative effect on the PK of the mAb (349). High DAR of an AAC could have negative effects on the PK of the AAC, high antibiotic loading could lead to immune stimulation, resulting in toxicity and higher clearance rates (373). Differences in linker chemistry and DAR could affect the PK of the mAb 3VIE5, and therefore the AAC therapy, further PK studies are essential once a finalised heterogeneous AAC product has been generated.

Here we have shown that there is potential in the development of an AAC for melioidosis. A ciprofloxacin AAC has been developed, in collaboration with Global Access Diagnostics. The AAC has demonstrated efficacy against *B. thailandensis in vitro,* in both cell infection assays and bacterial MIC assays. The 3VIE5 mAb has been well characterised in this project, and specific PK parameters of the mAb determined. There is scope to engineer and enhance the antibody in future projects, building upon the initial proof of concept AAC generated and tested in this research project. Various options exist for improving PK properties of the antibody, and enhancing antibiotic conjugation to the antibody, all of which should be taken into account for future development of the AAC.

6.6. Appendix.

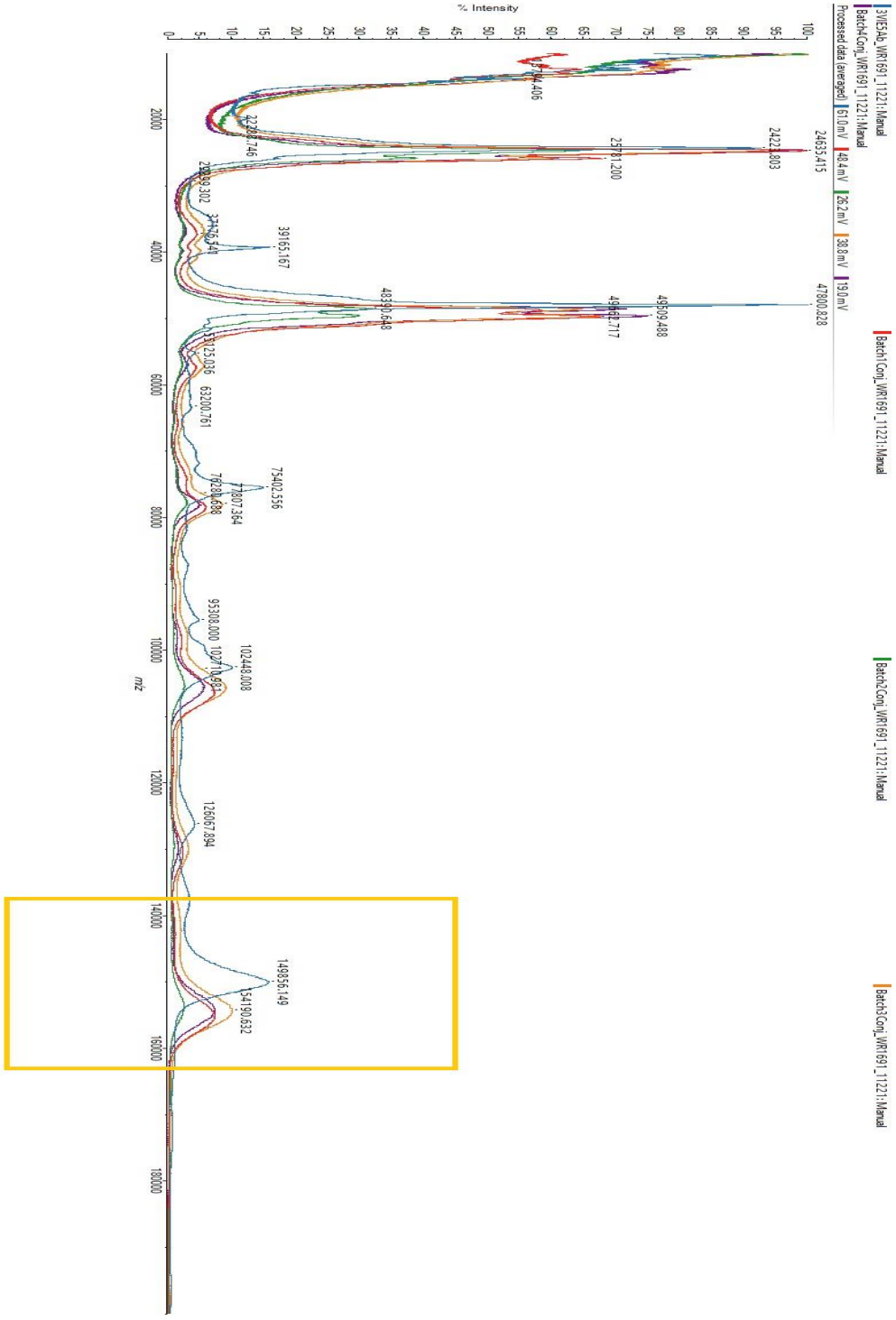

A.6.1. MALDI mass spectrometry trace for AAC batch WR1691, the shift in the peaks highlighted by the gold box indicates conjugation of ciprofloxacin-linker to mAb 3VIE5. Data provided by Global Access Diagnostics.

A.6.2. PK estimations based on ELISA LLOQ data and estimation of antibody half-life. This estimation of PK properties was used to determine the time points used in the murine PK study plan. This PK estimation spreadsheet was generated by S. Armstrong at Dstl. Data was analysed in Microsoft Excel®, Microsoft Office® professional 2016.

7. Conclusions and discussion.

7.1 Summary of results.

Monoclonal antibodies are opsonising in a RAW macrophage-like cell infection assay. The anti-capsule mAb 3VIE5, significantly reduces *B. thailandensis* actin tail formation *in vitro*.

In this research project, a panel of monoclonal antibodies were analysed for opsonisation of *B. thailandensis* and *B. pseudomallei* in a RAW cell infection assay. Data was generated from CFU enumeration and imaging flow cytometry. Imaging flow cytometry is a technique that combines the imaging of microscopy and the high throughput of flow cytometry. This technique has previously been used at Dstl to analyse infection of macrophages by *B. thailandensis* (244), and the uptake of polymersomes by macrophages (240). A sample of cells is processed by a fluidics system and passes through a flow cell, individual cells are exposed to lasers and high definition imaging using cameras. Imaging flow cytometry has the potential to analyse thousands of cells per second, providing a high throughput of single cell analysis. In comparison, CFU analysis analyses the cell population as a whole. Imaging flow cytometry therefore provides a greater level of detail, by analysing cell infection individually. A high level of detail is achievable in the quantification of Intracellular bacteria, details such as the intracellular location of bacteria and bacterial phenotypes, can be assessed using imaging flow cytometry (374). In this study, RAW cells are either fixed in paraformaldehyde or analysed live by imaging flow cytometry. In comparison, RAW cells are lysed prior to analysis by CFU enumeration. This enabled the RAW cell infection to be analysed in greater detail by imaging flow cytometry, providing a percentage of cell infection, together with spot counting of individual fluorescent bacteria. Imaging flow cytometry struggles to distinguish between live and dead fluorescent bacteria, whereas CFU analysis only represents the live culturable bacteria. Therefore, Imaging flow cytometry and CFU analysis together provide an enhanced method to analyse cell infection.

Both CFU and imaging flow cytometry demonstrated that each mAb opsonised *B. thailandensis* and *B. pseudomallei*. Additionally, the anti-CPS mAbs were opsonising

at a lower concentration, when compared to the anti-LPS mAb. The anti-CPS mAb 3VIE5 was selected to take forward for incorporation into an AAC.

The fate of opsonised bacteria was assessed by analysing bacterial actin tail formation and intracellular bacterial killing, following opsonisation with mAb 3VIE5. *B. thailandensis* opsonised with mAb 3VIE5 had a significantly reduced actin tail formation, compared to non-opsonised controls. A significant reduction in bacterial CFU was observed with mAb 3VIE5 opsonised bacteria, compared to the controls. Although, the reduction in bacterial CFU data did not correlate with imaging flow cytometry data. Data indicated there was no significant bacterial association with the lysosomal maker LAMP-1, following mAb 3VIE5 opsonisation. The mAb 3VIE5 however, significantly reduces bacterial actin tail formation, this could be a benefit as a therapeutic. Actin tail formation is required for bacterial intracellular motility, and therefore an important bacterial virulence factor. The mAb 3VIE5 could help prevent spread of the intracellular infection, and have potential synergistic effects with antibiotics as a combination therapy.

Verapamil shows promise for repurposing as an anti-microbial compound.

In parallel to AAC development, a panel of FDA approved compounds were investigated for repurposing as host directed and anti-microbial compounds. This project was an alternative approach, due to the inherent difficulty involved in developing an AAC. This provided an alternative strand of research, in the event of the AAC development proving unsuccessful. The panel of compounds were selected based on previous data in the literature, demonstrating host directed anti-microbial effects against intracellular pathogens such as *M. tuberculosis*. The compounds verapamil, norverapamil, carbamazepine and valproic acid, were all analysed in a *B. thailandensis* RAW cell infection assay. All compounds decreased intracellular bacterial CFU at 24 hours of incubation, with verapamil and norverapamil decreasing bacterial CFU to a greater extent. Verapamil and norverapamil were selected for further investigation, based on the extent of bacterial killing observed in the RAW cell infection assay. The cell is essential to observe bacterial killing, the compounds alone

do not kill *B. thailandensis* without the RAW cell being present. Cytotoxicity data was generated for both compounds at a range of concentrations, with each compound incubated with RAW cells over 24 hours. Verapamil was less cytotoxic to RAW cells than norverapamil, therefore verapamil was taken forward as the primary compound for further investigation. RAW cell infection assays demonstrated that a concentration of 100μM and greater of verapamil, significantly reduced intracellular bacterial CFU at 4 and 24 hours post-infection. Additionally, Imaging flow cytometry data mirrored the CFU data with a concentration of 100μM verapamil or greater, significantly reducing the percentage of cells infected with *B. thailandensis* at 24 hours incubation.

Verapamil is a potential autophagy inducing compound, therefore the role of autophagy in reducing intracellular bacteria was investigated. RAW cells were incubated with concentrations of verapamil, and subsequently stained with LC3 and LAMP-1 specific fluorescent mAbs. A RAW cell infection assay was analysed by imaging flow cytometry, with co-localisation of LC3 and LAMP-1 indicating autolysosomes within the RAW cell. Imaging flow cytometry was used to analyse infected RAW cells for an increase in autolysosome formation, when incubated with or without verapamil dilutions. The data did show a general trend towards an increase in autolysosome formation with an increased verapamil concentration, although this trend in the data was not determined to be significant. This was due to large variations in the autolysosome formation data between experimental replicates, especially at the higher concentrations of verapamil tested.

The role of kanamycin in combination with verapamil was investigated. Removing kanamycin from the culture media did significantly increase bacterial CFU at 24 hours incubation, although it was determined that kanamycin was not solely responsible or required for verapamil to induce bacterial killing. Therefore, the reduction in intracellular CFU observed with verapamil incubation is not dependent on kanamycin being present.

Verapamil shows promise as a therapeutic compound in this study, as a compound that could potentially be repurposed as an anti-microbial for melioidosis. There is significantly more work to be done in determining the mode of action of verapamil. Additional studies are required to determine a concentration that would be anti-microbial *in vivo*, with minimal toxicity, and achievable when administered

therapeutically. The RAW macrophage-like cell infection assay is a tool that can be used to screen other FDA approved compounds, to repurpose as an anti-microbial for melioidosis.

A proof of principle antibody-antibiotic conjugate has been developed for melioidosis.

A proof of principle AAC has been generated in collaboration with Global Access Diagnostics. The AAC consists of mAb 3VIE5 conjugated to ciprofloxacin, via a cathepsin cleavable linker. Initially, ciprofloxacin and finafloxacin were both tested in MIC assays as cleaved antibiotic-stub molecules, this data revealed that both antibiotics are active in their cleaved form. The finafloxacin-stub molecule suffered with suspected precipitation issues, and a reduced MIC compared to the control finafloxacin, therefore ciprofloxacin was selected for generation of the first proof of concept AAC.

A cathepsin cleavage assay was used to test batches of AAC, this involved cathepsin B cleavage of AAC preparations and analysis by MIC assays. Data from MIC and MBC assays proved that the AAC was cleavable by cathepsin B *in vitro*. The AAC displayed no killing activity against *B. thailandensis* in the intact non-cleaved form. Cathepsin B cleavage of the AAC released ciprofloxacin, which then demonstrated antimicrobial activity in MIC and MBC assays.

A RAW cell infection assay was used to assess the ciprofloxacin AAC for ability to reduce intracellular *B. thailandensis*. The AAC demonstrated functionality in the RAW cell infection assay. The AAC was opsonising at 2 hours incubation, with a significant increase in intracellular CFU, compared to the bacterial control. A concentration of AAC from 10 μg mL^{-1} significantly reduced bacterial CFU, at 24 hours incubation. Bacterial killing was observed when the AAC was added both pre and post-infection, with a greater level of killing with the AAC added post-infection. This *in vitro* data provides evidence that the AAC is able to enter the RAW cell, and deliver ciprofloxacin to kill the intracellular *B. thailandensis*.

Pharmacokinetic properties of mAb 3VIE5 have been determined.

The pharmacokinetic properties of mAb 3VIE5 were assessed in BALB/c mice. A group of mice received intravenous mAb 3VIE5, and groups of mice were subsequently culled over a period of 18 days. The sera was collected from each mouse by cardiac puncture and tested by ELISA. An immobilised antigen ELISA was developed in this study to detect mAb 3VIE5 in murine sera. The ELISA data generated was used to determine pharmacokinetics of mAb 3VIE5. A half-life of 83.5 hours was determined for 3VIE5 in BALB/c mice and a clearance rate of 0.83 mL hr kg^{-1}. This data will inform future murine *in vivo* studies involving mAb 3VIE5, including PK assessments of mAb 3VIE5 as an AAC.

7.2 Conclusions.

Monoclonal antibodies recognising the CPS and LPS of *B. pseudomallei*, are opsonising in a RAW macrophage-like cell infection assay. Opsonisation is a criteria that can be used to select an antibody for incorporation into an AAC. Opsonisation can be analysed successfully by both CFU enumeration and imaging flow cytometry, with consistent results across techniques and bacterial strains. A previously unknown effect of mAb opsonisation has been discovered, with an anti-CPS mAb 3VIE5 significantly reducing *B. thailandensis* actin tail formation in the RAW cell. Reducing this important bacterial virulence factor is a benefit for this antibody based therapy, by potentially reducing bacterial spread between cells and therefore intracellular disease progression.

An AAC has the potential to be a future therapeutic for melioidosis. An AAC can specifically target *B. pseudomallei* bacteria, increasing antibiotic delivery to the intracellular environment, therefore killing intracellular *B. pseudomallei* in protected sites of infection. This approach improves the use of antibiotics by targeting delivery to the site of infection, this limits off target effects, which is a benefit from an anti-microbial resistance point of view. The mAb 3VIE5 and the antibiotic ciprofloxacin, have both been successfully incorporated into an AAC. The AAC is able to opsonise *B. thailandensis* and deliver antibiotic to the intracellular site of infection. Within the

intracellular environment, the cathepsin cleavable linker is cleaved, releasing antibiotic in an active form to kill intracellular bacteria. This proof of principle *in vitro* data represents an initial step in the development of an AAC therapy for melioidosis. The AAC concept has proved successful *in vitro*, and leads the way for further developments to enhance the AAC therapy for melioidosis.

The AAC could be administered as an IV post exposure therapy to improve antibiotic therapy for melioidosis patients. This could be in combination with current front line antibiotics, or as a standalone therapy. Most likely is that the AAC will be used in combination with current IV antibiotics, this is due to the AAC antibiotic only being active when cleaved in the intracellular environment. The major benefit of the AAC is the ability to target delivery of antibiotic to the intracellular site of infection, thereby potentially reducing or eliminating latent *B. pseudomallei* infections. If the AAC was used in combination with front line IV antibiotic therapy, then the AAC could be administered with the sole purpose of eliminating the intracellular bacterial infection at protected sites. This could speed up the current prolonged antibiotic therapy that is required to clear the infection, and additionally reduce the risk of treatment failure and relapse in infection.

The AAC has potential to minimise off target cytotoxic effects, therefore reducing the risk from side effects of antibiotics in the patient. ADCs are successfully licenced as cancer therapeutics, whereby highly toxic compounds are conjugated as an ADC to reduce toxic side effects of the therapy. If toxic antibiotics could be conjugated as an AAC and limit cytotoxicity in the patient, then this could increase the antibiotics available for melioidosis therapy. Fluoroquinolones can have rare but significant side effects in some patients, including tendinopathy and neuropathy (375-377). The AAC approach in targeting antibiotic delivery, could help in reducing side effects such as these. Additionally, by including more potentially toxic antibiotics, the AAC approach could increase the available antibiotic options in cases of antibiotic resistance and treatment failure.

There is potential in repurposing current FDA approved compounds as anti-microbial therapies. The RAW cell infection assay has been successfully used as a tool to screen compounds for anti-bacterial activity *in vitro*. This led to verapamil being

assessed *in vitro* and significantly reducing intracellular *B. thailandensis*. Although the mechanism of action of verapamil remains unclear, the reduction in intracellular bacteria by verapamil was consistent between both CFU and imaging flow cytometry experimental techniques. Verapamil shows promise for repurposing as a host directed anti-microbial compound, as observed from the initial screening in the RAW cell infection assay. Before this compound can be considered a therapeutic for melioidosis further analysis is required, to determine both the mechanism of action on the intracellular bacteria and on the cell itself. This project represents a small scale screen of compounds, performed in parallel to development of an AAC therapy for melioidosis. The RAW macrophage-like cell infection assay represents a tool that could be used in future work to screen many more potential anti-microbial compounds, to identify early stage potential in repurposing drugs as a melioidosis therapy.

Melioidosis is difficult to treat, the antibiotic therapy is often prolonged and with a risk of relapse in infection. This is in part due to *B. pseudomallei* occupying an intracellular niche, an intracellular site of infection protected from the majority of antibiotic therapies. Here we have shown that we can successfully target the intracellular site of infection *in vitro*, with antibody based antibiotic delivery and also with repurposed anti-microbial compounds. The AAC has potential to work in synergy with current front line melioidosis therapies, delivering antibiotic to the intracellular infection, potentially reducing the overall therapy duration and risk of relapse in patients. Reducing antibiotic therapy duration and using antibiotics in a targeted way, supports the effort in reducing the threat caused by anti-microbial resistance. Although the risk of anti-microbial resistance is generally considered less for melioidosis than other bacterial diseases, it is still important to be aware of possible future antibiotic resistance issues that may arise. Researching into alternative therapeutics for melioidosis, with the aim of refining the current antibiotic regimen, would be a good start to address the potential threat from antibiotic resistance.

7.3 Future research.

There are three main areas of future research from this project. Additional *in vivo* studies of the mAb 3VIE5, further development of the AAC, and repurposing of antimicrobial compounds.

A major focus of future work will be on enhancing the AAC. This could include antibody engineering, linker optimisation and increasing drug delivery. To be a successful therapeutic, a humanised, chimeric, or a fully human version of mAb 3VIE5 will need to be developed. This is crucial to minimise anti-species reactions, such as the generation of human anti-mouse antibodies (HAMA). The HAMA response can cause severe allergic reactions in the patient, additionally the efficacy of the therapy will be significantly reduced (378). Humanised and chimeric mAbs help prevent the HAMA response in patients, whilst maintaining the desirable binding interactions of the mAb (317). Humanised mAbs retain the complementarity determining regions (CDRs) of the murine mAb, typically by grafting the CDRs onto a human antibody framework (317). This approach would retain the original CPS antigen binding specificity of the mAb 3VIE5. Chimeric antibodies retain the murine Fab regions and combine these with human Fc regions, this approach would also retain the antigen binding specificity of mAb 3VIE5. The human antibody framework itself can be engineered, to improve effector functions or select specific antibody properties. Specific antibody isotypes can be selected for improved Fc receptor interactions, such as the IgG1 isotype for efficient promotion of antibody dependent cellular toxicity (378).

The reduction of lysine residues on the antibody as conjugation sites, leads to a heterogeneous AAC with a variable DAR (373). This heterogeneity has been observed during this research project in the generation of the proof of concept AAC for melioidosis. Although this approach is viable, especially for a proof of concept AAC, future research should prioritise generating a homogenous AAC product for a melioidosis therapy. A human antibody framework can be engineered to contain specific conjugation sites for linker-antibiotic binding, such as engineered cysteine residues (165), this would enable generation of a homogeneous AAC therapy with a specific DAR. The THIOMAB™ approach (379), used in the development of the *S.*

aureus AAC (165), engineered specific cysteine conjugation sites on the antibody for a specific DAR. A homogeneous AAC is desirable for a successful therapeutic, this enables well characterised and consistent PK properties, without variation between AAC batches. A well-defined and stable therapeutic will be required for successful licensure of a melioidosis AAC therapy in the future.

Future research involving the AAC linker should include enhancing drug delivery to the intracellular environment. This could be achieved by increasing the DAR of the AAC to increase efficacy, although there is a balance to be met between increasing DAR and possible negative effects on antibody function and PK of the AAC therapy. Increasing DAR is possible by engineering multiple cystine conjugation sites on the antibody for a homogeneous AAC product, or increasing reductions in antibody lysine residues for a heterogeneous AAC product. A scaffold type approach could enable multiple antibiotic molecules to be conjugated per linker, therefore greatly increasing the drug-antibody ratio for enhanced bacterial killing. A scaffold approach has been developed for the *S. aureus* THIOMAB™ AAC, consisting of a recombinant XTEN polypeptide (380). This approach allows for a higher DAR (up to 18), avoiding the potential negative effects (poor efficacy and PK) that can occur at high DARs (above 4) with cysteine and lysine conjugation methods (380). In addition, this high DAR technique allows for generation of a higher potency homogenous AAC, potentially allowing for a simpler and more cost effective therapy formulation compared to other AAC formulations (380). Future research involving high DAR AAC, will require assessment of DAR on antibody function and antibiotic efficacy *in vitro*, in addition the effect of higher DAR on the PK of the AAC will need to be assessed *in vivo*.

The antibody is a crucial component of the AAC and selection of an antibody is based on various factors. In addition to selecting antibodies based on the Fab region for target specificity, it is also important to consider the Fc region that regulates serum half-life through FcRn binding and also governs binding to Fcγ receptors (381). Antibody modifications commonly used to improve effector functions and PK properties include modification of glycosylation sites, together with modification of FcRn and FcγR interaction sites (382). Glycosylation of the Fc portion of therapeutic antibodies is crucial for function, such as binding to FcγRs. Glycoengineering of therapeutic antibodies is potential route to increase desirable effector functions, such as binding to activating FcγRs and phagocytosis. This is particularly important when

the background IgG levels in the body (approximately 15 mg mL) is considered to occupy the majority of cellular FcγRs (137). Glycosylation is poorly understood, and together with natural variation in receptor glycobiology, makes therapeutic engineering to specific FcγRs challenging. There is potential for future personalised medicines based on individual's receptor glycoforms being identified, and therapeutics designed specifically to increase or dampen effector functions of immune cells (137).

Antibody subclass should be considered for future AACs, although subclass can be switched if deemed necessary. IgG1 is the most common subclass selected for AAC development due to the high affinity binding to activating Fcγ receptors, the only subclass of IgG which is generally avoided is IgG3 due to the low serum half-life (381, 383).

Further work investigating conjugation of finafloxacin to the AAC should be investigated. Finafloxacin has enhanced activity under low pH conditions, and therefore the antibiotic activity will be enhanced within the intracellular environment. Initial work has shown that finafloxacin is active as an antibiotic-stub, although further work is required to overcome potential solubility issues. This should be a focus of future AAC research, so that a finafloxacin AAC version is available as a comparator to the ciprofloxacin AAC.

In this study, the pharmacokinetic properties of 3VIE5 were determined in BALB/c mice. The 3VIE5 mAb has previously been tested in a murine *in vivo* protection study at Dstl (113), and demonstrated a level of protection against a *B. pseudomallei* challenge. Future studies with this mAb *in vivo*, should include a *B. pseudomallei* protection study whereby 3VIE5 is tested at a range of concentrations, both pre and post-infection. This will determine the concentration at which the mAb is protective, and if this protection can be achieved when the mAb is given as a pre or post-exposure therapy. This will inform future *in vivo* protection studies, whereby mAb 3VIE5 is compared to an AAC therapy. Future studies should also include PK studies of the AAC, to determine the effect of AAC conjugation on the PK properties of the antibody and antibiotic. Additionally, future studies should include the AAC in *B. pseudomallei* protection studies, to prove efficacy of the AAC *in vivo*. Detailed

characterisation of the *in vivo* PK and protection studies are crucial for the successful future licensure of the AAC therapy.

Screening current FDA approved drugs, with the aim to repurpose as host directed and anti-microbial compounds, has the potential to discover new therapeutics for melioidosis. Compounds that demonstrate bacterial killing for other intracellular bacteria, such as *M. tuberculosis*, should be screened for ability to kill *B. pseudomallei*. The cell infection assay is a method that should be used to screen compounds, and down-select compounds for further analysis. In this research project, verapamil has demonstrated early potential as an anti-bacterial compound. Further analysis of verapamil is required, to determine if this compound would be a suitable therapeutic option for melioidosis.

Various studies in the literature have tested the synergistic effects of verapamil with anti-tuberculosis drugs, demonstrating an increase in the efficacy of the drugs in combination with verapamil (219-221, 224, 225, 231, 291). Verapamil has been shown to have synergistic effects in combination with a tobramycin antibiotic, in studies with *Burkholderia cepacia in vitro* (384, 385). Verapamil demonstrates ability to increase host cell autophagy (227, 292), and reduce intracellular *M. tuberculosis* as a standalone drug (207). Despite all the promise of verapamil as a combination therapy, it is yet to be repurposed as an anti-bacterial therapy.

Verapamil has not been tested against *B. thailandensis* or *B. pseudomallei* in any other previous studies in the literature, and the data in this chapter is the first known test of verapamil as an anti-bacterial compound against *B. thailandensis in vitro*. The synergistic effect of verapamil and antibiotics has not been studied here, potential synergy with antibiotics *in vitro* should be examined in future studies with this compound. This would determine any beneficial effects of verapamil in combination with melioidosis relevant drugs. Initial *in vitro* assessment of verapamil in combination with antibiotics will reveal any potential synergy, this could lead to *in vivo* murine protection studies to demonstrate the benefit of the synergy on survival. If verapamil can increase the efficacy of antibiotics, then this could improve current antibiotic therapy regimens for melioidosis, and potentially even increase the repertoire of antibiotics available as therapies.

The data in this thesis represents a very early stage *in vitro* assessment of the effect of verapamil on intracellular *B. thailandensis*. Without further assessment, it is difficult to determine the full potential of repurposing verapamil as an anti-bacterial compound for melioidosis. Future studies should additionally include an extensive analysis of the mechanism of action, including analysing verapamil induced autophagy at additional time points and concentrations. There is potential for future studies investigating verapamil as a standalone anti-bacterial therapy, and additionally as a combination therapy with antibiotics.

8. Bibliography.

1. Whitmore A. 1913. An Account of a Glanders-like Disease occurring in Rangoon. The Journal of Hygiene 13:1-34.1.
2. Titball RW, Russell P, Cuccui J, Easton A, Haque A, Atkins T, Sarkar-Tyson M, Harley V, Wren B, Bancroft GJ. 2008. Burkholderia pseudomallei: animal models of infection. Trans R Soc Trop Med Hyg 102 Suppl 1:S111-6.
3. Gilad J, Harary I, Dushnitsky T, Schwartz D, Amsalem Y. 2007. Burkholderia mallei and Burkholderia pseudomallei as bioterrorism agents: national aspects of emergency preparedness. Isr Med Assoc J 9:499-503.
4. Wuthiekanun V, Smith MD, Dance DAB, Walsh AL, Pitt TL, White NJ. 1996. Biochemical characteristics of clinical and environmental isolates of Burkholderia pseudomallei. Journal of Medical Microbiology 45:408-412.
5. Hantrakun V, Thaipadungpanit J, Rongkard P, Srilohasin P, Amornchai P, Langla S, Mukaka M, Chantratita N, Wuthiekanun V, Dance DAB, Day NPJ, Peacock SJ, Limmathurotsakul D. 2018. Presence of B. thailandensis and B. thailandensis expressing B. pseudomallei-like capsular polysaccharide in Thailand, and their associations with serological response to B. pseudomallei. PLoS Negl Trop Dis 12:e0006193.
6. Ngamdee W, Tandhavanant S, Wikraiphat C, Reamtong O, Wuthiekanun V, Salje J, Low DA, Peacock SJ, Chantratita N. 2015. Competition between Burkholderia pseudomallei and B. thailandensis. BMC Microbiol 15:56.
7. Gee JE, Elrod MG, Gulvik CA, Haselow DT, Waters C, Liu L, Hoffmaster AR. 2018. Burkholderia thailandensis Isolated from Infected Wound, Arkansas, USA. Emerg Infect Dis 24:2091-2094.
8. Chang K, Luo J, Xu H, Li M, Zhang F, Li J, Gu D, Deng S, Chen M, Lu W. 2017. Human Infection with Burkholderia thailandensis, China, 2013. Emerging infectious diseases 23:1416-1418.
9. Glass MB, Gee JE, Steigerwalt AG, Cavuoti D, Barton T, Hardy RD, Godoy D, Spratt BG, Clark TA, Wilkins PP. 2006. Pneumonia and septicemia caused by Burkholderia thailandensis in the United States. J Clin Microbiol 44:4601-4.
10. Dance DAB, Sarovich D, Price EP, Limmathurotsakul D, Currie BJ. 2018. Human Infection with Burkholderia thailandensis, China, 2013. Emerg Infect Dis 24:953-954.
11. Brett PJ, DeShazer D, Woods DE. 1998. Burkholderia thailandensis sp. nov., a Burkholderia pseudomallei-like species. Int J Syst Bacteriol 48 Pt 1:317-20.
12. Smith MD, Angus BJ, Wuthiekanun V, White NJ. 1997. Arabinose assimilation defines a nonvirulent biotype of Burkholderia pseudomallei. Infect Immun 65:4319-21.
13. Sim BM, Chantratita N, Ooi WF, Nandi T, Tewhey R, Wuthiekanun V, Thaipadungpanit J, Tumapa S, Ariyaratne P, Sung WK, Sem XH, Chua HH, Ramnarayanan K, Lin CH, Liu Y, Feil EJ, Glass MB, Tan G, Peacock SJ, Tan P. 2010. Genomic acquisition of a capsular polysaccharide virulence cluster by non-pathogenic Burkholderia isolates. Genome Biol 11:R89.
14. Amiss AS, Webb JR, Mayo M, Currie BJ, Craik DJ, Henriques ST, Lawrence N. 2020. Safer In Vitro Drug Screening Models for Melioidosis Therapy Development. Am J Trop Med Hyg doi:10.4269/ajtmh.20-0248.

15. Kovacs-Simon A, Hemsley CM, Scott AE, Prior JL, Titball RW. 2019. Burkholderia thailandensis strain E555 is a surrogate for the investigation of Burkholderia pseudomallei replication and survival in macrophages. BMC Microbiol 19:97.
16. Kespichayawattana W, Intachote P, Utaisincharoen P, Sirisinha S. 2004. Virulent Burkholderia pseudomallei is more efficient than avirulent Burkholderia thailandensis in invasion of and adherence to cultured human epithelial cells. Microbial Pathogenesis 36:287-292.
17. Wand ME, Muller CM, Titball RW, Michell SL. 2011. Macrophage and Galleria mellonella infection models reflect the virulence of naturally occurring isolates of B. pseudomallei, B. thailandensis and B. oklahomensis. BMC Microbiol 11:11.
18. Gutierrez MG, Warawa JM. 2016. Attenuation of a select agent-excluded Burkholderia pseudomallei capsule mutant in hamsters. Acta Tropica 157:68-72.
19. Bayliss M, Donaldson MI, Nepogodiev SA, Pergolizzi G, Scott AE, Harmer NJ, Field RA, Prior JL. 2017. Structural characterisation of the capsular polysaccharide expressed by Burkholderia thailandensis strain E555:: wbiI (pKnock-KmR) and assessment of the significance of the 2-O-acetyl group in immune protection. Carbohydr Res 452:17-24.
20. Limmathurotsakul D, Golding N, Dance DA, Messina JP, Pigott DM, Moyes CL, Rolim DB, Bertherat E, Day NP, Peacock SJ, Hay SI. 2016. Predicted global distribution of Burkholderia pseudomallei and burden of melioidosis. Nat Microbiol 1.
21. Currie BJ. 2015. Melioidosis: evolving concepts in epidemiology, pathogenesis, and treatment. Semin Respir Crit Care Med 36:111-25.
22. Hantrakun V, Kongyu S, Klaytong P, Rongsumlee S, Day NPJ, Peacock SJ, Hinjoy S, Limmathurotsakul D. 2019. Clinical Epidemiology of 7126 Melioidosis Patients in Thailand and the Implications for a National Notifiable Diseases Surveillance System. Open Forum Infect Dis 6:ofz498.
23. O'Connor C, Kenna D, Walsh A, Zamarreño DV, Dance D. 2020. Imported melioidosis in the United Kingdom: Increasing incidence but continued under-reporting. Clinical Infection in Practice 7-8:100051.
24. Currie BJ, Ward L, Cheng AC. 2010. The epidemiology and clinical spectrum of melioidosis: 540 cases from the 20 year Darwin prospective study. PLoS Negl Trop Dis 4:e900.
25. Wiersinga WJ, Virk HS, Torres AG, Currie BJ, Peacock SJ, Dance DAB, Limmathurotsakul D. 2018. Melioidosis. Nat Rev Dis Primers 4:17107.
26. Maharjan B, Chantratita N, Vesaratchavest M, Cheng A, Wuthiekanun V, Chierakul W, Chaowagul W, Day NP, Peacock SJ. 2005. Recurrent melioidosis in patients in northeast Thailand is frequently due to reinfection rather than relapse. J Clin Microbiol 43:6032-4.
27. Sarovich DS, Ward L, Price EP, Mayo M, Pitman MC, Baird RW, Currie BJ. 2014. Recurrent melioidosis in the Darwin Prospective Melioidosis Study: improving therapies mean that relapse cases are now rare. J Clin Microbiol 52:650-3.
28. Singh M, Mahmood M. 2017. Melioidosis: the great mimicker. J Community Hosp Intern Med Perspect 7:245-247.
29. Wiersinga WJ, van der Poll T, White NJ, Day NP, Peacock SJ. 2006. Melioidosis: insights into the pathogenicity of Burkholderia pseudomallei. Nat Rev Micro 4:272-282.

30. Morris JL, Fane A, Sarovich DS, Price EP, Rush CM, Govan BL, Parker E, Mayo M, Currie BJ, Ketheesan N. 2017. Increased Neurotropic Threat from Burkholderia pseudomallei Strains with a B. mallei-like Variation in the bimA Motility Gene, Australia. Emerg Infect Dis 23.
31. Chaichana P, Jenjaroen K, Amornchai P, Chumseng S, Langla S, Rongkard P, Sumonwiriya M, Jeeyapant A, Chantratita N, Teparrukkul P, Limmathurotsakul D, Day NPJ, Wuthiekanun V, Dunachie SJ. 2018. Antibodies in Melioidosis: The Role of the Indirect Hemagglutination Assay in Evaluating Patients and Exposed Populations. Am J Trop Med Hyg 99:1378-1385.
32. Harris PN, Ketheesan N, Owens L, Norton RE. 2009. Clinical features that affect indirect-hemagglutination-assay responses to Burkholderia pseudomallei. Clin Vaccine Immunol 16:924-30.
33. Kaestli M, Richardson LJ, Colman RE, Tuanyok A, Price EP, Bowers JR, Mayo M, Kelley E, Seymour ML, Sarovich DS, Pearson T, Engelthaler DM, Wagner DM, Keim PS, Schupp JM, Currie BJ. 2012. Comparison of TaqMan PCR assays for detection of the melioidosis agent Burkholderia pseudomallei in clinical specimens. J Clin Microbiol 50:2059-62.
34. Houghton RL, Reed DE, Hubbard MA, Dillon MJ, Chen H, Currie BJ, Mayo M, Sarovich DS, Theobald V, Limmathurotsakul D, Wongsuvan G, Chantratita N, Peacock SJ, Hoffmaster AR, Duval B, Brett PJ, Burtnick MN, Aucoin DP. 2014. Development of a prototype lateral flow immunoassay (LFI) for the rapid diagnosis of melioidosis. PLoS Negl Trop Dis 8:e2727.
35. Currie BJ, Woerle C, Mayo M, Meumann EM, Baird RW. 2022. What is the Role of Lateral Flow Immunoassay for the Diagnosis of Melioidosis? Open Forum Infect Dis 9:ofac149.
36. Woods KL, Boutthasavong L, NicFhogartaigh C, Lee SJ, Davong V, AuCoin DP, Dance DAB. 2018. Evaluation of a Rapid Diagnostic Test for Detection of Burkholderia pseudomallei in the Lao People's Democratic Republic. J Clin Microbiol 56.
37. Dunachie S, Chamnan P. 2019. The double burden of diabetes and global infection in low and middle-income countries. Transactions of the Royal Society of Tropical Medicine and Hygiene 113:56-64.
38. Jenjaroen K, Chumseng S, Sumonwiriya M, Ariyaprasert P, Chantratita N, Sunyakumthorn P, Hongsuwan M, Wuthiekanun V, Fletcher HA, Teparrukkul P, Limmathurotsakul D, Day NP, Dunachie SJ. 2015. T-Cell Responses Are Associated with Survival in Acute Melioidosis Patients. PLoS Negl Trop Dis 9:e0004152.
39. Kronsteiner B, Chaichana P, Sumonwiriya M, Jenjaroen K, Chowdhury FR, Chumseng S, Teparrukkul P, Limmathurotsakul D, Day NPJ, Klenerman P, Dunachie SJ. 2019. Diabetes alters immune response patterns to acute melioidosis in humans. Eur J Immunol 49:1092-1106.
40. Limmathurotsakul D, Kanoksil M, Wuthiekanun V, Kitphati R, deStavola B, Day NPJ, Peacock SJ. 2013. Activities of Daily Living Associated with Acquisition of Melioidosis in Northeast Thailand: A Matched Case-Control Study. PLOS Neglected Tropical Diseases 7:e2072.
41. Limmathurotsakul D, Wongsuvan G, Aanensen D, Ngamwilai S, Saiprom N, Rongkard P, Thaipadungpanit J, Kanoksil M, Chantratita N, Day NP, Peacock SJ. 2014. Melioidosis caused by Burkholderia pseudomallei in drinking water, Thailand, 2012. Emerg Infect Dis 20:265-8.

42. Hinjoy S, Hantrakun V, Kongyu S, Kaewrakmuk J, Wangrangsimakul T, Jitsuronk S, Saengchun W, Bhengsri S, Akarachotpong T, Thamthitiwat S, Sangwichian O, Anunnatsiri S, Sermswan R, Lertmemongkolchai G, Sitthidet Tharinjaroen C, Preechasuth K, Udpaun R, Chuensombut P, Waranyasirikul N, Anudit C, Narenpitak S, Jutrakul Y, Teparrukkul P, Teerawattanasook N, Thanvisej K, Suphan A, Sukbut P, Ploddi K, Sirichotirat P, Chiewchanyon B, Rukseree K, Hongsuwan M, Wongsuwan G, Sunthornsut P, Wuthiekanun V, Sachaphimukh S, Wannapinij P, Chierakul W, Chewapreecha C, Thaipadungpanit J, Chantratita N, Korbsrisate S, Taunyok A, Dunachie S, Palittapongarnpim P, Sirisinha S, Kitphati R, Iamsirithaworn S, Chaowagul W, Chetchotisak P, et al. 2018. Melioidosis in Thailand: Present and Future. Tropical Medicine and Infectious Disease 3:38.
43. Mukhopadhyay C, Shaw T, Varghese G, Dance D. 2018. Melioidosis in South Asia (India, Nepal, Pakistan, Bhutan and Afghanistan). Tropical Medicine and Infectious Disease 3:51.
44. Rolim D, Lima R, Ribeiro A, Colares R, Lima L, Rodríguez-Morales A, Montúfar F, Dance D. 2018. Melioidosis in South America. Tropical Medicine and Infectious Disease 3:60.
45. Limmathurotsakul D, Dance DA, Wuthiekanun V, Kaestli M, Mayo M, Warner J, Wagner DM, Tuanyok A, Wertheim H, Yoke Cheng T, Mukhopadhyay C, Puthucheary S, Day NP, Steinmetz I, Currie BJ, Peacock SJ. 2013. Systematic review and consensus guidelines for environmental sampling of Burkholderia pseudomallei. PLoS Negl Trop Dis 7:e2105.
46. Vongphayloth K, Rattanavong S, Moore CE, Phetsouvanh R, Wuthiekanun V, Sengdouangphachanh A, Phouminh P, Newton PN, Buisson Y. 2012. Burkholderia pseudomallei detection in surface water in southern Laos using Moore's swabs. The American journal of tropical medicine and hygiene 86:872-877.
47. Corea E. 2018. Melioidosis: a neglected tropical disease. Ceylon Med J 63:1-4.
48. Savelkoel J, Dance DAB, Currie BJ, Limmathurotsakul D, Wiersinga WJ. 2021. A call to action: time to recognise melioidosis as a neglected tropical disease. Lancet Infect Dis doi:10.1016/s1473-3099(21)00394-7.
49. Birnie E, James A, Peters F, Olajumoke M, Traore T, Bertherat E, Trung T, Dhamari N, Steinmetz I, Wiersinga WJ, Oladele R, Akanmu A. 2022. Melioidosis in Africa: Time to Raise Awareness and Build Capacity for Its Detection, Diagnosis, and Treatment. Am J Trop Med Hyg doi:10.4269/ajtmh.21-0673.
50. Birnie E, Wiersinga WJ, Limmathurotsakul D, Grobusch MP. 2015. Melioidosis in Africa: should we be looking more closely? Future Microbiol 10:273-81.
51. Steinmetz I, Wagner G, Kanyala E, Sawadogo M, Soumeya H, Teferi M, Andargie E, Yeshitela B, Yaba Atsé-Achi L, Sanogo M, Bonfoh B, Rakotozandrindrainy R, Pongombo Shongo C, Shongoya Pongombo M, Kasamba Ilunga E, Lichtenegger S, Assig K, May J, Bertherat E, Owusu M, Owusu-Dabo E, Adu-Sarkodie Y. 2018. Melioidosis in Africa: Time to Uncover the True Disease Load. Tropical Medicine and Infectious Disease 3:62.
52. Stephens DP, Thomas JH, Ward LM, Currie BJ. 2016. Melioidosis Causing Critical Illness: A Review of 24 Years of Experience From the Royal Darwin Hospital ICU. Crit Care Med 44:1500-5.
53. Dance D. 2014. Treatment and prophylaxis of melioidosis. International Journal of Antimicrobial Agents 43:310-318.

54. Lipsitz R, Garges S, Aurigemma R, Baccam P, Blaney DD, Cheng AC, Currie BJ, Dance D, Gee JE, Larsen J, Limmathurotsakul D, Morrow MG, Norton R, O'Mara E, Peacock SJ, Pesik N, Rogers LP, Schweizer HP, Steinmetz I, Tan G, Tan P, Wiersinga WJ, Wuthiekanun V, Smith TL. 2012. Workshop on treatment of and postexposure prophylaxis for Burkholderia pseudomallei and B. mallei Infection, 2010. Emerg Infect Dis 18:e2.
55. Lemaire S, Van Bambeke F, Tulkens PM. 2011. Activity of finafloxacin, a novel fluoroquinolone with increased activity at acid pH, towards extracellular and intracellular Staphylococcus aureus, Listeria monocytogenes and Legionella pneumophila. Int J Antimicrob Agents 38:52-9.
56. Barnes KB, Hamblin KA, Richards MI, Laws TR, Vente A, Atkins HS, Harding SV. 2017. Demonstrating the protective efficacy of the novel fluoroquinolone finafloxacin against an inhalational exposure to Burkholderia pseudomallei. Antimicrob Agents Chemother doi:10.1128/aac.00082-17.
57. Medzhitov R. 2007. Recognition of microorganisms and activation of the immune response. Nature 449:819-826.
58. Vignali DAA, Collison LW, Workman CJ. 2008. How regulatory T cells work. Nature Reviews Immunology 8:523-532.
59. Akira S, Uematsu S, Takeuchi O. 2006. Pathogen recognition and innate immunity. Cell 124.
60. Akira S, Takeda K, Kaisho T. 2001. Toll-like receptors: critical proteins linking innate and acquired immunity. Nat Immunol 2.
61. Ley K, Pramod AB, Croft M, Ravichandran KS, Ting JP. 2016. How Mouse Macrophages Sense What Is Going On. Front Immunol 7:204.
62. Krakauer T. 2019. Inflammasomes, Autophagy, and Cell Death: The Trinity of Innate Host Defense against Intracellular Bacteria. Mediators Inflamm 2019:2471215.
63. West TE, Chierakul W, Chantratita N, Limmathurotsakul D, Wuthiekanun V, Emond MJ, Hawn TR, Peacock SJ, Skerrett SJ. 2012. Toll-Like Receptor 4 Region Genetic Variants are Associated with Susceptibility to Melioidosis. Genes and immunity 13:38-46.
64. West TE, Ernst RK, Jansson-Hutson MJ, Skerrett SJ. 2008. Activation of Toll-like receptors by Burkholderia pseudomallei. BMC Immunology 9:1-10.
65. Tan KS, Chen Y, Lim YC, Tan GY, Liu Y, Lim YT, Macary P, Gan YH. 2010. Suppression of host innate immune response by Burkholderia pseudomallei through the virulence factor TssM. J Immunol 184:5160-71.
66. White NJ. 2003. Melioidosis. The Lancet 361:1715-1722.
67. Lazar Adler NR, Govan B, Cullinane M, Harper M, Adler B, Boyce JD. 2009. The molecular and cellular basis of pathogenesis in melioidosis: how does Burkholderia pseudomallei cause disease? FEMS Microbiol Rev 33:1079-99.
68. Vandana KE, Mukhopadhyay C, Tellapragada C, Kamath A, Tipre M, Bhat V, Sathiakumar N. 2016. Seroprevalence of Burkholderia pseudomallei among Adults in Coastal Areas in Southwestern India. PLoS Negl Trop Dis 10:e0004610.
69. Raj S, Sistla S, Melepurakkal Sadanandan D, Kadhiravan T, Chinnakali P. 2022. Estimation of seroprevalence of melioidosis among adult high risk groups in Southeastern India by indirect Hemagglutination assay. PLOS Global Public Health 2:e0000431.

70. Stone JK, DeShazer D, Brett PJ, Burtnick MN. 2014. Melioidosis: molecular aspects of pathogenesis. Expert Rev Anti Infect Ther 12:1487-99.
71. Willcocks SJ, Denman CC, Atkins HS, Wren BW. 2016. Intracellular replication of the well-armed pathogen Burkholderia pseudomallei. Curr Opin Microbiol 29:94-103.
72. Whiteley L, Meffert T, Haug M, Weidenmaier C, Hopf V, Bitschar K, Schittek B, Kohler C, Steinmetz I, West TE, Schwarz S. 2017. Entry, intracellular survival and multinucleated giant cell-forming activity of Burkholderia pseudomallei in human primary phagocytic and non-phagocytic cells. Infect Immun doi:10.1128/iai.00468-17.
73. Allwood EM, Devenish RJ, Prescott M, Adler B, Boyce JD. 2011. Strategies for Intracellular Survival of Burkholderia pseudomallei. Front Microbiol 2:170.
74. Gong L, Cullinane M, Treerat P, Ramm G, Prescott M, Adler B, Boyce JD, Devenish RJ. 2011. The Burkholderia pseudomallei type III secretion system and BopA are required for evasion of LC3-associated phagocytosis. PLoS One 6:e17852.
75. Burtnick MN, Brett PJ, Nair V, Warawa JM, Woods DE, Gherardini FC. 2008. Burkholderia pseudomallei type III secretion system mutants exhibit delayed vacuolar escape phenotypes in RAW 264.7 murine macrophages. Infect Immun 76:2991-3000.
76. Holden MTG, Titball RW, Peacock SJ, Cerdeño-Tárraga AM, Atkins T, Crossman LC, Pitt T, Churcher C, Mungall K, Bentley SD, Sebaihia M, Thomson NR, Bason N, Beacham IR, Brooks K, Brown KA, Brown NF, Challis GL, Cherevach I, Chillingworth T, Cronin A, Crossett B, Davis P, DeShazer D, Feltwell T, Fraser A, Hance Z, Hauser H, Holroyd S, Jagels K, Keith KE, Maddison M, Moule S, Price C, Quail MA, Rabbinowitsch E, Rutherford K, Sanders M, Simmonds M, Songsivilai S, Stevens K, Tumapa S, Vesaratchavest M, Whitehead S, Yeats C, Barrell BG, Oyston PCF, Parkhill J. 2004. Genomic plasticity of the causative agent of melioidosis, Burkholderia pseudomallei. Proceedings of the National Academy of Sciences of the United States of America 101:14240-14245.
77. Vander Broek CW, Stevens JM. 2017. Type III Secretion in the Melioidosis Pathogen Burkholderia pseudomallei. Front Cell Infect Microbiol 7:255.
78. Stevens MP, Wood MW, Taylor LA, Monaghan P, Hawes P, Jones PW, Wallis TS, Galyov EE. 2002. An Inv/Mxi-Spa-like type III protein secretion system in Burkholderia pseudomallei modulates intracellular behaviour of the pathogen. Molecular Microbiology 46:649-659.
79. Stevens MP, Haque A, Atkins T, Hill J, Wood MW, Easton A, Nelson M, Underwood-Fowler C, Titball RW, Bancroft GJ. 2004. Attenuated virulence and protective efficacy of a Burkholderia pseudomallei bsa type III secretion mutant in murine models of melioidosis. Microbiology 150:2669-2676.
80. Vander Broek CW, Zainal Abidin N, Stevens JM. 2017. BipC, a Predicted Burkholderia pseudomallei Type 3 Secretion System Translocator Protein with Actin Binding Activity. Front Cell Infect Microbiol 7:333.
81. Suparak S, Kespichayawattana W, Haque A, Easton A, Damnin S, Lertmemongkolchai G, Bancroft GJ, Korbsrisate S. 2005. Multinucleated giant cell formation and apoptosis in infected host cells is mediated by Burkholderia pseudomallei type III secretion protein BipB. J Bacteriol 187:6556-60.
82. Stevens MP, Haque A, Atkins T, Hill J, Wood MW, Easton A, Nelson M, Underwood-Fowler C, Titball RW, Bancroft GJ, Galyov EE. 2004. Attenuated virulence and

protective efficacy of a Burkholderia pseudomallei bsa type III secretion mutant in murine models of melioidosis. Microbiology 150:2669-76.
83. Kang WT, Vellasamy KM, Chua EG, Vadivelu J. 2015. Functional characterizations of effector protein BipC, a type III secretion system protein, in Burkholderia pseudomallei pathogenesis. J Infect Dis 211:827-34.
84. Kang WT, Vellasamy KM, Rajamani L, Beuerman RW, Vadivelu J. 2016. Burkholderia pseudomallei type III secreted protein BipC: role in actin modulation and translocation activities required for the bacterial intracellular lifecycle. PeerJ 4:e2532.
85. Vander Broek CW, Chalmers KJ, Stevens MP, Stevens JM. 2015. Quantitative proteomic analysis of Burkholderia pseudomallei Bsa type III secretion system effectors using hypersecreting mutants. Mol Cell Proteomics 14:905-16.
86. Stevens MP, Friebel A, Taylor LA, Wood MW, Brown PJ, Hardt W-D, Galyov EE. 2003. A Burkholderia pseudomallei Type III Secreted Protein, BopE, Facilitates Bacterial Invasion of Epithelial Cells and Exhibits Guanine Nucleotide Exchange Factor Activity. Journal of Bacteriology 185:4992-4996.
87. Muangman S, Korbsrisate S, Muangsombut V, Srinon V, Adler NL, Schroeder GN, Frankel G, Galyov EE. 2011. BopC is a type III secreted effector protein of Burkholderia pseudomallei. FEMS Microbiol Lett 323:75-82.
88. Srinon V, Muangman S, Imyaem N, Muangsombut V, Lazar Adler NR, Galyov EE, Korbsrisate S. 2013. Comparative assessment of the intracellular survival of the Burkholderia pseudomallei bopC mutant. J Microbiol 51:522-6.
89. Ray K, Marteyn B, Sansonetti PJ, Tang CM. 2009. Life on the inside: the intracellular lifestyle of cytosolic bacteria. Nat Rev Micro 7:333-340.
90. Benanti EL, Nguyen CM, Welch MD. 2015. Virulent Burkholderia species mimic host actin polymerases to drive actin-based motility. Cell 161:348-60.
91. Kespichayawattana W, Rattanachetkul S, Wanun T, Utaisincharoen P, Sirisinha S. 2000. Burkholderia pseudomallei induces cell fusion and actin-associated membrane protrusion: a possible mechanism for cell-to-cell spreading. Infect Immun 68:5377-84.
92. Lamason RL, Welch MD. 2017. Actin-based motility and cell-to-cell spread of bacterial pathogens. Current Opinion in Microbiology 35:48-57.
93. Stevens MP, Stevens JM, Jeng RL, Taylor LA, Wood MW, Hawes P, Monaghan P, Welch MD, Galyov EE. 2005. Identification of a bacterial factor required for actin-based motility of Burkholderia pseudomallei. Mol Microbiol 56:40-53.
94. Srinon V, Chaiwattanarungruengpaisan S, Korbsrisate S, Stevens JM. 2019. Burkholderia pseudomallei BimC Is Required for Actin-Based Motility, Intracellular Survival, and Virulence. Frontiers in Cellular and Infection Microbiology 9.
95. Choe JE, Welch MD. 2016. Actin-based motility of bacterial pathogens: mechanistic diversity and its impact on virulence. Pathog Dis doi:10.1093/femspd/ftw099.
96. Welch MD, Way M. 2013. Arp2/3-mediated actin-based motility: a tail of pathogen abuse. Cell Host Microbe 14:242-55.
97. Lazar Adler NR, Stevens MP, Dean RE, Saint RJ, Pankhania D, Prior JL, Atkins TP, Kessler B, Nithichanon A, Lertmemongkolchai G, Galyov EE. 2015. Systematic mutagenesis of genes encoding predicted autotransported proteins of Burkholderia pseudomallei identifies factors mediating virulence in mice, net intracellular

replication and a novel protein conferring serum resistance. PloS one 10:e0121271-e0121271.
98. Jitprasutwit N, Zainal-Abidin N, Vander Broek C, Kurian D, Korbsrisate S, Stevens MP, Stevens JM. 2016. Identification of Candidate Host Cell Factors Required for Actin-Based Motility of Burkholderia pseudomallei. J Proteome Res 15:4675-4685.
99. Toesca IJ, French CT, Miller JF. 2014. The Type VI Secretion System Spike Protein VgrG5 Mediates Membrane Fusion during Intercellular Spread by Pseudomallei Group Burkholderia Species. Infection and Immunity 82:1436-1444.
100. Stockton JL, Torres AG. 2020. Multinucleated Giant Cell Formation as a Portal to Chronic Bacterial Infections. Microorganisms 8.
101. Suparak S, Muangsombut V, Riyapa D, Stevens JM, Stevens MP, Lertmemongkolchai G, Korbsrisate S. 2011. Burkholderia pseudomallei-induced cell fusion in U937 macrophages can be inhibited by monoclonal antibodies against host cell surface molecules. Microbes and Infection 13:1006-1011.
102. Ninan F, Mishra AK, John AO, Iyadurai R. 2018. Splenic granuloma: Melioidosis or Tuberculosis? J Family Med Prim Care 7:271-273.
103. Krakauer T. 2018. Living dangerously: Burkholderia pseudomallei modulates phagocyte cell death to survive. Med Hypotheses 121:64-69.
104. Cullinane M, Gong L, Li X, Lazar-Adler N, Tra T, Wolvetang E, Prescott M, Boyce JD, Devenish RJ, Adler B. 2008. Stimulation of autophagy suppresses the intracellular survival of Burkholderia pseudomallei in mammalian cell lines. Autophagy 4:744-53.
105. Rubinsztein DC, Bento CF, Deretic V. 2015. Therapeutic targeting of autophagy in neurodegenerative and infectious diseases. J Exp Med 212:979-90.
106. Rubinsztein DC, Codogno P, Levine B. 2012. Autophagy modulation as a potential therapeutic target for diverse diseases. Nat Rev Drug Discov 11:709-30.
107. DiRita VJ, Reckseidler SL, DeShazer D, Sokol PA, Woods DE. 2001. Detection of Bacterial Virulence Genes by Subtractive Hybridization: Identification of Capsular Polysaccharide ofBurkholderia pseudomallei as a Major Virulence Determinant. Infection and Immunity 69:34-44.
108. Reckseidler-Zenteno SL, DeVinney R, Woods DE. 2005. The capsular polysaccharide of Burkholderia pseudomallei contributes to survival in serum by reducing complement factor C3b deposition. Infect Immun 73:1106-15.
109. Reckseidler-Zenteno SL. 2012. Capsular Polysaccharides Produced by the Bacterial Pathogen Burkholderia pseudomallei, p Ch. 05. *In* Karunaratne DN (ed), The Complex World of Polysaccharides doi:10.5772/50116. InTech, Rijeka.
110. Reckseidler-Zenteno SL, Viteri DF, Moore R, Wong E, Tuanyok A, Woods DE. 2010. Characterization of the type III capsular polysaccharide produced by Burkholderia pseudomallei. J Med Microbiol 59:1403-14.
111. Cuccui J, Milne TS, Harmer N, George AJ, Harding SV, Dean RE, Scott AE, Sarkar-Tyson M, Wren BW, Titball RW, Prior JL. 2012. Characterization of the Burkholderia pseudomallei K96243 Capsular Polysaccharide I Coding Region. Infection and Immunity 80:1209-1221.
112. Burtnick MN, Heiss C, Roberts RA, Schweizer HP, Azadi P, Brett PJ. 2012. Development of capsular polysaccharide-based glycoconjugates for immunization against melioidosis and glanders. Front Cell Infect Microbiol 2:108.
113. Jones SM, Ellis JF, Russell P, Griffin KF, Oyston PC. 2002. Passive protection against Burkholderia pseudomallei infection in mice by monoclonal antibodies against

capsular polysaccharide, lipopolysaccharide or proteins. J Med Microbiol 51:1055-62.
114. Zhang S, Feng SH, Li B, Kim HY, Rodriguez J, Tsai S, Lo SC. 2011. In Vitro and In Vivo studies of monoclonal antibodies with prominent bactericidal activity against Burkholderia pseudomallei and Burkholderia mallei. Clin Vaccine Immunol 18:825-34.
115. AuCoin DP, Reed DE, Marlenee NL, Bowen RA, Thorkildson P, Judy BM, Torres AG, Kozel TR. 2012. Polysaccharide Specific Monoclonal Antibodies Provide Passive Protection against Intranasal Challenge with Burkholderia pseudomallei. PLOS ONE 7:e35386.
116. Scott AE, Laws TR, D'Elia RV, Stokes MG, Nandi T, Williamson ED, Tan P, Prior JL, Atkins TP. 2013. Protection against experimental melioidosis following immunization with live Burkholderia thailandensis expressing a manno-heptose capsule. Clin Vaccine Immunol 20:1041-7.
117. Anuntagool N, Panichakul T, Aramsri P, Sirisinha S. 2000. Shedding of lipopolysaccharide and 200-kDa surface antigen during the in vitro growth of virulent Ara- and avirulent Ara+ Burkholderia pseudomallei. Acta Trop 74:221-8.
118. Nualnoi T, Kirosingh A, Pandit SG, Thorkildson P, Brett PJ, Burtnick MN, AuCoin DP. 2016. In vivo Distribution and Clearance of Purified Capsular Polysaccharide from Burkholderia pseudomallei in a Murine Model. PLOS Neglected Tropical Diseases 10:e0005217.
119. Nuti DE, Crump RB, Dwi Handayani F, Chantratita N, Peacock SJ, Bowen R, Felgner PL, Davies DH, Wu T, Lyons CR, Brett PJ, Burtnick MN, Kozel TR, AuCoin DP. 2011. Identification of circulating bacterial antigens by in vivo microbial antigen discovery. mBio 2.
120. Organization WH. 2014. Antimicrobial resistance: global report on surveillance. World Health Organization.
121. CDC. 2019. Antibiotic Resistance Threats in the United States. Atlanta, GA: US Department of Health and Human Services, CDC; 2019.
122. Murray CJL, Ikuta KS, Sharara F, Swetschinski L, Robles Aguilar G, Gray A, Han C, Bisignano C, Rao P, Wool E, Johnson SC, Browne AJ, Chipeta MG, Fell F, Hackett S, Haines-Woodhouse G, Kashef Hamadani BH, Kumaran EAP, McManigal B, Agarwal R, Akech S, Albertson S, Amuasi J, Andrews J, Aravkin A, Ashley E, Bailey F, Baker S, Basnyat B, Bekker A, Bender R, Bethou A, Bielicki J, Boonkasidecha S, Bukosia J, Carvalheiro C, Castañeda-Orjuela C, Chansamouth V, Chaurasia S, Chiurchiù S, Chowdhury F, Cook AJ, Cooper B, Cressey TR, Criollo-Mora E, Cunningham M, Darboe S, Day NPJ, De Luca M, Dokova K, et al. Global burden of bacterial antimicrobial resistance in 2019: a systematic analysis. The Lancet doi:10.1016/S0140-6736(21)02724-0.
123. Schweizer HP. 2012. Mechanisms of antibiotic resistance in Burkholderia pseudomallei: implications for treatment of melioidosis. Future Microbiol 7:1389-99.
124. Rhodes KA, Schweizer HP. 2016. Antibiotic resistance in Burkholderia species. Drug Resistance Updates 28:82-90.
125. Podnecky NL, Rhodes KA, Schweizer HP. 2015. E ffl ux pump-mediated drug resistance in Burkholderia. Front Microbiol 6:305.
126. Godfrey A, Wong S, Dance D, Chaowagul W, Bryan L. 1991. Pseudomonas pseudomallei resistance to beta-lactam antibiotics due to alterations in the

chromosomally encoded beta-lactamase. Antimicrobial agents and chemotherapy 35:1635-1640.
127. Sarovich DS, Webb JR, Pitman MC, Viberg LT, Mayo M, Baird RW, Robson JM, Currie BJ, Price EP. 2018. Raising the stakes: Loss of efflux-pump regulation decreases meropenem susceptibility in Burkholderia pseudomallei. Clin Infect Dis doi:10.1093/cid/ciy069.
128. Piliouras P, Ulett GC, Ashhurst-Smith C, Hirst RG, Norton RE. 2002. A comparison of antibiotic susceptibility testing methods for cotrimoxazole with Burkholderia pseudomallei. Int J Antimicrob Agents 19:427-9.
129. Lumbiganon P, Tattawasatra U, Chetchotisakd P, Wongratanacheewin S, Thinkhamrop B. 2000. Comparison between the antimicrobial susceptibility of Burkholderia pseudomallei to trimethoprim-sulfamethoxazole by standard disk diffusion method and by minimal inhibitory concentration determination. J Med Assoc Thai 83:856-60.
130. Wuthiekanun V, Cheng AC, Chierakul W, Amornchai P, Limmathurotsakul D, Chaowagul W, Simpson AJ, Short JM, Wongsuvan G, Maharjan B, White NJ, Peacock SJ. 2005. Trimethoprim/sulfamethoxazole resistance in clinical isolates of Burkholderia pseudomallei. J Antimicrob Chemother 55:1029-31.
131. KÖHler G, Milstein C. 1975. Continuous cultures of fused cells secreting antibody of predefined specificity. Nature 256:495.
132. Vidarsson G, Dekkers G, Rispens T. 2014. IgG Subclasses and Allotypes: From Structure to Effector Functions. Frontiers in Immunology 5:520.
133. Schroeder HW, Cavacini L. 2010. Structure and Function of Immunoglobulins. The Journal of allergy and clinical immunology 125:S41-S52.
134. Janeway CA Jr TP, Walport M and Shlomchik MJ. 2001. The structure of a typical antibody molecule. *In* (ed), Immunobiology: The Immune System in Health and Disease. Garland Science, New York. https://www.ncbi.nlm.nih.gov/books/NBK27144/.
135. Mazumdar S. 2009. Raxibacumab. MAbs 1:531-8.
136. Dunkelberger JR, Song W-C. 2010. Complement and its role in innate and adaptive immune responses. Cell Research 20:34-50.
137. Hayes JM, Wormald MR, Rudd PM, Davey GP. 2016. Fc gamma receptors: glycobiology and therapeutic prospects. J Inflamm Res 9:209-219.
138. Guilliams M, Bruhns P, Saeys Y, Hammad H, Lambrecht BN. 2014. The function of Fc[gamma] receptors in dendritic cells and macrophages. Nat Rev Immunol 14:349-349.
139. Bruhns P, Jonsson F. 2015. Mouse and human FcR effector functions. Immunol Rev 268:25-51.
140. Nimmerjahn F, Ravetch JV. 2008. Fcgamma receptors as regulators of immune responses. Nat Rev Immunol 8:34-47.
141. Rhodes DA, Isenberg DA. 2017. TRIM21 and the Function of Antibodies inside Cells. Trends in Immunology 38:916-926.
142. James LC. 2014. Intracellular antibody immunity and the cytosolic Fc receptor TRIM21. Curr Top Microbiol Immunol 382:51-66.
143. Foss S, Watkinson R, Sandlie I, James LC, Andersen JT. 2015. TRIM21: a cytosolic Fc receptor with broad antibody isotype specificity, vol 268, p 328-339.

144. Sockolosky JT, Szoka FC. 2015. The neonatal Fc receptor, FcRn, as a target for drug delivery and therapy. Advanced drug delivery reviews 91:109-124.
145. Borrok MJ, Wu Y, Beyaz N, Yu XQ, Oganesyan V, Dall'Acqua WF, Tsui P. 2015. pH-dependent binding engineering reveals an FcRn affinity threshold that governs IgG recycling. J Biol Chem 290:4282-90.
146. Vaughn DE, Bjorkman PJ. 1998. Structural basis of pH-dependent antibody binding by the neonatal Fc receptor. Structure 6:63-73.
147. Sparrow E, Friede M, Sheikh M, Torvaldsen S. 2017. Therapeutic antibodies for infectious diseases. Bulletin of the World Health Organization 95:235-237.
148. Greig SL. 2016. Obiltoxaximab: First Global Approval. Drugs 76:823-30.
149. Yamamoto BJ, Shadiack AM, Carpenter S, Sanford D, Henning LN, Gonzales N, O'Connor E, Casey LS, Serbina NV. 2016. Obiltoxaximab Prevents Disseminated Bacillus anthracis Infection and Improves Survival during Pre- and Postexposure Prophylaxis in Animal Models of Inhalational Anthrax. Antimicrob Agents Chemother 60:5796-805.
150. Tsai CW, Morris S. 2015. Approval of Raxibacumab for the Treatment of Inhalation Anthrax Under the US Food and Drug Administration "Animal Rule". Front Microbiol 6:1320.
151. Fenton C, Scott LJ, Plosker GL. 2004. Palivizumab: a review of its use as prophylaxis for serious respiratory syncytial virus infection. Paediatr Drugs 6:177-97.
152. Wilcox MH, Gerding DN, Poxton IR, Kelly C, Nathan R, Birch T, Cornely OA, Rahav G, Bouza E, Lee C, Jenkin G, Jensen W, Kim Y-S, Yoshida J, Gabryelski L, Pedley A, Eves K, Tipping R, Guris D, Kartsonis N, Dorr M-B. 2017. Bezlotoxumab for Prevention of Recurrent Clostridium difficile Infection. New England Journal of Medicine 376:305-317.
153. Sayburn A. 2014. WHO gives go ahead for experimental treatments to be used in Ebola outbreak. Bmj 349:g5161.
154. Qiu X, Audet J, Wong G, Pillet S, Bello A, Cabral T, Strong JE, Plummer F, Corbett CR, Alimonti JB, Kobinger GP. 2012. Successful Treatment of Ebola Virus–Infected Cynomolgus Macaques with Monoclonal Antibodies. Science Translational Medicine 4:138ra81-138ra81.
155. Qiu X, Wong G, Audet J, Bello A, Fernando L, Alimonti JB, Fausther-Bovendo H, Wei H, Aviles J, Hiatt E. 2014. Reversion of advanced Ebola virus disease in nonhuman primates with ZMapp. Nature 514:47-53.
156. Geisbert TW. 2014. Ebola therapy protects severely ill monkeys. Nature 514:41-43.
157. Casadevall A, Dadachova E, Pirofski LA. 2004. Passive antibody therapy for infectious diseases. Nat Rev Microbiol 2:695-703.
158. Nagy E, Nagy G, Power CA, Badarau A, Szijarto V. 2017. Anti-bacterial Monoclonal Antibodies. Adv Exp Med Biol 1053:119-153.
159. Motley MP, Banerjee K, Fries BC. 2019. Monoclonal antibody-based therapies for bacterial infections. Curr Opin Infect Dis 32:210-216.
160. Rouha H, Weber S, Janesch P, Maierhofer B, Gross K, Dolezilkova I, Mirkina I, Visram ZC, Malafa S, Stulik L, Badarau A, Nagy E. 2018. Disarming Staphylococcus aureus from destroying human cells by simultaneously neutralizing six cytotoxins with two human monoclonal antibodies. Virulence 9:231-247.
161. Gébleux R, Casi G. 2016. Antibody-drug conjugates: Current status and future perspectives. Pharmacology & Therapeutics 167:48-59.

162. Rowe JM, Löwenberg B. 2013. Gemtuzumab ozogamicin in acute myeloid leukemia: a remarkable saga about an active drug. Blood 121:4838.
163. Peters C, Brown S. 2015. Antibody–drug conjugates as novel anti-cancer chemotherapeutics. Bioscience Reports 35:e00225.
164. Peddi PF, Hurvitz SA. 2013. Trastuzumab emtansine: the first targeted chemotherapy for treatment of breast cancer. Future oncology (London, England) 9:10.2217/fon.13.7.
165. Lehar SM, Pillow T, Xu M, Staben L, Kajihara KK, Vandlen R, DePalatis L, Raab H, Hazenbos WL, Hiroshi Morisaki J, Kim J, Park S, Darwish M, Lee B-C, Hernandez H, Loyet KM, Lupardus P, Fong R, Yan D, Chalouni C, Luis E, Khalfin Y, Plise E, Cheong J, Lyssikatos JP, Strandh M, Koefoed K, Andersen PS, Flygare JA, Wah Tan M, Brown EJ, Mariathasan S. 2015. Novel antibody–antibiotic conjugate eliminates intracellular S. aureus. Nature 527:323-328.
166. Zhou C, Lehar S, Gutierrez J, Rosenberger CM, Ljumanovic N, Dinoso J, Koppada N, Hong K, Baruch A, Carrasco-Triguero M, Saad O, Mariathasan S, Kamath AV. 2016. Pharmacokinetics and pharmacodynamics of DSTA4637A: A novel THIOMAB™ antibody antibiotic conjugate against Staphylococcus aureus in mice. mAbs 8:1612-1619.
167. Kajihara KK, Pantua H, Hernandez-Barry H, Hazen M, Deshmukh K, Chiang N, Ohri R, Castellanos ER, Martin L, Matsumoto ML, Payandeh J, Storek KM, Schneider K, Smith PA, Koehler MFT, Tsai SP, Vandlen R, Loyet KM, Nakamura G, Pillow T, Seshasayee D, Kapadia SB, Hazenbos WLW, Projan SJ. 2021. Potent Killing of Pseudomonas aeruginosa by an Antibody-Antibiotic Conjugate. mBio 0:e00202-21.
168. Kamath AV. 2016. Translational pharmacokinetics and pharmacodynamics of monoclonal antibodies. Drug Discovery Today: Technologies 21-22:75-83.
169. Ryman JT, Meibohm B. 2017. Pharmacokinetics of Monoclonal Antibodies. CPT: Pharmacometrics & Systems Pharmacology 6:576-588.
170. Kim J, Hayton WL, Robinson JM, Anderson CL. 2007. Kinetics of FcRn-mediated recycling of IgG and albumin in human: pathophysiology and therapeutic implications using a simplified mechanism-based model. Clin Immunol 122:146-55.
171. Marchetti R, Dillon MJ, Burtnick MN, Hubbard MA, Kenfack MT, Bleriot Y, Gauthier C, Brett PJ, AuCoin DP, Lanzetta R, Silipo A, Molinaro A. 2015. Burkholderia pseudomallei Capsular Polysaccharide Recognition by a Monoclonal Antibody Reveals Key Details toward a Biodefense Vaccine and Diagnostics against Melioidosis. ACS Chem Biol 10:2295-302.
172. Weehuizen TA, Lankelma JM, De Jong HK, De Boer OJ, Roelofs JJ, Day NP, Gram H, De Vos AF, Wiersinga WJ. 2016. Therapeutic Administration of a Monoclonal Anti-Il-1beta Antibody Protects Against Experimental Melioidosis. Shock 46:566-574.
173. Ceballos-Olvera I, Sahoo M, Miller MA, Del Barrio L, Re F. 2011. Inflammasome-dependent pyroptosis and IL-18 protect against Burkholderia pseudomallei lung infection while IL-1β is deleterious. PLoS Pathog 7:e1002452.
174. Breitbach K, Köhler J, Steinmetz I. 2008. Induction of protective immunity against Burkholderia pseudomallei using attenuated mutants with defects in the intracellular life cycle. Transactions of the Royal Society of Tropical Medicine and Hygiene 102:S89-S94.
175. Silva EB, Goodyear A, Sutherland MD, Podnecky NL, Gonzalez-Juarrero M, Schweizer HP, Dow SW. 2013. Correlates of immune protection following cutaneous

immunization with an attenuated Burkholderia pseudomallei vaccine. Infection and Immunity 81:4626-4634.
176. Amemiya K, Dankmeyer JL, Biryukov SS, Treviño SR, Klimko CP, Mou SM, Fetterer DP, Garnes PG, Cote CK, Worsham PL. 2019. Deletion of two genes in Burkholderia pseudomallei MSHR668 that target essential amino acids protect acutely infected BALB/c mice and promote long term survival. Vaccines 7:196.
177. Atkins T, Prior R, Mack K, Russell P, Nelson M, Prior J, Ellis J, Oyston PC, Dougan G, Titball RW. 2002. Characterisation of an acapsular mutant of Burkholderia pseudomallei identified by signature tagged mutagenesis. J Med Microbiol 51:539-47.
178. Müller CM, Conejero L, Spink N, Wand ME, Bancroft GJ, Titball RW. 2012. Role of RelA and SpoT in Burkholderia pseudomallei virulence and immunity. Infection and immunity 80:3247-3255.
179. Khakhum N, Bharaj P, Myers JN, Tapia D, Kilgore PB, Ross BN, Walker DH, Endsley JJ, Torres AG. 2019. Burkholderia pseudomallei DeltatonB Deltahcp1 Live Attenuated Vaccine Strain Elicits Full Protective Immunity against Aerosolized Melioidosis Infection. mSphere 4.
180. Puangpetch A, Anderson R, Huang YY, Saengsot R, Sermswan RW, Wongratanacheewin S. 2014. Comparison of the protective effects of killed Burkholderia pseudomallei and CpG oligodeoxynucleotide against live challenge. Vaccine 32:5983-8.
181. Henderson A, Propst K, Kedl R, Dow S. 2011. Mucosal immunization with liposome-nucleic acid adjuvants generates effective humoral and cellular immunity. Vaccine 29:5304-5312.
182. Sarkar-Tyson M, Smither SJ, Harding S, Atkins TP, Titball RW. 2009. Protective efficacy of heat-inactivated B. thailandensis, B. mallei or B. pseudomallei against experimental melioidosis and glanders. Vaccine 27:4447-4451.
183. Harland DN, Chu K, Haque A, Nelson M, Walker NJ, Sarkar-Tyson M, Atkins TP, Moore B, Brown KA, Bancroft G. 2007. Identification of a LolC homologue in Burkholderia pseudomallei, a novel protective antigen for melioidosis. Infection and immunity 75:4173-4180.
184. Hara Y, Mohamed R, Nathan S. 2009. Immunogenic Burkholderia pseudomallei outer membrane proteins as potential candidate vaccine targets. PloS one 4:e6496.
185. Burtnick MN, Brett PJ, Harding SV, Ngugi SA, Ribot WJ, Chantratita N, Scorpio A, Milne TS, Dean RE, Fritz DL. 2011. The cluster 1 type VI secretion system is a major virulence determinant in Burkholderia pseudomallei. Infection and immunity 79:1512-1525.
186. Whitlock GC, Deeraksa A, Qazi O, Judy BM, Taylor K, Propst KL, Duffy AJ, Johnson K, Kitto GB, Brown KA. 2010. Protective response to subunit vaccination against intranasal Burkholderia mallei and B. pseudomallei challenge. Procedia in vaccinology 2:73-77.
187. Titball RW, Burtnick MN, Bancroft GJ, Brett P. 2017. Burkholderia pseudomallei and Burkholderia mallei vaccines: Are we close to clinical trials? Vaccine 35:5981-5989.
188. Scott AE, Burtnick MN, Stokes MG, Whelan AO, Williamson ED, Atkins TP, Prior JL, Brett PJ. 2014. Burkholderia pseudomallei capsular polysaccharide conjugates provide protection against acute melioidosis. Infect Immun 82:3206-13.

189. Burtnick MN, Shaffer TL, Ross BN, Muruato LA, Sbrana E, DeShazer D, Torres AG, Brett PJ. 2017. Development of subunit vaccines that provide high-level protection and sterilizing immunity against acute inhalational melioidosis. Infection and immunity 86:e00724-17.
190. Scott AE, Christ WJ, George AJ, Stokes MG, Lohman GJ, Guo Y, Jones M, Titball RW, Atkins TP, Campbell AS. 2016. Protection against experimental melioidosis with a synthetic manno-heptopyranose hexasaccharide glycoconjugate. Bioconjugate chemistry 27:1435-1446.
191. Scott AE, Ngugi SA, Laws TR, Corser D, Lonsdale CL, D'Elia RV, Titball RW, Williamson ED, Atkins TP, Prior JL. 2014. Protection against experimental melioidosis following immunisation with a lipopolysaccharide-protein conjugate. Journal of immunology research 2014.
192. Chapartegui-González I, Bowser S, Torres AG, Khakhum N. 2021. Recent Progress in Shigella and Burkholderia pseudomallei Vaccines. Pathogens 10:1353.
193. Scott AE, Burtnick MN, Stokes MG, Whelan AO, Williamson ED, Atkins TP, Prior JL, Brett PJ. 2014. Burkholderia pseudomallei capsular polysaccharide conjugates provide protection against acute melioidosis. Infection and immunity 82:3206-3213.
194. Su YC, Wan KL, Mohamed R, Nathan S. 2010. Immunization with the recombinant Burkholderia pseudomallei outer membrane protein Omp85 induces protective immunity in mice. Vaccine 28:5005-11.
195. Casey WT, Spink N, Cia F, Collins C, Romano M, Berisio R, Bancroft GJ, McClean S. 2016. Identification of an OmpW homologue in Burkholderia pseudomallei, a protective vaccine antigen against melioidosis. Vaccine 34:2616-21.
196. Charuchaimontri C, Suputtamongkol Y, Nilakul C, Chaowagul W, Chetchotisakd P, Lertpatanasuwun N, Intaranongpai S, Brett PJ, Woods DE. 1999. Antilipopolysaccharide II: an antibody protective against fatal melioidosis. Clin Infect Dis 29:813-8.
197. Patel N, Conejero L, Easton A, DeReynal M, Bancroft G, Titball R. 2011. Development of Vaccines Against Burkholderia Pseudomallei. Frontiers in Microbiology 2.
198. Casadevall A. 2018. Antibody-based vaccine strategies against intracellular pathogens. Curr Opin Immunol 53:74-80.
199. Luangasanatip N, Flasche S, Dance DAB, Limmathurotsakul D, Currie BJ, Mukhopadhyay C, Atkins T, Titball R, Jit M. 2019. The global impact and cost-effectiveness of a melioidosis vaccine. BMC Medicine 17:129.
200. de Duve C, Pressman BC, Gianetto R, Wattiaux R, Appelmans F. 1955. Tissue fractionation studies. 6. Intracellular distribution patterns of enzymes in rat-liver tissue. Biochemical Journal 60:604-617.
201. Klionsky DJ. 2008. Autophagy revisited: a conversation with Christian de Duve. Autophagy 4:740-3.
202. Levine B, Kroemer G. 2008. Autophagy in the pathogenesis of disease. Cell 132:27-42.
203. Levine B, Mizushima N, Virgin HW. 2011. Autophagy in immunity and inflammation. Nature 469:323-35.
204. Choi AMK, Ryter SW, Levine B. 2013. Autophagy in Human Health and Disease. New England Journal of Medicine 368:651-662.
205. Boya P, Reggiori F, Codogno P. 2013. Emerging regulation and functions of autophagy. Nat Cell Biol 15:713-20.

206. Jung CH, Ro S-H, Cao J, Otto NM, Kim D-H. 2010. mTOR regulation of autophagy. FEBS letters 584:1287-1295.
207. Abate G, Ruminiski PG, Kumar M, Singh K, Hamzabegovic F, Hoft DF, Eickhoff CS, Selimovic A, Campbell M, Chibale K. 2016. New Verapamil Analogs Inhibit Intracellular Mycobacteria without Affecting the Functions of Mycobacterium-Specific T Cells. Antimicrobial Agents and Chemotherapy 60:1216-1225.
208. Renna M, Jimenez-Sanchez M, Sarkar S, Rubinsztein DC. 2010. Chemical Inducers of Autophagy That Enhance the Clearance of Mutant Proteins in Neurodegenerative Diseases. The Journal of Biological Chemistry 285:11061-11067.
209. Shang L, Chen S, Du F, Li S, Zhao L, Wang X. 2011. Nutrient starvation elicits an acute autophagic response mediated by Ulk1 dephosphorylation and its subsequent dissociation from AMPK. Proceedings of the National Academy of Sciences of the United States of America 108:4788-4793.
210. Heitman J, Movva NR, Hall MN. 1991. Targets for cell cycle arrest by the immunosuppressant rapamycin in yeast. Science 253:905-9.
211. Li J, Kim SG, Blenis J. 2014. Rapamycin: one drug, many effects. Cell metabolism 19:373-379.
212. Zumla A, Rao M, Wallis RS, Kaufmann SH, Rustomjee R, Mwaba P, Vilaplana C, Yeboah-Manu D, Chakaya J, Ippolito G, Azhar E, Hoelscher M, Maeurer M. 2016. Host-directed therapies for infectious diseases: current status, recent progress, and future prospects. Lancet Infect Dis 16:e47-63.
213. Wallis RS, Zumla A. 2016. Vitamin D as Adjunctive Host-Directed Therapy in Tuberculosis: A Systematic Review. Open Forum Infect Dis 3:ofw151.
214. Wallis RS, Hafner R. 2015. Advancing host-directed therapy for tuberculosis. Nat Rev Immunol 15:255-63.
215. Degner NR, Wang JY, Golub JE, Karakousis PC. 2018. Metformin Use Reverses the Increased Mortality Associated With Diabetes Mellitus During Tuberculosis Treatment. Clin Infect Dis 66:198-205.
216. Yew WW, Chang KC, Chan DP, Zhang Y. 2019. Metformin as a host-directed therapeutic in tuberculosis: Is there a promise? Tuberculosis 115:76-80.
217. Singhal A, Jie L, Kumar P, Hong GS, Leow MK, Paleja B, Tsenova L, Kurepina N, Chen J, Zolezzi F, Kreiswirth B, Poidinger M, Chee C, Kaplan G, Wang YT, De Libero G. 2014. Metformin as adjunct antituberculosis therapy. Sci Transl Med 6:263ra159.
218. Dutta NK, Bruiners N, Pinn ML, Zimmerman MD, Prideaux B, Dartois V, Gennaro ML, Karakousis PC. 2016. Statin adjunctive therapy shortens the duration of TB treatment in mice. J Antimicrob Chemother 71:1570-7.
219. Adams KN, Szumowski JD, Ramakrishnan L. 2014. Verapamil, and its metabolite norverapamil, inhibit macrophage-induced, bacterial efflux pump-mediated tolerance to multiple anti-tubercular drugs. J Infect Dis 210:456-66.
220. de Knegt GJ, van der Meijden A, de Vogel CP, Aarnoutse RE, de Steenwinkel JE. 2017. Activity of moxifloxacin and linezolid against Mycobacterium tuberculosis in combination with potentiator drugs verapamil, timcodar, colistin and SQ109. Int J Antimicrob Agents doi:10.1016/j.ijantimicag.2016.11.027.
221. Demitto FdO, do Amaral RCR, Maltempe FG, Siqueira VLD, Scodro RBdL, Lopes MA, Caleffi-Ferracioli KR, Canezin PH, Cardoso RF. 2015. In Vitro Activity of Rifampicin and Verapamil Combination in Multidrug-Resistant Mycobacterium tuberculosis. PLOS ONE 10:e0116545.

222. Gupta A, Misra A, Deretic V. 2016. Targeted pulmonary delivery of inducers of host macrophage autophagy as a potential host-directed chemotherapy of tuberculosis. Adv Drug Deliv Rev 102:10-20.
223. Gupta A, Pant G, Mitra K, Madan J, Chourasia MK, Misra A. 2014. Inhalable particles containing rapamycin for induction of autophagy in macrophages infected with Mycobacterium tuberculosis. Mol Pharm 11:1201-7.
224. Gupta S, Tyagi S, Almeida DV, Maiga MC, Ammerman NC, Bishai WR. 2013. Acceleration of tuberculosis treatment by adjunctive therapy with verapamil as an efflux inhibitor. Am J Respir Crit Care Med 188:600-7.
225. Gupta S, Tyagi S, Bishai WR. 2015. Verapamil increases the bactericidal activity of bedaquiline against Mycobacterium tuberculosis in a mouse model. Antimicrob Agents Chemother 59:673-6.
226. Schiebler M, Brown K, Hegyi K, Newton SM, Renna M, Hepburn L, Klapholz C, Coulter S, Obregón-Henao A, Henao Tamayo M, Basaraba R, Kampmann B, Henry KM, Burgon J, Renshaw SA, Fleming A, Kay RR, Anderson KE, Hawkins PT, Ordway DJ, Rubinsztein DC, Floto RA. 2014. Functional drug screening reveals anticonvulsants as enhancers of mTOR-independent autophagic killing of Mycobacterium tuberculosis through inositol depletion. EMBO Molecular Medicine 7:127.
227. Juarez E, Carranza C, Sanchez G, Gonzalez M, Chavez J, Sarabia C, Torres M, Sada E. 2016. Loperamide Restricts Intracellular Growth of Mycobacterium tuberculosis in Lung Macrophages. Am J Respir Cell Mol Biol 55:837-847.
228. Kohler LJ, Roy CR. 2017. Autophagic targeting and avoidance in intracellular bacterial infections. Current Opinion in Microbiology 35:36-41.
229. Bergson P, Lipkind G, Lee SP, Duban M-E, Hanck DA. 2011. Verapamil block of T-type calcium channels. Molecular pharmacology 79:411-419.
230. Pule CM, Sampson SL, Warren RM, Black PA, van Helden PD, Victor TC, Louw GE. 2016. Efflux pump inhibitors: targeting mycobacterial efflux systems to enhance TB therapy. J Antimicrob Chemother 71:17-26.
231. Gupta S, Cohen KA, Winglee K, Maiga M, Diarra B, Bishai WR. 2014. Efflux inhibition with verapamil potentiates bedaquiline in Mycobacterium tuberculosis. Antimicrob Agents Chemother 58:574-6.
232. Spengler G, Kincses A, Gajdacs M, Amaral L. 2017. New Roads Leading to Old Destinations: Efflux Pumps as Targets to Reverse Multidrug Resistance in Bacteria. Molecules 22.
233. Sharma A, Gupta VK, Pathania R. 2019. Efflux pump inhibitors for bacterial pathogens: From bench to bedside. The Indian journal of medical research 149:129-145.
234. Auda IG, Ali Salman IM, Odah JG. 2020. Efflux pumps of Gram-negative bacteria in brief. Gene Reports 20:100666.
235. Olivares N, Rodriguez Y, Zatarain-Barron ZL, Marquina B, Mata-Espinosa D, Barrios-Payan J, Parada C, Moguel B, Espitia-Pinzon C, Estrada I, Hernandez-Pando R. 2017. A significant therapeutic effect of immunoglobulins administered alone, or in combination with conventional chemotherapy, in experimental pulmonary tuberculosis caused by drug-sensitive or drug-resistant strains. Pathog Dis 75.
236. Su F-Y, Srinivasan S, Lee B, Chen J, Convertine AJ, Eoin West T, Ratner DM, Skerrett SJ, Stayton PS. 2018. Macrophage-targeted drugamers with enzyme-cleavable

linkers deliver high intracellular drug dosing and sustained drug pharmacokinetics against alveolar pulmonary infections. Journal of Controlled Release doi:https://doi.org/10.1016/j.jconrel.2018.08.014.
237. Ye M, Zhao Y, Wang Y, Yodsanit N, Xie R, Gong S. 2020. pH-Responsive Polymer–Drug Conjugate: An Effective Strategy to Combat the Antimicrobial Resistance. Advanced Functional Materials n/a:2002655.
238. Meiers J, Zahorska E, Röhrig T, Hauck D, Wagner S, Titz A. 2020. Directing Drugs to Bugs: Antibiotic-Carbohydrate Conjugates targeting Biofilm-associated Lectins of Pseudomonas aeruginosa. Journal of Medicinal Chemistry doi:10.1021/acs.jmedchem.0c00856.
239. D'Elia RV, Woods S, Butcher W, McGahon J, Khadke S, Perrie Y, Williamson ED, Roberts CW. 2019. Exploitation of the bilosome platform technology to formulate antibiotics and enhance efficacy of melioidosis treatments. J Control Release 298:202-212.
240. Porges E, Jenner D, Taylor AW, Harrison JSP, De Grazia A, Hailes AR, Wright KM, Whelan AO, Norville IH, Prior JL, Mahajan S, Rowland CA, Newman TA, Evans ND. 2021. Antibiotic-Loaded Polymersomes for Clearance of Intracellular Burkholderia thailandensis. ACS Nano doi:10.1021/acsnano.1c05309.
241. Xie S, Li S, Zhang Z, Chen M, Ran P, Li X. 2020. Bacterial ghosts for targeting delivery and subsequent responsive release of ciprofloxacin to destruct intracellular bacteria. Chemical Engineering Journal doi:https://doi.org/10.1016/j.cej.2020.125700:125700.
242. Le H, Arnoult C, Dé E, Schapman D, Galas L, Le Cerf D, Karakasyan C. 2021. Antibody-Conjugated Nanocarriers for Targeted Antibiotic Delivery: Application in the Treatment of Bacterial Biofilms. Biomacromolecules doi:10.1021/acs.biomac.1c00082.
243. de Chaumont F, Dallongeville S, Chenouard N, Hervé N, Pop S, Provoost T, Meas-Yedid V, Pankajakshan P, Lecomte T, Le Montagner Y, Lagache T, Dufour A, Olivo-Marin J-C. 2012. Icy: an open bioimage informatics platform for extended reproducible research. Nature Methods 9:690-696.
244. Jenner D, Ducker C, Clark G, Prior J, Rowland CA. 2016. Using multispectral imaging flow cytometry to assess an in vitro intracellular Burkholderia thailandensis infection model. Cytometry A doi:10.1002/cyto.a.22809.
245. Wikler MA. 2006. Methods for dilution antimicrobial susceptibility tests for bacteria that grow aerobically: approved standard. CLSI (NCCLS) 26:M7-A7.
246. Wright AE, Douglas SR, Burdon-Sanderson JS. 1904. An experimental investigation of the rôle of the blood fluids in connection with phagocytosis. Proceedings of the Royal Society of London 72:357-370.
247. Pyzik M, Rath T, Lencer WI, Baker K, Blumberg RS. 2015. FcRn: The architect behind the immune and non-immune functions of IgG and albumin. Journal of immunology (Baltimore, Md : 1950) 194:4595-4603.
248. Roopenian DC, Akilesh S. 2007. FcRn: the neonatal Fc receptor comes of age. Nature Reviews Immunology 7:715-725.
249. Beck A, Wurch T, Bailly C, Corvaia N. 2010. Strategies and challenges for the next generation of therapeutic antibodies. Nat Rev Immunol 10:345-52.
250. Mulye M, Bechill MP, Grose W, Ferreira VP, Lafontaine ER, Wooten RM. 2014. Delineating the importance of serum opsonins and the bacterial capsule in affecting

the uptake and killing of Burkholderia pseudomallei by murine neutrophils and macrophages. PLoS Negl Trop Dis 8:e2988.
251. Chaichana P, Kronsteiner B, Rongkard P, Teparrukkul P, Limmathurotsakul D, Chantratita N, Day NPJ, Fletcher HA, Dunachie SJ. 2020. Serum From Melioidosis Survivors Diminished Intracellular Burkholderia pseudomallei Growth in Macrophages: A Brief Research Report. Front Cell Infect Microbiol 10:442.
252. Welkos S, Blanco I, Okaro U, Chua J, DeShazer D. 2020. A DUF4148 family protein produced inside RAW264.7 cells is a critical Burkholderia pseudomallei virulence factor. Virulence 11:1041-1058.
253. Brett PJ, Burtnick MN, Su H, Nair V, Gherardini FC. 2008. iNOS activity is critical for the clearance of Burkholderia mallei from infected RAW 264.7 murine macrophages. Cellular Microbiology 10:487-498.
254. Chiang CY, Ulrich RL, Ulrich MP, Eaton B, Ojeda JF, Lane DJ, Kota KP, Kenny TA, Ladner JT, Dickson SP, Kuehl K, Raychaudhuri R, Sun M, Bavari S, Wolcott MJ, Covell D, Panchal RG. 2015. Characterization of the murine macrophage response to infection with virulent and avirulent Burkholderia species. BMC Microbiol 15:259.
255. Taciak B, Białasek M, Braniewska A, Sas Z, Sawicka P, Kiraga Ł, Rygiel T, Król M. 2018. Evaluation of phenotypic and functional stability of RAW 264.7 cell line through serial passages. PLoS ONE 13:e0198943.
256. Fuentes AL, Millis L, Vapenik J, Sigola L. 2014. Lipopolysaccharide-mediated enhancement of zymosan phagocytosis by RAW 264.7 macrophages is independent of opsonins, laminarin, mannan, and complement receptor 3. J Surg Res 189:304-12.
257. Welkos SL, Klimko CP, Kern SJ, Bearss JJ, Bozue JA, Bernhards RC, Trevino SR, Waag DM, Amemiya K, Worsham PL, Cote CK. 2015. Characterization of Burkholderia pseudomallei Strains Using a Murine Intraperitoneal Infection Model and In Vitro Macrophage Assays. PLoS One 10:e0124667.
258. Place DE, Briard B, Samir P, Karki R, Bhattacharya A, Guy CS, Peters JL, Frase S, Vogel P, Neale G, Yamamoto M, Kanneganti T-D. 2020. Interferon inducible GBPs restrict Burkholderia thailandensis motility induced cell-cell fusion. PLoS pathogens 16:e1008364-e1008364.
259. Andreu N, Phelan J, de Sessions PF, Cliff JM, Clark TG, Hibberd ML. 2017. Primary macrophages and J774 cells respond differently to infection with Mycobacterium tuberculosis. Scientific Reports 7:42225.
260. Brezden A, Mohamed MF, Nepal M, Harwood JS, Kuriakose J, Seleem MN, Chmielewski J. 2016. Dual Targeting of Intracellular Pathogenic Bacteria with a Cleavable Conjugate of Kanamycin and an Antibacterial Cell-Penetrating Peptide. Journal of the American Chemical Society 138:10945-10949.
261. Moule MG, Spink N, Willcocks S, Lim J, Guerra-Assuncao JA, Cia F, Champion OL, Senior NJ, Atkins HS, Clark T, Bancroft GJ, Cuccui J, Wren BW. 2016. Characterization of New Virulence Factors Involved in the Intracellular Growth and Survival of Burkholderia pseudomallei. Infect Immun 84:701-10.
262. Lu R, Popov V, Patel J, Eaves-Pyles T. 2012. Burkholderia mallei and Burkholderia pseudomallei stimulate differential inflammatory responses from human alveolar type II cells (ATII) and macrophages. Frontiers in Cellular and Infection Microbiology 2.

263. Guimarães MCC, Amaral LG, Rangel LBA, Silva IV, Matta CGF, de Matta MFR. 2009. Growth inhibition of Staphylococcus aureus by chicken egg yolk antibodies. Archivum Immunologiae et Therapiae Experimentalis 57:377-382.
264. Lennings J, West TE, Schwarz S. 2018. The Burkholderia Type VI Secretion System 5: Composition, Regulation and Role in Virulence. Front Microbiol 9:3339.
265. Stevens JM, Ulrich RL, Taylor LA, Wood MW, DeShazer D, Stevens MP, Galyov EE. 2005. Actin-Binding Proteins from Burkholderia mallei and Burkholderia thailandensis Can Functionally Compensate for the Actin-Based Motility Defect of a Burkholderia pseudomallei bimA Mutant. Journal of Bacteriology 187:7857-7862.
266. Hotinger JA, May AE. 2020. Antibodies Inhibiting the Type III Secretion System of Gram-Negative Pathogenic Bacteria. Antibodies (Basel, Switzerland) 9:35.
267. Asano K, Sashinami H, Osanai A, Hirose S, Ono HK, Narita K, Hu D-L, Nakane A. 2016. Passive immunization with anti-ActA and anti-listeriolysin O antibodies protects against Listeria monocytogenes infection in mice. Scientific reports 6:39628-39628.
268. Kocks C, Gouin E, Tabouret M, Berche P, Ohayon H, Cossart P. 1992. L. monocytogenes-induced actin assembly requires the actA gene product, a surface protein. Cell 68:521-31.
269. Joller N, Weber SS, Muller AJ, Sporri R, Selchow P, Sander P, Hilbi H, Oxenius A. 2010. Antibodies protect against intracellular bacteria by Fc receptor-mediated lysosomal targeting. Proc Natl Acad Sci U S A 107:20441-6.
270. Joller N, Weber SS, Oxenius A. 2011. Antibody-Fc receptor interactions in protection against intracellular pathogens. Eur J Immunol 41:889-97.
271. Laws TR, Taylor AW, Russell P, Williamson D. 2019. The treatment of melioidosis: is there a role for repurposed drugs? A proposal and review. Expert Review of Anti-infective Therapy doi:10.1080/14787210.2018.1496330:1-11.
272. Inglis TJJ, Sagripanti J-L. 2006. Environmental Factors That Affect the Survival and Persistence of Burkholderia pseudomallei. Applied and Environmental Microbiology 72:6865-6875.
273. Li L, Mendis N, Trigui H, Oliver JD, Faucher SP. 2014. The importance of the viable but non-culturable state in human bacterial pathogens. Frontiers in Microbiology 5.
274. Cubitt AB, Heim R, Adams SR, Boyd AE, Gross LA, Tsien RY. 1995. Understanding, improving and using green fluorescent proteins. Trends in Biochemical Sciences 20:448-455.
275. Lowder M, Unge A, Maraha N, Jansson JK, Swiggett J, Oliver JD. 2000. Effect of Starvation and the Viable-but-Nonculturable State on Green Fluorescent Protein (GFP) Fluorescence in GFP-Tagged Pseudomonas fluorescens A506. Applied and Environmental Microbiology 66:3160-3165.
276. Eskelinen E-L. 2006. Roles of LAMP-1 and LAMP-2 in lysosome biogenesis and autophagy. Molecular Aspects of Medicine 27:495-502.
277. Hunziker W, Geuze HJ. 1996. Intracellular trafficking of lysosomal membrane proteins. Bioessays 18:379-89.
278. Andrejewski N, Punnonen E-L, Guhde G, Tanaka Y, Lüllmann-Rauch R, Hartmann D, von Figura K, Saftig P. 1999. Normal Lysosomal Morphology and Function in LAMP-1-deficient Mice*. Journal of Biological Chemistry 274:12692-12701.
279. Winchester BG. 2001. Lysosomal membrane proteins. European Journal of Paediatric Neurology 5:11-19.

280. Pierzyńska-Mach A, Janowski PA, Dobrucki JW. 2014. Evaluation of acridine orange, LysoTracker Red, and quinacrine as fluorescent probes for long-term tracking of acidic vesicles. Cytometry Part A 85:729-737.
281. Yapici NB, Bi Y, Li P, Chen X, Yan X, Mandalapu SR, Faucett M, Jockusch S, Ju J, Gibson KM, Pavan WJ, Bi L. 2015. Highly Stable and Sensitive Fluorescent Probes (LysoProbes) for Lysosomal Labeling and Tracking. Scientific Reports 5:8576.
282. Freundt EC, Czapiga M, Lenardo MJ. 2007. Photoconversion of Lysotracker Red to a green fluorescent molecule. Cell Research 17:956-958.
283. Rosales C, Uribe-Querol E. 2017. Phagocytosis: A Fundamental Process in Immunity. Biomed Res Int 2017:9042851.
284. Manivannan S, Rao NV, Ramanathan VD. 2012. Role of complement activation and antibody in the interaction between Mycobacterium tuberculosis and human macrophages. Indian J Exp Biol 50:542-50.
285. Taylor A, Jenner D, Rowland C, Laws T, Norville I, Prior J. 2021. Monoclonal antibodies opsonise Burkholderia and reduce intracellular actin tail formation in a macrophage infection assay. J Bacteriol doi:10.1128/jb.00244-21:Jb0024421.
286. O'Neill J. 2016. Tackling drug-resistant infections globally: Final report and recommendations. HM Government.
287. Ross BN, Myers JN, Muruato LA, Tapia D, Torres AG. 2018. Evaluating New Compounds to Treat Burkholderia pseudomallei Infections. Frontiers in Cellular and Infection Microbiology 8.
288. Tapia D, Sanchez-Villamil JI, Torres AG. 2019. Emerging role of biologics for the treatment of melioidosis and glanders. Expert Opinion on Biological Therapy 19:1319-1332.
289. Boyd NK, Teng C, Frei CR. 2021. Brief Overview of Approaches and Challenges in New Antibiotic Development: A Focus On Drug Repurposing. Frontiers in Cellular and Infection Microbiology 11.
290. Farha MA, Brown ED. 2019. Drug repurposing for antimicrobial discovery. Nature Microbiology 4:565-577.
291. Parumasivam T, Chan JG, Pang A, Quan DH, Triccas JA, Britton WJ, Chan HK. 2016. In Vitro Evaluation of Inhalable Verapamil-Rifapentine Particles for Tuberculosis Therapy. Mol Pharm 13:979-89.
292. Kania E, Pajak B, O'Prey J, Sierra Gonzalez P, Litwiniuk A, Urbanska K, Ryan KM, Orzechowski A. 2017. Verapamil treatment induces cytoprotective autophagy by modulating cellular metabolism. Febs j doi:10.1111/febs.14064.
293. Nieto-Patlán E, Serafín-López J, Wong-Baeza I, Pérez-Tapia SM, Cobos-Marín L, Estrada-Parra S, Estrada-García I, Chávez-Blanco AD, Chacón-Salinas R. 2019. Valproic acid promotes a decrease in mycobacterial survival by enhancing nitric oxide production in macrophages stimulated with IFN-γ. Tuberculosis 114:123-126.
294. Garg R, Shaw T, Vandana KE, Magazine R, Mukhopadhyay C. 2020. Melioidosis In Suspected Recurrent Tuberculosis: A disease in disguise. J Infect Dev Ctries 14:312-316.
295. Koh GC, Schreiber MF, Bautista R, Maude RR, Dunachie S, Limmathurotsakul D, Day NP, Dougan G, Peacock SJ. 2013. Host responses to melioidosis and tuberculosis are both dominated by interferon-mediated signaling. PLoS One 8:e54961.
296. Poolchanuan P, Unagul P, Thongnest S, Wiyakrutta S, Ngamrojanavanich N, Mahidol C, Ruchirawat S, Kittakoop P. 2020. An anticonvulsive drug, valproic acid (valproate),

has effects on the biosynthesis of fatty acids and polyketides in microorganisms. Scientific Reports 10:9300.
297. López S, Prieto M, Dijkstra J, Dhanoa MS, France J. 2004. Statistical evaluation of mathematical models for microbial growth. Int J Food Microbiol 96:289-300.
298. Tanida I, Ueno T, Kominami E. 2008. LC3 and Autophagy. Methods Mol Biol 445:77-88.
299. Pugsley HR. 2016. Quantifying autophagy: Measuring LC3 puncta and autolysosome formation in cells using multispectral imaging flow cytometry. Methods doi:http://dx.doi.org/10.1016/j.ymeth.2016.05.022.
300. Korzeniewski C, Callewaert DM. 1983. An enzyme-release assay for natural cytotoxicity. J Immunol Methods 64:313-20.
301. Van den Bossche S, Vandeplassche E, Ostyn L, Coenye T, Crabbé A. 2020. Bacterial Interference With Lactate Dehydrogenase Assay Leads to an Underestimation of Cytotoxicity. Frontiers in Cellular and Infection Microbiology 10.
302. Follath F, Ha HR, Schütz E, Bühler F. 1986. Pharmacokinetics of conventional and slow-release verapamil. British journal of clinical pharmacology 21 Suppl 2:149S-153S.
303. Information NCfB. 2022. PubChem Compound Summary for CID 2520, Verapamil. https://pubchem.ncbi.nlm.nih.gov/compound/Verapamil. Accessed March 25.
304. Rinchai D, Riyapa D, Buddhisa S, Utispan K, Titball RW, Stevens MP, Stevens JM, Ogawa M, Tanida I, Koike M, Uchiyama Y, Ato M, Lertmemongkolchai G. 2015. Macroautophagy is essential for killing of intracellular Burkholderia pseudomallei in human neutrophils. Autophagy 11:748-55.
305. Chen C, Gardete S, Jansen RS, Shetty A, Dick T, Rhee KY, Dartois V. 2018. Verapamil Targets Membrane Energetics in Mycobacterium tuberculosis. Antimicrobial agents and chemotherapy 62:e02107-17.
306. Rajan R, Karbowniczek M, Pugsley HR, Sabnani MK, Astrinidis A, La-Beck NM. 2015. Quantifying autophagosomes and autolysosomes in cells using imaging flow cytometry. Cytometry A 87:451-8.
307. Dunachie SJ, Jenjaroen K, Reynolds CJ, Quigley KJ, Sergeant R, Sumonwiriya M, Chaichana P, Chumseng S, Ariyaprasert P, Lassaux P, Gourlay L, Promwong C, Teparrukkul P, Limmathurotsakul D, Day NPJ, Altmann DM, Boyton RJ. 2017. Infection with Burkholderia pseudomallei - immune correlates of survival in acute melioidosis. Sci Rep 7:12143.
308. Dunachie S, Jenjaroen K, Limmathurotsakul D, Chumseng S, Ariyaprasert P, Teparrukkul P, P. J Day N. 2019. Metformin is associated with increased survival in melioidosis doi:10.6084/m9.figshare.9849119.v1. figshare.
309. Diamos AG, Hunter JGL, Pardhe MD, Rosenthal SH, Sun H, Foster BC, DiPalma MP, Chen Q, Mason HS. 2020. High Level Production of Monoclonal Antibodies Using an Optimized Plant Expression System. Frontiers in Bioengineering and Biotechnology 7.
310. Sifniotis V, Cruz E, Eroglu B, Kayser V. 2019. Current Advancements in Addressing Key Challenges of Therapeutic Antibody Design, Manufacture, and Formulation. Antibodies (Basel, Switzerland) 8:36.
311. Yamashita M, Katakura Y, Shirahata S. 2007. Recent advances in the generation of human monoclonal antibody. Cytotechnology 55:55-60.

312. Gupta SK, Shukla P. 2017. Sophisticated Cloning, Fermentation, and Purification Technologies for an Enhanced Therapeutic Protein Production: A Review. Frontiers in Pharmacology 8.
313. Motley MP, Fries BC. 2017. A New Take on an Old Remedy: Generating Antibodies against Multidrug-Resistant Gram-Negative Bacteria in a Postantibiotic World. mSphere 2:e00397-17.
314. Kollef MH, Betthauser KD. 2021. Monoclonal antibodies as antibacterial therapies: thinking outside of the box. The Lancet Infectious Diseases 21:1201-1202.
315. Zurawski DV, McLendon MK. 2020. Monoclonal Antibodies as an Antibacterial Approach Against Bacterial Pathogens. Antibiotics (Basel) 9.
316. Stockwin LH, Holmes S. 2003. Antibodies as therapeutic agents: vive la renaissance! Expert Opin Biol Ther 3:1133-52.
317. Lu R-M, Hwang Y-C, Liu IJ, Lee C-C, Tsai H-Z, Li H-J, Wu H-C. 2020. Development of therapeutic antibodies for the treatment of diseases. Journal of Biomedical Science 27:1.
318. Elgundi Z, Reslan M, Cruz E, Sifniotis V, Kayser V. 2017. The state-of-play and future of antibody therapeutics. Advanced Drug Delivery Reviews 122:2-19.
319. Kim H-Y, Stojadinovic A, Weina PJ, Kim HS, Lo S-C, Izadjoo MJ. 2011. Monoclonal Antibody-Based Therapeutics for Melioidosis and Glanders. American Journal of Immunology 7:14.
320. Ho M, Schollaardt T, Smith MD, Perry MB, Brett PJ, Chaowagul W, Bryan LE. 1997. Specificity and functional activity of anti-Burkholderia pseudomallei polysaccharide antibodies. Infect Immun 65:3648-53.
321. Domenech M, Sempere J, de Miguel S, Yuste J. 2018. Combination of Antibodies and Antibiotics as a Promising Strategy Against Multidrug-Resistant Pathogens of the Respiratory Tract. Frontiers in immunology 9:2700-2700.
322. Casal J, Aguilar L, Jado I, Yuste J, Gimenez MJ, Prieto J, Fenoll A. 2002. Effects of specific antibodies against Streptococcus pneumoniae on pharmacodynamic parameters of beta-lactams in a mouse sepsis model. Antimicrob Agents Chemother 46:1340-4.
323. Yuste J, Fenoll A, Casal J, Gimenez MJ, Aguilar L. 2002. Combined effect of specific antibodies (as serotherapy or preimmunization) and amoxicillin doses in treatment of Streptococcus pneumoniae sepsis in a mouse model. Antimicrob Agents Chemother 46:4043-4.
324. DiGiandomenico A, Keller AE, Gao C, Rainey GJ, Warrener P, Camara MM, Bonnell J, Fleming R, Bezabeh B, Dimasi N, Sellman BR, Hilliard J, Guenther CM, Datta V, Zhao W, Gao C, Yu XQ, Suzich JA, Stover CK. 2014. A multifunctional bispecific antibody protects against Pseudomonas aeruginosa. Sci Transl Med 6:262ra155.
325. Song Y, Baer M, Srinivasan R, Lima J, Yarranton G, Bebbington C, Lynch SV. 2012. PcrV antibody–antibiotic combination improves survival in Pseudomonas aeruginosa-infected mice. European Journal of Clinical Microbiology & Infectious Diseases 31:1837-1845.
326. Hua L, Hilliard JJ, Shi Y, Tkaczyk C, Cheng LI, Yu X, Datta V, Ren S, Feng H, Zinsou R, Keller A, O'Day T, Du Q, Cheng L, Damschroder M, Robbie G, Suzich J, Stover CK, Sellman BR. 2014. Assessment of an anti-alpha-toxin monoclonal antibody for prevention and treatment of Staphylococcus aureus-induced pneumonia. Antimicrob Agents Chemother 58:1108-17.

327. Hilliard JJ, Datta V, Tkaczyk C, Hamilton M, Sadowska A, Jones-Nelson O, O'Day T, Weiss WJ, Szarka S, Nguyen V, Prokai L, Suzich J, Stover CK, Sellman BR. 2015. Anti-alpha-toxin monoclonal antibody and antibiotic combination therapy improves disease outcome and accelerates healing in a Staphylococcus aureus dermonecrosis model. Antimicrob Agents Chemother 59:299-309.
328. Migone TS, Bolmer S, Zhong J, Corey A, Vasconcelos D, Buccellato M, Meister G. 2015. Added benefit of raxibacumab to antibiotic treatment of inhalational anthrax. Antimicrob Agents Chemother 59:1145-51.
329. Biron B, Beck K, Dyer D, Mattix M, Twenhafel N, Nalca A. 2015. Efficacy of ETI-204 monoclonal antibody as an adjunct therapy in a New Zealand white rabbit partial survival model for inhalational anthrax. Antimicrob Agents Chemother 59:2206-14.
330. Tong JTW, Harris PWR, Brimble MA, Kavianinia I. 2021. An Insight into FDA Approved Antibody-Drug Conjugates for Cancer Therapy. Molecules (Basel, Switzerland) 26:5847.
331. Fu Z, Li S, Han S, Shi C, Zhang Y. 2022. Antibody drug conjugate: the "biological missile" for targeted cancer therapy. Signal transduction and targeted therapy 7:93-93.
332. Anonymous. 2019. Polatuzumab Vedotin Approved for DLBCL. Cancer Discov 9:Of2.
333. Deeks ED. 2019. Polatuzumab Vedotin: First Global Approval. Drugs 79:1467-1475.
334. Leung D, Wurst JM, Liu T, Martinez RM, Datta-Mannan A, Feng Y. 2020. Antibody Conjugates-Recent Advances and Future Innovations. Antibodies (Basel) 9.
335. Nakada T, Sugihara K, Jikoh T, Abe Y, Agatsuma T. 2019. The Latest Research and Development into the Antibody-Drug Conjugate, [fam-] Trastuzumab Deruxtecan (DS-8201a), for HER2 Cancer Therapy. Chem Pharm Bull (Tokyo) 67:173-185.
336. MacGregor P, Gonzalez-Munoz AL, Jobe F, Taylor MC, Rust S, Sandercock AM, Macleod OJS, Van Bocxlaer K, Francisco AF, D'Hooge F, Tiberghien A, Barry CS, Howard P, Higgins MK, Vaughan TJ, Minter R, Carrington M. 2019. A single dose of antibody-drug conjugate cures a stage 1 model of African trypanosomiasis. PLOS Neglected Tropical Diseases 13:e0007373.
337. Umotoy JC, de Taeye SW. 2021. Antibody Conjugates for Targeted Therapy Against HIV-1 as an Emerging Tool for HIV-1 Cure. Frontiers in immunology 12:708806-708806.
338. Mariathasan S, Tan M-W. 2017. Antibody–Antibiotic Conjugates: A Novel Therapeutic Platform against Bacterial Infections. Trends in Molecular Medicine doi:http://dx.doi.org/10.1016/j.molmed.2016.12.008.
339. Easmon CS, Crane JP, Blowers A. 1986. Effect of ciprofloxacin on intracellular organisms: in-vitro and in-vivo studies. J Antimicrob Chemother 18 Suppl D:43-8.
340. Easmon CS, Crane JP. 1985. Uptake of ciprofloxacin by macrophages. J Clin Pathol 38:442-4.
341. Château MT, Caravano R. 1993. Rapid fluorometric measurement of the intra-cellular concentration of ciprofloxacin in mouse peritoneal macrophages. J Antimicrob Chemother 31:281-7.
342. Podnecky NL, Rhodes KA, Schweizer HP. 2015. Efflux pump-mediated drug resistance in Burkholderia. Frontiers in microbiology 6:305-305.
343. Russell P, Eley SM, Ellis J, Green M, Bell DL, Kenny DJ, Titball RW. 2000. Comparison of efficacy of ciprofloxacin and doxycycline against experimental melioidosis and glanders. J Antimicrob Chemother 45:813-8.

344. Dance DA, Wuthiekanun V, Chaowagul W, White NJ. 1989. The antimicrobial susceptibility of Pseudomonas pseudomallei. Emergence of resistance in vitro and during treatment. J Antimicrob Chemother 24:295-309.
345. Chaowagul W, Suputtamongkul Y, Smith MD, White NJ. 1997. Oral fluoroquinolones for maintenance treatment of melioidosis. Trans R Soc Trop Med Hyg 91:599-601.
346. Randall LB, Georgi E, Genzel GH, Schweizer HP. 2017. Finafloxacin overcomes Burkholderia pseudomallei efflux-mediated fluoroquinolone resistance. The Journal of antimicrobial chemotherapy 72:1258-1260.
347. Chalhoub H, Harding SV, Tulkens PM, Van Bambeke F. 2019. Influence of pH on the activity of finafloxacin against extracellular and intracellular Burkholderia thailandensis, Yersinia pseudotuberculosis, and Francisella philomiragia and on its cellular pharmacokinetics in THP-1 monocytes. Clin Microbiol Infect doi:10.1016/j.cmi.2019.07.028.
348. Ovacik M, Lin K. 2018. Tutorial on Monoclonal Antibody Pharmacokinetics and Its Considerations in Early Development. Clin Transl Sci 11:540-552.
349. Deng R, Zhou C, Li D, Cai H, Sukumaran S, Carrasco-Triguero M, Saad O, Nazzal D, Lowe C, Ramanujan S, Kamath AV. 2019. Preclinical and translational pharmacokinetics of a novel THIOMAB antibody-antibiotic conjugate against Staphylococcus aureus. MAbs doi:10.1080/19420862.2019.1627152:1-13.
350. Huang W, Zhang Q, Li W, Chen Y, Shu C, Li Q, Zhou J, Ye C, Bai H, Sun W, Yang X, Ma Y. 2019. Anti-outer Membrane Vesicle Antibodies Increase Antibiotic Sensitivity of Pan-Drug-Resistant Acinetobacter baumannii. Frontiers in microbiology 10:1379-1379.
351. Collins HH, Cross AS, Dobek A, Opal SM, McClain JB, Sadoff JC. 1989. Oral Ciprofloxacin and a Monoclonal Antibody to Lipopolysaccharide Protect Leukopenic Rats from Lethal Infection with Pseudomonas aeruginosa. The Journal of Infectious Diseases 159:1073-1082.
352. Peterson JW, Comer JE, Noffsinger DM, Wenglikowski A, Walberg KG, Chatuev BM, Chopra AK, Stanberry LR, Kang AS, Scholz WW, Sircar J. 2006. Human monoclonal anti-protective antigen antibody completely protects rabbits and is synergistic with ciprofloxacin in protecting mice and guinea pigs against inhalation anthrax. Infect Immun 74:1016-24.
353. Vieira P, Rajewsky K. 1988. The half-lives of serum immunoglobulins in adult mice. Eur J Immunol 18:313-6.
354. Diehl KH, Hull R, Morton D, Pfister R, Rabemampianina Y, Smith D, Vidal JM, van de Vorstenbosch C. 2001. A good practice guide to the administration of substances and removal of blood, including routes and volumes. J Appl Toxicol 21:15-23.
355. Mort JS, Buttle DJ. 1997. Cathepsin B. The International Journal of Biochemistry & Cell Biology 29:715-720.
356. Delamarre L, Pack M, Chang H, Mellman I, Trombetta ES. 2005. Differential lysosomal proteolysis in antigen-presenting cells determines antigen fate. Science 307:1630-4.
357. Caculitan NG, dela Cruz Chuh J, Ma Y, Zhang D, Kozak KR, Liu Y, Pillow TH, Sadowsky J, Cheung TK, Phung Q, Haley B, Lee B-C, Akita RW, Sliwkowski MX, Polson AG. 2017. Cathepsin B Is Dispensable for Cellular Processing of Cathepsin B-Cleavable Antibody–Drug Conjugates. Cancer Research 77:7027-7037.
358. Poreba M. 2020. Protease-activated prodrugs: strategies, challenges, and future directions. The FEBS Journal n/a.

359. Turk V, Stoka V, Vasiljeva O, Renko M, Sun T, Turk B, Turk D. 2012. Cysteine cathepsins: From structure, function and regulation to new frontiers. Biochimica et Biophysica Acta (BBA) - Proteins and Proteomics 1824:68-88.
360. Vidak E, Javoršek U, Vizovišek M, Turk B. 2019. Cysteine Cathepsins and their Extracellular Roles: Shaping the Microenvironment. Cells 8:264.
361. Behrens CR, Liu B. 2014. Methods for site-specific drug conjugation to antibodies. MAbs 6:46-53.
362. Agarwal P, Bertozzi CR. 2015. Site-specific antibody-drug conjugates: the nexus of bioorthogonal chemistry, protein engineering, and drug development. Bioconjug Chem 26:176-92.
363. Yao H, Jiang F, Lu A, Zhang G. 2016. Methods to Design and Synthesize Antibody-Drug Conjugates (ADCs). International journal of molecular sciences 17:194.
364. Wang-Lin SX, Zhou C, Kamath AV, Hong K, Koppada N, Saad OM, Carrasco-Triguero M, Khojasteh C, Deng R. 2018. Minimal physiologically-based pharmacokinetic modeling of DSTA4637A, A novel THIOMAB antibody antibiotic conjugate against Staphylococcus aureus, in a mouse model. MAbs doi:10.1080/19420862.2018.1494478:1-13.
365. Burn GL, Foti A, Marsman G, Patel DF, Zychlinsky A. 2021. The Neutrophil. Immunity 54:1377-1391.
366. Laws TR, Smither SJ, Lukaszewski RA, Atkins HS. 2011. Neutrophils are the predominant cell-type to associate with Burkholderia pseudomallei in a BALB/c mouse model of respiratory melioidosis. Microb Pathog 51:471-5.
367. Easton A, Haque A, Chu K, Lukaszewski R, Bancroft GJ. 2007. A critical role for neutrophils in resistance to experimental infection with Burkholderia pseudomallei. J Infect Dis 195:99-107.
368. Haque A, Easton A, Smith D, O'Garra A, Van Rooijen N, Lertmemongkolchai G, Titball RW, Bancroft GJ. 2006. Role of T cells in innate and adaptive immunity against murine Burkholderia pseudomallei infection. J Infect Dis 193:370-9.
369. Santanirand P, Harley VS, Dance DA, Drasar BS, Bancroft GJ. 1999. Obligatory role of gamma interferon for host survival in a murine model of infection with Burkholderia pseudomallei. Infect Immun 67:3593-600.
370. Miyagi K, Kawakami K, Saito A. 1997. Role of reactive nitrogen and oxygen intermediates in gamma interferon-stimulated murine macrophage bactericidal activity against Burkholderia pseudomallei. Infection and Immunity 65:4108-4113.
371. Geraghty P, Rogan MP, Greene CM, Boxio RMM, Poiriert T, O'Mahony M, Belaaouaj A, O'Neill SJ, Taggart CC, McElvaney NG. 2007. Neutrophil Elastase Up-Regulates Cathepsin B and Matrix Metalloprotease-2 Expression. The Journal of Immunology 178:5871-5878.
372. Lah TT, Hawley M, Rock KL, Goldberg AL. 1995. Gamma-interferon causes a selective induction of the lysosomal proteases, cathepsins B and L, in macrophages. FEBS Lett 363:85-9.
373. Cavaco M, Castanho MARB, Neves V. 2022. The Use of Antibody-Antibiotic Conjugates to Fight Bacterial Infections. Frontiers in Microbiology 13.
374. Power AL, Barber DG, Groenhof SRM, Wagley S, Liu P, Parker DA, Love J. 2021. The Application of Imaging Flow Cytometry for Characterisation and Quantification of Bacterial Phenotypes. Frontiers in Cellular and Infection Microbiology 11.

375. Baggio D, Ananda-Rajah MR. 2021. Fluoroquinolone antibiotics and adverse events. Australian prescriber 44:161-164.
376. Marchant J. 2018. When antibiotics turn toxic. Nature 555:431-433.
377. Bennett AC, Bennett CL, Witherspoon BJ, Knopf KB. 2019. An evaluation of reports of ciprofloxacin, levofloxacin, and moxifloxacin-association neuropsychiatric toxicities, long-term disability, and aortic aneurysms/dissections disseminated by the Food and Drug Administration and the European Medicines Agency. Expert Opin Drug Saf 18:1055-1063.
378. Breedveld FC. 2000. Therapeutic monoclonal antibodies. Lancet 355:735-40.
379. Adhikari P, Zacharias N, Ohri R, Sadowsky J. 2020. Site-Specific Conjugation to Cys-Engineered THIOMAB™ Antibodies. Methods Mol Biol 2078:51-69.
380. Zacharias N, Podust VN, Kajihara KK, Leipold D, Del Rosario G, Thayer D, Dong E, Paluch M, Fischer D, Zheng K, Lei C, He J, Ng C, Su D, Liu L, Masih S, Sawyer W, Tinianow J, Marik J, Yip V, Li G, Chuh J, Morisaki JH, Park S, Zheng B, Hernandez-Barry H, Loyet KM, Xu M, Kozak KR, Phillips GL, Shen BQ, Wu C, Xu K, Yu SF, Kamath A, Rowntree RK, Reilly D, Pillow T, Polson A, Schellenberger V, Hazenbos WLW, Sadowsky J. 2022. A homogeneous high-DAR antibody-drug conjugate platform combining THIOMAB antibodies and XTEN polypeptides. Chem Sci 13:3147-3160.
381. Hoffmann RM, Coumbe BGT, Josephs DH, Mele S, Ilieva KM, Cheung A, Tutt AN, Spicer JF, Thurston DE, Crescioli S, Karagiannis SN. 2018. Antibody structure and engineering considerations for the design and function of Antibody Drug Conjugates (ADCs). Oncoimmunology 7:e1395127.
382. Fonseca MHG, Furtado GP, Bezerra MRL, Pontes LQ, Fernandes CFC. 2018. Boosting half-life and effector functions of therapeutic antibodies by Fc-engineering: An interaction-function review. Int J Biol Macromol 119:306-311.
383. Bruhns P, Iannascoli B, England P, Mancardi DA, Fernandez N, Jorieux S, Daeron M. 2009. Specificity and affinity of human Fcgamma receptors and their polymorphic variants for human IgG subclasses. Blood 113:3716-25.
384. Cohn RC, Rudzienski L, Putnam RW. 1995. Verapamil-tobramycin synergy in Pseudomonas cepacia but not Pseudomonas aeruginosa in vitro. Chemotherapy 41:330-3.
385. Treerat P, Widmer F, Middleton PG, Iredell J, George AM. 2008. In vitro interactions of tobramycin with various nonantibiotics against Pseudomonas aeruginosa and Burkholderia cenocepacia. FEMS Microbiology Letters 285:40-50.